

LIFETIME PREDICTIONS FOR THE FIRST WALL AND BLANKET STRUCTURE OF FUSION REACTORS

**PROCEEDINGS OF A TECHNICAL COMMITTEE MEETING
ON LIFETIME PREDICTIONS FOR THE
FIRST WALL AND BLANKET STRUCTURE OF FUSION REACTORS
ORGANIZED BY THE
INTERNATIONAL ATOMIC ENERGY AGENCY
AND HELD IN KARLSRUHE, 5-7 NOVEMBER 1985**



**A TECHNICAL DOCUMENT ISSUED BY THE
INTERNATIONAL ATOMIC ENERGY AGENCY, VIENNA, 1986**

LIFETIME PREDICTIONS FOR THE
FIRST WALL AND BLANKET STRUCTURE OF FUSION REACTORS
IAEA, VIENNA, 1986
IAEA-TECDOC-393

Printed by the IAEA in Austria
November 1986

**PLEASE BE AWARE THAT
ALL OF THE MISSING PAGES IN THIS DOCUMENT
WERE ORIGINALLY BLANK**

The IAEA does not normally maintain stocks of reports in this series.
However, microfiche copies of these reports can be obtained from

INIS Clearinghouse
International Atomic Energy Agency
Wagramerstrasse 5
P.O. Box 100
A-1400 Vienna, Austria

Orders should be accompanied by prepayment of Austrian Schillings 100,—
in the form of a cheque or in the form of IAEA microfiche service coupons
which may be ordered separately from the INIS Clearinghouse.

FOREWORD

Lifetime analysis of the first wall including the divertor and limiter is an important subject for the design of fusion reactors. These components are exposed to severe mechanical, thermal and irradiation effects, that limit their useful structural life and their design lifetime has a large influence on the selection of major reactor design parameters.

The Technical Committee on Lifetime Predictions for the First Wall and Blanket Structure of Fusion Reactors was convened by the International Atomic Energy Agency in Karlsruhe on the invitation of the Government of the Federal Republic of Germany. The meeting was hosted by the Nuclear Research Centre Karlsruhe and chaired by Dr. J. Vetter, KFK Karlsruhe. The purpose of the meeting was to provide an international forum for reviewing and discussing the state of the art of lifetime predictions for the first wall, divertor and limiter of fusion reactors, and to identify areas in which additional research and development are needed. The meeting emphasized the review of life limiting mechanisms and their influence on plasma facing components of fusion reactors. Particular attention was given to the discussion of different approaches and models for the prediction of component lifetimes.

The Technical Committee was subdivided into three technical sessions:

- 1) Life-limiting Mechanisms
- 2) Stress Analysis and Lifetime Evaluation
- 3) Erosion and Depository Effects

At the end of the meeting a round table discussion was held on Future Goals and Needs in Lifetime Assessments.

The meeting was attended by 34 participants from 11 countries and 2 International Organizations presenting 18 papers.

The present volume contains all papers and session summaries of this meeting.

CONTENTS

Session summaries by the Chairmen	7
Round table discussion	15

LIFE-LIMITING MECHANISMS (Session 1)

Lifetime limitation of first wall structures by fatigue crack propagation	23
<i>E. Diegele, T. Fett, D. Munz</i>	
Creep lifetime of austenitic steels as determined by high temperature helium embrittlement studies	51
<i>H. Schroeder</i>	
Thermal shock effects on type 316L austenitic steel and vanadium base alloys	59
<i>H.Th. Klippel, B. van der Schaaf, W. van Witzenburg</i>	
An overview of the PIREX program	71
<i>S.L. Green, W.V. Green, D. Gavillet, F. Hegedus, P. Marmy, U. Stiefel, M.P. Victoria</i>	

STRESS ANALYSIS AND LIFETIME EVALUATION (Session 2)

High temperature thermal creep of materials under non-stationary stress and/or temperature loading conditions (<i>Abstract only</i>)	83
<i>M. Boček, M. Hoffmann</i>	
Thermo-mechanical stresses in structural components close to the plasma	85
<i>A. Ludwig</i>	
The RCC-MR design code for LMFBR components. A useful basis for fusion reactor design tools development	97
<i>D. Acker, G. Chevereau</i>	
An analytical and experimental study on lifetime predictions for fusion reactor first walls and divertor plates	107
<i>T. Horie, T. Aruga, N. Miki, A. Minato, M. Seki, K. Shiraishi, S. Tsujimura, T. Watanabe, T. Tone</i>	

STRESS ANALYSIS AND LIFETIME EVALUATION (cont.) (Session 3)

Lifetime analysis of plasma side components	137
<i>R.F. Mattas</i>	
Estimated thermal fatigue limits for the first wall of NET	149
<i>G.O. Vieider, A. Cardella</i>	
Stress analysis of the NET outboard first wall box	151
<i>A. Cardella, H. Gorenflo</i>	
Possibilities and limitations of first-wall lifetime analyses by means of analytical methods	161
<i>W. Dänner</i>	
Tools and procedures for structural lifetime evaluation of NET first wall design concepts	173
<i>E. Zolti</i>	

EROSION AND DEPOSITION EFFECTS (Session 4)

Material damage in the first wall of TOKAMAKs by plasma wall interaction	187
<i>K. Koizlik, H. Nickel</i>	
Mechanisms of wall erosion in fusion devices	203
<i>R. Behrisch</i>	
Redistribution of limiter and wall materials in JET	221
<i>J. Ehrenberg, R. Behrisch, P.E. Stott, J.P. Coad, L. de Kock, G.M. McCracken</i>	
The depositions of hydrogen isotopes on carbonised fusion reactor walls	233
<i>B.Y. Emmoth, H. Bergsaker</i>	
List of participants and observers	239

Session Summaries

LIFE-LIMITING MECHANISMS

M. BOČEK

Kernforschungszentrum Karlsruhe,
Karlsruhe, Federal Republic of Germany

Plasma burning with periodic refueling in fusion reactors will produce temperature and thermal stress cycling. The cyclic stress in the first wall structural material is likely to be reversing in the tension-compression sense. The response of materials to such mechanical loading is the development of fatigue damage. It is expected that crack growth will lead to component failure.

It is obvious that materials' properties will change during their lifetime. For instance helium implantation and radiation damage will affect bulk properties. Sputtering, redeposition etc. will influence the surface conditions, i.e. the metallurgical structure and composition of materials will depend on the loading conditions and hence both will vary in time.

In this session a model for lifetime prediction was presented (Diegele, Fett, Munz) to outline the general procedure and to demonstrate the behaviour of structures facing the plasma. In detail temperature distributions and elastic stresses due to thermal loading were calculated taking into account the redistribution of stresses due to irradiation induced creep and swelling. Cracks of different initial sizes were assumed in the inner and outer wall surface and the lifetime was estimated by means of crack extension computations. It was concluded that crack growth on the outer wall surface is more serious than on the inner surface. In comparison to austenitic steel (SS 316) martensitic steel (1.4914) has a longer lifetime under same boundary conditions.

In one of the lectures (Schröder) results of experimental and theoretical investigations concerning the influence of helium on creep properties and on material lifetime as conducted in different laboratories were reported. Therefrom "maps" can be established which allow the estimation of the lifetime limiting failure mechanisms in austenitic stainless steels for given load conditions.

Klippel and van der Schaaf examined-by means of laser light pulses-thermal shock effects on the lifetime of crept and strain cycled SS 316 and vanadium based alloys. Metallographic investigations revealed eroded areas with plenty of cracks. Under comparable conditions the lifetime of these specimens turned out to be appreciably lower than those of the "unirradiated" specimens. Although the quantification of the effect is difficult, the method demonstrated could be used for simulation of plasma-wall interactions.

The paper of Green et al. gives an overview about the PIREX program. The facility (under installation) will allow to evaluate the microstructural and mechanical effects expected to be generated in the first wall and blanket structure by the combination of the environmental loading and radiation damage.

STRESS ANALYSIS AND LIFETIME EVALUATION

R.F. MATTAS

Argonne National Laboratory,
Argonne, Illinois,
United States of America

The first part of Session B consisted of four papers which examined various aspects of stress analysis and lifetime evaluation.

The first paper by M. Bocek entitled, "Constitutive Equations for High Temperature Creep Under Non-Stationary Stress and/or Temperature Loading Conditions" considered creep-rupture lifetime predictions of materials where the lifetime was limited by cavitation damage. Constitutive equations have been developed which describe the accumulation of damage during creep-rupture. The equations can then be used to predict the shape of the creep curves and the lifetime of materials under time dependent loading and temperature conditions. The inclusion of the time dependence of stress and temperature represents a considerable advance in creep-rupture modeling. The equations have been used to successfully describe high temperature burst tests of Zircaloy. An important restriction in developing the analytic solutions to the equations is that the metallurgical state of the system is assumed to remain the same during the application of stress and high temperature. This restriction means that fundamental changes in microstructure during the stress/temperature history, such as irradiation induced changes, are not presently taken into account by the model. Much of the discussion involved the initial assumptions used in developing the model and the limits of applicability. Dr. Bocek stated that he based the model on measurable macroscopic quantities, rather than microscopic parameters, so that it could easily be verified against existing data. The model is presently limited to predicting lifetimes at high levels of strain and does not consider the primary creep stage.

The second paper by A. Ludwig entitled, "Thermo-Mechanical Stress in Structural Components Close to the Plasma," describes the modeling of the long term cyclic response of the first wall. The computer code TSTRELT has been developed for this purpose. In TSTRELT, which is based upon the code TSTRESS written at the University of Wisconsin, the first wall structure is represented by a plate element which is uniformly loaded over its surface. The TSTRELT code uses an approximative extrapolation procedure where the actual rates of creep, swelling, and wall erosion are replaced by average values.

This procedure results in a greatly reduced number of calculations without losing important information about the history of the first wall. The code has been used to predict the structural response of the INTOR and JET first walls. The results, which are presented using computer generated "3-D" time, stress, and depth plots, show the evolution of the first wall stress when radiation creep and swelling are considered.

The third paper by D. Acker and G. Chevereau entitled, "The RCC-MR Design Code for LMFBR Components; A Useful Basis for Fusion Reactor Design Tools Development," describes the applicability of LMFBR design codes to fusion reactor design. In several areas, it appears that LMFBR codes can be successfully applied because of similarities in operating temperature levels (550-600°C), structural materials (stainless steel), stress loading conditions, and irradiation effects. The RCC-MR code, which was developed for the French LMFBR program, was specifically addressed. This code considers temperatures and stresses during both normal and off-normal operation, the effects of creep, the ratchetting limits of materials, fatigue and creep-fatigue damage limits and buckling. The authors believe that the RCC-MR code can serve as the basis for developing a fusion reactor design code.

The final paper of the session by T. Horio, et al., and entitled, "An Analytical and Experimental Study on Lifetime Predictions for Fusion Reactor First Walls and Divertor Plates," describes recent work in Japan in several areas related to lifetime studies. The items described in the paper are the materials data base system, a one-dimensional lifetime analysis of the first wall and divertor plate, 2-D elastic-plastic finite element analyses of the first wall and divertor plates, and experimental results of thermal and stress fatigue tests of divertor plate duplex structures. The main conclusions from this work are: 1) Erosion and fatigue appear to be lifetime limiting rather than creep or swelling in near term reactors; 2) Induced plastic stresses during disruptions will enhance ratchetting strain in the first wall; 3) Fatigue failure tests in tungsten-copper duplex structures show that failure occurs in tungsten at high strain ranges and in copper at low strain ranges; and 4) 2-D elastic-plastic analyses are believed to be required to fully understand the behavior of the first wall and divertor plates.

In summary, these papers show that considerable progress has been made in developing design codes and lifetime models for fusion components. Similar approaches have been taken by various researchers in developing the lifetime models. The major long term needs for further development are a reduction in uncertainties in materials properties, particularly radiation effects, and direct verification of model predictions with experiments.

STRESS ANALYSIS AND LIFETIME EVALUATION (cont.)

T. TONE

Japan Atomic Energy Research Institute,
Naka-machi, Naka-gun, Ibaraki-ken,
Japan

Three of four presentations put an emphasis on the methodology of lifetime predictions and the characteristics resulting from exemplified applications (B5, B7, B8), while the other one (B6) discusses numerical results obtained from one-, two- and three-dimensional models applied to the stress analysis of the NET first wall structures. Two one-dimensional computer programs developed for lifetime predictions are reported (B5, B7), with an emphasis on their usefulness and adequacy to perform extensive analysis studies for a wide variety of operating conditions and design parameters under the present big uncertainties of input parameters (materials properties, loading conditions, etc.). In addition, through further discussions on the suitable and practical methodology under the present problematic areas and uncertainties in lifetime predictions, the simplification concept of computational procedures and a draft of simplified structural design criteria are presented (B8).

Individual papers presented are briefly summarized as follows.

The one-dimensional computer code developed for the lifetime prediction of first wall and impurity control components is capable of examining sputtering erosion, swelling, creep, fatigue and crack growth, and their synergistic effects (B5). The lifetime analysis applied to INTOR first wall and divertor plates indicates that both the INTOR first wall and divertor will have acceptable lifetimes, though the considerable uncertainties in the analysis are recognized. Since the INTOR first wall has little operating margin, impact of uncertainties on the lifetime is large. For example, a small increase in surface heat load or erosion rate could reduce the lifetime to an unacceptable level. A need to verify code predictions is proposed. In the absense of direct verification by experiment, it is pointed out that it is desirable to compare predictions of different codes with each other, e.g., through the use of benchmark problems.

The modeling of one-, two- and three-dimensional thermo-mechanical analysis applied to the NET first wall is discussed (B6). The 3-D first

wall geometry is simulated by the first wall-box model. The results obtained show that the ratio of peak 3D-stress to peak 1-D stress is in the range of 1.07 ~ 1.15. Influence of the first wall coolant channel geometry on the peak 2-D thermal stresses is well represented by a linear relationship with the aspect ratio of coolant channel to front plate of the first wall. Stress concentration factors in grooved first wall are analyzed for three types of groove geometry. Parametric calculations are conducted to examine the range of thermal fatigue limits for the NET first wall with austenitic stainless steel. With some conditions, the conclusion says that the type 316 SS first wall of NET appears to be marginally feasible for the required 10^5 burn cycles, and that grooved protection layers are not applicable due to high stress concentrations.

An analytical methodology for predicting the first wall lifetime in simple geometries (cylindrical and spherical shell) is presented(B7). The usefulness of the analytical methods for the first wall long-term behavior is concluded by demonstrating the important results of general nature. As for the inelastic response the ratio of the swelling and creep rates is important. If the ratio is linear in dose the additional stresses saturate. If the ratio is larger than one a continuous stress increase will lead to an early life termination. In case of a DEMO power reactor first wall made of 20% cold worked 316 SS the most important lifetime limitations are the tolerable amounts of swelling and creep deformation.

Main problems in first wall lifetime predictions, particularly from the viewpoint of computational methods, design criteria, and analysis modeling and procedures, are discussed and summarized(B8). As for computational methods, it is addressed that no model describes completely the complex plastic and creep behavior. The hypotheses in the material model developed by Oak Ridge National Laboratory, which is implemented in the finite element computer codes such as ADINA, MARC, and ANSYS, are reviewed. It is pointed out that their validity to be applied to first wall plastic and thermal creep analysis is to be verified for the first wall material conditions. A first draft of simplified criteria is proposed for use in the predesign phase of the NET project. The major differences between the predesign criteria and the ASME-code are identified. In the predesign criteria operational loading conditions are grouped into 2 categories, while in the ASME-code into

6 categories. The major conclusion is that simplified method for lifetime assessment are essential particularly in the predesign phase with considerations of the present uncertainties, and for comparative evaluation of different design options.

Round Table Discussion

FUTURE GOALS AND NEEDS IN LIFETIME ASSESSMENT

D.R. HARRIES

The NET Team,

Garching near Munich

The Chairman, Dr.D.R. Harries (The NET Team, Garching bei München), opened the session by listing the principal areas on which the subsequent discussion was centred. The main conclusions and recommendations arising from the very lively, 1.5 hour discussion on the future goals and needs for assessing the lifetimes of the first wall and other plasma facing components may be summarised as follows:

1. Plasma physics boundary conditions

The need for more precise data on the loadings from the plasma to the surrounding components was emphasised. In particular, the physicists were strongly urged to supply data on the particles, energies, electrical fields and, in the case of plasma disruptions, a systematic analysis of the global experience from large tokamaks.

2. Materials requirements and data bases

(i) Materials

First Wall

The materials of primary interest for the first wall in the next step Tokamak fusion devices are: solution annealed or cold worked 316 type austenitic steels and quenched and tempered 9-12%Cr martensitic steels. The candidate materials for later reactors include titanium modified 316 type austenitic steels, vanadium base alloys and the low activation materials which are currently being developed.

First Wall protection

A metallic first wall will not be able to withstand plasma disruptions without excessive surface damage and detrimental effects on the integrity of the structure. There is no guarantee at this stage that plasma

disruptions can be completely avoided in large Tokamaks and methods of protecting the first wall have to be considered.

The favoured protection material is graphite as it sublimates and only melts at temperatures of $>4000^{\circ}\text{C}$ and at a pressure of >100 atmospheres. However, it exhibits excessive irradiation growth and swelling and has unfavourable hydrogen recycling characteristics; a grade of graphite with better irradiation resistance or graphite impregnated with silicon could be used but periodic replacement of the protection would still have to be contemplated. Other materials, such as ceramics, composites and low Z (beryllium) and high Z (tungsten and molybdenum) elements have also been considered but their resistance to plasma disruptions is inferior to that of graphite.

Divertor

Low physical sputtering coefficient tungsten, molybdenum and their respective alloys are currently considered as armour materials for the divertor impurity control system, with copper and copper alloys proposed as heat sink and coolant tube materials respectively in some of the present design concepts. The choice of materials for the divertor armour is still a matter of some concern as the sputtered atoms of the high Z elements are effective in quenching the plasma and resistance to plasma disruption effects is required.

Limiter

A number of metallic and non-metallic materials are being explored as potential limiter materials in TEXTOR and carbon and beryllium considered for JET.

(ii) Data bases

Experimental data on the following materials bulk properties and behaviour, in the form of constitutive equations or rules, are required for predicting the lifetimes of the plasma facing components:

- (a) Physical, chemical and magnetic properties.
- (b) Mechanical properties (tensile, creep, relaxation and rupture, low cycle fatigue, fatigue crack growth, creep-fatigue, thermal fatigue and fracture toughness) in the unirradiated and irradiated conditions

as well as irradiation-induced micro-chemical and - structural changes, void swelling and creep. The possibility of failure by thermal fatigue is a major concern since the first wall is subjected to alternating thermal stresses induced by the surface and volumetric heating from the plasma and the pulsed nature of the operation.

The possibility of hydrogen isotope embrittlement of the plasma facing component materials is a major concern since high concentrations of deuterium and tritium are injected from the plasma and hydrogen is formed by (n,p) reactions. Data are also required on the synergistic effects of helium (He^3 formed by decay of the tritium, He^4 produced by (n, α) reactions and injected from the plasma), hydrogen and displacement damage on the mechanical properties.

For the metallic structures, data on the properties of the welds and heat-affected zones, and brazings are required in addition to those on the parent materials.

(c) Interactions with the coolants, particularly with respect to localised effects such as stress corrosion, stress assisted and caustic cracking; influence of irradiation on these phenomena as well as on the general corrosion of the materials in contact with the coolants.

(d) The properties of rewelded, tritiated and irradiated materials.

With respect to plasma surface interactions and their influence on the lifetimes of the plasma facing components, data are primarily required on: the physical and chemical erosion, the properties of the sputtered and redeposited materials and the effects of plasma disruptions, run-away electrons and arcing.

(iii) Test facilities and irradiation sources

Since a large volume, high 14 MeV neutron flux facility is not available, data on the bulk properties will continue to be obtained during and following irradiations in thermal and fast reactors and with charged particles in accelerators and cyclotrons. Since these approaches do not exactly simulate the fusion neutron environment, theoretical and experimental studies have to be continued in an

attempt to establish fission-fusion and charged particle-fusion correlations.

For surface damage investigations, a dedicated facility is required to determine the properties of the redeposited materials. The effects of plasma disruptions can be usefully simulated in high heat flux test facilities utilising intense electron or laser beam heating. The use of existing fusion devices such as JET, TFTR, TEXTOR and JT-60 for exposing samples or probes to the plasma should continue but it is paramount that the experimental conditions are sufficiently well defined and controlled to allow the data to be fully interpreted.

(iv) Models and equations

The development of phenomenological and physically based models will significantly enhance the interpretation of the materials data and contribute to the formulation of the constitutive equations of the materials behaviour required for the lifetime assessments.

3. Computational tools and procedures

The thermostructural response of the plasma facing components in a fusion system can, to a large extent, be predicted using existing finite element codes. However, the validity of the basic assumptions in the mathematical representations of the materials behaviour has to be qualified for the component materials, loading and environmental conditions and geometries. The loading conditions and geometries can be idealised in first estimations of the lifetimes but less conservative and more refined approaches will be necessary in the longer term.

4. Failure criteria

The computed structural responses have to be evaluated with respect to the potential failure modes. Thus, limits have to be defined for the material integrity and for the component functional requirements. The structural design code ASME Section III and Code Case 47 forms a valuable starting base but the effects of irradiation on the failure limits have to be included and fracture mechanics approaches also considered in extended versions.

The up-dating and finalisation of the failure criteria will, of necessity, require many years of dedicated effort.

5. Lifetime evaluations

The predictions of the component lifetime analyses need to be compared with experimental results; for example, data obtained from high heat flux tests would form an extremely useful basis for some of the comparisons. In addition, uncertainty analyses of the estimates of the component lifetimes will be required.

The discussion concluded with the following recommendations for promoting and implementing further work relevant to this topic of lifetime assessments for the plasma facing components in fusion reactors:

- (i) Arrange specialist meetings on specific topics.
- (ii) Establish working groups in specific areas.
- (iii) Undertake reviews of the literature and materials data bases.
- (iv) Compile materials handbooks.
- (v) Organise benchmark or "round-robin" exercises.

Session 1

LIFE-LIMITING MECHANISMS

LIFETIME LIMITATION OF FIRST WALL STRUCTURES BY FATIGUE CRACK PROPAGATION

E. DIEGELE, T. FETT, D. MUNZ
Kernforschungszentrum Karlsruhe,
Karlsruhe, Federal Republic of Germany

Abstract

The extension of small cracks by cyclic thermal stresses caused by the cyclic operation seems to be the most important failure mode of first wall structures of fusion reactors. The change of stress during one cycle at different locations of the first wall is dependent on the heat flux, the details of the geometry of the first wall structure and the cooling conditions. In addition the stress distribution is affected by the creep and swelling behaviour of the material.

To investigate the effect of the different influencing parameters first the behavior of pressurized tubes was considered. The lifetime calculations were performed in the following steps: temperature distribution, stress distribution, cyclic stress intensity factor, cyclic crack growth rate, lifetime. For stainless steel the redistribution of the stresses due to radiation creep and swelling changes the mean stress.

This affects the crack propagation at different locations of the tube during the lifetime.

At the present time the calculations are extended in the following directions:

- replacing the longitudinal cracks by more realistic semi-elliptical surface cracks
- comparison of austenitic and martensitic steels
- considering more complex structures, proposed by the NET-team.

The results, available at the time of the meeting, shall be presented.

1. Introduction

Different failure modes have to be considered in the design of the first wall and blanket of fusion reactors; namely

- excessive plastic deformation due to exceeding of the yield strength or to creep,

- creep rupture,
- crack propagation due to cyclic loading,
- wall erosion due to sputtering.

Crack extension by cyclic operation of a fusion reactor seems to be the most important failure mode. Cracks can be generated during fabrication as welding cracks, during normal operation as fatigue cracks or during plasma disruptions.

The stress distribution is caused by external heating and by internal pressure of the cooling medium. This stress distribution changes during operation because of radiation creep and swelling. The change of the stress field during the burn-off phase is superimposed to this gradually changing stress distribution.

In the past, lifetime calculations were performed often for constrained plates /1-4/. In /5, 6/ these results were extended to include tubes of stainless steel SS 316 (20% CW). Here results are presented for a first wall with square cooling channels (NET design). In addition a preliminary comparison of stainless steel with the martensitic 10.5 % Cr steel (German designation 1.4914) is given.

2. Temperature and Stress Distribution

2.1 Geometry

One of the designs proposed by NET is a water cooled first wall with 'square' channels and inner tubes at 240°/280°C temperature and breeder material liquid $\text{Li}_{17}\text{Pb}_{83}$ (Fig. 1). Calculations are made for a set of parameters. For example the thickness d of the first wall front side and the curvature radius R of the 'square' channel are varied. Here results are presented for $d = 8$ mm and $R = 6$ mm. The other geometric data, given by the NET team, can be taken from Figs. 1 and 2.

2.2 Finite element meshes

Temperature calculations are performed on a two dimensional structure using 1169 nodes and 352 elements with the FE program ADINAT. Thermal stresses are computed for a 3-D structure with ADINA. The mesh, modeled with 1709 nodes

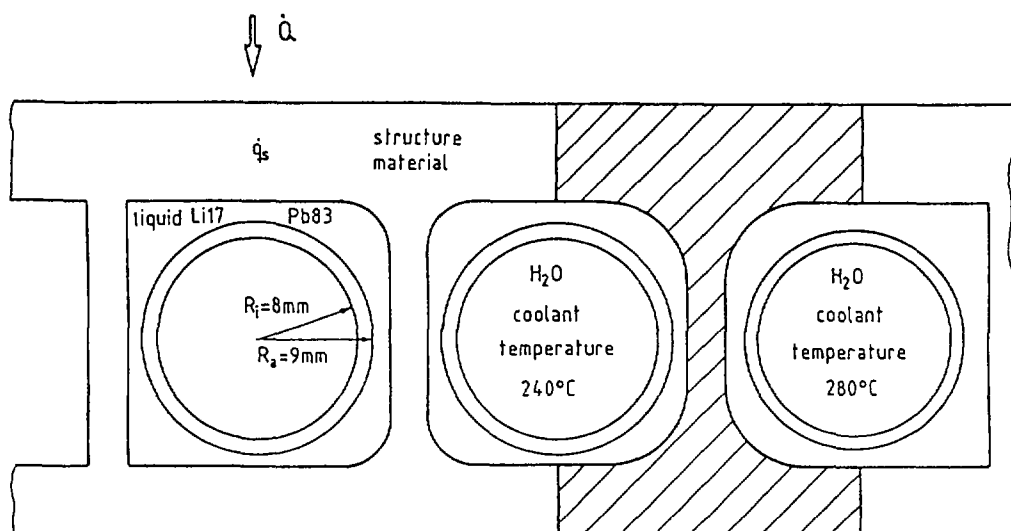


Fig. 1 First wall

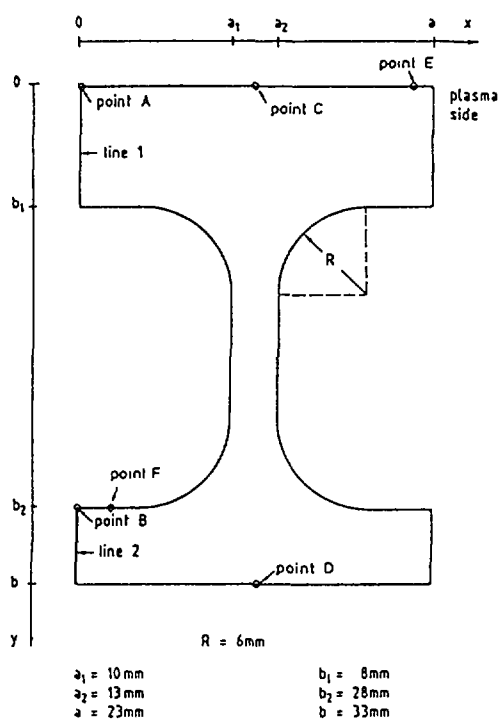


Fig. 2

Geometric data - structure material

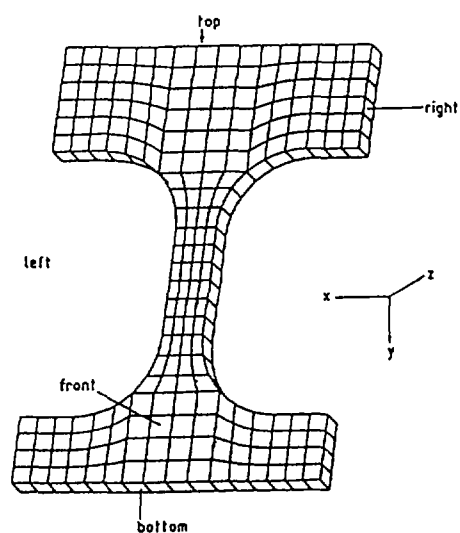


Fig. 3

Finite element mesh

and 208 elements, is explained in more detail in Fig. 3. To simplify the model, the cooling pipes and breeder material have been neglected in the stress analysis; besides, it was assumed that no internal pressure acts on the structure.

2.3 Thermal loads

The plasma side first wall is subjected to surface heating and heat deposition due to power release by neutrons. A surface heat flux \dot{Q} of 15 W/cm^2 and an internal heat generation rate \dot{q}_s of 15 W/cm^3 (over the whole structure) are assumed during the burn-time of the plasma. We furthermore suppose the maximal values of \dot{q} and \dot{Q} to be reached linearly within 10 s after plasma ignition, a burn-time of 250 s with constant \dot{q} and \dot{Q} , a linear decrease of the surface heat flux and volumetric heating to 0 within 10 s after burn-off time, and a dwell time of 50 s.

2.4 Boundary conditions for temperature calculations

We use adiabatic boundaries, except for the inner side of the coolant tube for which an environmental temperature of the cooling medium H_2O of $240^\circ/280^\circ\text{C}$ is fixed. The heat transfer coefficient is $0.5 \text{ W/cm}^2/\text{K}$.

2.5 Material properties

Austenitic 316 SS and martensitic 1.4914 steel are considered as structure materials. The temperature dependence of the Young's modulus, thermal conductivity, thermal expansion and volumetric specific heat are documented in Figs. 4, 5 and 6. Data for the breeder material $\text{Li}_{17}\text{Pb}_{83}$ are shown in Fig. 7. As maximal volumetric heat generation in this material was assumed to be 20 W/cm^3 .

2.6 Displacement constraints

A thermal stress analysis was carried out while fixing some points of the mesh. The left side has deleted degrees of freedom in the x-direction. In order to keep the cut of the first wall (Fig. 2) free from bending, the displacements on the right side are subject to constraint. The structure can expand in the x-direction keeping the right side parallel to the left. The same consideration was made for the 'front/back' sides.

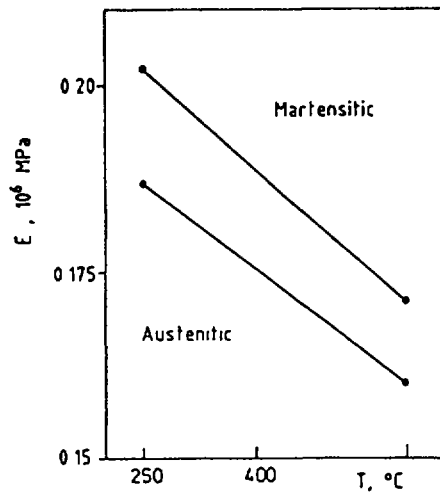


Fig. 4 Young's modulus

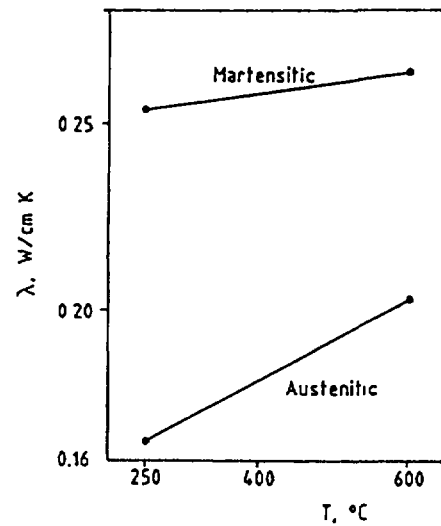


Fig. 5 Thermal conductivity

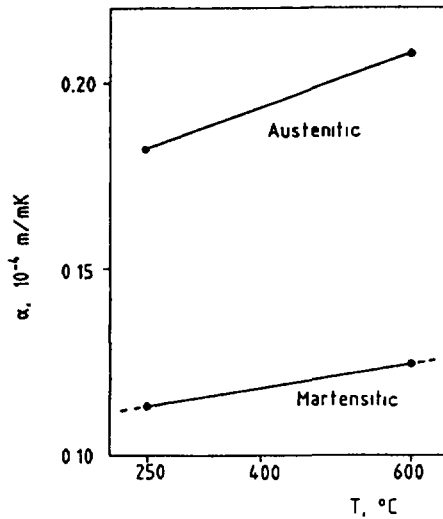


Fig. 6 Coefficient of thermal expansion

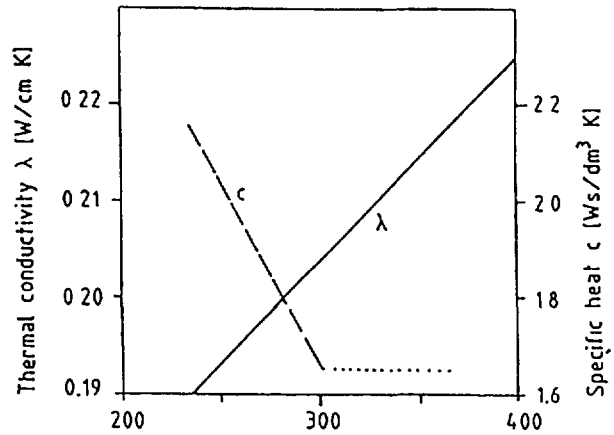


Fig. 7 Material data Li₁₇Pb₈₃

2.7 Temperature analysis

A transient analysis was performed. The structure was heated from the initial conditions (260°C) until steady state, then cooled with a dwell-time of 50 sec and heated again from minimal temperature. The time dependence at the point of maximal temperature (Point A in Fig. 2) is documented in Fig. 8. The maximum temperature is 488°C and 455°C, respectively, for the austenitic and the martensitic steels. Furthermore, we show two contour plots at the end of the burn-time for the two materials examined, Figs. 9 and 10.

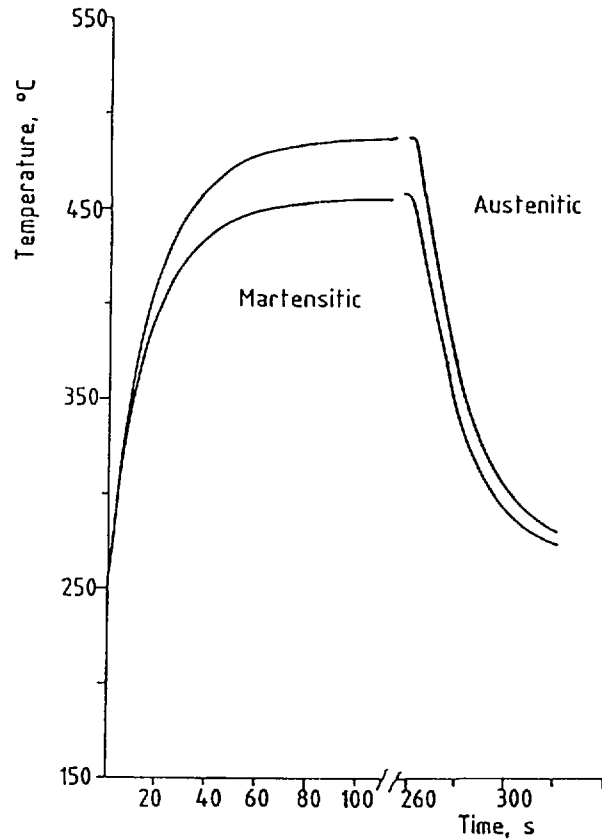


Fig. 8 Temperature at point A during one cycle
Austenitic and Martensitic Steel

The temperature variation ($T_{\max} - T_{\min}$) of martensitic steel is 15% less than for austenitic steel.

The temperature distribution is not symmetric with respect to the middle axis because of different inlet and outlet cooling temperatures.

2.8 Stress analysis

The structure is assumed to be free from stresses under the initial condition (260°C). The distribution of stresses at the end of the burn time (maximal temperature) and after the dwell time (minimal temperature) are of greatest interest. As expected by the temperature distribution, there are compressive stresses on the plasma side and tensile stresses on the back side of the first wall in any direction. This can be documented by contour plots for the nodal stresses. In Fig. 11 stresses for austenitic steel and in Fig. 12 stresses for martensitic steel are shown.

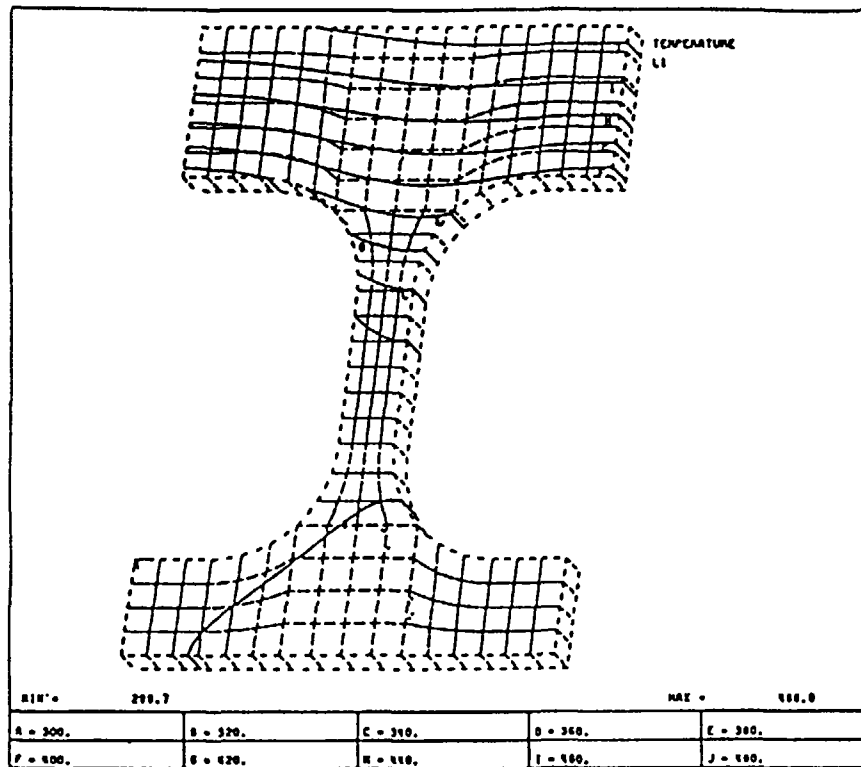


Fig. 9 Temperature distribution, austenitic steel

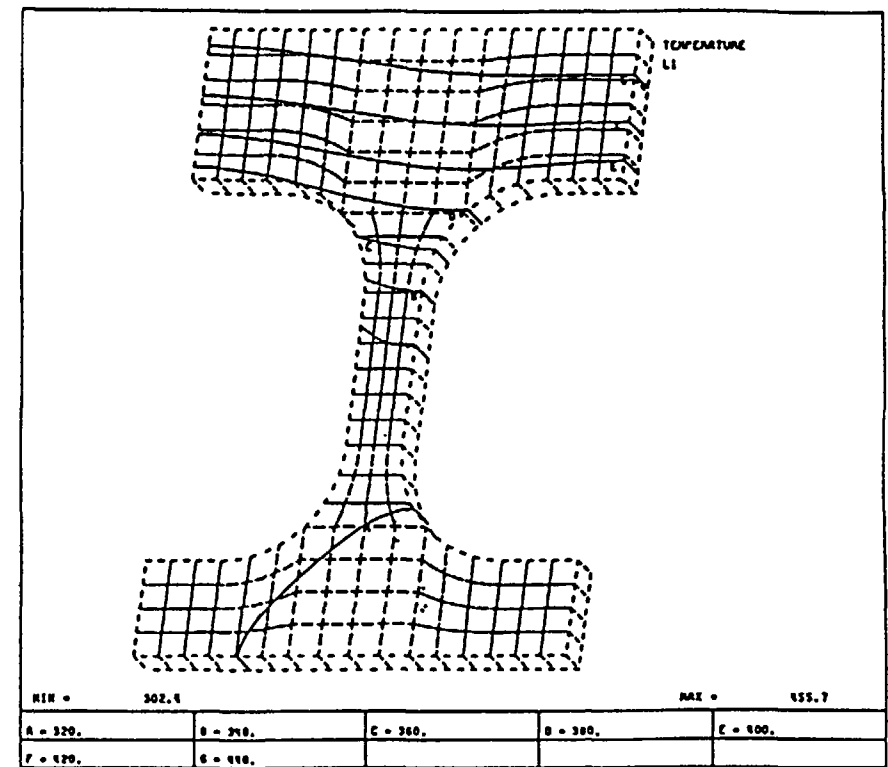


Fig. 10 Temperature distribution, martensitic steel

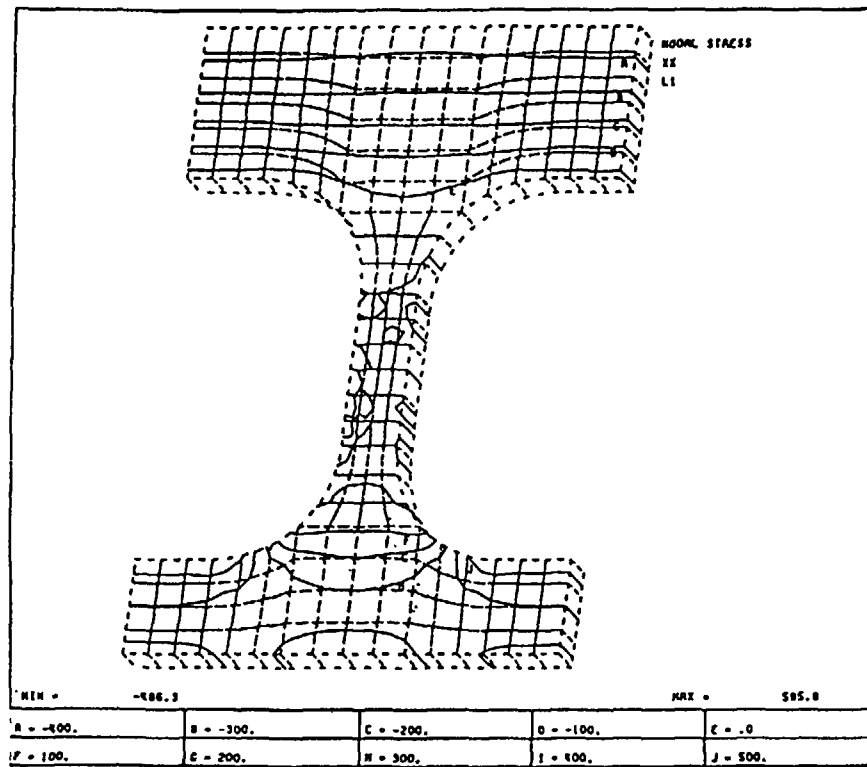


Fig. 11.1 Thermal stresses, x-direction, austenitic

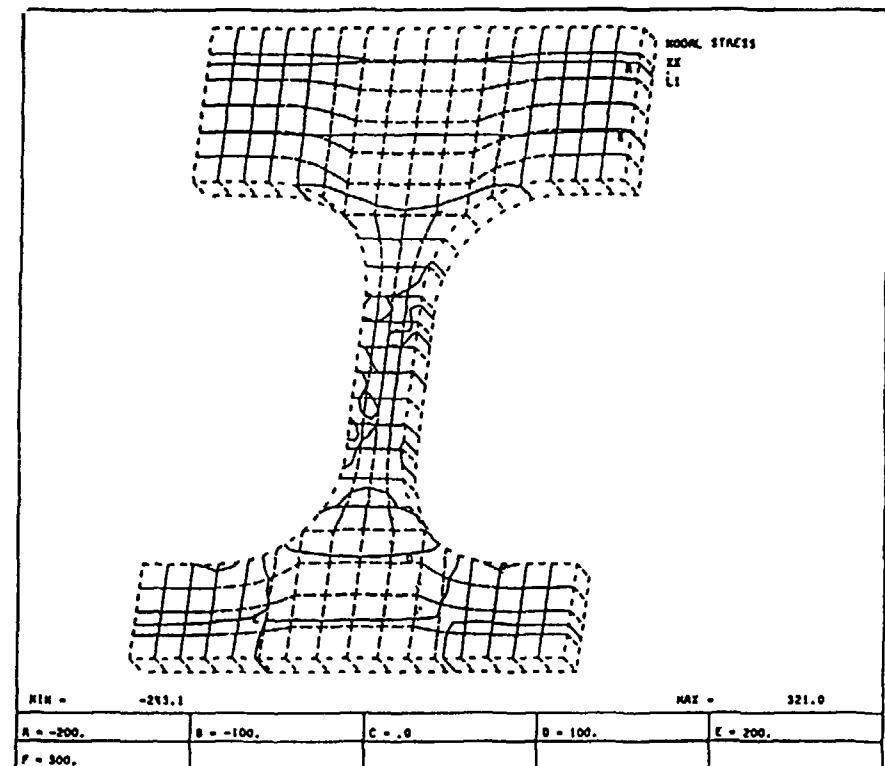


Fig. 12.1 Thermal stresses, x-direction, martensitic

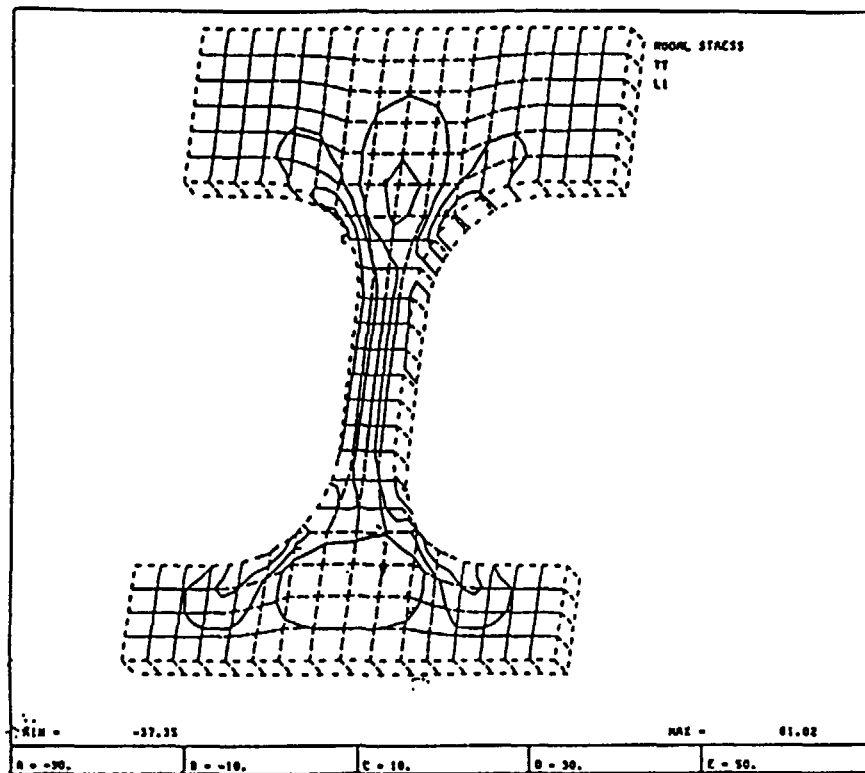


Fig. 11.2 Thermal stresses, y-direction, austenitic

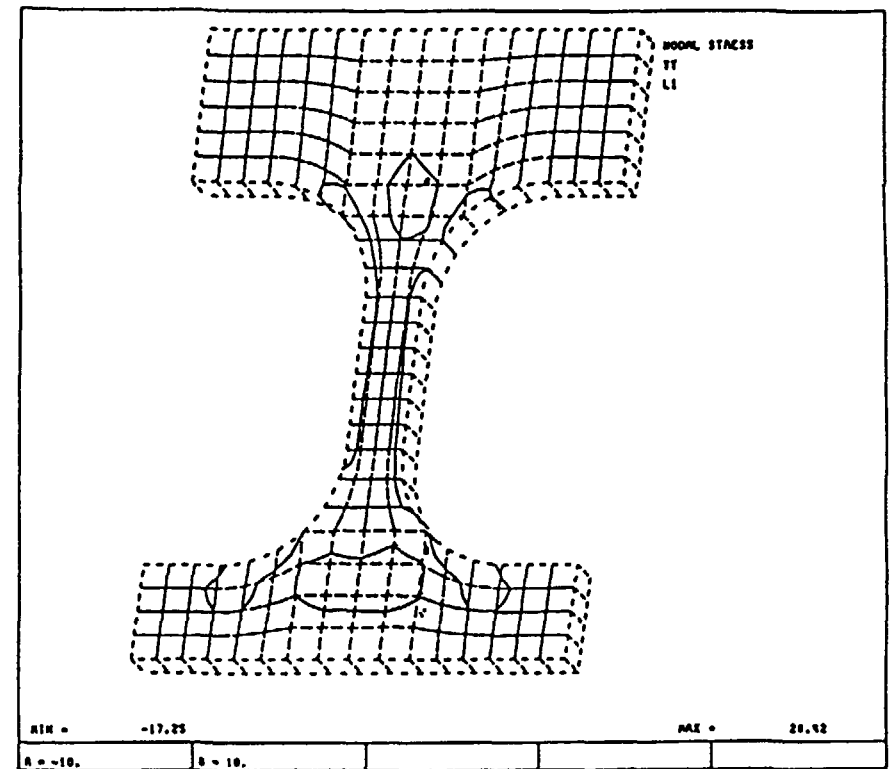


Fig. 12.2 Thermal stresses, y-direction, martensitic

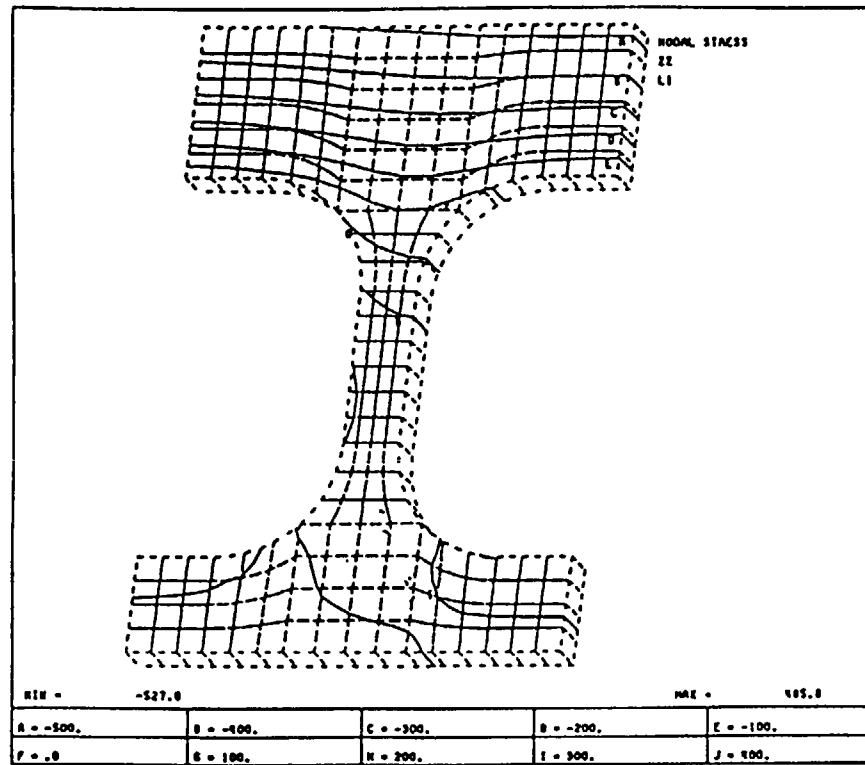


Fig. 11.3 Thermal stresses, z-direction, austenitic

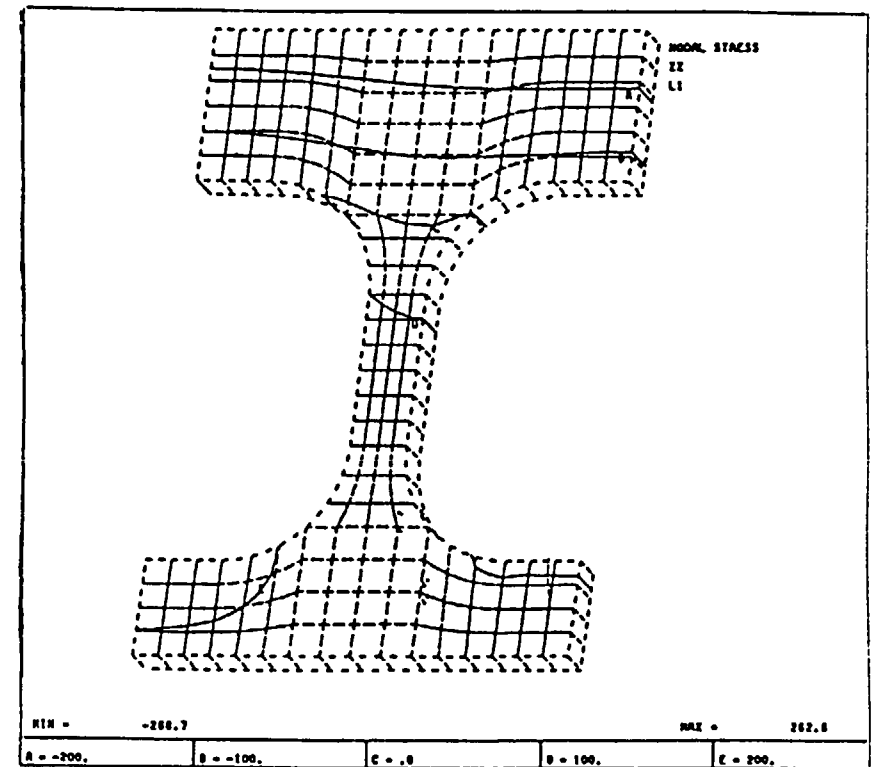


Fig. 12.3 Thermal stresses, z-direction, martensitic

Maximal tensile stresses for austenitic and martensitic steel are:

in x direction	596/321	MPa (at Point F)
in y direction	61/28	MPa
in z direction	486/263	MPa (at Point B)

Maximal compressive stresses are reached at point E (-527/-292 MPa) in x direction.

The first conclusion is, that for martensitic steel the stresses are about 45% less than for austenitic steel. Considering the components it seems to be suitable to neglect in some calculations the stresses in the y-direction as they are about 10% of stresses in the x and z- directions. The highest stresses across the whole first wall appear in the x-direction (axial direction).

The failure behavior of the first wall cracks is considered at points A and B of Fig. 2. The stresses along the lines L_1 , L_2 must be known for the calculations of crack growth. In Figs. 13 - 16 these stresses acting in the x and z- directions are indicated.

3. Stress Intensity Factors

The intention of this report is to demonstrate the general treatment of lifetime predictions under the aspects of fatigue. Therefore, the procedure will be outlined in detail for cracks on the cutting line "A - B" for the austenitic steel in Fig. 17. For this line the results of the FE-calculations can be represented by polynomials.

For $y \leq b_1$ one obtains

$$\begin{aligned}
 T &= 487 - 64.4\xi - 9.1\xi^2 - 35.5\xi^3 + 14.2\xi^4 \\
 \sigma_x &= -481 + 383\xi - 8.3\xi^2 + 261\xi^3 - 123\xi^4 \\
 \sigma_y &< 1 \\
 \sigma_z &= -526 + 311\xi + 311\xi^2 - 262\xi^3 + 147\xi^4
 \end{aligned}
 \tag{1}$$

$$\xi = \frac{y}{b_1}$$

and for $b_2 \leq y \leq b$ it yields

$$\begin{aligned}
 T &\approx 330^\circ\text{C} \\
 \sigma_x &= 544 - 314\kappa + 50.3\kappa^2 \\
 \sigma_y &\leq 30\text{MPa}
 \end{aligned}
 \tag{2}$$

$$\kappa = \frac{y - b_2}{b - b_2}$$

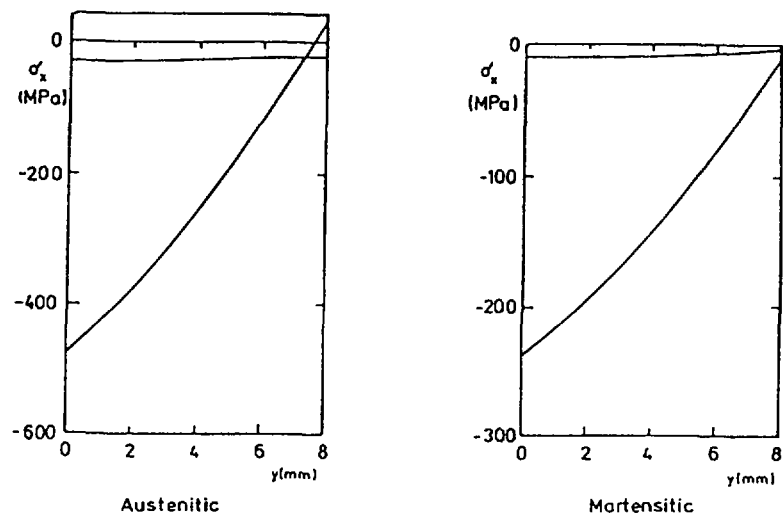


Fig. 13 σ_x along line 1

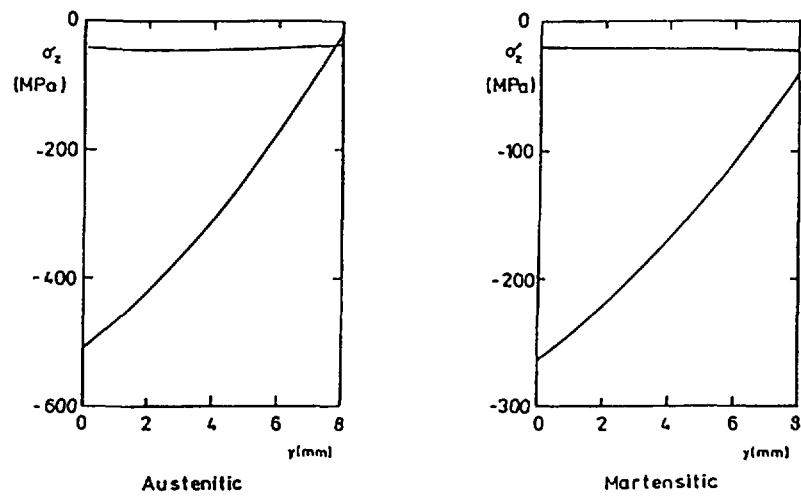


Fig. 14 σ_z along line 1

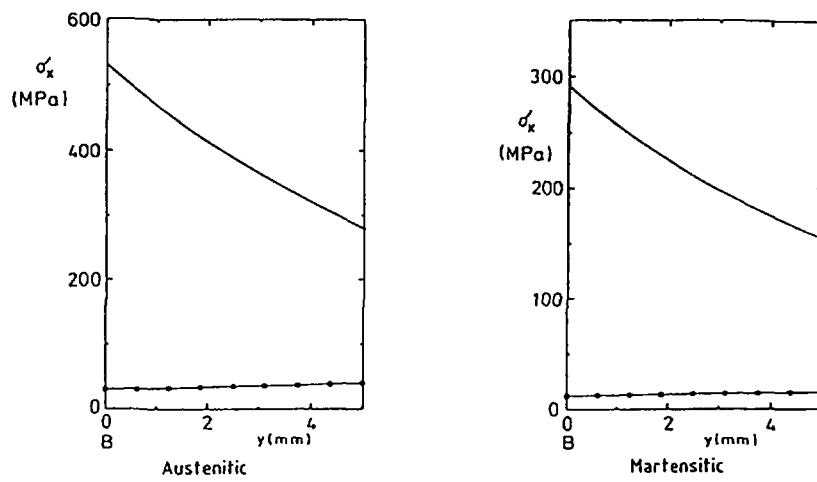


Fig. 15 σ_x along line 2

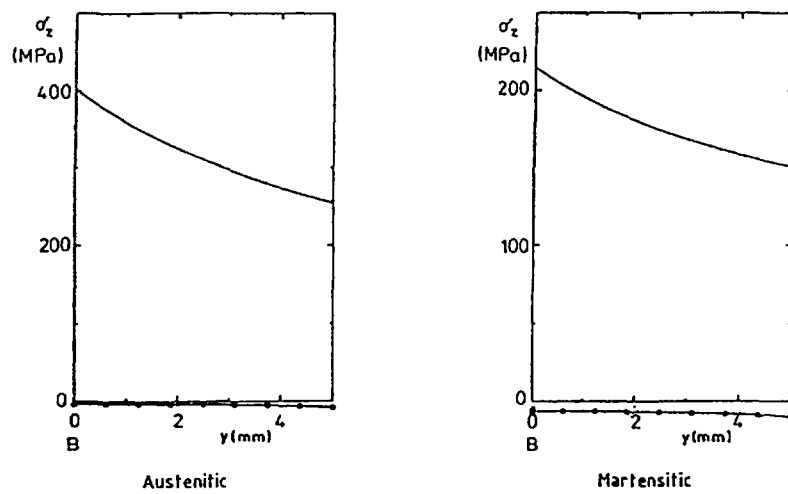


Fig. 16 σ_z along line 2

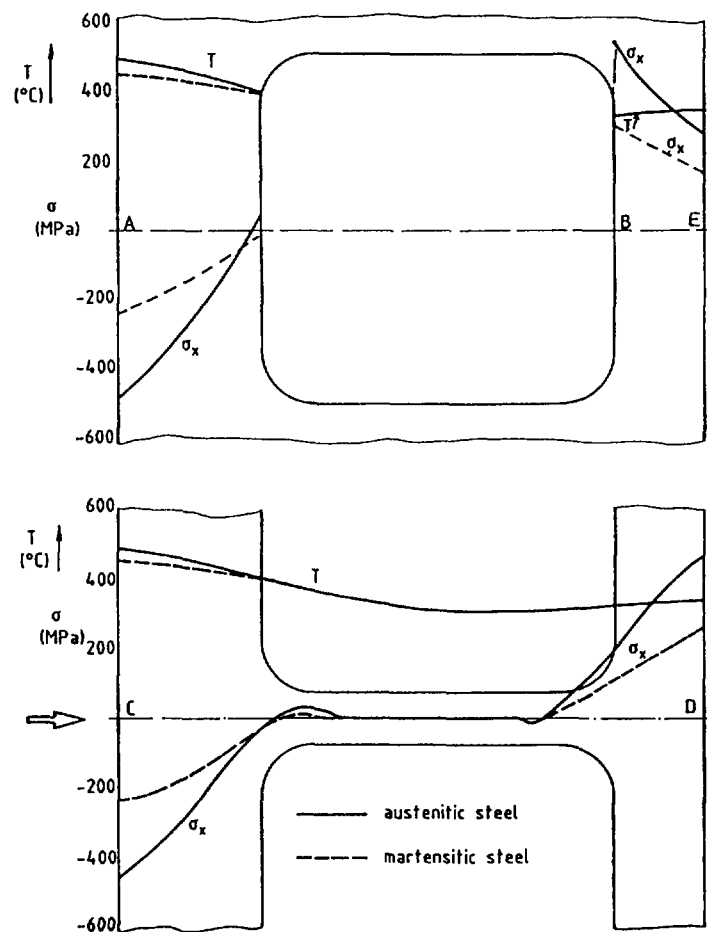


Fig. 17 Temperatures and thermal stresses.

3.1 Time dependent stress development

The initial stresses are influenced by irradiation creep and swelling.

3.1.1 Swelling

The basic effect is the displacement of atoms from their lattice sites, thus producing vacancies and interstitials. Such defects can interact in two ways. Vacancies and interstitials can recombine to annihilate each other, or vacancies can nucleate and grow, producing so-called cavities or "voids". By the latter process the volume of the material will increase. The effect of volume expansion is called "swelling", abbreviated S, and given by

$$S = \Delta V/V \quad (3)$$

Swelling is dependent on the temperature and the irradiation dose ϕt . Void swelling is strongly temperature dependent with maximum values in the range of 500 - 600°C for stainless steel, as can be seen from Fig. 18. The insert

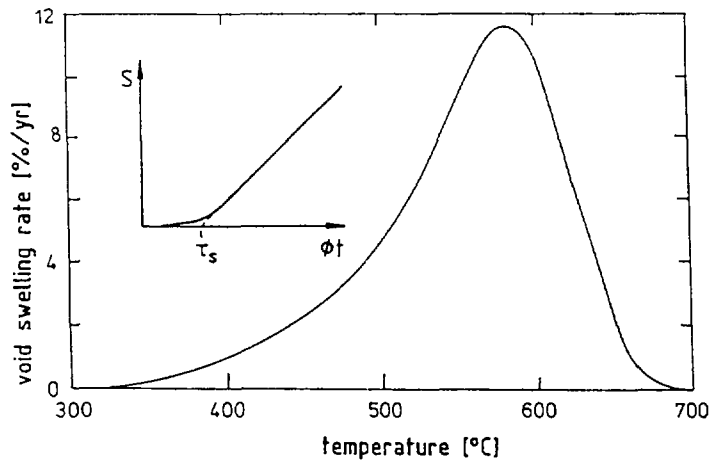


Fig. 18 Void swelling rate for $\phi = 22$ dpa/yr /7/ (Insert: time dependency of swelling, schematical)

in Fig. 18 shows the dose dependency schematically. There is an incubation dose τ_s with an approximately linear dependency. An empirical expression known from fast breeder technology is /7/

$$S(t) = R \left[\phi t + \frac{1}{\alpha} \ln \left(\frac{1 + e^{\alpha(\tau - \phi t)}}{1 + e^{\alpha\tau}} \right) \right] \quad (4)$$

$$R(T) = 0.002 \exp [0.042 + 1.498\beta + 0.122\beta^2 - 0.332\beta^3 - 0.441\beta^4] \quad \text{dpa}^{-1}$$

$$\tau_s = 5 (4.742 - 0.2326\beta + 2.717\beta^2) \quad \text{dpa}$$

$$\alpha = 0.15 \quad \text{dpa}^{-1}$$

$$\beta = (T - 500)/100 \quad T \text{ in } ^\circ\text{C}$$

3.1.2 Irradiation creep

A metal subjected to neutron irradiation and non-hydrostatic stresses shows an effect of inelastic deformation, the so-called "irradiation creep." Neglecting a correlation between irradiation creep and swelling, the creep law can be expressed by a power law

$$\dot{\epsilon}_{ijc} = \frac{3}{2} C \sigma_{\text{eff}}^{n-1} S_{ij} \quad (5)$$

where S_{ij} is the deviatoric and σ_{eff} an effective stress. The deviatoric stresses are

$$\begin{aligned} S_{11} = S_x &= \frac{2}{3} [\sigma_x - \frac{1}{2}(\sigma_y + \sigma_z)] \\ S_{22} = S_y &= \frac{2}{3} [\sigma_y - \frac{1}{2}(\sigma_x + \sigma_z)] \\ S_{33} = S_z &= \frac{2}{3} [\sigma_z - \frac{1}{2}(\sigma_x + \sigma_y)] \end{aligned} \quad (6)$$

and the effective stress is given by

$$\sigma_{\text{eff}} = \left[\frac{2}{3} S_{ij}^2 \right]^{1/2} \quad (7)$$

The creep parameters are

$$n = 1 \quad ; \quad C \approx 1.5 \cdot 10^{-6} \quad \text{MPa}^{-1} \text{dpa}^{-1}$$

for various austenitic stainless steels /8, 9/. In the interesting temperature range of $T < 550^\circ\text{C}$ thermal creep can be neglected.

The total deformation rate of a volume element can be composed by superposition of elastic, creep and swell strains. Under conditions of general plane strain and neglecting the very low stresses in the y-direction, as found in the FE-calculations (Fig. 11.2), one obtains

$$\begin{aligned}\dot{\epsilon}_x &= \frac{1}{E} (\dot{\sigma}_x - \mu \dot{\sigma}_z) + \dot{\epsilon}_{cx} + \frac{1}{3} \dot{S} \neq f(y) \\ \dot{\epsilon}_z &= \frac{1}{E} (\dot{\sigma}_z - \mu \dot{\sigma}_x) + \dot{\epsilon}_{cz} + \frac{1}{3} \dot{S} \neq f(x,y)\end{aligned}\quad (8)$$

As there are no normal forces, one obtains a system of differential equations by integrating the total strain rates $\dot{\epsilon}_x$ and $\dot{\epsilon}_z$ over the height b and the x-y-cross-section.

$$\begin{aligned}\dot{\sigma}_x &= \frac{E}{1-\mu^2} \left[-\dot{\epsilon}_{cx} - \mu \dot{\epsilon}_{cz} - \frac{1+\mu}{3} \dot{S} + \frac{1}{b'} \int_0^b (\dot{\epsilon}_{cx} + \mu \dot{\epsilon}_{cz} + \frac{1+\mu}{3} \dot{S}) dy \right] \\ \dot{\sigma}_z &= \frac{E}{1-\mu^2} \left[-\dot{\epsilon}_{cz} - \mu \dot{\epsilon}_{cx} - \frac{1+\mu}{3} \dot{S} + \frac{1}{F} \int_F (\dot{\epsilon}_{cz} + \mu \dot{\epsilon}_{cx} + \frac{1+\mu}{3} \dot{S}) dx dy \right]\end{aligned}\quad (9)$$

where

$$b' = \begin{cases} b & \text{for cutting line A-B} \\ b+b_1-b_2 & \text{for cutting line C-D} \end{cases}\quad (10)$$

These two differential equations can be solved numerically step by step. To do this a distribution of neutron irradiation has to be assumed. In the present investigation it was assumed that only the surface layer should be affected by neutron radiation and the other parts are totally shaded due to the breeder material in the inner channels (Fig. 1).

The calculations were carried out for the state of constant operation. From Figs. 19 and 20 the complete history of stresses can be understood. Almost immediately after the start of operation the stress state is given by the

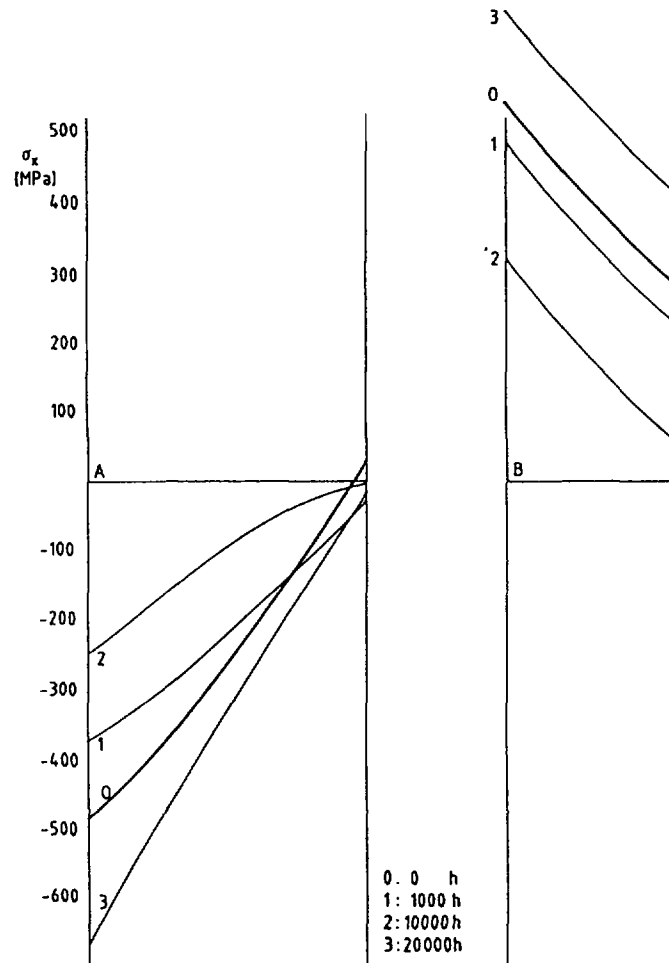


Fig. 19 Time dependent stresses σ_x along symmetry line A - B for different times.

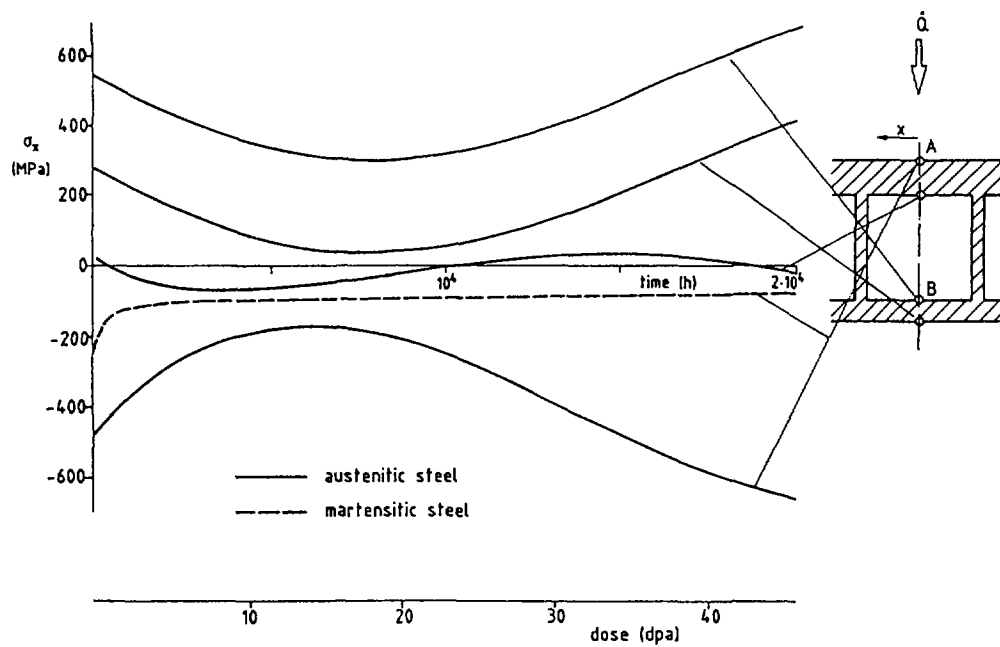


Fig. 20 Stress development for 4 points on cutting line A - B.

thermoelastic stresses because the internal pressure in the channels can be neglected. These stresses relax towards zero due to irradiation creep. After swelling becomes noticeable compressive stresses are generated in high temperature regions and tensile stresses in low temperature regions because swelling at high temperatures is higher than swelling at low temperatures. The compressive stresses near the plasma side become very high because of the completely prevented bending deformations. In a more realistic elastic-plastic analysis all compressive stresses in the outer region of the wall would be reduced due to plastic flow if the effective stress exceeded the temperature dependent yield stress. This effect will be taken into account in a later study.

3.2 Cyclic stresses in the wall

In most fusion reactors the plasma is heated by direct-current, with the plasma acting as a secondary winding of a transformer. The magnetic field varies with constant slope creating a constant current in the plasma. Before the magnetic field reaches saturation, reactor operation has to be interrupted. Consequently, reactor operation becomes cyclic.

As a consequence of these cycles the thermal stresses change periodically. If the burn-off times are long enough, the temperature in the whole wall will become nearly equal to the temperature T_0 of the coolant medium. Due to this temperature changes $\Delta T = T - T_0$ cyclic thermoelastic stresses occur. For shorter interruptions the assumption of complete temperature balance in the wall becomes a worst case assumption with respect to crack growth behavior.

3.3 Calculation of stress intensity factors

Cyclic stresses are responsible for crack growth. In welded structures pre-existing cracks cannot be excluded because defects can only be detected above a minimum size. The fracture mechanical loading quantity characterizing the stress state at the crack tip is the stress-intensity factor K . If a is the depth of a crack and $\sigma(y)$ the stress distribution in the uncracked wall, the stress intensity factor for two-dimensional crack problems is given by the basic equation

$$K(a) = \int_0^a \sigma(y) H(y,a) dy \quad (11)$$

where $H(y,a)$ is the so-called weight function. In this report only continuous cracks (i.e. cracks are as long as the wall) have been taken into account, because they are the most serious ones. Lifetimes calculated with such cracks obviously become conservative. This means that more realistic cracks with the same crack depth, i.e. semi-elliptical cracks, will fail later. In a normalized representation Eq. (11) can be expressed as

$$K = \sqrt{W} \int_0^{\alpha} \sigma(\xi) h(\xi, \alpha) d\xi \quad (12)$$

$$\xi = y/W \quad ; \quad \alpha = a/W \quad W = \text{wall thickness}$$

The weight function of the edge crack given by Bückner /10/ is

$$h(\xi, \alpha) = \sqrt{\frac{2}{\pi\alpha}} \frac{1}{\sqrt{1-\xi/\alpha}} [1 + m_1(1-\xi/\alpha) + m_2(1-\xi/\alpha)^2] \quad (13)$$

$$m_1 = c_0 + c_1 \alpha^2 + c_2 \alpha^6$$

$$m_2 = d_0 + d_1 \alpha^2 + d_2 \alpha^6$$

$$c_0 = 0,6147$$

$$d_0 = 0,2502$$

$$c_1 = 17,1844$$

$$d_1 = 3,2889$$

$$c_2 = 8,7822$$

$$d_2 = 70,0444$$

Equation (13) is valid in the range $0 < \alpha < 0.5$.

To simplify the calculations the stress distributions for each time step were expressed by polynomials of the 4th order using Newton's interpolation formula. The distribution is described by the coefficients a, b, c, d, e in

$$\sigma = a + b\xi + c\xi^2 + d\xi^3 + e\xi^4 \quad (14)$$

Replacing $q = \xi/\alpha$ by

$$\sigma = a + b\alpha q + c\alpha^2 q^2 + d\alpha^3 q^3 + e\alpha^4 q^4$$

one can write the K-factor

$$\tilde{K} = K \frac{\pi}{2\alpha W} = \int_0^1 (a + b\alpha q + c\alpha^2 q^2 + d\alpha^3 q^3 + e\alpha^4 q^4) \frac{1 + m_1(1-q) + m_2(1-q)^2}{\sqrt{1-q}} dq \quad (15)$$

The integration can be made taking into account

$$I_n = \int_0^1 \frac{q^n}{\sqrt{1-q}} dq = \sum_{k=0}^n \frac{2}{2n-2k+1} \binom{n}{k} (-1)^{n-k} \quad (16)$$

The result is

$$K = A(\alpha; a, b, c, d, e) \sqrt{\frac{2\alpha W}{\pi}} \quad (17)$$

$$\begin{aligned} A = & 2aM + \frac{4}{3}(bM\alpha - aN) + \frac{16}{15}(am_2 - bN\alpha + cM\alpha^2) \\ & + \frac{32}{35}(bm_2\alpha - cN\alpha^2 + dM\alpha^3) \\ & + \frac{256}{315}(cm_2\alpha^2 - dN\alpha^3 + eM\alpha^4) \\ & + \frac{512}{693}(dm_2\alpha^3 - eN\alpha^4) + \frac{2048}{3003}m_2e\alpha^4 \end{aligned}$$

with

$$M = 1 + m_1 + m_2 \quad N = m_1 + 2m_2$$

Cyclic operation of a fusion reactor causes cyclic thermal stresses. Due to these stresses a cyclic stress intensity factor ΔK results from Eq. (11). Superposition of K-values during constant operation and ΔK -values due to thermal cycling gives the complete K-behavior.

4. Lifetime

The propagation of cracks in cyclically loaded structures is mainly a consequence of plastic deformations at the crack tip. These deformations and hence the crack growth rate are controlled by ΔK . Other crack growth mechanisms caused by static load in a corrosive environment shall be excluded. For ΔK -controlled crack growth numerous relationships have been developed since

the early 1960's. Taking into account a threshold ΔK_0 below which no crack growth occurs, and an acceleration of crack growth rate near the critical stress intensity factor K_{Ic} , a modified Forman equation proposed by Speidel /11/ seems to be most effectively adopted. It reads

$$\frac{da}{dN} = \frac{C_1 \lambda^m [f \Delta K - \Delta K_0]^n}{K_{Ic} - \lambda f \Delta K} \quad (18)$$

where

$$\lambda = 1/(1-R)$$

and $f = E(T_1)/E(T)$ is a correction factor allowing to model the temperature effect caused by the temperature dependent Young's modulus. T_1 stands for room temperature.

R is given by

$$R = K_{min}/K_{max}$$

The material constants for stainless steels are taken from Watson /7/ for room temperature and air as the environment

$$C_1 = 3.122 \cdot 10^{-9} \quad \text{m/cycle}$$

$$n = 2.95$$

$$K_{Ic} = 150 \text{ MPa} \sqrt{\text{m}}$$

$$m = \begin{cases} 1 - 0.31R - 1.23 R^2 & R > 0 \\ 1.88 & R < 0 \end{cases}$$

$$\Delta K_0 = \begin{cases} 5.4 (1 - 0.9R) & \text{MPa} \sqrt{\text{m}} \quad R > 0 \\ 5.4 (1 - 0.2R) & R < 0 \end{cases}$$

The wall investigated fails when K_{max} reaches the critical stress intensity factor K_{Ic} . On account of irradiation embrittlement this K_{Ic} is not a constant, but decreases with the neutron dose. Our calculations were carried out with an equation quoted in /7/

$$K_{Ic} = 115 \exp(-0.25 \phi t) + 35 \exp(-0.0134 \phi t)$$

Calculated crack growth curves are depicted in Figs. 21 and 22. In Fig. 21 K_{\max} , ΔK and the minimum values

$$K_{\min} = K_{\max} - \Delta K \quad (19)$$

are represented for cracks of the initial size $a_0 = 0.1$ mm at two different locations. For two points on the cutting line A - B the maximum stress intensity factors K_{\max} are plotted versus the time of operation (Fig. 22). Failure occurs when the rapidly increasing parts of the curves crosses the K_{Ic} -curve.

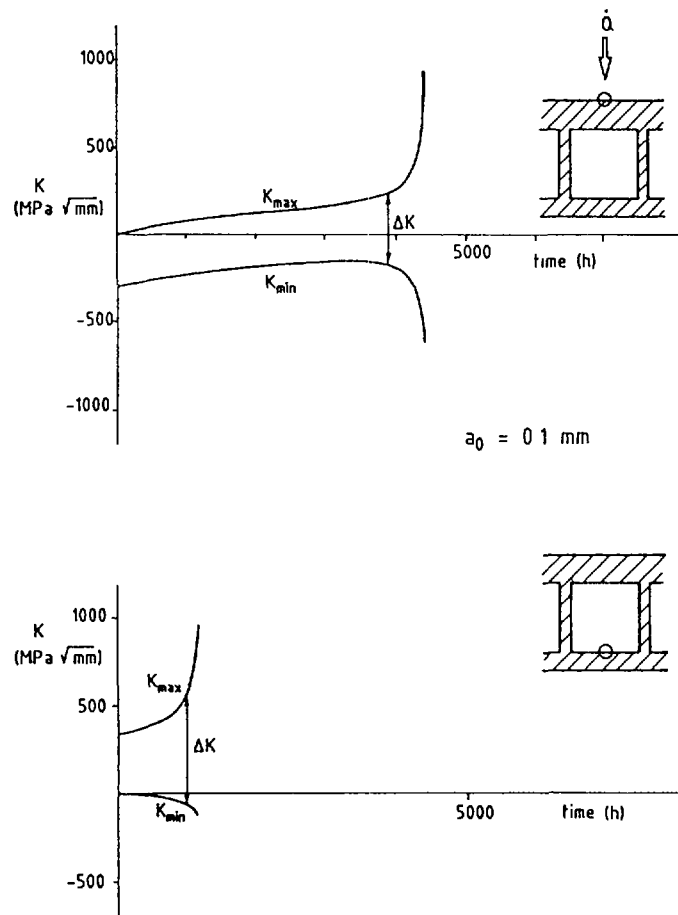


Fig. 21 Stress intensity factors for two cracks of initial crack size $a_0=0.1$ mm.

It can be concluded that cracks in the back side of the first wall give shorter lifetimes compared with cracks of the same size which are situated in the hottest region.

Figure 23 shows the lifetimes for these cracks as a function of their initial size.

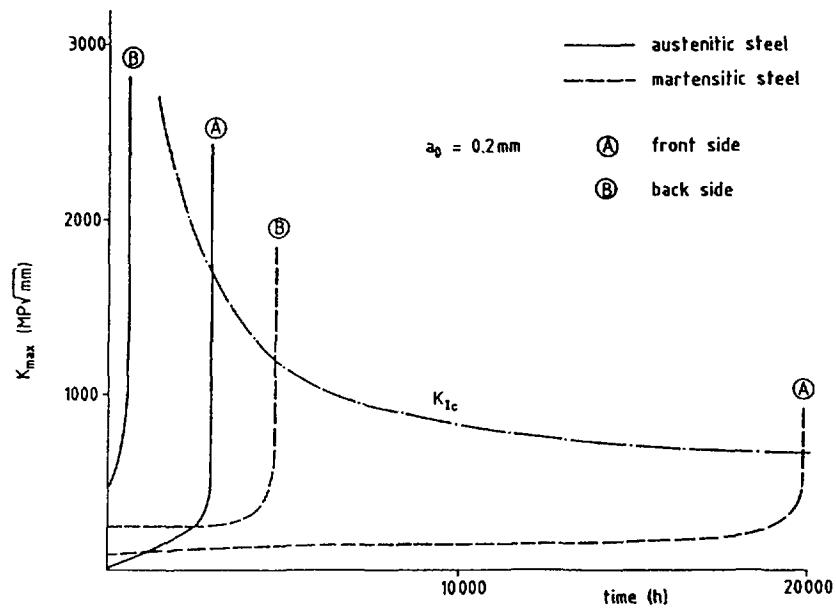


Fig. 22 Crack extension due to cyclic operation for cracks situated in the front and the rear part of the first wall

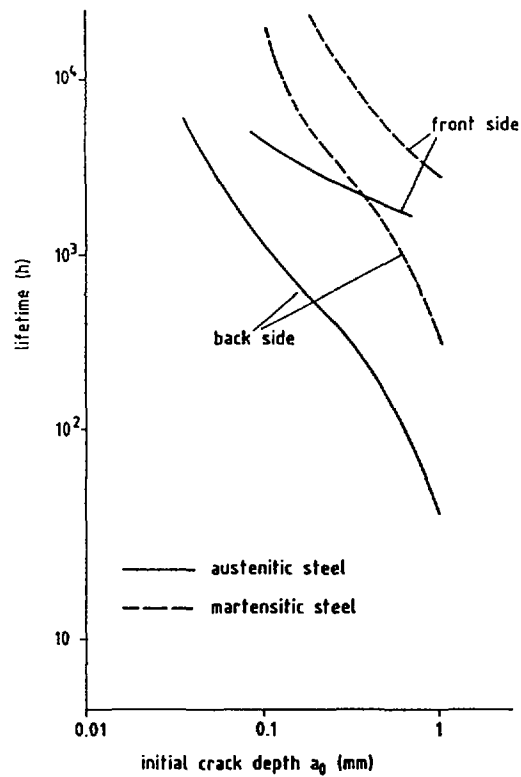


Fig. 23 Lifetime in dependence of initial crack size a_0

5. Comparison between Austenitic and Martensitic Steels

While a lot of data exist for austenitic steel SS 316 only a small data base is available for the second material proposed for NET-first-wall, the martensitic steel 1.4914. Nevertheless, first rough calculations shall be presented. Starting with the temperatures and thermo-elastic stresses obtained by FE-calculations, a treatment similar to that for SS 316 was performed. The following material properties were used.

I. Irradiation creep

In-pile creep tests can be described by /12/

$$\dot{\epsilon}_c = C \sigma^n \exp(-3\text{eV}/kT) \quad [\text{dpa}^{-1}]$$

$$\text{with } n=5 \quad C = 2 \cdot 10^6$$

II. Swelling

Swelling can be neglected. The maximum values found are $\dot{S} < 0.07\%/ \text{dpa}$.

III. Crack growth behavior

Results from fatigue measurements were not available. But from other martensitic steels the crack growth behavior can be estimated. Fig. 24 shows fatigue measurements carried out with various different martensitic steels. In addition, the crack growth rates for SS 316 represented by the modified Forman equation, are plotted as solid line. Due to the good agreement with the results for martensitic steels, we used Eq. (18) for 1.4914 too.

IV. Irradiation embrittlement

The embrittlement due to irradiation seems to be not as important as in case of SS 316. Nevertheless, in a conservative calculation the same decrease of K_{IC} with neutron dose was assumed.

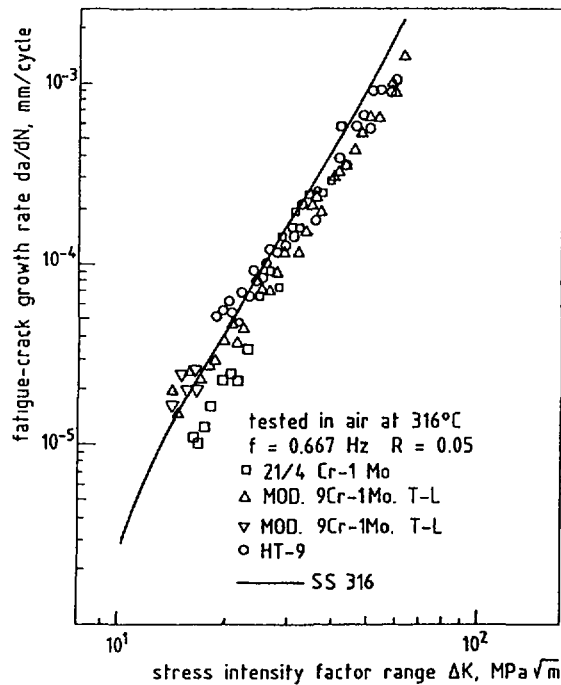


Fig. 24 Crack growth behaviour of some martensitic steels compared with the results for SS 316 [12]

The results obtained for 1.4914 are plotted as dashed lines in Figs. 17, 20, 22 and 23. A comparison shows a distinctly improved lifetime behavior. From the standpoint of fatigue a superiority of martensitic steel has to be stated. This result is due to the lower coefficient of expansion and the higher conductivity.

6. Outlook

In this report preliminary results are presented for a proposed first wall structure. The aim was to show the general procedure for lifetime calculations, to demonstrate the principal behavior of plasma faced structures, to explain the radiation effects and to give a first idea of the expected lifetime. Further refinement of the calculations are necessary, especially:

- improvement of the stress calculations for swelling and irradiation creep (with FE-program ABAQUS);
- improvement of the fracture mechanics model (incorporation of 2 D-cracks);
- inclusion of crack initiation.

In addition, other design proposals have to be considered (first wall with grooves, ceramic tiles).

Finally, it is obvious that better results about the material behavior after radiation damage are urgently needed.

7. Summary

The treatment of lifetime predictions for the first wall of a fusion reactor is outlined in case of an actual NET-design:

- The temperature distribution and elastic stresses due to thermal loading were calculated by FE-methods in generalized plane strain.
- The change of stresses during operation caused by irradiation creep and swelling was considered.
- Cracks of different initial crack size were assumed to exist in the front and in the backward parts of the wall.
- Due to cyclic operation of the reactor, cyclic stresses occur in the whole structure and the cracks can grow.
- Crack extension computations by means of a modified Forman equation allow to predict the time of failure.

It could be stated:

- Crack extension in the backward structure region is much more serious than in the front parts.
- A structure made of martensitic steel (1.4914) shows a distinctly improved lifetime behavior compared with austenitic steel (SS 316).

8. References

- /1/ R.F. Mattas, D.L. Smith, "Model for life-limiting properties of fusion reactor structural materials," Nuclear Technology, 38 (1978), pp. 186-198.
- /2/ W. Daenner, "Results of strategic calculations for optimizing the first wall life in a tokamak fusion reactor," Transact. 6th Intern. Conf. on Struct. Mech. in Reactor Techn., Paris, Aug. 1981, Paper N 4/1.
- /3/ R.W. Watson, R.R. Peterson, W.G. Wolfer, "Lifetime analysis of fusion reactor first wall components," Transactions of the ASME, Journ. of Pressure Vessel Technology, 105 (1983), pp. 144-152.

- /4/ A.O. Adegbulugbe, "Comparison of lifetime calculation for fusion reactor first walls based on two creep-fatigue design criteria," Nuclear Engineering and Design/Fusion 1 (1984) 301-305.
- /5/ T. Fett, A. Müller, D. Munz, H. Stamm, "Stress distribution and fatigue crack growth in pressurized tubes including the effect of swelling and radiation creep", in Fusion Technology 1984, Volume 2, Proceedings of the 13th SOFT 1984, pp. 973-978.
- /6/ T. Fett, D. Munz, "Stress and lifetime calculations for first wall and blanket structural components", Part I: Crack propagation in tubes, KfK 3875, 1985.
- /7/ R.D. Watson, "The impact of inelastic deformation, radiation effects, and fatigue damage on fusion reactor first wall lifetime," Thesis, University of Wisconsin, 1981, UWFD-460.
- /8/ K. Ehrlich, "Irradiation creep and interrelation with swelling in austenitic stainless steels," Journ. of Nucl. Materials 100 (1981) 149-166.
- /9/ W. Schneider, K. Herschbach, K. Ehrlich, "Interdependence of In-pile Creep and Void Swelling in Ti- and Nb-stabilized Stainless Steels," ASTM STP 782 (1982) 30-42.
- /10/ H.F. Bueckner, "Field singularities and related integral expressions," Mechanics of Fracture 1, - Methods of Analysis and Solution of Crack Problems, Nordhoff Int. 1973.
- /11/ M.O. Speidel, "Fatigue crack growth at high temperatures," Proc. of the Symposium on high-temperature materials in gas turbines, Switzerland, 1974, 207-251.
- /12/ K. Ehrlich, private communication.

CREEP LIFETIME OF AUSTENITIC STEELS DETERMINED BY HIGH TEMPERATURE HELIUM EMBRITTLEMENT STUDIES

H. SCHROEDER

Institut für Festkörperforschung,
Kernforschungsanlage Jülich GmbH,
Jülich, Federal Republic of Germany

Abstract

The influence of helium on the creep properties, i.e. lifetime, ductility and strain rate, have been investigated for some austenitic stainless steels with variations of many parameters such as stress, temperature, helium implantation rate, implanted helium concentration, test mode etc. These experiments were accompanied by a) extensive electron microscope studies in order to establish correlations between the creep data and the fracture behaviour (SEM) and the (helium bubble) microstructure (TEM) and b) theoretical modelling in order to interpret the experimental results and "understand" the basic mechanisms of the helium embrittlement. All these efforts resulted in a qualitative map of lifetime controlling mechanisms for creep rupture in austenitic stainless steels.

1. Introduction

The detrimental effect of helium on the mechanical properties of reactor materials has been recognized long time ago and has been studied in the materials programs for fast reactors. Helium effects, in general, /1/ and helium embrittlement, in particular, are of much more interest in the fusion reactor materials research because of the much higher generation rates of helium via (n, α) nuclear reactions in the harder fusion neutron spectrum, compared to a fast reactor environment. For example, the helium to dpa ratio for austenitic stainless steel is about 10-15 appm He/dpa in a fusion reactor which leads to about 155 appm He/MWy/m² in AISI 316SS. The corresponding numbers for a fast reactor (such as EBRII) are 0.2 - 0.3 appm He/dpa and 10 appm He/y.

Because of the lack of an intense, high energy neutron source, it is very time consuming and expensive to simulate expected high

helium levels (up to end-of-life concentrations) with the existing fission reactors. This is different if one simulates the helium generation by homogeneous α -particle implantation at a cyclotron (with rates up to several hundred appm helium per hour). The energy of the α -beam should be large enough to penetrate foils thick enough to perform mechanical tests representing bulk properties.

Such a method has been used to investigate the influence of implanted helium on the creep properties of austenitic steels. The results will be reported in the form of an extended summary because they have already been published in very detail /2-6/ and also been described in a very recent review /7/ and some conference papers /8,9/.

2. Experimental

The creep rupture tests have been performed on 100 μm thick foil tensile specimens in vacuum for post-implantation tests and in ultra-pure helium atmosphere for "in-beam" tests. The creep properties, i.e. creep rate $\dot{\epsilon}$, rupture strain ϵ_R and creep lifetime t_R have been determined for a wide set of parameters such as

- a) test mode: "in-beam" test (i.e. creep rupture test during helium implantation) and post-implantation tests ($T_{\text{impl}} = T_{\text{test}}$)
- b) tensile stress σ : 0-300 MPa
- c) helium implantation rate \dot{c}_{He} : $8 \cdot 10^{-4} - 3 \cdot 10^{-2}$ appm He/s
- d) helium concentration c_{He} : 0-2500 appm He
- e) implantation and test temperature T : 973 K - 1073 K
- f) microstructure: by using different austenitic steels the microstructure was varied: (i) AISI 316 L, solution annealed and aged 24 h at 1073 K; this treatment resulted in a clean, dislocation and precipitation free matrix and only large grain boundary precipitates of the type $M_{23}C_6$. (ii) DIN 1.4970, solution annealed, 13 % cold worked and aged 24 h at 1073 K; this treatment resulted in a fine dispersion of TiC particles ($\varnothing \sim 5$ nm) in the matrix, mostly nucleated at dislocations and somewhat coarser TiC particles and other carbides ($M_{23}C_6$) in the grain boundaries. As the 1.4970 steel is dispersion hardened, it is much stronger than the 316 under same conditions.

After the creep tests many of the specimens have been checked for type of fracture and cracks in the scanning electron microscope (SEM). All the helium containing specimens have been investigated in the transmission electron microscope (TEM) to determine the helium bubble microstructure in different microstructural regions such as matrix, grain boundaries, precipitate interfaces. The bubbles have been characterized by density ρ and average radius \bar{r} .

3. Results

3.A. Creep properties

The main results of the creep rupture test in both austenitic steels are:

(i) All samples containing helium show helium embrittlement, i.e. compared to helium free control specimen they show reduced rupture times, reduced rupture strains, transition from transgranular to intergranular fracture.

(ii) The degree of embrittlement is dependent on all in section 2 mentioned parameters:

a) The most pronounced differences were observed in the different test "modes": For example, the time to rupture, t_R , as a function of stress, σ , was much less stress dependent in "in-beam" experiments than in post-implantation tests: Using a power law $t_R \propto \sigma^{-n}$, "in-beam" test could be described by $n = 3 \dots 4$, while post-implantation tests showed high stress dependence, $n = 8-12$, similar to the helium free controls. The lower stress dependence in the case of "in-beam" tests resulted in increasing reductions of rupture times, t_R , and rupture strains, ϵ_R , with decreasing stress, σ , compared to the post-implantation and the control cases, respectively. However, one should remember that decreasing stress in a "in-beam" test means increasing rupture time, i.e. increasing helium content (at a fixed implantation rate, in most cases $3 \cdot 10^{-2}$ appm He/s) while the post-implantation tests were done at constant helium concentration (100 appm He).

- b) In post-implantation experiments the creep properties were drastically reduced above a critical helium concentration.
- c) In post-implantation tests the helium embrittlement increased with decreasing implantation rate.
- d) The degree of embrittlement was higher in the (clean) AISI 316 than in the (dispersion hardened) DIN 1.4970.

3.B. Helium bubble microstructure

Very detailed investigations on the helium bubble microstructure have been performed for the AISI 316 SS because these studies are much easier to do in such a "single" microstructure compared to the heterogeneous microstructure of the DIN 1.4970 SS. Although the grain boundary bubbles are believed to induce the observed embrittlement and hence are most important also the matrix bubbles have been studied because they may have large influence on the growth properties of the grain boundary bubbles, e.g. if they act as sinks for the diffusing helium atoms, they control the flux of helium atoms into the boundaries. Consequently, the bubble sizes and densities have been determined in all different microstructural regions, namely matrix, grain boundary, coherent and incoherent (grain boundary) precipitate interfaces.

The most important results of the TEM work and correlations of the bubble microstructure to the creep properties are summarized:

- a) Although bubble sizes and densities in the different microstructural regions can be quite different, the dependencies on the test parameter are generally similar, i.e. plotting bubble sizes and densities as a function of any test parameter one gets nearly parallel curves for the different regions. From that one may conclude that in all regions similar nucleation and growth mechanisms of the helium bubbles are working.
- b) After stress free high temperature helium implantation, in general, the bubble sizes are largest in the matrix, followed by grain boundary bubbles in precipitate free regions. The smallest are those at grain boundary precipitate interfaces. The number densities show the opposite sequence.

c) The bubble microstructure after implantation without stress represents the starting microstructure for all post-implantation tests. The following implantation parameters have been changed:

(i) Implantation temperature: increasing temperature results in increasing bubble sizes, but lower densities.

(ii) Implantation rate: decreasing rate results in increasing sizes, but lower densities.

(iii) Implantation time (helium concentration): bubble radii increase with concentration, while bubble densities are independent (or slightly decreasing) on concentration.

The general effect is: The coarser the bubble microstructure (i.e. larger size, lower density) the higher is the detrimental helium effect on the post-implantation creep tests under otherwise identical conditions.

d) For "in-beam" test, i.e. high temperature implantation under stress, the correlations between bubble microstructure and creep properties were less straightforward because of three reasons:

(i) the parameters stress, lifetime and helium concentration are not independent on each other;

(ii) the creep strain and hence the dislocation movement seem to influence the bubble microstructure at least in the primary creep stage, in which the strain rates are quite high in this solution annealed material.

(iii) At fracture the bubble microstructure, especially in the grain boundaries, is very inhomogeneous, because some bubbles underwent catastrophic growth creating cracks and inducing fracture, other bubbles did not. So, the TEM results depend strongly on the additional external parameters such as angle between stress direction and grain boundary normal, shape of the grain boundary such as serrated (stress concentrations !) or straight, etc.

e) Nevertheless some "trends" have been observed:

(i) After fracture the bubble radii are larger at lower stresses, which is not surprising because lower stress involves larger (life-) time at high temperatures and higher

helium concentration. The bubble densities are smaller at lower stresses (as expected from the larger radii), but the variations are quite small. To uncouple influence of stress, test time and helium concentration two additional TEM series have been studied taking "snapshots" during (uncompleted) "in-beam" tests.

(ii) After 1 hour test time, i.e. constant helium concentration, at different stresses (and different strains !): The higher the stress (and strain) the smaller the matrix bubbles and the larger the matrix bubble density. The grain boundary bubbles showed similar trends but less dependence on stress.

(iii) At constant stress after different creep test times (i.e. also different strains and different helium concentration): During the primary creep stage the radii were practically independent on stress while the densities increased monotonically, indicating continuous nucleation. The opposite behaviour was observed in the stress free case (see 3.B.c.(iii)). In the steady state creep regime up to fracture the behaviour changed to that of the stress free case: Increasing radii and decreasing densities with increasing time and helium concentration.

4. Lifetime controlling mechanisms

The lifetime of a creep sample tested at high temperature under helium generating conditions (i.e. in-reactor or "in-beam" thermal creep test) may be divided into several periods which may be characterized in correlation to the nucleation and growth of helium-vacancy clusters or bubbles in grain boundaries. In close connection to the experimental data collection described in the previous sections Trinkaus /9/ has suggested the following time periods: a) Establishment of quasi-stationary point defect concentration; during this incubation time, t_{inc} , no significant helium-point defect clustering will occur; b) helium bubble nucleation time, t_n , during which stable helium-vacancy clusters are created which act as nuclei for the helium bubbles; c) stable gas driven growth period, t_{bubble} ; during this time existing small bubbles grow in a stable manner by collecting the newly generated

or implanted helium; d) cavity growth period, t_{cavity} ; growth due to collection of vacancies in the case of vacancy supersaturation induced by stress and/or irradiation; e) crack growth period, t_{crack} , induced by linking up of cavities. Hence the rupture time, t_R , can be written as a sum of all these periods,

$$t_R = t_{\text{inc}} + t_n + t_{\text{bubble}} + t_{\text{cavity}} + t_{\text{crack}}$$

If one of these periods dominates, it determines the rupture time. This is of course dependent on all the parameters listed in section 2. Trinkaus has pointed out /9/, that under high temperature implantation conditions (i.e. high helium and point defect generation rates) the rupture time is probably dominated by gas driven bubble growth after very short incubation and nucleation periods. Because of the high vacancy supersaturation due to stress and implantation also the cavity and crack growth periods (which takes place after the bubble-to-cavity (void)-transition, depending on critical parameters) should be short. One indication of the gas driven growth mechanism is the stress dependence of the rupture time, $t_R \propto \sigma^{-n}$. The exponent n theoretically is close to 3 for gas driven growth, while the "in-beam" experiments in both austenitic steels yield 3-4. Another indication that the gas driven growth mechanism is working under the given conditions of high temperature implantation (with or without stress) is the verification of a critical parameter for the bubble-void transition, $N\sigma^2$; N is the number of helium bubbles, which also can be transformed into the bubble radius using the appropriate gas law; σ is the tensile stress. In addition the critical bubble radius was determined by TEM and agreed quite well with theoretical predictions /6/.

Trinkaus /9/ has also computed the other times and their dependencies on the external parameters. As the helium generation rate using α -particle implantation is much too high compared with the rates expected in fusion technology or with the operating high flux fission reactors it would be interesting how to extrapolate the simulation data obtained at a cyclotron. Or in other words: Do the mechanisms of helium induced embrittlement change if one changes important parameters such as helium generation rate orders of magnitude?

Trinkauss /9/ developed a mechanism map for helium embrittlement in AISI 316 SS for the parameter set helium generation rate/stress, using the creep rupture data described in this paper. It turned out that a) one has indeed to be careful to extrapolate over orders of magnitude and b) that the gas driven growth mechanism is only one possibility of helium effects on creep properties, which is realized only in a certain section of the multi-parameter space.

References

- /1/ Proceedings of the Int. Symp. on Fundamental Aspects of Helium in Metals, Ed.: H. Ullmaier, Radiation Effects 78 (1983) 1-426.
- /2/ H. Schroeder and P. Batfalsky, J. Nucl. Mater. 103&104 (1981) 839.
- /3/ H. Schroeder and P. Batfalsky, J. Nucl. Mater. 117 (1983) 287.
- /4/ P. Batfalsky and H. Schroeder, Proc. Third Topical Meeting on Fusion Reactor Materials, Albuquerque, USA, Sept. 1983, J. Nucl. Mater. 122&123 (1984) 1475-1480.
- /5/ P. Batfalsky, Thesis, Report KFA Jülich, Jül-1923 (June 1984).
- /6/ H. Schroeder and P. Batfalsky, ASTM STP 870, pp. 745 (1985).
- /7/ H. Schroeder, W. Kesternich and H. Ullmaier, Nuclear Eng. and Des./Fusion 2 (1985) 65-95.
- /8/ H. Ullmaier, J. Nucl. Mat. 133&134 (1985) 100-104.
- /9/ H. Trinkaus, J. Nucl. Mater. 133&134 (1985) 105-112.

THERMAL SHOCK EFFECTS ON TYPE 316L AUSTENITIC STEEL AND VANADIUM BASE ALLOYS

H.Th. KLIPPEL, B. van der SCHAAF,
H. van WITZENBURG
Netherlands Energy Research Foundation, ECN,
Petten, Netherlands

Abstract

Under abnormal conditions magnetically confined plasma can disrupt and hit the first wall. The unshielded structural alloy of the wall will then partially melt, evaporate and show crack initiation and propagation by the imposed high thermal stresses. Depending on the frequency and location of occurrence, the life-time of the first wall will be affected.

The present work gives the results of thermal shock effects on the surface of plate from the 316L European reference heat and V-1Cr-0.1Ti alloy. Thermal shocks were generated by a laser beam with energy pulses of 20 J. Pulse length, frequency and number were varied with energy densities in the range of 2 MJ.m^{-2} to 10 MJ.m^{-2} per pulse, which is the range expected for plasma disruptions. With increasing number of pulses both steel and V increasingly evaporate. Short pulse durations promote evaporation. In and underneath melt layers intergranular cracks develop.

Additionally fatigue specimens of Type 316 were exposed to laser pulses, simulating plasma disruption. Subsequently, fatigue tests have been performed. Strain ranges and frequencies are varied and the effects on cyclic life are discussed.

1. INTRODUCTION

The first generation of TOKAMAK-type fusion reactors will be operated discontinuously. Plasma burn times in the range of 100 to 1000 s are foreseen in the NET-design. Considering the heat loads and the number of plasma burns in its lifetime (about 10^5) the first wall of NET will be subjected to high cycle fatigue loads. Additionally the structural material is exposed to high fluxes of 14 MeV neutrons, resulting for NET in 30 dpa end of life.

It is expected that during its life-time a TOKAMAK-type reactor first wall will suffer from several thousands of plasma disruptions,

Under such abnormal conditions the plasma hits the wall resulting in heat loads in the range from 2 MJ.m^{-2} to 10 MJ.m^{-2} . The unshielded structural alloy of the wall will then partially melt, evaporate and redeposit itself. These phenomena can cause crack initiation from the very high thermal stresses imposed during such abnormal transients. Normal operation with its high cycle fatigue nature will promote propagation of the cracks formed during disruption.

Quataert [1] presented a study of thermal shocks, generated by electron beams, on a wide variety of materials. The study describes the observed mass transport and cracks initiations in detail. Similar work by Brossa [2] demonstrates the beneficial effect of ceramic surface coatings.

The present study describes the use of laser beams for the production of thermal shocks in a vanadium base alloy and the European Reference Heat of Type 316 steel, aimed at assessing disruption effects. The thermal shock effects are described. Further some fatigue properties of shock-affected specimens have been determined. The consequences of plasma disruptions for life-time predictions are discussed.

2. PROCEDURE

2.1. Material and specimens

The austenitic stainless steel Type 316 used for this study is the European Reference Heat. The tensile, fatigue and creep properties have been reported by Van der Schaaf [3]. For the primary study of laser energy deposition on the steel blocks of $9 \times 20 \times 90 \text{ mm}$ were used. One surface of $20 \times 90 \text{ mm}$ has been ground before exposure to laser flashes.

An hourglass shaped low cycle fatigue specimen, with a minimum diameter of 8.8 mm , was used for elevated temperature testing under strain control, Fig. 1.

The specimens were exposed to laser flashes prior to fatigue testing.

From the vanadium base alloy, V-1Cr-0.1Ti, plates of $3 \times 12 \times 100 \text{ mm}$ were exposed to laser light in the primary study. The surface was in the cold-rolled condition. Additionally lead, aluminium and copper have been used to study the laser energy deposition/reflection ratio. These materials were pure: the impurity contents are below $0.5 \text{ wt.}\%$.

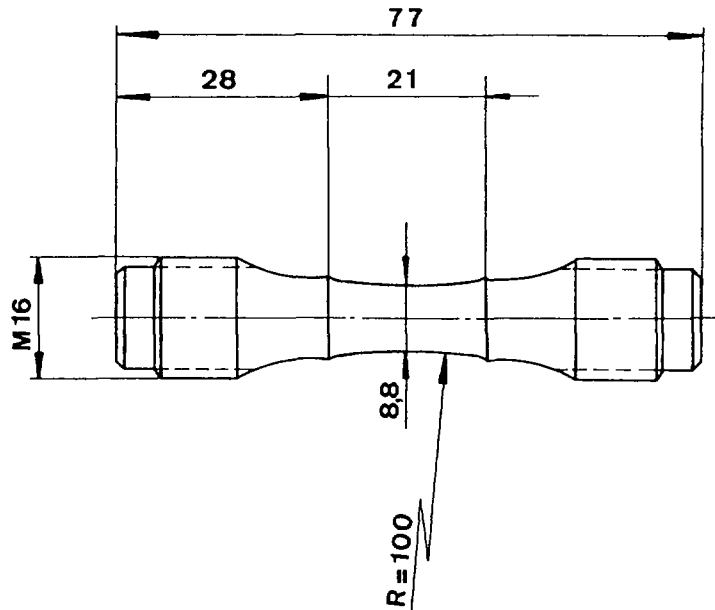


Fig. 1. Low cycle fatigue specimen.

2.2. Laser beam facility

A Nd-YAG solid laser was applied for the generation of thermal shocks, with multimode, unpolarized light rays of $1.06 \mu\text{m}$ wavelength. The pulse form is approximately rectangular; the pulse length can be chosen in the range from 0.2 to 20 ms; the maximum pulse energy is 70 J. The pulse performance amounts to about 20 J in order to keep a reasonable lamp life.

Laser parameters and object table are both under CNC-control and so is the focus distance. The objects to be thermally shocked are positioned in an inert gas stream: flow from $1.5\text{--}2.5 \text{ l.min}^{-1}$. Cylindrical specimens are rotated under the laser beam in an independent fixture to assure the right location for the laser flash.

2.3. Fatigue testing

All fatigue testing was performed in a servo-mechanical machine which allows a maximum frequency of 2 Hz. The hourglass specimens were subjected to strain controlled low cycle fatigue at a temperature of 700 K. The total strain range was in the interval from 0.4 to 1.0%. The failure criterion in this investigation is the reduction of the cyclic tensile stress to half that of the saturation stress. The frequency of the 700 K tests was in the range from 0.02 Hz to 0.05 Hz (strain rate 10^{-3} s^{-1}). The R-ratio amounts to -1: fully push-pull.

3. RESULTS

3.1. Energy deposition efficiency

The energy produced in the focus area of the laser beam is known to an accuracy of about 10%. It is difficult to measure the amount of energy reflected by the illuminated surface, it highly depends on the surface conditions.

From comparisons of metallography and two-dimensional calculations we estimate the absorbed energy for stainless steel and vanadium alloy being about 40% of the incident beam energy. The optical metallography comprised sections perpendicular to the melt layer to measure the profile of the layer boundary. The diameters of the melt layers were determined with scanning electron microscopy. Details of this analysis will be given in a forthcoming paper.

The accurate determination of the laser beam efficiency and also the determination of the energy distribution across the affected area, necessary for the direct comparison with plasma disruption heat fluxes, will require more experimental work.

The diameter of the laser beam affected area is in the range from 1 to 2 mm depending on material and beam conditions. The range of beam and power parameters allows variation from no effect up to the production of holes, even in vanadium base alloys, after 100 laser pulses by metal evaporation. The reproducibility of laser flash damage in stainless steel is good when alignment of lamp lenses and object tables are under close control. The argon flow is necessary to avoid oxidation of the illuminated material but this flow also cools the surface. All materials have been subjected to the same gas flow of 1.4 l/min., but the effects might be different because of the difference in heat conductivity of the objects.

3.2. Energy deposition variation effects

The investigations have been limited to two pulse lengths: 2 and 20 ms. Four sets of pulse numbers have been applied 1, 10, 100 and 1000. The focus location was varied in steps of 5 mm in the range from 0 to 15 mm. Only pulses of 20 J were used.

The following tendencies have been observed for both vanadium and type 316 austenitic steel.

- With a pulse length of 2 ms after 100 and 1000 pulses holes were

observed in steel at least 4 mm in depth. Even after ten pulses penetration was observed down to 0.5 mm.

- With a pulse length of 20 ms the drilling phenomenon was observed after 100 and 1000 shots in steel, but to limited depth. In vanadium limited melting occurs after 100 pulses, after 1 and 10 pulses no melting has been observed. Austenitic steel shows melt layers after 1, 10 and 100 pulses with thicknesses in the range from 0-400 μm depending on the focus condition. With increasing focus distance the thickness of the melt layer decreases.
- After 1 or 10 pulses, out-of-focus, only evaporation was observed in stainless steel, while vanadium is unaffected.

Figure 2 shows a scanning electron micrograph of Type 316 steel subjected to 10 pulses of 20 J (20 ms duration) in focussed beam condition. The cracks caused by the solidification are clearly visible.

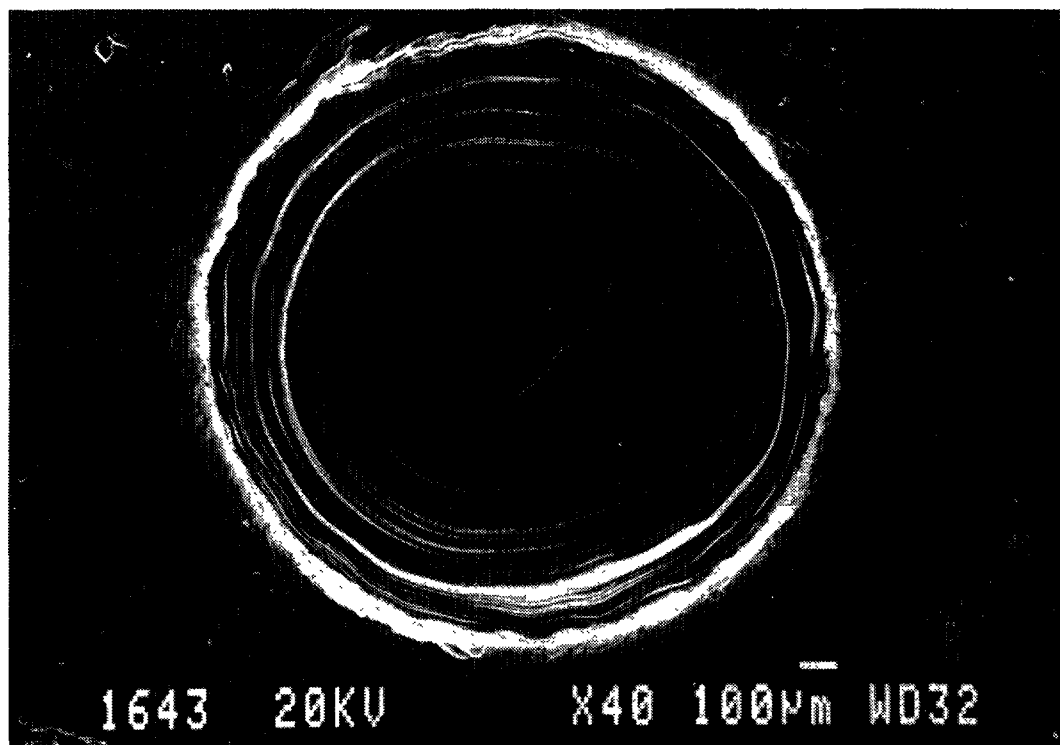


Fig. 2. Scanning electron micrograph of austenitic steel after 10 pulses of 20 J in focussed laser beam condition.

In Fig. 3 a metallographic section (in two magnifications) is shown of a melt layer in austenitic steel. The crack in the melt layer does not extend into the base metal. However, from the higher magnification it is clear that the grain boundaries are affected by the thermal shocks. In vanadium, Fig. 4, cracks cannot be observed in the

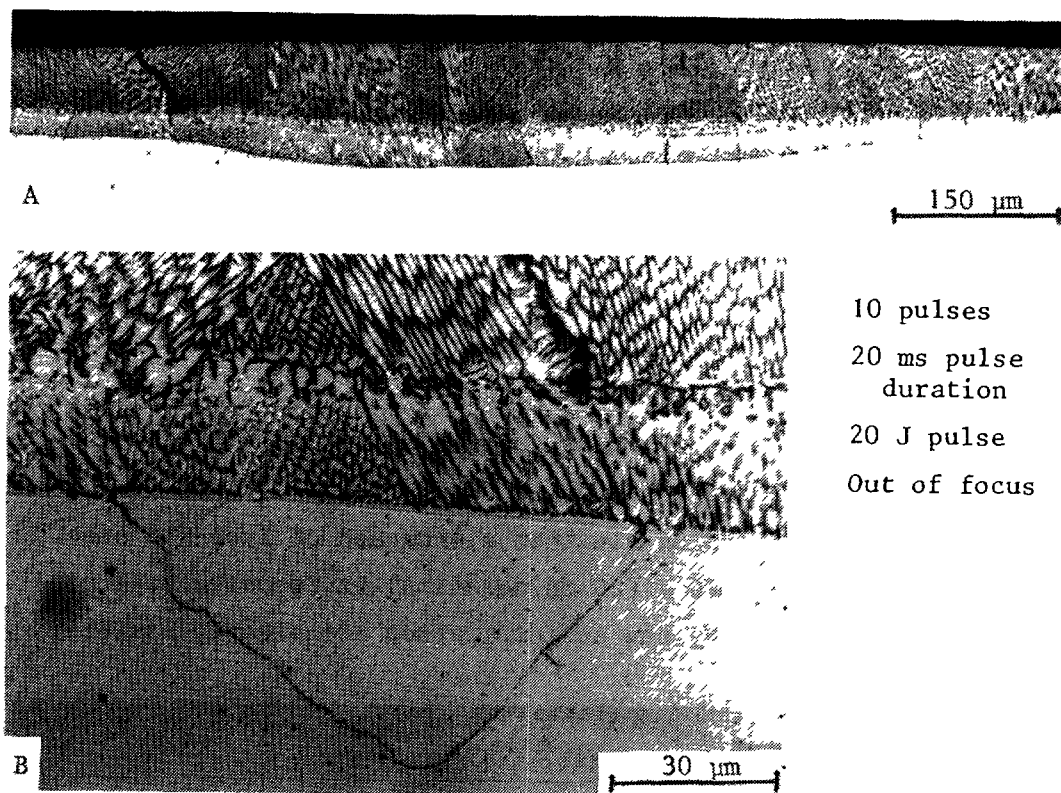


Fig. 3A. Metallographic section of a laser beam induced melt layer including an interdendritic crack in stainless steel.

Fig. 3B. Magnification of the fusion zone: the boundary between melt layer and base metal. The grain boundary is heat-affected.

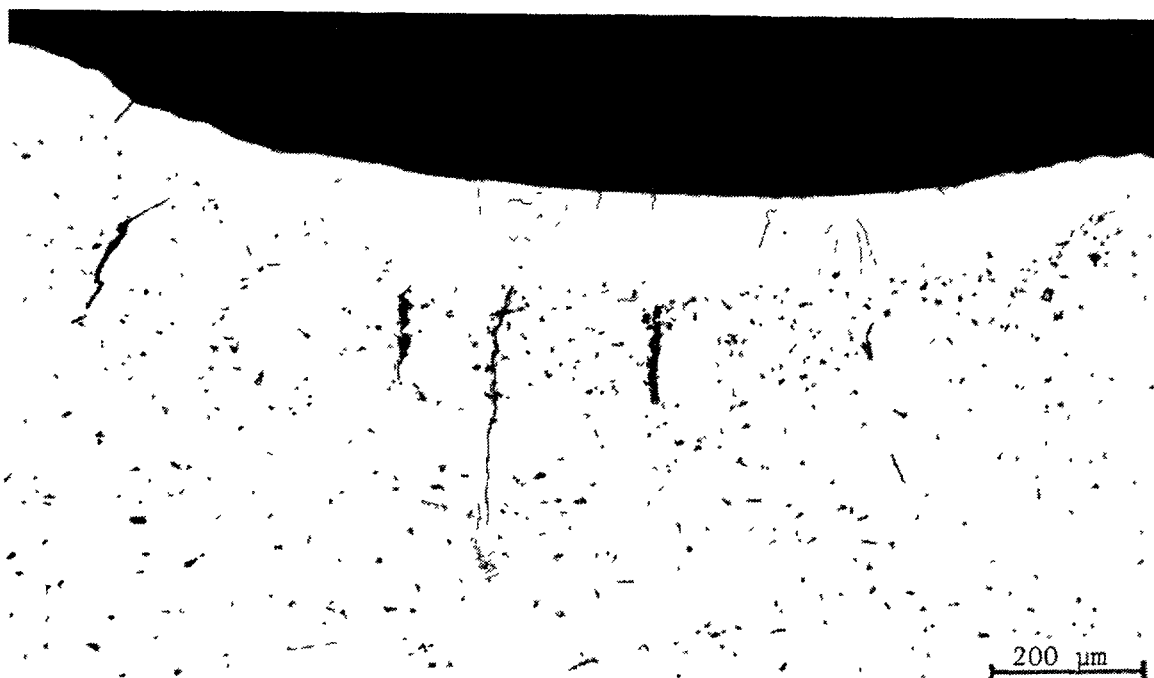


Fig. 4. Metallographic section of vanadium with a laser beam induced melt layer and associated microcracks: 100 pulses, 2 ms pulse duration, in focus.

melt layer, but have formed solely in the heat-affected zone under severe illumination condition: 100 pulses, 2 ms pulse duration.

3.3. Fatigue properties of thermally shocked 316 L austenitic steel

A limited number of low cycle fatigue specimens shown in Fig. 1 have been exposed to two laser beam conditions: 5 mm and 10 mm out of focus respectively (pulse length: 20 ms, pulse energy 20 J, number of pulses: 10). At the thinnest section 6 such spots with 60° difference in rotation were produced. Each individual spot has a diameter of about 1.2 mm. The melt layers have a thickness of 200 μm and 100 μm respectively, representing absorbed energy densities of 4 MJ.m^{-2} and 2.5 MJ.m^{-2} respectively [4]. In the first case cracks are observed in the melt layer, but grain boundaries in a metallographic section are decorated.

The specimens were subjected to low cycle fatigue at 700 K with total strain ranges of 0.4%, 0.6% and 1.0%, with a strain rate of 10^{-3} s^{-1} (triangular wave form $R = -1$). In Fig. 5 the number of cycles measured for thermal shocked steel can be compared with fatigue properties of virgin material under identical test conditions.

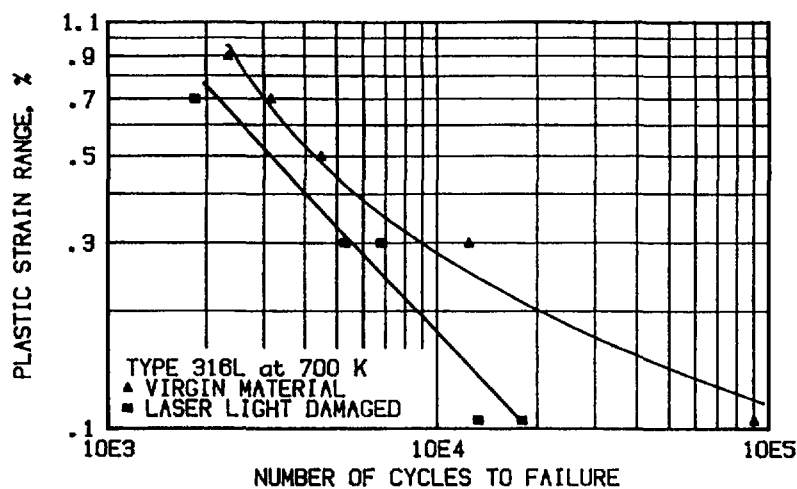


Fig. 5. The total strain range versus the number of cycles to failure of thermally shocked and virgin Type 316 austenitic steel.

It can be concluded that with decreasing total strain amplitude the effect of melt layers on fatigue endurance increases. With decreasing total strain amplitude the high cycle fatigue mechanism grows in importance. The crack initiation phase becomes fatigue life controlling. The presence of cracks in melt layers or weakened grain bounda-

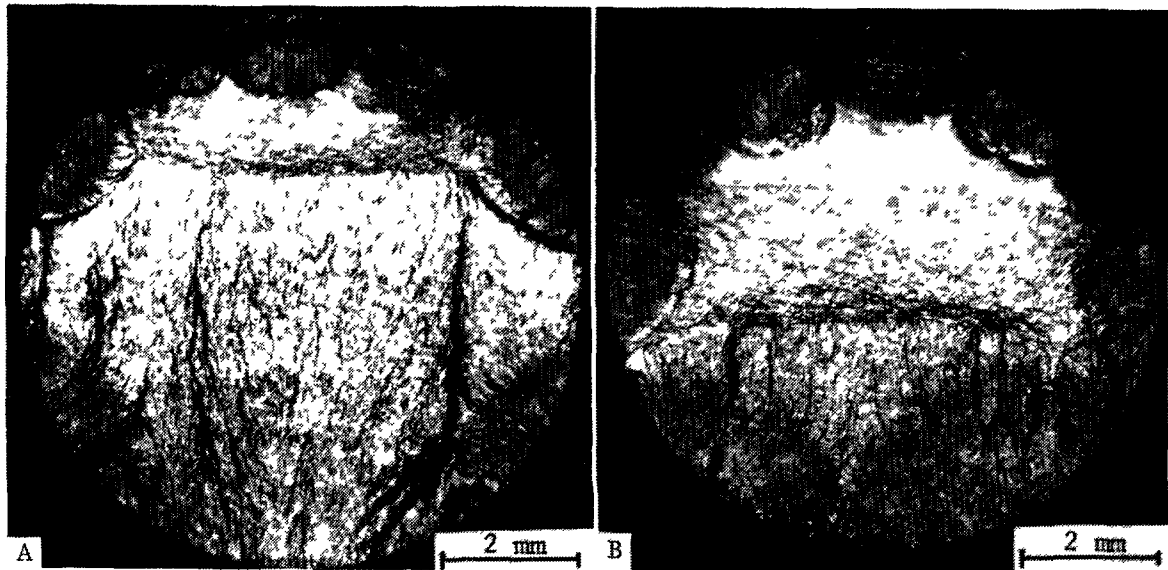


Fig. 6A. Fractography of a fatigue crack initiated from only one melt layer in stainless steel.

Fig. 6B. Fractography of a fatigue crack with multiple initiation melt layers.

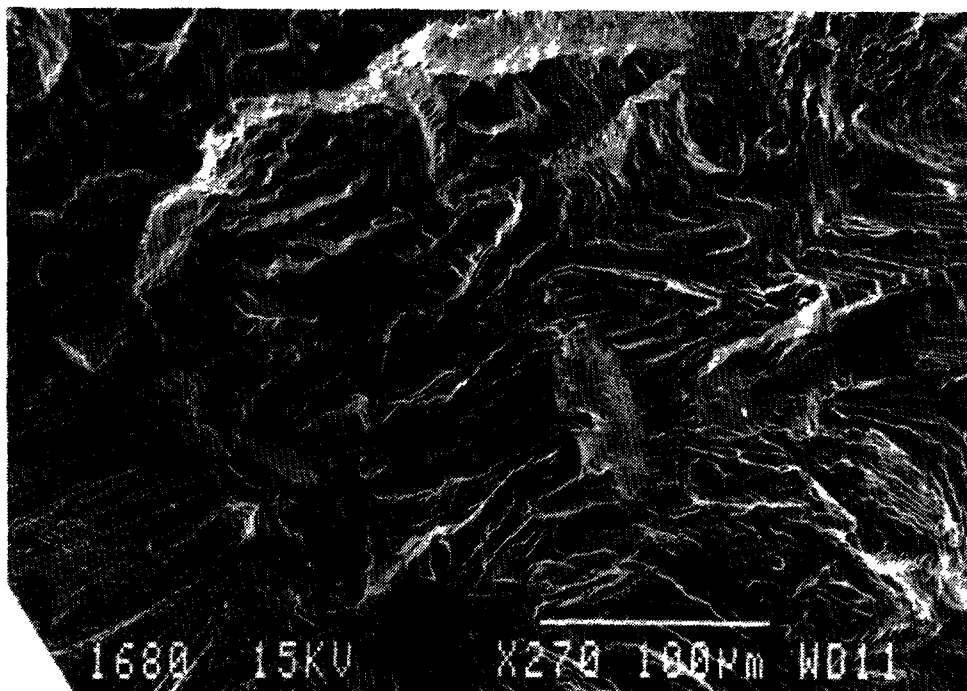


Fig. 7. Detail of an initiating melt layer with intergranular cracks in the heat-affected zone of stainless steel.

ries in the heat-affected zone reduces the duration of the initiation phase considerably. This is evident from fractography of the fatigue specimens. In Fig. 6A the main fatigue crack originates from one spot. In Fig. 6B two initiation spots contribute to the main fatigue crack growth. The importance of the weakness of grain boundaries for fatigue crack initiation is shown in Fig. 7 en Fig. 8. Figure 7 shows intergranular failure in the parent metal underneath the interdendritic failure of the melt layer. In Fig. 8 a detail of the fusion zone, the melt layer-base metal boundary, shows clearly the intergranular failure in the heat-affected zone.

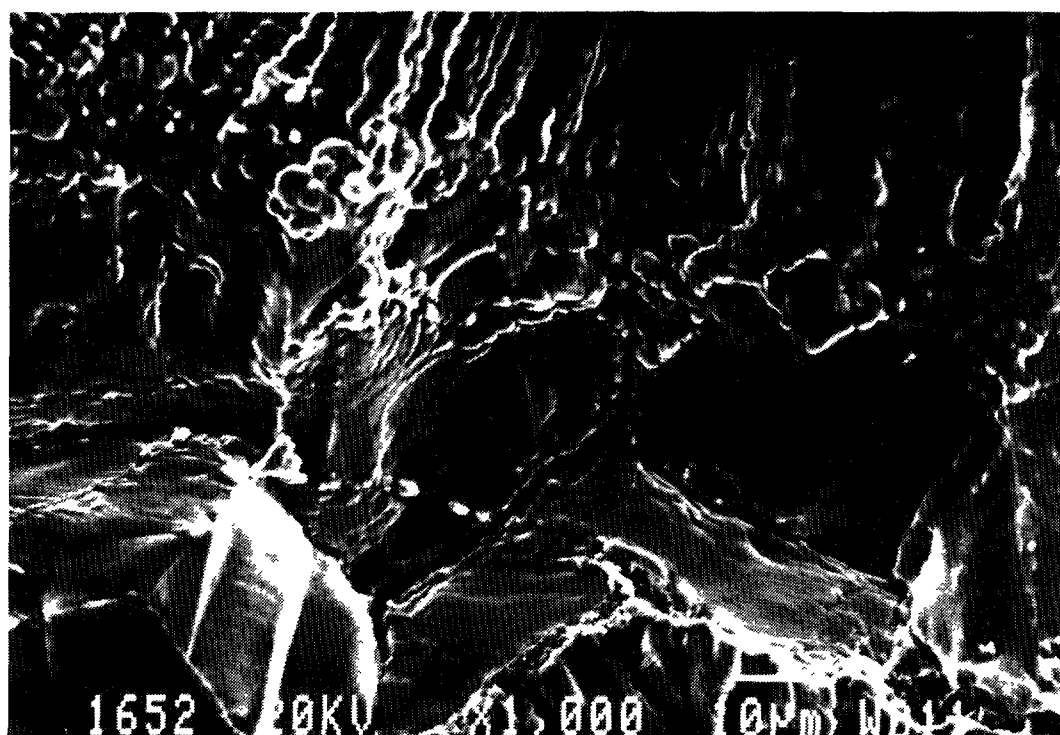


Fig. 8. Fractography of the fusion zone between a melt layer and the intergranularly fractured heat-affected zone underneath.

4. DISCUSSION

4.1. Laser beams for plasma disruption simulations

In principle laser beam facilities are suitable for simulating plasma disruption. Pulse duration, energy flux and number of pulses can be performed in a sufficiently wide range of parameters. Improvement of efficiency determination is required in the near future (reflection and heat transport by shield gas and metal vapour are to be measured

independently). Also the energy distribution in the illuminated surface should be obtained in detail.

Our present results concerning melt layers and cracks on Type 316 austenitic steel are very similar to those reported by Quataert, who used an electron beam welder for simulation. The efficiency and distribution measurements of electron beam energy fluxes into the exposed material also poses some problems.

4.2. Differences between Type 316 steel and vanadium

Melt layers and cracks develop in vanadium after more intense pulses than in austenitic stainless steel. Otherwise there is only a gradual difference between the two alloys. Assuming an equal efficiency of the laser beam for steel and vanadium leads to the conclusion that vanadium starts suffering from disruption under NET first wall conditions after at least 10 times as many disruptions as for steel.

The starter cracks in the vanadium originate from the same area as in steel: in the heat-affected zone underneath the melt layer. This is in accordance with results from creep fatigue testing Type 304 austenitic steel weldments [5].

4.3. Plasma disruptions and first wall life-time prediction

The experimental results of Quataert [1], calculations by Klippel [4] and the present experimental results indicate that first walls need a coating to reduce peak heat loads. The high heat fluxes cause evaporation and melting of the structural alloy, but even more threatening to the life of the first wall is the formation of cracks in the heat-affected zone which form in both vanadium and steel. Since the initiation phase is fatigue life controlling under first wall conditions, these cracks under melt layers have a large influence (factors of 10) on the life-time.

Most future effort on reducing disruption effects should be devoted to coatings on first walls. The coating should not only prevent melting, but in the case of austenitic steel, it should also limit the intergranular structural damage. In this way intergranular fracture under low cycle fatigue conditions should be suppressed. On the other hand it is necessary to measure crack growth rates of the particular alloys in order to assess the resistance against growth of small cracks eventually developing under coatings.

For the use of experimental data of disruption simulations, a more accurate figure is required for both laser and electron beam efficiency. The uncertainties at present are too high for life time evaluations.

5. CONCLUSION

Laser beam welding equipment provides parameter ranges quite suitable for disruption simulation work. The differences between Type 316 and vanadium alloys are only quantitative. Both suffer from cracks under melt layers, but vanadium shows this after a factor of 10 more thermal shocks. The reduction in low cycle fatigue life of thermally shocked Type 316 austenitic steel is considerable. For the low strain amplitudes, where initiation controls fatigue life, the reduction in number of cycles to failure can be ten or more.

Future experimental work should be aimed at the creation of ceramic layers, which shall prevent both melting and crack formation in heat-affected zones. Nevertheless study of crack growth properties is required to determine the threshold stress intensity values.

6. REFERENCES

- [1] Quataert, D., Brossa, F., Moretto, P., Rigon, G.,
Electron Beam Disruption Simulation of First Wall Material,
Proc. of the 13th Symposium on Fusion Technology, Varese,
September 1984, for CEC by Pergamon Press, Vol. 1, pp 401-408.
- [2] Brossa, F., Ferro, C., Franconi, E.,
Characterization of TiC coatings on AISI 316 stainless steel
limiters, *ibid*, Vol. II, pp 1267-1273.
- [3] Schaaf, B. van der,
Mechanical Properties of the European 316L Reference Heat for
NET First Wall and Blanket Materials R&D, *ibid*, Vol. II,
pp 1045-1052.
- [4] Klippel, H.Th.,
The thermal response of the first wall of a fusion reactor blanket to plasma disruptions, Report ECN-137, Netherlands Energy Research Foundation, ECN, Petten, September 1983.

- [5] Schaaf, B. van der, Vries, M.I. de, Elen, J.D.,
The Effect of Irradiation on Creep, Fatigue and their Interaction of DIN 1.4948 (Type 304) Stainless Steel Plate and Welded Joints at 823 K,
Proc. of Int. Conf. on Eng. Aspects of Creep, Sheffield, Sept. 1980, Inst. of Mech. Eng., London, pp 147-153.

AN OVERVIEW OF THE PIREX PROGRAM

S.L. GREEN, W.V. GREEN, D. GAVILLET,
F. HEGEDUS, P. MARMY, U. STIEFEL,
M.P. VICTORIA
Swiss Federal Reactor Institute,
Würenlingen, Switzerland

Abstract

Materials in the first wall and blanket structure of a fusion reactor are likely to experience a highly destructive environment combining radiation damage, high temperature and cyclic stressing. A new facility is under installation that will combine the equivalent conditions. Its use will allow the microstructural and mechanical effects to be evaluated.

1 INTRODUCTION

Plasma burning with periodic refueling in fusion reactors will produce temperature and thermal stress cycling. The cyclic stress in the first wall structural material is likely to be reversing in the tension-compression sense. The stress in divertor plates of tungsten bonded to copper, on the other hand, is likely to be more complex: tension-tension in the low thermal expansion tungsten and compression-compression in the copper. The response of metals to such mechanical loading is inevitable: either low cycle fatigue (LCF) crack growth or cyclic creep crack growth will terminate in component failure. It is necessary to know if the service life that is desired is longer or shorter than the LCF or creep rupture life, whichever is shorter.

These two processes are quite different, however: LCF involves the propagation of transgranular cracks driven by the stress intensity. Little direct thermal assistance is involved in the deformation processes at the tip of the growing crack. Each cycle of stress advances the crack. In contrast, thermal creep involves the time dependent growth of intercrystalline cracks driven by sustained stressing that is thermally assisted. A deformation map could be determined experimentally: it would define regions in the stress, temperature and hold time space where LCF or creep dominate. It would be used as a design aid in life time prediction.

Radiation damage will occur at the same time as the competing deformation processes, and interact with them. The radiation damage by the fusion reactor neutron spectra will include production of high energy displacement cascades, hydrogen, helium and metallic impurity production. Lattice defect mobility will lead to helium bubble formation, bubble and void swelling, phase separation, and radiation

hardening through dislocation loop formation and radiation produced "alloying".

Theory alone can not hope to predict whether failure would be dominated by fatigue processes, creep processes, or by warpage and distortion due to gradients in neutron flux. Experiments combining radiation damage, elevated temperature and stress cycling must guide lifetime prediction model development.

One installation designed to combine the relevant environmental conditions is the PIREX II facility at the Swiss Institute for Nuclear Research (SIN) proton accelerator. Its use will allow simultaneous irradiation and cyclic stressing at controlled elevated temperatures of metals or alloys of importance to fusion reactor first walls and divertors. In addition to in-situ testing, post irradiation mechanical testing will allow the evaluation of brittle ductile transition temperature increases which will be important to machine maintenance and service.

2 CALCULATIONS

Calculations of the radiation damage effects produced by 600 MeV protons have already been reported (1), for many materials. The collision of a 600 MeV proton with a target atom is calculated using the intranuclear cascade-evaporation model. The collision time is so short that the incident proton does not interact with the nucleus as a whole, but with the individual protons and neutrons in the nucleus. These collisions usually lead to one or more energetic particles escaping the nucleus. The nucleus is left in a highly excited state and enters the evaporation phase, where neutrons and light nuclei are emitted. These processes are calculated using high energy nuclear transport codes which use the Monte Carlo technique.

The energy of the residual nucleus is partly dissipated as heat and partly by high energy collisions with atoms in the host lattice. These are the source of atomic displacement cascades similar to those that would be induced by the neutron flux in the first wall, divertor, and blanket structure of a fusion reactor. The LSS theory is used to calculate the damage efficiency and the resulting damage energy for each nucleus produced in the previous calculations. These values are then combined with the production cross sections to produce the damage energy cross section for the target material. A modified Kinchin-Pease model can then be used to relate the displacements per atom site (dpa) to the proton fluence.

This spallation process is the source of He and H gas and metallic impurities that would be produced via nonelastic reactions in the fusion spectra. Spallation reactions induced by 600 MeV protons are

produced homogenously in bulk material as the range is long and the energy loss rate of 600 MeV protons is so low. TABLE 1 shows the characteristics of 600 MeV proton irradiation to materials to be irradiated in the PIREX II program.

TABLE 1: MEDIUM ENERGY PROTON
IRRADIATION CHARACTERISTICS

MATERIAL	W	AL	CU	1.4914 CR STEEL
AVERAGE DAMAGE (KEV)	660	110	323	284
DAMAGE ENERGY CROSS SECTION (B-KEV)	1530	52	337	272
DAMAGE RATE* (X 10 ⁻⁵ DPA/SEC)	1.7	.31	1.12	.68
HELIUM / DPA	80	143	29	45
600 MEV PROTON RANGE (M)	.145	.72	.25	.27
POWER DENSITY (W/G)	560	817	711	755

*AT 4 μ A/MM²

TABLE 2: CALCULATED IMPURITY PRODUCTION
IN IRON BY 600 MEV PROTONS
(APPM / DPA)

IMPURITY	AS PRODUCED	AFTER DECAY OF SHORT LIVED ISOTOPES	SOLUBLE IN IRON ?
MN	70	60	YES
CR	45	55	YES
V	30	30	YES
TI	25	28	YES
CO	2.5	1.4	YES
SC	16	10	? BEHAVES AS RARE EARTH
S	7	7	FORMS FeS *
P	5	4	YES *
CL	7	6	SHOULD FORM IRON CHLORIDE
AR	12	12	MAY FORM BUBBLES
HE	40-170	40-170	FORMS BUBBLES
H	840	840	DIFFUSES OUT OF BULK

* MAXIMUM ALLOWABLE IN CR STEELS - 600 APPM

The results of the Monte Carlo calculations are also used to predict the activity level in the targets during and after irradiation using an isotope generation and depletion code. Table 2 shows the spallation impurities that will be produced in Fe by 600 MeV proton irradiation, and those remaining after the radioactive decay of the short lives species.

3 PIREX I

A prototype facility, PIREX I, has been operated by the Swiss Federal Reactor Institute, EIR, at SIN since early 1980; a series of publications (2-12) resulted. The proton beam of the SIN accelerator was used to irradiate thin Al targets. These parasitic irradiations were restricted to thin Al as the samples spread the beam and there was no provision for remote handling, which would be required for most other materials. The microstructural studies concluded that a dominate feature was a distribution of pressurized He bubbles, that were uniformly distributed throughout the microstructure, but were often larger and or more numerous on the grain boundaries and along dislocations. Bubble strengthening, and grain boundary embrittlement were expected.

Tensile testing of a series of proton irradiated samples was recently completed (13) which showed that there was an increment of radiation hardening that was actually greater than hardening produced by the bubbles. The dominant increment of hardening was proportional to the fluence or dose. The bubble density was established early in the irradiations and the average bubble size only grew slowly with increasing dose. The hardening effect of the impurities produced by the spallation reactions was simulated by making alloys containing the same elements as those produced by the irradiation. The solid solution hardening was measured and found to be much less than the dominant hardening increment. It is believed that irradiation produced impurities must interact with displacement cascades as they are produced. The resulting hardening effect would be proportional to the fluence in the way observed. These results demonstrate the need for experimental mechanical test data on material irradiated to a damage state equivalent to that of fusion reactor components.

4 DOSIMETRY

The production cross sections for Na-22, Na-24, and Be-7 have been established (14,15) for Al irradiated with 600 and 800 MeV protons. An irradiation of a set of seven materials of interest in the PIREX program is in progress at the present time. Each material has a companion Al foil for proton dosimetry. This bombardment is in the LAMPF proton accelerator in the USA where the spatial gradient of proton flux is so small that the flux can be considered constant

across the diameter of the dosimetry discs. Subsequent radiochemical evaluations of the resulting decay schemes for the various materials will allow us to choose reactions that are convenient for dosimetry from the standpoints of half life and gamma energy.

As in earlier work in the PIREX I program, gamma scan counting through a collimator can be used to map the induced activities as a function of position. The stage translates, in steps, the irradiated sample across the collimator during the counting and thereby maps the intensity of the activation. The proton fluence is mapped.

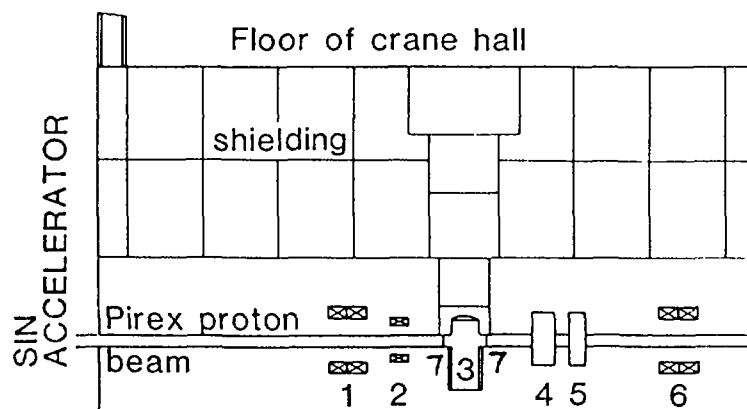
Helium analysis is also used where the helium is measured with a mass spectrograph when a sample of the irradiated material is melted. The irradiation in progress at LAMPF includes samples for helium analysis so that cross sections determined by experiment can be compared to the cross sections derived from the HETC calculation.

5 PIREX II

The PIREX II proton irradiation facility is being installed in its own dedicated beam line of the SIN accelerator, Fig. 1. It incorporates beam optics to control the position, size, shape, and therefore the current density of the proton beam bombarding the sample or target under irradiation. Profile monitors are used to measure the position and size of the beam during an irradiation. A beam stop immediately behind the target station allows the beam spreading to be tolerated

Figure 1: PIREX II Beam line

1. Focusing magnet
2. Steering magnet
3. Irradiation head
4. Degradar
5. Collimator
6. Focusing magnet
7. Profile monitor



without interfering with other experiments. Local shielding, and provision for remote handling will allow safe handling of irradiated materials, Fig. 2.

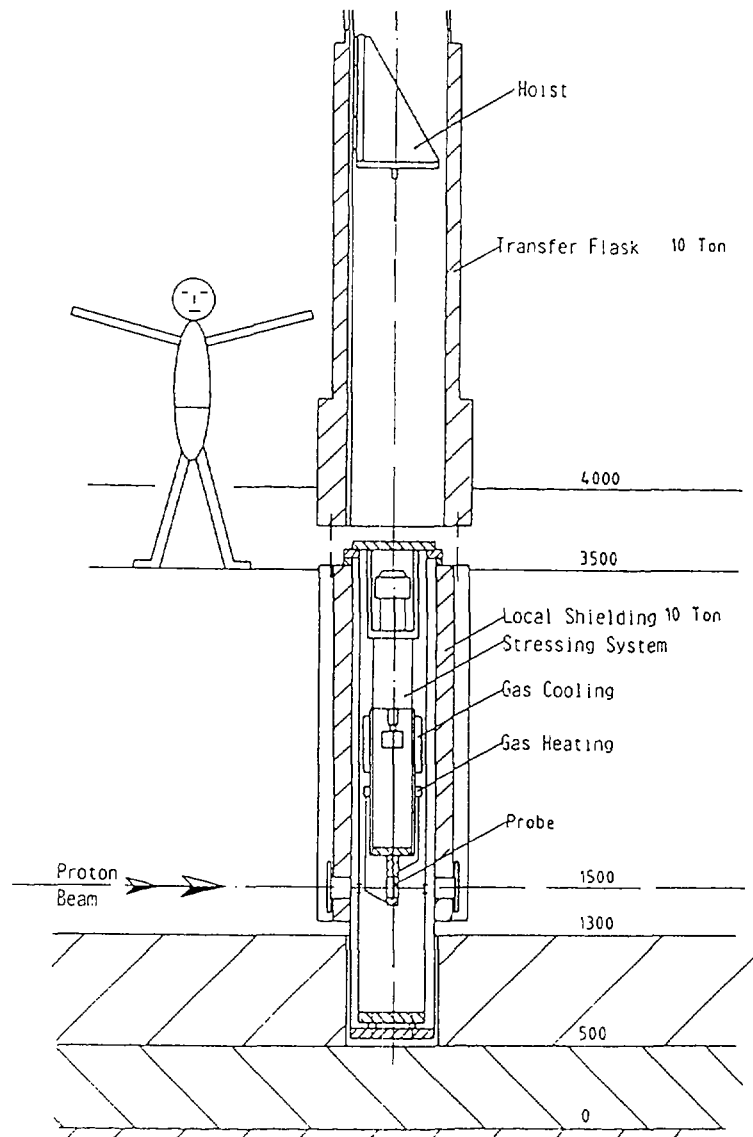


Figure 2: Irradiation head exchange system.

The temperature of the material under irradiation can be controlled between 110 C and 500 C using the system described below. The stress acting on the material under irradiation can be controlled using an electromechanical loading system, and the deformation determined by a measuring system based on linear variable differential system (LVDT), Fig. 3.

5.1 Temperature Control

He gas, at a controlled temperature, will flow over the sample in the beam and extract the heating effect of the beam, Fig. 4. The energy lost by 600 MeV protons in He gas is insignificant. The temperature

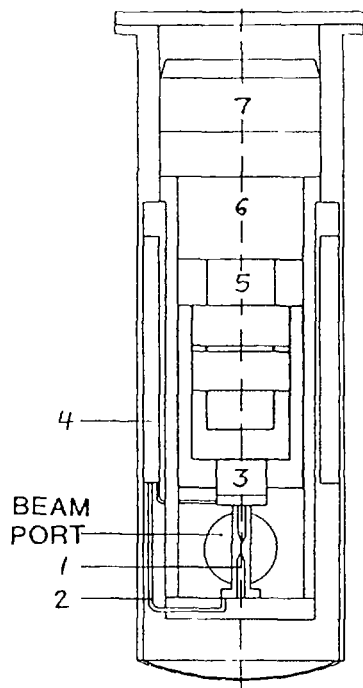


Figure 3: Irradiation head components

1. Sample with cooling tube
2. Helium manifold
3. Load cell
4. Heat exchanger
5. Screw
6. Gear box
7. Low inertia motor

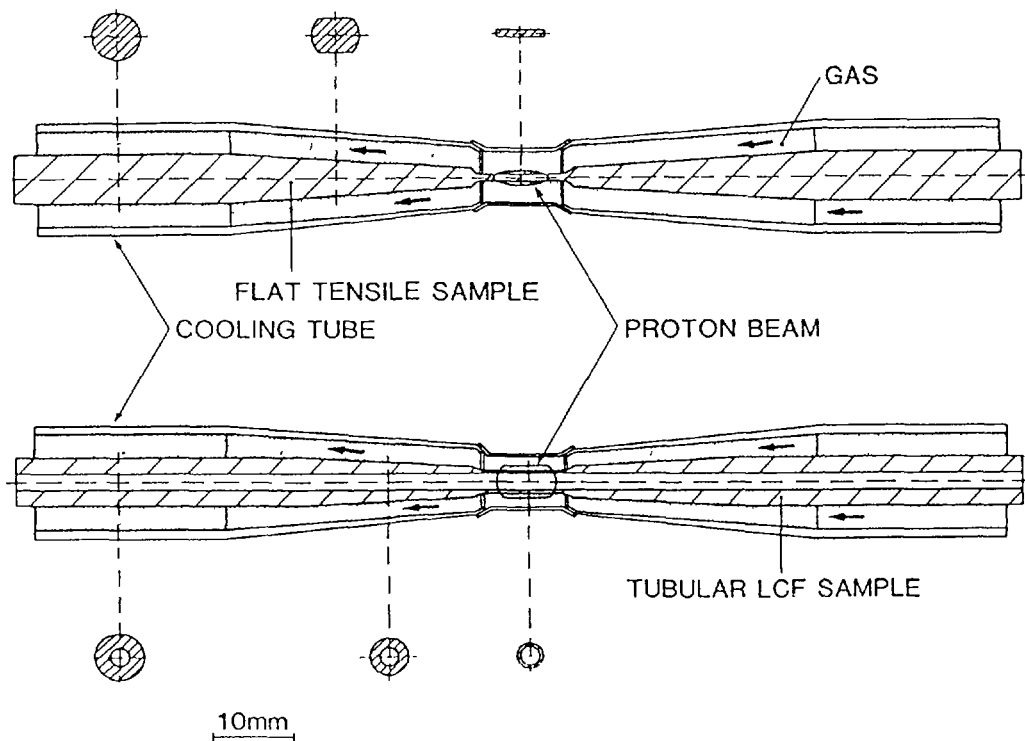


Figure 4: The sample, He cooling gas, cooling tube arrangement.

of the flowing gas will be regulated with an electrical heater of 9 kW and a counterflow heat recuperator of 29 kW that cools the gas that exits the target structure. The heat input to the sample by the beam depends on the target material and dimensions, and the current, but will always be less than 100 W.

The mass flow rate of He gas is controllable between 5 and 15 g per s; the gas pressure is controllable between 11 and 51 bars. The gas velocity will be 80 m per s, or less. Problems with turbulent flow would develop if the gas velocity exceeded about 1/10 the sonic velocity, i.e., about 110 m per s. The gas temperature will only rise a few degrees as it extracts the heat deposited in the target structure. The temperature of the gas will stabilize in about 1/2 h. The system is capable of extracting approximately 150 W per cm², and controlling the irradiation temperature to any desired value between 150 and 550 C.

Simulation experiments are used to model the target and He gas temperature conditions, using electron beam heating to simulate the proton beam heating, and flowing air or He to provide the cooling. Temperatures are measured by thermocouples in the simulation experiment.

The He gas system incorporates the largest gas purifier commercially available. At full flow, only one third of the circulating He gas can be processed, but at lower flow rates, all the gas can undergo continuous purification. The impurities remaining in the gas at the exit of the purifier will be 1 ppm by volume for each of the significant impurities. The impurities will build up in the He gas over a several hour period.

5.2 Target Structure

The proton target includes the cooling tube and the sample. The sample is either a flat strip tensile specimen or a hollow, thin walled tube LCF test sample cooled on its outside. The thickness of the wall of the LCF sample can be 0.5 mm for a 1.4914 Cr steel sample, or 0.25 mm for a W or W-Re sample.

The cooling tube is heated by the beam around only part of its circumference. This will produce a temperature gradient and therefore a thermal stress gradient. The pressurized gas inside the tube is not balanced by an equal outside pressure, so hoop stresses will be present. The combined stress will be a function of the wall thickness and will be a minimum when the wall is 0.07 mm thick. The stress in Inconel X-750 will be slightly less than 1/2 of its yield stress at the irradiation temperature.

5.3 In-Situ Stressing

An electromechanical drive from a compact commercial LCF testing machine has been modified to fit the irradiation head structure in a location where it is partially shielded. Any length change will be detected by the LVDT devices, with alumina rods acting to transfer the relative displacement to the LVDT core. An in-situ mechanical

test can be conducted during the irradiation, or the sample can undergo irradiation at temperature and with an applied constant or cyclic stress for post irradiation testing or examination.

If in-situ stressing is not involved in a particular irradiation, up to three samples can be irradiated simultaneously under controlled conditions of dose and temperature. These would be used for post irradiation testing or examination.

5.4 Sample Handling

The PIREX is being installed in its own experimental hall with a floor area of 31 by 20 m. The shielding is being stacked to a height of 7 m, which is adequate to reduce the radiation field to an acceptable level with a beam current of 20 μ A. A 20 ton crane is available for moving the shielding, irradiation plug and other experimental facilities. All the information and controls are located in a separate, air conditioned measuring room.

After the completion of an irradiation, the irradiation head is raised into a transfer cask of 10 ton for transfer to the hot cell facilities of EIR. The cell facility includes electrospark cutting and electrolytic preparation for TEM and mechanical testing with a commercial LFC testing machine.

6 PIREX PROGRAM

The materials to be studied include 1.4914 Cr steel, W and W-Re alloys, and Cu. These materials are candidates in the NET design study of EURATOM. The PIREX irradiations are allotted 150 days of beam time per year, with a beam current of 20 μ A. The irradiation doses will be up to 10 dpa and 1000 appm of He gas.

ACKNOWLEDGEMENT

The authors express their appreciation for the support provided by EURATOM and the Swiss government and the encouragement from R. Brogli and the EIR Direction. Many others, too numerous to list, have contributed to the design and development of the new PIREX facility.

REFERENCES

1. S.L.Green, J. Nucl. Mater. 126 (1984) 30.
2. W.V.Green, S.L.Green, B.N.Singh and T Leffers, J. Nucl. Mater. 104 (1981) 1221.

3. B.N.Singh, T.Leffers, W.V.Green and S.L.Green, Scripta Met. 15 (1981) 1355.
4. B.N.Singh, T.Leffers, W.V.Green and S.L.Green, J. Nucl. Mater. 105 (1982) 1.
5. M.Victoria, W.V.Green, B.N.Singh, T.Leffers, J. Nucl. Mater. 122-123 (1984) 737.
6. B.N.Singh, T.Leffers, W.V.Green, and M. Victoria, J. Nucl. Mater. 122-123 (1984) 703.
7. B.N.Singh, T.Leffers, W.V.Green and M.Victoria, J. Nucl. Mater. 125 (1984) 287.
8. D. Gavillet, J.L.Martin, M. Victoria and W.V.Green, Ann. Chim Fr. 9 (1984) 275.
9. D.Gavillet, R.Gotthardt, J.L.Martin, S.L.Green, W.V.Green and M. Victoria, Effects of Radiation on Materials: Twelfth Conf. ASTM (1984).
10. J,K,Kjems, B.N.Singh, B.Sjoberg, M.Victoria, and S.L.Green, Microstructural Characterization of Materials by Non-Microscopic Techniques, Riso National Laboratory, Roskilde, Denmark (1984).
11. K.O. Jensen, B.N.Singh, M. Eldrup, M. Victoria and W.V.Green, Microstructural Characterization of Materials by Non-Microscopic Techniques, Riso National Laboratory, Roskilde, Denmark (1984).
12. W.V.Green, M.P.Victoria, and S.L.Green, J. Nucl. Mater. 133 and 134 (1985) 58.
13. D. Gavillet, W.V.Green, M.Victoria and J.L.Martin, presented at the Second Int. Workshop on The Relationship Between Mechanical Properties and Microstructure under Fusion Irradiation Conditions, Ebeltort, Dk. To be published in Workshop issue of Radia. Effects.
14. H.R.Heydegger, A.L.Turkevich, A.Van Ginneken and P.H.Walpole, Phys.Rev. c 14, 1506 (1976).
15. A. Grutter, Int. Jnl. Appl. Radiat. Isot. 33,725 (1982).

Session 2

STRESS ANALYSIS AND LIFETIME EVALUATION

HIGH TEMPERATURE THERMAL CREEP OF MATERIALS UNDER NON-STATIONARY STRESS AND/OR TEMPERATURE LOADING CONDITIONS*

M. BOČEK, M. HOFFMANN**

Institut für Material- und Festkörperforschung,
Kernforschungszentrum Karlsruhe,
Karlsruhe, Federal Republic of Germany

Abstract

The object of this paper is to describe the thermal creep behavior and the lifetime prediction of materials subjected to non-stationary tensile loading conditions. The calculations are based on HART's tensile test equation and on a phenomenological cavitation damage model. From this model the life fraction rule (LFR) is derived. Analytical expressions for the lifetimes are derived, which contain only stationary stress rupture data. The creep behavior of non-cavitating and ideally plastic materials is derived from the solution of the tensile test equation for the particular loading conditions considered. Cavitation damage is known to influence the creep behavior by reducing the load bearing capability. The corresponding constitutive equation containing the loading conditions as well as the damage function is derived.

The following loading conditions were considered: (i) creep at constant load F and temperature T ; (ii) creep at linearly increasing load and $T = \text{const.}$; (iii) creep at constant load amplitude cycling and $T = \text{const.}$; (iv) creep at constant load and linearly increasing T ; (v) creep at constant load and temperature cycling and (vi) creep at superimposed load and temperature cycling.

* The full text of this paper was published in Nuclear Engineering and Design/Fusion 2 (1985) 29-52, North-Holland, Amsterdam.

** Now Staatliche Materialprüfungsanstalt, Universität Stuttgart, Pfaffenwaldring 32, D-7000 Stuttgart 80, Federal Republic of Germany.

THERMO-MECHANICAL STRESSES IN STRUCTURAL COMPONENTS CLOSE TO THE PLASMA

A. LUDWIG

Institut für Reaktorentwicklung,
Kernforschungszentrum Karlsruhe,
Karlsruhe, Federal Republic of Germany

Abstract

Structural components of fusion devices will be exposed to severe thermal and irradiational loadings, either over long time periods of cyclic operation, or in short transients caused by any accidental events. In both cases, an analysis of the resulting stresses and strains should comprise a suitable simulation of the long-term behaviour, since also the initial conditions, and hence the consequences of any short-term transients depend on the loading history suffered by the structure, due to the non-linear effects of creep, swelling, and wall erosion.

As one tool for such analyses, the computer code TSTRELT has been developed, based on the code TSTRESS which had been written at the University of Wisconsin, Madison. In TSTRELT, like in its predecessor, the structure is represented by a plate element which is uniformly loaded over its surface. Several kinematical boundary conditions may optionally be adopted to the element.

The main extension of the code is concerned with the simulation of cyclic long-term operations. Its method is distinguished from previous approaches by an approximative extrapolation procedure: the actual rates of creep, swelling, and wall erosion are replaced by average values which result from repeatedly inserted short-term calculations covering a small integer number of operational cycles. As a by-product, the peak stresses over the plate and the bounds of the stress ranges for zones near to the surfaces are traced as functions of time. These data may be used for low cycle fatigue investigations and life time predictions. The approach to short-term investigations is similar to known methods, but realistic initial conditions may be provided using the long-term algorithms. Thus an efficient tool has been prepared for estimating the thermo-mechanical behaviour of heavily loaded components.

The relative simple geometrical model used in TSTRELT appears to be adequate to limiting estimations in the present phase. It may soon become necessary, however, to consider also geometrically more complex structures. Then efficient long-term simulations will be even more urgent. For this aim, the long-term extrapolation techniques of TSTRELT could be combined with a more powerful structural model.

The present paper sketches the mathematical model of TSTRELT and the principles of its realization. Then some results of example calculations are aimed to demonstrate the capabilities of the code. The input data for these examples approximate the conditions which the first wall of INTOR will undergo, and the behaviour of the carbon protection tiles which are applied in front of the first wall of JET, respectively.

1. Introduction

In future nuclear fusion devices, there will be a lot of structural components which are exposed to high thermal and irradiational loadings, even at normal operational conditions. For most present designs of fusion machines (except only the tandem mirror and the stellarator designs), the significance of these loadings is enhanced by the necessarily cyclic operation modes.

Any malfunction of the device may cause especially the thermal loadings to increase even more, leading to more or less severe accidents. The stresses within the first wall, for instance, which are induced by such events, have to be analysed in order to prove the integrity of the first wall or to estimate the aftermath of its failure. It will not be sufficient, however, to start such analyses from single well defined states of the structure; due to the inelastic effects of creep and swelling, the properties of the structural material will change during the lifetime of a device, and wall erosion effects will additionally alter the geometrical configuration. Therefore, the consequences of any incident depend on the loading history which has been experienced by the structure.

Furthermore, besides realistic initial conditions for transient processes, the long-term behaviour may be of interest itself. For example, if lifetime considerations are to be performed, the long-term changes of stress levels and strains as well as of the amplitudes of the stress swing (induced by cyclic operation) are very important for the evaluation of fatigue models.

In principle, such investigations would demand for an analysis of the total lifetime of a component from the first start-up to the event under consideration, or to its pre-designed end of life. In most cases, however, such a procedure is prohibited by the huge computational efforts, because the time increments of the analysis had to be determined according to the changes within a single operational cycle.

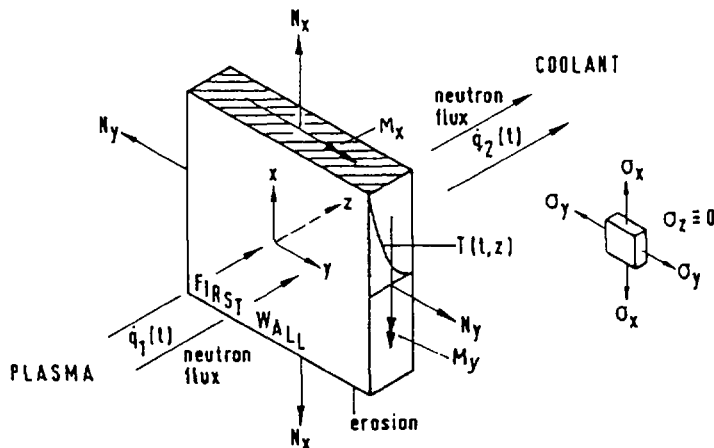


Figure 1: Plate Element Used in TSTRELT

A simple structural model, which will be suitable for fast estimations. Material properties as well as constitutive equations for swelling and creep are provided within separate subroutines which may easily be exchanged for different materials.

Therefore, approximate methods are needed which avoid the requirement of simulating the full lifetime of a component in all details. One such method has been developed by KfK and is reported in the present paper. It is aimed to simulate the long-term inelastic behaviour of structural components which are exposed to cyclic thermal and irradiational loadings.

The method has been realized in the computer code TSTRELT, combined with a

Since the emphasis of this paper is drawn to the long-term simulation, however, the structural modelling will be sketched only briefly, and the constitutive equations will not be discussed at all, though their formulation represents the best state of knowledge which was available to the author.

2. Structural Model

The structural model of TSTRELT is based on that of the code TSTRESS [1] which has been developed at the University of Wisconsin, Madison, several years ago. Thus the structural equations are essentially the same in both codes. TSTRESS was designed for the investigation of inelastic structural responses due to thermal and irradiational loadings like TSTRELT, but it does not contain any special features for long-term analyses.

In order to facilitate investigations into the inelastic behaviour and, in the case of TSTRELT, the development of the long-term algorithms, a rather simple structural model has been chosen. It considers shell-type structures which are restricted to plane stress states; i.e., the stresses normal to the surfaces are presumed to vanish identically. Furthermore, only such loadings are allowed, which are uniformly distributed over the surface. Consequently, also the time-dependent temperature distribution, which has to be input to the code, must not depend on the surface coordinates, x and y , but only on the depth into the wall, z . Figure 1 illustrates the general situation underlying the code.

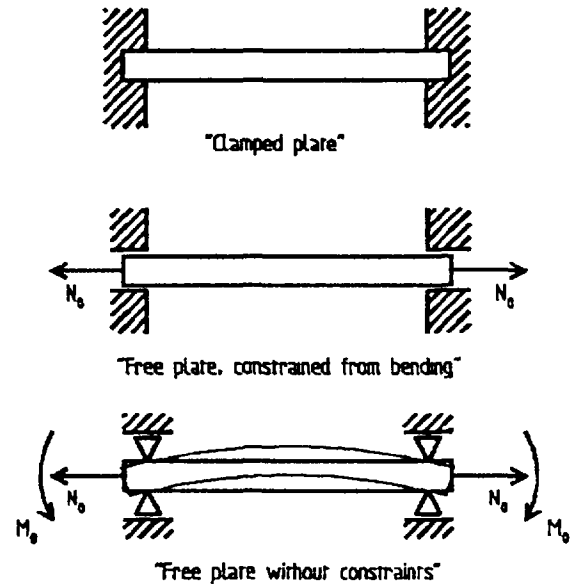


Figure 2: Boundary Conditions Available in TSTRELT

The "plate", defined in this way, is subjected to kinematical boundary conditions, which severely influence the cross-sectional distribution of strains and stresses. Three different sets of boundary conditions have been provided alternatively, which cover a wide range of interest. They may be characterized as follows (see also Figure 2):

- o Conditions of a "clamped plate": The total strains have to vanish identically throughout the wall thickness.
- o Conditions of a "free plate, constrained from bending": The total strains do not depend on the depth into the wall, but they may vary with time. They are subject to the equilibrium between the stress resultants over the wall and imposed membrane loads at each instant of time.
- o Conditions of a "free plate without constraints": Here also bending may occur, and the total strains are allowed to vary linearly with the depth into the wall. Their time-dependent distribution is again subject to the balance between imposed membrane and bending loads and the resultants of stresses and stress-moments.

The stress equations are derived in a general formulation. First Hooke's law is written in terms of the principal stresses, σ_x , σ_y , and σ_z , and of the differences of total and inelastic principal strains. After the condition of plane stress, $\sigma_z = 0$, has been introduced, the remaining stress equations are transformed using the transformation rules $\sigma = \frac{1}{2}(\sigma_x + \sigma_y)$, $\tau = \sigma_x - \sigma_y$, and corresponding rules for the strains. This yields formally independent equations for the "transformed" stresses:

$$\sigma(z) = \frac{E(z)}{1-\nu(z)} [\epsilon(z) - e(z)] \quad (1)$$

$$\tau(z) = \frac{E(z)}{1+\nu(z)} [\eta(z) - g(z)] \quad (2)$$

where ε and η are the "transformed" total strains, and e and g are the "transformed" inelastic strains. $\varepsilon(z)$ and $\eta(z)$ are linear functions of z , according to the respective boundary conditions. e and g comprise contributions from thermo-elastics, swelling, and creep.

Due to the plane stress condition, the total normal strain reads

$$\varepsilon_z(z) = e_z(z) - \frac{2\nu(z)}{1-\nu(z)} [\varepsilon(z) - e(z)] \quad (3)$$

with e_z being the inelastic normal strain.

Equations (1) through (3) are used in TSTRELT in order to calculate initial conditions. The stress-rate equations, which are the relevant expressions, are essentially got by taking the time-derivatives of the equations above. If the material properties do not depend significantly on the temperature, and hence the time, their time-derivatives may be neglected, and the stress-rate equations may be written in the following way (in all subsequent equations it is presumed that all terms are functions of the depth into the wall and of the time; a dot denotes derivation with respect to time):

$$\dot{\sigma} = \frac{E}{1-\nu} [\dot{\varepsilon} - \dot{e}] \quad (4)$$

$$\dot{\tau} = \frac{E}{1+\nu} [\dot{\eta} - \dot{g}] \quad (5)$$

These equations are partial differential equations for a "clamped plate" (where $\varepsilon = \eta = 0$), but integro-differential equations with the other boundary conditions, because there $\dot{\varepsilon}$ and $\dot{\eta}$ become integrals over the wall thickness with $\dot{\sigma}$ or $\dot{\tau}$ appearing in the integrand.

The inelastic strain-rates are composed of contributions from thermal expansion, swelling, and creep:

$$\dot{e} = \alpha \dot{T} + \frac{1}{3} \dot{S} + \dot{e}_{\text{creep}} \quad (6)$$

$$\dot{g} = \dot{g}_{\text{creep}} \quad (7)$$

Here, α is the coefficient of linear thermal expansion, T the temperature, and \dot{S} is the volumetric swelling rate. The temperature distribution in time and space is presumed to be given. The swelling and creep rates are the subject of constitutive equations, which have to be provided for each material. In general, they depend on the stresses, the temperature, the neutron flux and the fluence, but also other effects may be taken into account.

The stress-rate equations (4) and (5) are completed by an equation for the total normal strain-rate, where the inelastic terms have already been partitioned into their constituents:

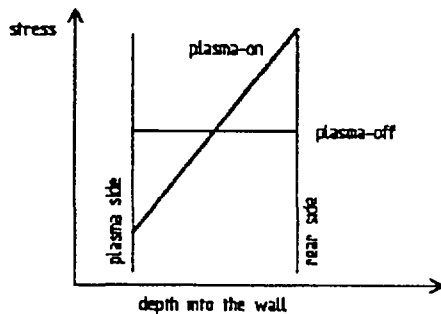
$$\dot{e}_z = [(1+\nu)(\alpha \dot{T} + \frac{1}{3} \dot{S}) - 2(1-2\nu)\dot{e}_{\text{creep}} - 2\nu\dot{\varepsilon}]/(1-\nu) \quad (8)$$

Integrating equation (8) over the plate thickness finally results in the change-rate equation for the thickness itself, where a change-rate due to wall erosion may be added.

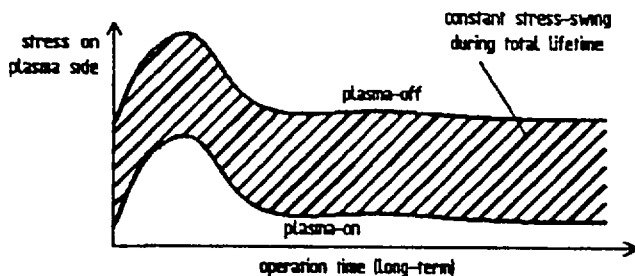
For simulating the stress history within the plate, equations (4) through (8) have to be integrated numerically, since closed form solutions do not exist. For this aim, the partial (integro-)differential equations are re-written as difference equations. In TSTRELT (like in TSTRESS), first order differences have been chosen, and an explicit time integration scheme has been adopted in combination with the trapezoidal rule for the spatial integration. The initial conditions are determined by use of equations (1) through (3).

3. Long-Term Simulation of the Response to Cyclic Loadings

The long-term behaviour of a structural component due to thermal and irradiational loadings is easily calculated, if steady-state loadings are considered. In this case, the time steps of the integration scheme may readily be increased in order to reduce the computational effort to reasonable limits.



a) Initial Stress Distributions



b) Stress History on the Plasma Side for "Plasma-on" and "Plasma-off" Conditions

Figure 3: Watson's Long-Term Approach [3]

counted for by superimposing the thermo-elastic stress-swing to the inelastic results.

This holds no longer for components which are exposed to cyclically oscillating loadings. Then the time steps have to be much smaller than the cycle period, and they are limited by the fast changes which occur within a cycle. As indicated above, it is generally impossible to follow the stress history in this case over long periods of time in full detail.

Therefore, approximative methods have been proposed by several authors, for instance by Dänner [2], Watson [3], and Fett [4]. In principle, they all separate the inelastic long-term effects from the short-term cycling, assuming that the latter is essentially due to the thermal loads. Thus the long-term calculation is done for continuous loadings, and the thermal cycling is ac-

In order to illustrate the differences to TSTRELT, first Watson's long-term procedure [3] will be sketched. He used essentially the same structural model as described above, because he applied the code TSTRESS.

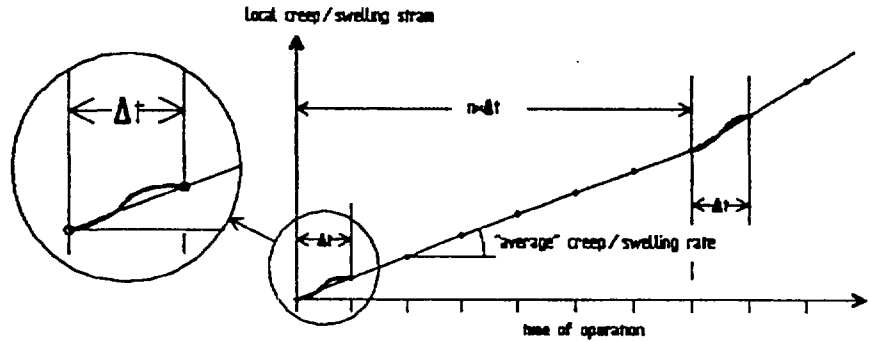
Watson considers the first wall of a tokamak reactor which is cyclically loaded by heat fluxes and neutral irradiation. He merely distinguishes between "plasma-on" and "plasma-off" conditions and calculates the initial stress distribution for both cases (Figure 3a). For "plasma-on", he imposes the stationary temperature distribution, which is reached within a cycle, when the inflowing heat flux is balanced by the cooling rate, and the maximal neutron

flux to the wall. Then he calculates the long-term behaviour under the assumption that the "plasma-on" loads are stationarily applied, yielding a long-term stress distribution history for "plasma-on". In order to evaluate the stress distributions under "plasma-off" conditions, merely the difference between both initial distributions (i.e., the initial "stress-swing" distribution) is subtracted from the long-term "plasma-on" distributions (see Figure 3b).

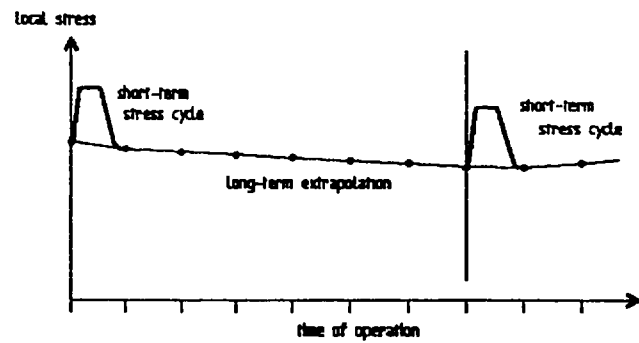
Such a procedure supposes the stress-swing distribution to remain unchanged during the lifetime of a component, and creep and swelling effects, which usually are very sensitive to temperature changes, are calculated according to the "hottest" temperature profile. These simplifications are suitable only then, if the wall thickness is not changed significantly by wall erosion and creep, and if the "plasma-off" time is short in comparison to the "plasma-on" time within a cycle.

The approach used with TSTRELT avoids these restrictions. Figure 4 gives a schematical illustration. Here, first the response history is calculated for one operational cycle,

using the full short-term equations and taking into account the varying loadings with respect to thermo-elastics as well as to irreversible processes like creep and swelling. The time step has to be appropriately short, but this is tolerable, since only one cycle has to be simulated. Now the local "cycle-average" rates of creep and swelling are calculated as



a) Averaging of Creep and Swelling Rates



b) Resulting Cycle-Initial Stresses

Figure 4: Long-Term Extrapolation in TSTRELT

$$\dot{S}_{av}^{\bullet}(z) = \frac{1}{\Delta t} \int_t^{t+\Delta t} \dot{S}^{\bullet}(z, t') dt' \quad (9)$$

$$\dot{e}_{creep, av}^{\bullet}(z) = \frac{1}{\Delta t} \int_t^{t+\Delta t} \dot{e}_{creep}^{\bullet}(z, t') dt' \quad (10)$$

$$\dot{g}_{creep, av}^{\bullet}(z) = \frac{1}{\Delta t} \int_t^{t+\Delta t} \dot{g}_{creep}^{\bullet}(z, t') dt' \quad (11)$$

and it is supposed that these average rates remain unchanged for some time which is significantly greater than the cycle period Δt , but much smaller than the lifetime of the component. Therefore, the creep and swelling rates are replaced in equations (6) through (8) by the expressions of equations (9) through (11), and now the equations (4) to (8), which have been modified in this way, are used to calculate the development of the cycle-initial conditions with time. The time step in this "long-term" calculation must be, consequently, an integer multiple of the cycle period. After some long-term time steps, the results of the long-term calculation are used as initial conditions for a new short-term analysis of one cycle, which yields again local cycle-averaged rates of creep and swelling. These new average values, which are different from the previous ones in general, are used in a subsequent long-term analysis as before. I.e., the short-term and long-term equations are integrated by turns along with the progress in problem time. Thus the procedure is characterized by an alternating sequence of short-term and long-term calculations, as it is indicated by the schematical flow-chart of Figure 5. Furtheron, it may be seen from this flow-chart that short-term analyses may be run independently with TSTRELT, but long-term investigations demand for previous and intermediate short-term calculations.

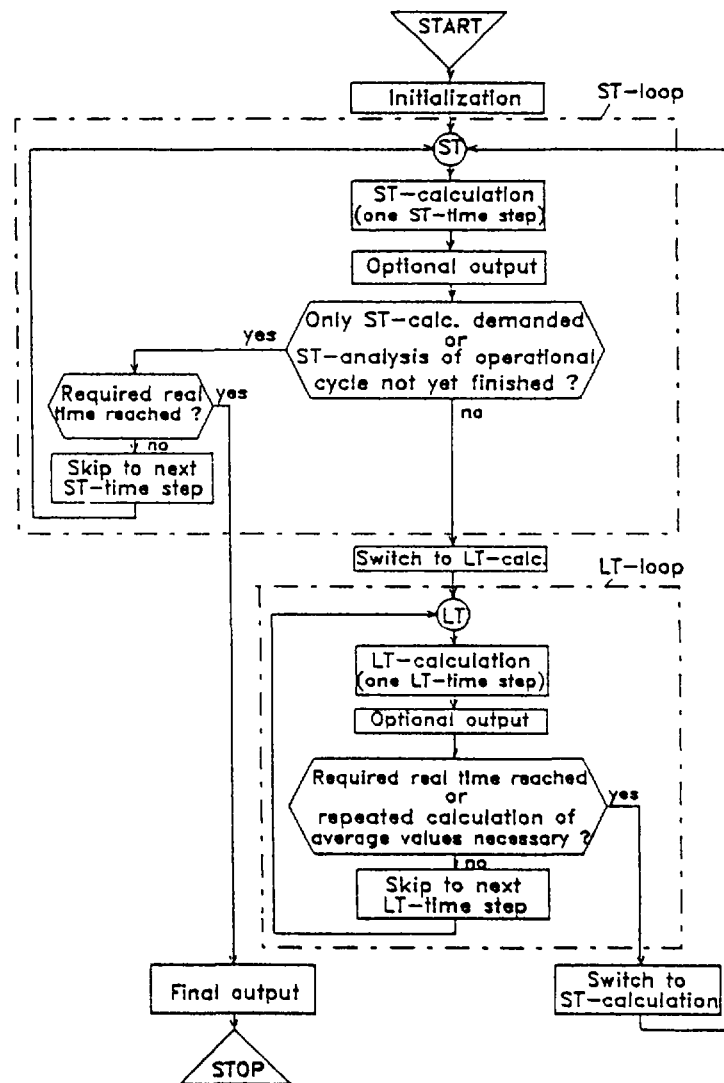


Figure 5: Schematic Flow-Chart of TSTRELT
(ST = Short-Term; LT = Long-Term)

This approach to the long-term simulation shows several advantages, which are briefly outlined in the following:

- o As only a small part of the problem time has to be analysed in detail (i.e., by a short-term calculation), the computing time is reduced significantly. The long-term extrapolation of cycle-initial conditions may be performed using relatively large time steps, and also the computational efforts for one long-term time step are diminished. The additional effort for computing the average rates, on the other hand, is rather small.
- o In spite of this reduced effort, the long-term effects are taken into account not only with regard to the creep and swelling strains, but also to cycling thermal stresses, since the short-term calculations are started from updated initial conditions each time. Besides this, also the vari-

ations of temperature and neutron flux within a cycle are accounted for with regard to creep and swelling.

- o Due to the repeatedly analysed cycle histories, the development of lower and upper stress levels, and hence of the stress-swing within an operational cycle is easily traced. This tracing takes place discontinuously, but it provides enough information for evaluating low cycle fatigue phenomena.
- o Although the long-term time step is confined to integer multiples of the cycle period and is usually settled to be constant over a computational run, it may yet be adapted to major changes of the average rates of creep and swelling which occur in the progress of operation time. In this case, a simple restart technique will allow to change the predefined values occasionally. The same technique allows to analyse a short transient which starts after a long period of cyclic operation.

The accuracy of the present approach depends, of course, on the long-term time steps and particularly on the frequency of the intermediate short-term calculations, as compared to the actual change-rates of the "average" creep and swelling. In the applications performed up to now, the long-term calculations covered about 80 to 160 operational cycles without updating the average rates, and no significant change in accuracy has been found with these variations. This statement severely depends, however, on the problem data and has to be checked for each application.

The approach could be refined, in principle, by an iterative procedure which updates the long-term results by taking into account the subsequent short-term analysis. Such a refined procedure would become even less sensitive to time steps and updating frequencies for the average rates. However, it has not been implemented in TSTRELT, as this code is restricted to estimative calculations, due to its simple structural model.

But the long-term extrapolation technique itself, which has been proposed in this section, could be used also in connection with more detailed structural models. If this is done, one has to balance the increased efforts for coding and computation against the additional gains in accuracy and time-step independency, which may be got from such a refinement.

4. Example Calculations

The code TSTRELT and its long-term algorithms have been used to simulate the long-term behaviour of two totally different structural components, each of which is part of the first wall of a fusion device. The original goal of these calculations was to provide realistic initial conditions for accidental transients; but, in the present context, only the long-term investigations will be discussed.

Most of the illustrations show "three-dimensional" plots which demand for some annotations. In these plots, normal stresses have been drawn along the vertical axis as functions of time (axis from back to front) and of the depth into the wall (z-axis, from left to right). In z-direction, the centers of computational zones have been traced. For this reason the z-axis does not start at zero and stops at a value lower than the wall thickness. Only a small part of the actually calculated time levels could be traced.

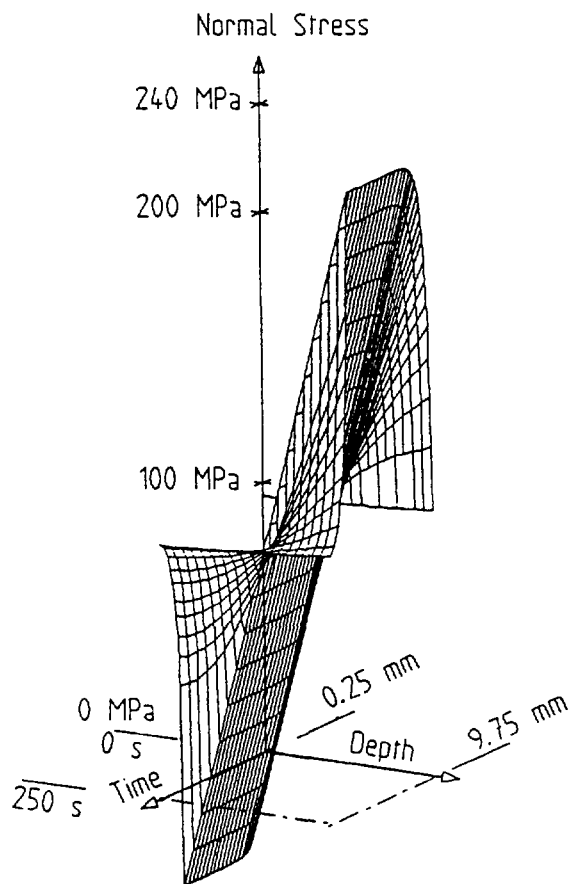


Figure 6: Stresses in the First Wall of an INTOR-Like Reactor During the First Operational Cycle

One investigation dealt with the first wall of a tokamak reactor, cyclically loaded under nominal operational conditions. Input parameters like material (SS 316), wall thickness (10 mm), cycle and burn time (250 s and 200 s), heat flux to the wall (120 kW/m^2 during burn time) and neutron flux ($1.5 \cdot 10^{15} \text{ n/(cm}^2\text{s)}$ in the average) have been extracted from the 1982 INTOR report [5]. Wall erosion has been neglected. Assuming a constant coolant temperature of 620 K, a maximum wall temperature at the plasma side of 689 K has been found from these data. The first wall has been analysed as a "clamped plate, constrained from bending", with imposed membrane loads of $1 \text{ MPa}\cdot\text{m}$ in the directions of both principal stresses due to the coolant pressure.

For understanding the long term results, it will be helpful to look first at the short-term stress cycle of the "virginal" plate. Figure 6 shows the normal stress distributions within the first cycle after operation start-up. It commences with a very flat distribution, corresponding to Watson's "plasma-off" condition. When the heat flux from the plasma sets in, the plasma side of the wall reaches higher temperatures and expands more rapidly than the rear side. This induces tensile stresses on the rear side and compressive stresses at the

plasma side to be superimposed to the initial stress distribution. After shut down of the plasma burn, the initial stress distribution is nearly reproduced. - Operational cycles, which start after some time of operation, show different initial distributions, which will be discussed below, but qualitatively the same behaviour is found.

The long-term development of the cycle-initial normal stress distributions during $4 \cdot 10^7 \text{ s}$ or about 15.3 months of operation has been plotted in Figure 7. The increased tensile stresses at the rear side during burn time induce there

higher creep rates than at the plasma side, and therefore compressive residual stresses are built up during the operation. Due to the restricted bending, these stresses cause, in turn, tensile residual stresses on the plasma side. This development of residual stresses is not stopped until swelling effects surpass the creep strains, which takes place after about $1.8 \cdot 10^7$ s or seven months of operation.

The long-term changes of the minimum and maximum stress levels within a cycle have been drawn in Figure 8 for the zones close to the plasma and close to the coolant. Two facts may be read from this figure: 1. The cycle-initial stresses coincide with the cycle-maxima at the plasma side and with the cycle-minima at the rear side. 2. The stress-swing is not changed significantly in this example during the operation time considered, because wall erosion has been neglected and only a low fluence is reached within this period, which results in small changes of the wall thickness due to creep (see equation (3)).

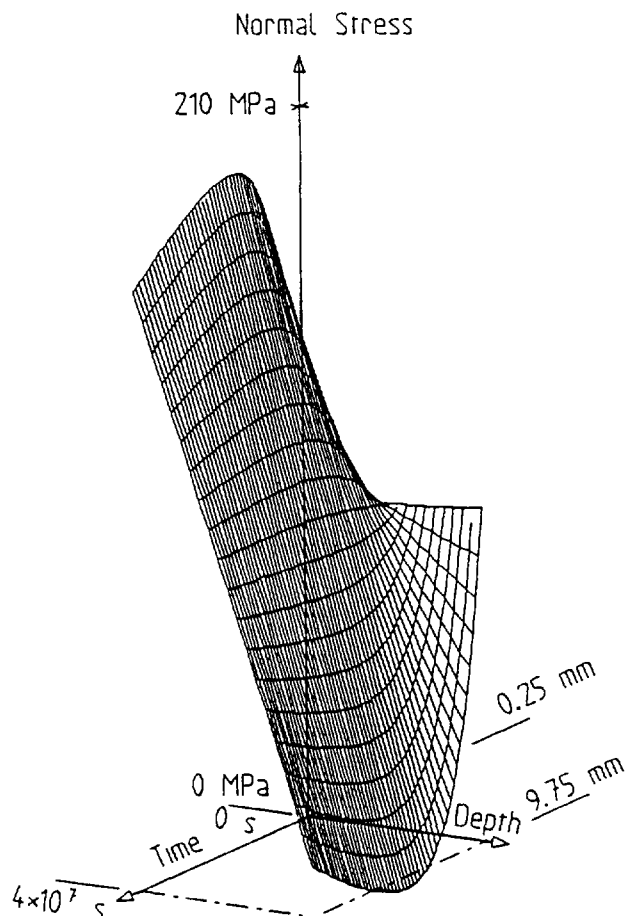


Figure 7: History of Cycle-Initial Stress Distributions in the First Wall of an INTOR-Like Reactor

As a second example, the graphite tiles have been investigated which protect the first wall of

JET from the shine through of the neutral heating beams. For this aim, the hot spot area has been determined, and the input data for TSTRELT have been chosen according to this area. Thus we have 17 mm thickness, a cycle period of 600 s with an - optimistic - burn time of 15 s. When JET will use a D-T plasma in its last phase, which comprises 10,000 cycles, the neutron flux will be about $8.75 \cdot 10^8$ n/(cm²s) in the average. The total heat flux to the hot spot area will be about 5 MW/m² during the burn time, the major part of which will be due to the neutral beam shine through. The

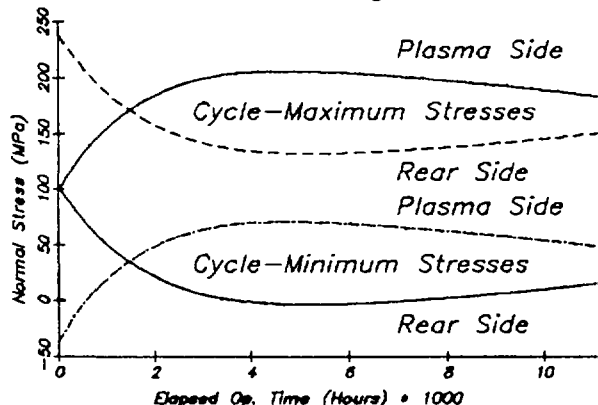


Figure 8: Stress-Swing Histories for the INTOR-Like First Wall

tiles are passively cooled by irradiation to cooler components, the temperature of which we have assumed to be about 520 K. Thus the tile is rapidly

heated within the burn time from the initial temperature of 760 K to about 1760 K at the plasma side and to 1660 K at the rear side. During the long dwell time they are slowly cooled down to the initial temperature.

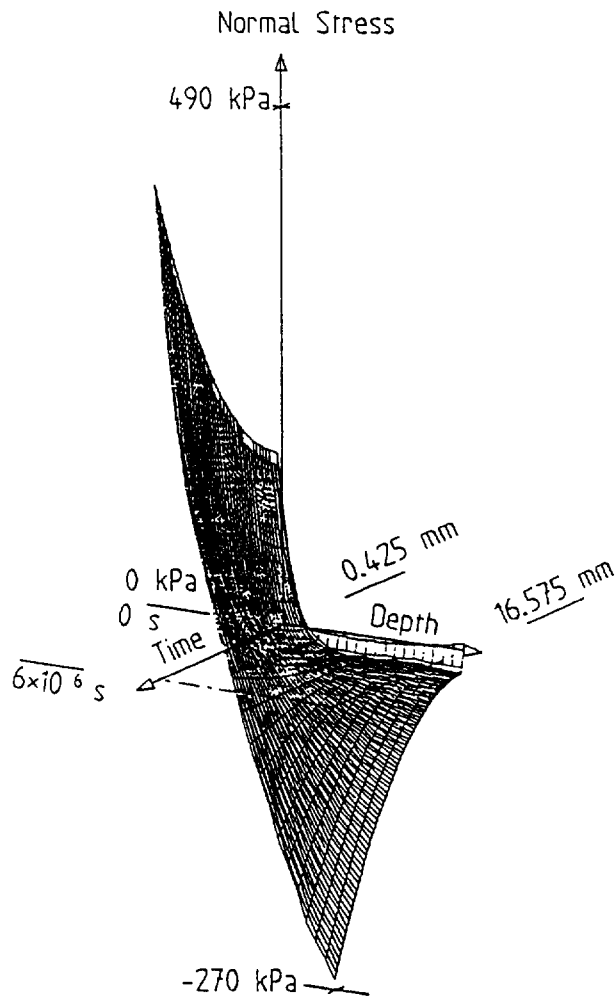


Figure 9: Cycle-Initial Stress
History of JET Protection Tiles:
"Plate Constrained from Bending"

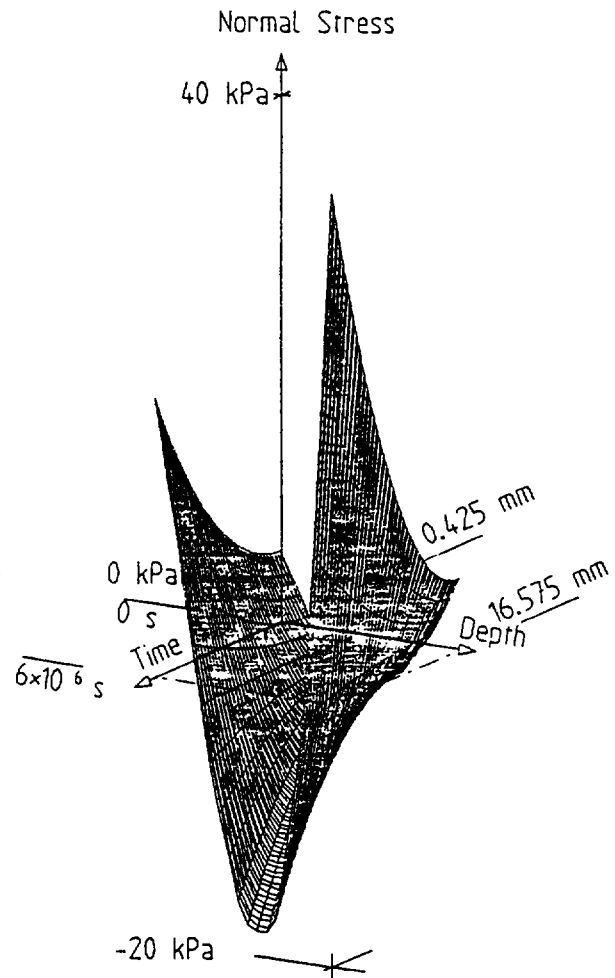


Figure 10: Cycle-Initial Stress
History of JET Protection Tiles:
"Free Plate Without Constraints"

For these TSTRELT calculations, swelling has been accounted for according to the formulas given in [6]. Creep effects turned out to be absolutely irrelevant. Two calculations have been performed, one of which considered the tile to be a "free plate, constrained from bending", whereas the other used the boundary conditions of a "free plate without constraints". Membrane or bending loads have not been imposed. It is anticipated that the real behaviour of the tile will be in between these limiting cases, as no bending constraint is provided by the design, but the heat flux is distributed non-uniformly, thus inducing internal constraints to bending.

In Figure 9, the development of cycle-initial (or residual) stresses is shown for the "plate, constrained from bending". Since the "swelling" of graphite is actually a shrinking for low values of the fluence, the overall image remembers that of Figure 7; there, however, the creep strains have induced the

residual stresses. Besides this, the figure over-emphasizes the swelling effects due to its enhanced stress-scale.

The corresponding distributions for the "plate without constraints" are given in Figure 10. The levels of the residual stresses are lower by more than one order of magnitude in this case; due to the freedom of bending they form an almost symmetrical profile across the plate thickness.

It should be mentioned, however, that the cycle-initial stresses remain insignificant for the JET tiles at all, as the thermally induced stress-swing has been found to reach up to 12.7 MPa with bending constraints and up to 1.8 MPa without constraints. In both cases, the cycle-initial stresses do not coincide with one of the extremal stresses within a cycle, which occur at the end of the burn time and after a short period of cooling, when heat conduction inside the tile is flattening the temperature profile.

5. Conclusions

An efficient method has been presented in this paper for simulating the long-term behaviour of cyclically loaded structures. It has been realized in the computer code TSTRELT, the short-term algorithms of which are equivalent to known methods, apart the fact that realistic initial conditions may be provided due to the long-term facilities.

The simple structural model of TSTRELT and its geometrical restrictions, especially to the spatial distributions of loadings, appear to be adequate to preliminary estimations of stresses and strains, as they have been done up to now in the design studies for fusion devices. It may become necessary in the near future, however, to consider also geometrically more complex structures. Then it will be even less feasible than for the present simple model, to simulate the development of stresses and strains in full detail for the total lifetime of a component. Presumably it would be advantageous in this case, to adopt the long-term extrapolation techniques of TSTRELT and to combine them with a more powerful structural model.

References

- [1] R.R. Peterson, R.D. Watson, W.G. Wolfer, G.A. Moses: TSTRESS - A Transient Stress Computer Code. Fusion Engrg. Program, Nucl. Engrg. Dep., University of Wisconsin - Madison, Madison, Wisc., Report UWFD-382, December 1980.
- [2] W. Dänner: FWLTB - A Computer Program for Estimating the First Wall Lifetime in a Fusion Reactor: A Status Report. Res Mechanica 6 (1983), 183-191.
- [3] R.D. Watson: The Impact of Inelastic Deformation, Radiation Effects, and Fatigue Damage on Fusion Reactor First Wall Lifetime. Ph.D.-Thesis. Fusion Engrg. Program, Nucl. Engrg. Dep., University of Wisconsin - Madison, Madison, Wisc., Report UWFD-460, December 1981.
- [4] T. Fett, D. Munz: Stress and Lifetime Calculations for First Wall and Blanket Structural Components, Part I: Crack Propagation in Tubes. Kernforschungszentrum Karlsruhe, Report KfK 3875, January 1985.
- [5] European Community Contribution to the INTOR Phase-Two-A Workshop. Rep. Commission of the European Communities, Brussels, 1982.
- [6] R.D. Watson, W.G. Wolfer: Mechanical Constitutive Laws for the Irradiation Behavior of Graphite. J. Nucl. Mat. 85 & 86 (1979), 159-164.

THE RCC-MR DESIGN CODE FOR LMFBR COMPONENTS

A useful basis for fusion reactor design tools development

D. ACKER, G. CHEVEREAU
CEA, Centre d'études nucléaires,
Saclay, France

Abstract

LMFBR and fusion reactors exhibit common features with regard to structural materials, temperature service level, loading types.

So, design and construction rules used in France for LMFBR, that is to say RCC-MR Code, can constitute a good basis for fusion reactors design.

Some original aspects of RCC-MR design rules are described, relating to insignificant creep, ratchetting effect, fatigue and creep damage limits, creep damage evaluation, fatigue damage evaluation, buckling.

The main originality of RCC-MR consists to propose comprehensive simplified rules based on elastic calculations and extended from classical cold temperatures to the elevated temperature domain.

- 1) The development of new nuclear plant prototype needs to gather a collection of design rules.

This step is necessary as game rules between public authorities, users and manufacturers. It is difficult because the construction of a prototype obviously starts before sufficient knowledge of problems is gained. Therefore, it is advisable to lean on the most recent progress in close domains in order to take advantages of larger experiences.

LMFBR differs from fusion plant in physical principles, reactor arrangement, and in some used materials. They are very similar in temperature level (550°C - 600°C), structural materials (stainless steels), loadings types (thermal loadings), and irradiation effects (in the core reactor).

Also, the LMFBR rules can be a useful basis for fusion reactor design and the necessary progress in design rules field are common to LMFBR and fusion reactors.

The RCC-MR rules for design and construction of LMFBR components focus the experience gained in construction of Rapsodie and Phenix and in

R. and D. progress due to setting up, developing and justifying Superphenix design analysis.

The RCC-MR building up was decided in 1978 by Commissariat à l'Energie Atomique, Electricité de France and Novatome, two years after the Superphenix building start and the first edition is published today, in 1985, November, at the same time as the Reactor start a chain reaction.

2) General layout of RCC-MR design rules

The RCC-MR has the same general organization as light water reactor codes as RCC-M or ASME III.

A more complete presentation was performed by R. NOEL at the 1st International Seminar on Construction Codes and Engineering Mechanics in Paris (August 26-27, 1985), and we focused our attention on the chapter 3200, corresponding to the general design rules. Its organization is drawn fig.1.

§ RB 3210 à 3240

Applicability domain, definitions, methods, materials
constitutive equations (1), significant creep test

Significant creep test

	No	Yes
Damages "type P"	RB 3251	RB 3252
Damages "type S"	RB 3261 (4)	RB 3262 (5)
Buckling	RB 3271 (3)	RB 3272 (3)
Bolting	RB 3281 (2)	RB 3282 (2)

Nota

- (1) Annexe A3 - Materials properties
- (2) Annexe A6 - Bolting analysis
- (3) Annexe A7 - Buckling analysis
- (4) Annexe A10 - Cyclic loadings,
elastoplastic analysis
- (5) Annexe A11 - Cyclic loadings,
elasto-visco-plastic analysis

Fig 1 - RB 3200 scheme
General rules of analysis

2-1) "Levels" of components.

Since the safety and system engineering specialists have chosen to keep the classical 3 classes of safety, the RCC-MR divides also the components in 3 levels.

But from the design methods, we can more easily conceive 2 levels only : the first with requirements of a complete behaviour analysis and limitative criteria versus every mechanical damage to avoid : excessive

deformation, plastic collapse, buckling, creep fatigue, ratcheting, and the second, with requirements limited to design by formulae.

That is why the writers decided to adopt practically the same design rules for "Level 1" and "Level 2" components, relating the main differences between the two level to fabrication prescriptions (weld design and NDE extent).

2-2) Levels of criteria

The LWR design codes distinguish 4 criteria levels.

The two firsts are corresponding to current in service loading or to practically unavoidable malfunctions and their limits differ slightly only on the allowable primary stress limits. It seemed more convenient to RCC-MR writers to define only one level for these situations which shall not interfere with the future plant working.

The two last levels corresponding to exceptional or hypothetical accidents are retained.

3) Design rules in the RCC-MR.

The basic idea of the RCC-MR rules is to extend as far as possible the elastic analysis domain.

A complete discussion of these rules and of their basis would be too long for this presentation and the subject will be limited to some original aspects.

3-1) Limit of "unsignificant creep"

The main aim of the RCC-MR is to provide a set of rules available both under "cold" temperature and under "hot" temperature.

These two domains are divided by a "creep cross over curve" and the allowable rules differ only by additional requirements but analysis methods are identical.

The "creep cross-over curve" is based on an idea first initiated by the CEA RAMSES Committee that short excursions at high temperature could be ignored -as regards creep damage-. An usable curve, drawn for each material concerned, is to be used with a cumulative method in $\sum t_i/T_i$ to assess the field of "unsignificant creep".

The principle is to ensure that the total rate of relaxation at the temperatures t_i , under assumed stresses of $3 S_m$, is lower than 10 %. Once this condition met, it enables the designer to perform his analysis with "cold" rules and criteria.

The limit curves are given for each materials, see fig. 2 for typical example.

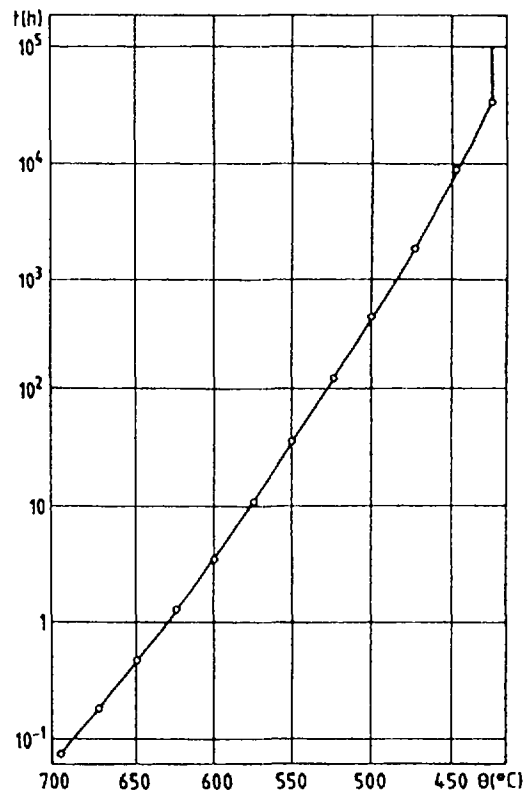


Fig. 2 - Creep cross over curve for 316L

3-2) Limits of Ratchetting effect

Progressive distortion by ratchetting must be strictly limited in order to avoid amplification of creep fatigue damages as well as to respect strains limits.

The classical rules against ratchetting are founded on theoretical works performed with very simple models of materials behaviour (elastic perfectly plastic, kinematic hardening), even though none of them is available to predict experimental results.

The method developed by RAMSES Committee from CEA, is based on experimental results analysis.

The RCC-MR rule leads to derive from primary stress P and cyclic secondary stress range ΔQ an "effective primary stress" P_{eff} . and apply

to this stress the same type of limitations as currently applied to primary stresses.

The fixed limits are :

1,2 Sm in the "cold" field, which corresponds to 0,45 % for stainless steels as a general membrane strain

creep usage factor lesser than one in the "hot" field (same limit as for common primary stresses).

The curve giving the "efficiency coefficient" P/P_{eff} , versus "rate of secondarity" $\Delta Q/P$ was originally drawn from experimental work performed by CEA. It has been progressively refined and confirmed by plotting any known experimental point gained home or abroad. It is presented with its experimental validation in figure 3.

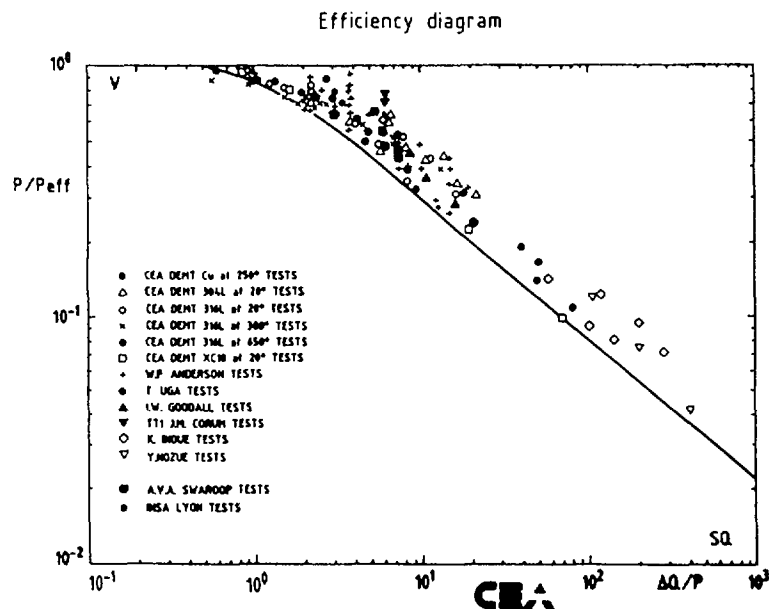


Fig. 3

3-3) Fatigue and Creep fatigue damage limits

The rule principles are similar to those adopted by the "Code Case N 47" :

The fatigue-damages and the creep damages are assessed separately.

The usual linear summation rule is used for both damages.

The creep fatigue interaction is assessed by means of the classical interaction diagram (fig.4).

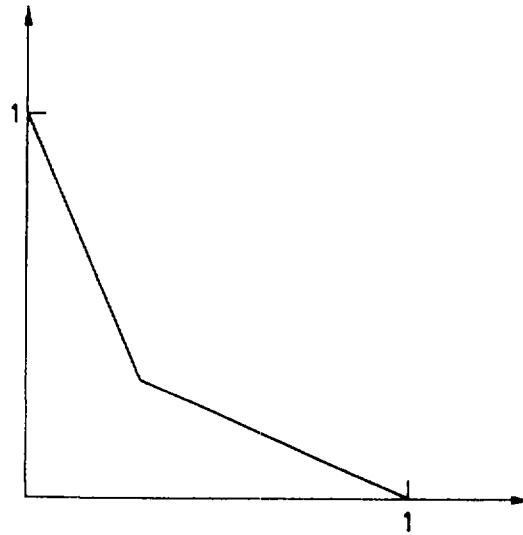


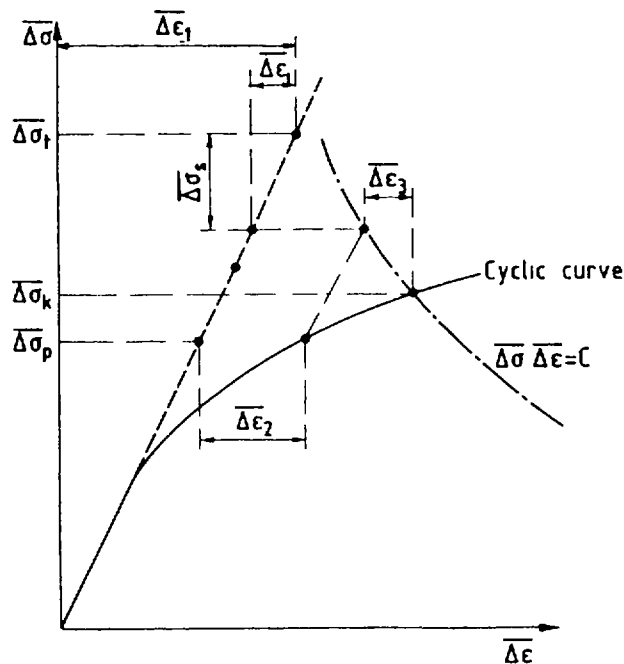
Fig. 4 - Creep fatigue damage interaction

3-3-1) Fatigue damage evaluations

The relevant parameter for the fatigue damage assessment is the usual VON MISES equivalent strain range $\overline{\Delta \epsilon}_t$ which is the sum of two contributions :

- a first contribution due to instantaneous elastoplasticity : $\overline{\Delta \epsilon}_{elpl}$.
- a second contribution due to creep : $\overline{\Delta \epsilon}_c$

$\overline{\Delta \epsilon}_{elpl}$ and $\overline{\Delta \epsilon}_c$ are derived from the local value (at the actual point under examination) of the elastically computed VON MISES stress range $\overline{\Delta \sigma}$.



Procedure

- 1 - To determine $\overline{\Delta \epsilon}_1$ from $\overline{\Delta \sigma}_t$
- 2 - To determine $\overline{\Delta \sigma}_s$ from $\overline{\Delta \epsilon}$ imposed

$$\overline{\Delta \sigma}_s = (3/2) (E/(1+\nu)) \overline{\Delta \epsilon}_1$$
- 3 - To determine $\overline{\Delta \epsilon}_2$ from $\overline{\Delta \sigma}_p$

$$\overline{\Delta \sigma}_p = \Delta(P_m - 0.67(P_b + P_L - P_m))$$
- 4 - To determine $\overline{\Delta \epsilon}_3$ from $\overline{\Delta \sigma} \overline{\Delta \epsilon} = C$
- 5 - To determine $\Delta \sigma_k$ from $\Delta \epsilon_3$

Fig 5 - Fatigue analysis procedure

$\overline{\Delta \xi}_{\text{elpl}}$ is evaluated by summation of four terms (fig.5)

$$\overline{\Delta \xi}_{\text{elpl}} = \overline{\Delta \xi}_1 + \overline{\Delta \xi}_2 + \overline{\Delta \xi}_3 + \overline{\Delta \xi}_4$$

where :

. $\overline{\Delta \xi}_1$ stands for the elastic part of the strain range

$$\overline{\Delta \xi}_1 = \frac{2}{3} \left(\frac{1+\nu}{E} \right) \overline{\Delta \sigma}$$

. $\overline{\Delta \xi}_2$ is a provision in case significant plasticity should arise from large primary stresses variation.

In most actual cases $\overline{\Delta \xi}_2$ is just equal to zero.

. $\overline{\Delta \xi}_3$ stands for plasticity induced by secondary and peak stresses

$$\overline{\Delta \xi}_3 = (K_{\xi} - 1) \overline{\Delta \xi}_1$$

The K_{ξ} function derives from the NEUBER's rule applied with the mean cyclic stress-strain curve of the material.

. $\overline{\Delta \xi}_4$ stands for the multiaxial effects

$$\overline{\Delta \xi}_4 = (K_{\nu} - 1) \overline{\Delta \xi}_1$$

K_{ν} is also a function of the temperature and of $\overline{\Delta \sigma}$ which is pretabulated.

If a part of the loading is strain controlled, the corresponding strain is not taken into account in the $\overline{\Delta \xi}_3$ evaluation (fig.5).

If significant creep effects are expected, $\overline{\Delta \xi}_c$ is evaluated as the creep strain induced by a sustained stress $\overline{\sigma}_k$ (the definition of $\overline{\sigma}_k$ is discussed below see § 4) during the given hold time of the cycle at the temperature of the steady state part of the cycle.

This creep strain is calculated from the creep laws specified for each material.

The fatigue damage is evaluated by use of fatigue curves without hold time and Minner rule.

3-3-2) Creep Damage evaluation

The creep damage is assessed from the life fraction rule with the maximum estimated stress $\overline{\sigma}_k$ which is generated during the cycles.

The $\overline{\sigma}_k$ value is appraised as follows

$$\overline{\sigma}_k = P_m + K_s \overline{\Delta \sigma}^*$$

where :

- . $\overline{\Delta \sigma}^*$ is the stress range corresponding on the mean cyclic curve, to the previously determined $\overline{\Delta \epsilon}_{elpl}$
- . K_s is the symetry factor. This symetry factor depends on the ratio of $\overline{\Delta \sigma}^*$ divided by twice the yield stress and is taken ~~into~~ account for the symetry effect which arise during cyclic straining (the main stress value vanishes, to some extend during cyclic straining). It is defined from experimental results.
- . P_m is the average sustained membrane stress during the hold time

3-3-3) Special case of crack like defect

In crack like defects, under insignificant creep limits, fatigue analysis shall be performed at a distance d from the defect line. The total strain $\Delta \epsilon_t$ evaluated at this point is divided by 1.5 before to assess the fatigue damage. The parameter d depends from the maxima specified ultimate strength R_{um} of the material and is equal to 0,05 mm when $R_{um} \leq 600$ MPa.

This rule was validated from experimental results on CT tests.

Any rule is available in the creep domain.

3-3-4) Comments

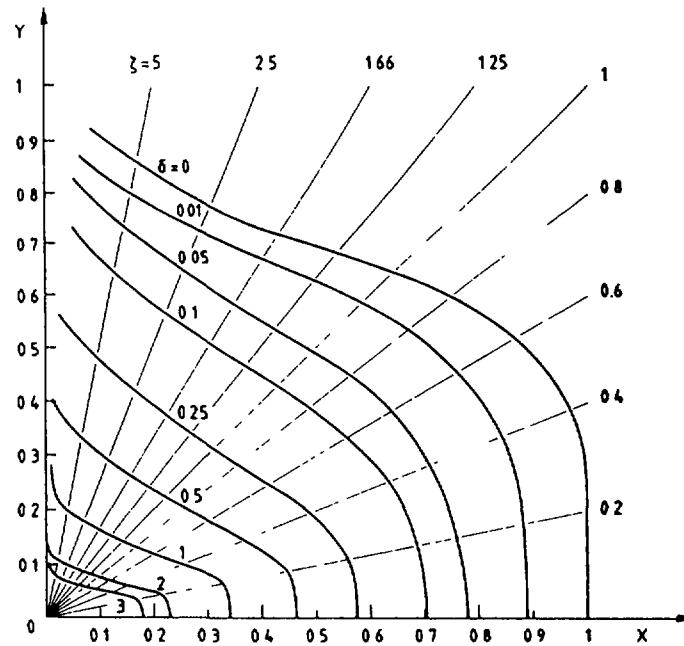
In the creep domain, the evaluation of the damage due to the creep seems very conservative since any relaxation effect is taken into account.

An important R and D effort is sustained about this point.

3-4) Buckling

The RCC-MR proposes a simplified analysis method based on an elastic analysis of the structure, without defect taken into account, in order to determine its elastic buckling load λ_E and its plastic load λ_y for which a point reaches the conventional elastic limit.

Then, λ_E must be corrected by a "Knock down" factor X , which depends on the "structure index" equal to the ratio λ_E/λ_y and on the "defect parameter", defined as the ratio of the tolerancies on the thickness.



The Knock-down factor X is given by computed diagrams (fig.6) depending from the material but not from the temperature.

They have been validated by comparison with many experimental results corresponding to number of structure types subjected to various loadings.

Conclusion -

We have briefly presented the RCC-MR code and its main originalities.

This code contains the experience acquired from setting up and justifying Superphenix design analysis and summarizes the results of the large R and D efforts performed as support for the design of this plant or at longer term perspective.

Its main originality is to propose a very comprehensive set of simplified rules founded on elastic calculations and extended from the classical "cold" temperatures to the elevated temperature domain. Some excessive conservatism could be lightened when R and D results will give justifications.

Actually used in industrial practice for SPX 2 project, it has still to be completed and improved and will take advantage of LMFBR European development.

Acknowledgments -

This paper was written with the support of the presentations performed by Mr R. NOEL and Mr J. TRIBOUT during the 1st International Seminar "Construction Codes and Engineering Mechanics, in Paris, France August 26-27, 1985".

AN ANALYTICAL AND EXPERIMENTAL STUDY ON LIFETIME PREDICTIONS FOR FUSION REACTOR FIRST WALLS AND DIVERTOR PLATES

T. HORIE, T. ARUGA, N. MIKI*, A. MINATO**, M. SEKI,
K. SHIRAIISHI, S. TSUJIMURA⁺, T. WATANABE⁺⁺, T. TONE
Naka Fusion Research Establishment,
Japan Atomic Energy Research Institute,
Naka-machi, Naka-gun, Ibaraki-Ken, Japan

Abstract

Analyses and experiments concerning lifetime predictions of the first wall and divertor plate of fusion reactors have been performed. Swelling and irradiation creep strain curves are recommended by the evaluation of materials data in open literatures. A parametric lifetime analysis based on a one-dimensional plate model has been performed. To examine the effects of elasto-plasticity and two-dimensional configuration, a two-dimensional elastic-plastic analysis has been applied. Based on thermal and mechanical experiments on a tungsten-copper bonded duplex structure, its fracture behavior and lifetime predictions are discussed.

1. INTRODUCTION

Lifetime analysis of first walls and divertor plates for tokamak fusion reactors, materials data evaluation, and fatigue tests of the bonded duplex structure have been performed to examine the life-limiting mechanisms and failure criteria.

There are uncertainties in neutron irradiation data of materials. Lifetime predictions are affected by the material data selected. In this paper, for the lifetime analysis, swelling and irradiation creep strain equations are recommended through the evaluation of the data compiled in the data base system developed at JAERI.

One- and two-dimensional stress analyses are performed for both the first wall and divertor plate of an experimental reactor [1], and the first wall of a power reactor [2]. In one-dimensional plate model, parametric lifetime analysis considering the effects of thermal cyclic strain, membrane force, irradiation creep, swelling, and erosion is performed. Its objective is to examine the influence of operating conditions and design parameters on the materials used.

Though lifetime analyses have been performed by many investigators [3-7] so far, the elastic-plastic finite element analysis considering the effects of swelling and irradiation creep has not been performed yet. To take account of the effects of elasto-plasticity and two-dimensional configuration a detailed stress and strain analysis is performed by finite element method. Since irradiation creep depends on a stress level, elastic-plastic analysis is important to evaluate the stress level. Problems in design criteria are discussed based on the results obtained.

*Toshiba Corporation.

** On leave from Kawasaki Heavy Industries, Ltd.

⁺On leave from Mitsubishi Heavy Industries, Ltd.

⁺⁺Century Research Center Corporation.

For divertor design studies [1,8], a tungsten protective armor bonded to a copper (or copper alloy) heat sink is selected as a reference design concept. Metallurgical bonds using techniques such as brazing or direct casting are preferable in terms of high thermal conductance. However, analyses for this duplex structure indicate that large shear stresses will appear at the tungsten-copper interface because of the difference in the thermal expansion coefficients of the two materials. The data base for the interface bond properties is small. To obtain the information on the properties of the bonded interface, mechanical and thermal cycle tests on fatigue properties at the interface of the tungsten-copper duplex have been conducted.

2. MATERIALS DATA BASE

2.1 Database system

The materials properties for Type 316 stainless steel and its related alloys appeared in open literatures have been evaluated and compiled in the FMDB-J database system. The system for fusion reactor materials data has been developed based on the database management system, PLANNER of computer system FACOM-M380 at JAERI. The materials data compiled in the system include tensile, creep, fatigue, crack growth, swelling and irradiation creep as well as fundamental physical and chemical properties. In the FMDB-J database system, the materials property data are expressed in property name and relevant numerical values as functions of experimental variables specifying specimen preparation, irradiation and test conditions. The variables are further expressed in the variables name and numerical values. Thus, the materials property is related to its numerical values with the variable names, and the data are stored interrelatedly in the form of data-table sets [9]. The data are entered into the system by a question-answer way using TSS terminal; numerical values given in figures are input with a tablet digitizer. Therefore, any property of specified materials is retrieved as a function of any specified experimental variables. The retrieved data are superposed after unit conversion, if necessary, on the CRT screen. Then, the materials property data from various data sources are efficiently displayed as a function of any specific variables.

2.2 Structural material

In Type 316 stainless steel as a blanket structural material, tensile, swelling, creep and fatigue properties are examined for lifetime prediction with FMDB-J database system. Tensile strength of the steel is increased by neutron irradiation at temperatures below 500°C. The coldworked steel is expected to have total elongation of larger than 2% in tensile testing after neutron irradiation when the irradiation and testing temperature is limited below 500°C, even if the steel contains high concentration of nuclear transmuted helium[10].

The swelling data for cold-worked 316 steel irradiated at relatively high temperature ($\geq 450^\circ\text{C}$) are fairly well compiled in FMDB-J. An example of the swelling data is presented in Fig. 1 for 450°C irradiations; the data for the samples irradiated at temperatures of 425 to 475°C are plotted in the figure. The fluence dependence of swelling can conveniently be described as a low-swelling transient period followed by an acceleration at a regime of linear swelling [11]. Furthermore, the swelling is little affected by nuclear transmuted helium at least at temperatures below 500°C, i.e. the data produced by experimental fast reactors can be used for predicting the

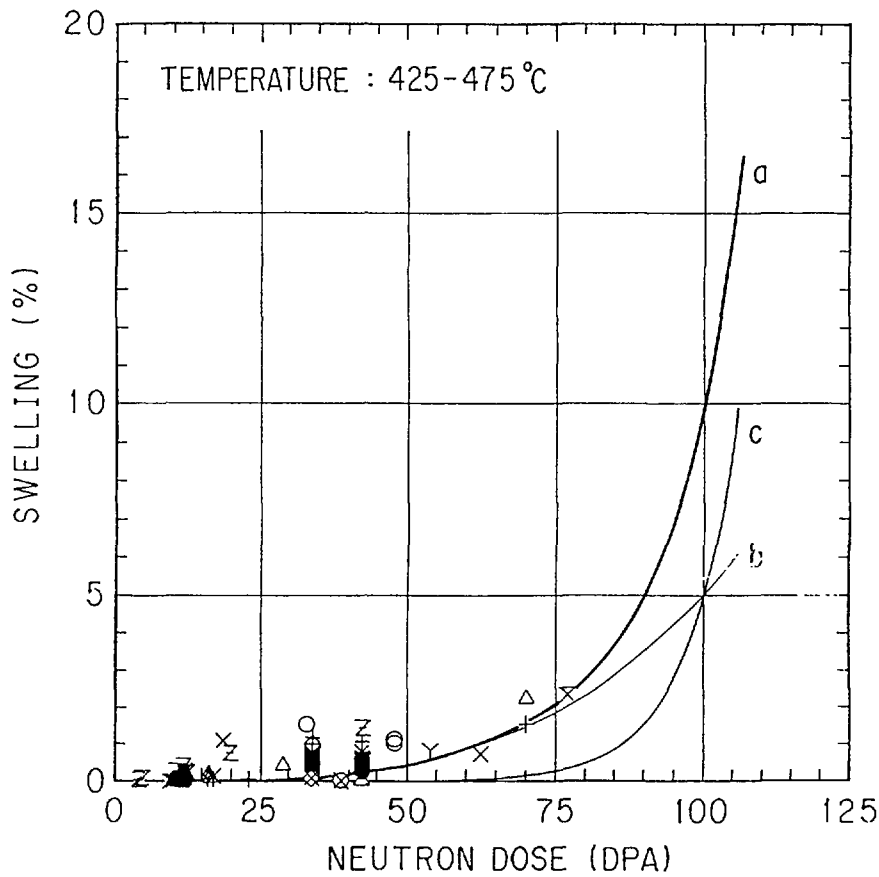


Fig. 1 Swelling as a function of neutron dose with fitting curves for 20% cold-worked Type 316 stainless steel.

$$(a) S = S_1 + S_2$$

$$(b) S_1 = 1.54 \times 10^{-12} \cdot \exp\left(\frac{T}{35.5}\right) \cdot D^{3.5}$$

$$(c) S_2 = 5.94 \times 10^{-11} \cdot \exp\left(\frac{T}{46.3}\right) \cdot D \cdot \exp(0.108 \cdot D)$$

$$T = 450$$

swelling behavior in fusion reactor environment. As the minor elements in 316 steel have been properly adjusted to alleviate the swelling, old data at low fluences are accounted to be overestimated at present. With above considerations, the swelling S (%) is assumed to be described as a function of dpa D ,

$$S = A \cdot D^n \quad . \quad (1)$$

The temperature dependent coefficient A and exponent n are determined with swelling data for 350, 400, 450, 500 and 550°C. Thus, the stress-free swelling of cold-worked 316 steel is expressed by

$$S = 1.54 \times 10^{-12} \cdot \exp\left(\frac{T}{35.5}\right) \cdot D^{3.5} \quad (2)$$

at temperature T , ranging from 350 to 550°C. The swelling given by eq.(2) represents the minimum value. The swelling data at temperatures of 450 to 550°C indicate that the swelling is in a transient region at around 70 dpa. The swelling curves given by eq.(2) are smoothly extrapolated to a regime of linear swelling by adding a term,

$$5.94 \times 10^{-11} \cdot \exp\left(\frac{T}{46.3}\right) \cdot D \cdot \exp(0.108 \cdot D) \quad (3)$$

at least, to a swelling of 15%. The swelling given by

$$S = 1.54 \times 10^{-12} \cdot \exp\left(\frac{T}{35.5}\right) \cdot D^{3.5} + 5.94 \times 10^{-11} \cdot \exp\left(\frac{T}{46.3}\right) \cdot D \cdot \exp(0.108 \cdot D) \quad (4)$$

is considered to represent the maximum value at high fluences (>70 dpa). The swelling curves given by eqs. (2)~(4) are drawn in Fig. 1. The swelling curves of eq.(4) are shown in Fig. 2 for temperatures of 350 to 550°C with measured data compiled in FMDB-J. It is noted that only a few swelling data are available at high dpa, especially no data are seen in the figure for examining the validity of eq.(4) at temperatures below 450°C.

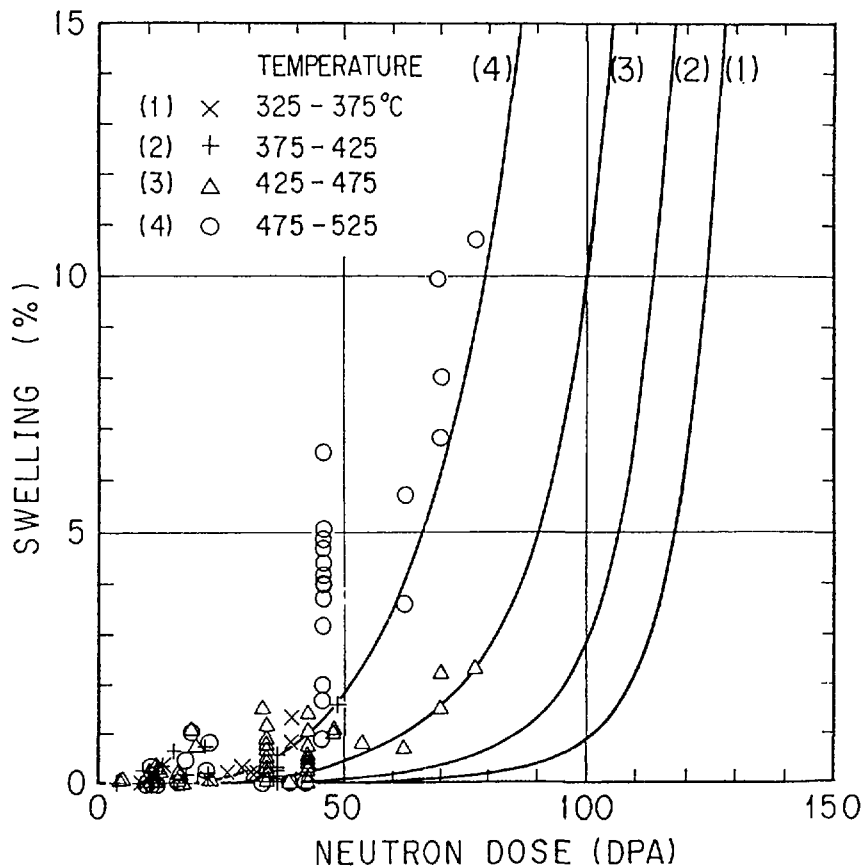


Fig. 2 Swelling as a function of neutron dose with fitting curves at temperatures of 350 to 500°C for 20% cold-worked Type 316 stainless steel.

Irradiation creep is almost independent of temperature but influenced by swelling. Thus, the creep strain ϵ under a constant stress σ (MPa) is expressed by the following equation,

$$\epsilon/\sigma = B \cdot D + C \cdot S \quad (5)$$

where, B and C are constants, D the neutron dose [12]. Irradiation creep data for cold-worked 316 steel compiled in FMDB-J can be fitted to eq. (5) with $B = 1 \times 10^{-6} \text{ MPa}^{-1} \text{ dpa}^{-1}$ and $C = 3 \times 10^{-5} \%^{-1} \text{ MPa}^{-1}$; the irradiation creep data at temperatures of 450 and 550°C compiled in the system are also fitted with the constants. An example is shown in Fig. 3, where normalized creep strain is plotted as a function of neutron dose with the fitting curve. In the analysis of the irradiation creep, swelling is assumed to be described by eq.(4). The creep strains measured at high neutron doses are distributed above the fitting curve, since swelling given by eq. (4) is smaller than the value for actual specimens.

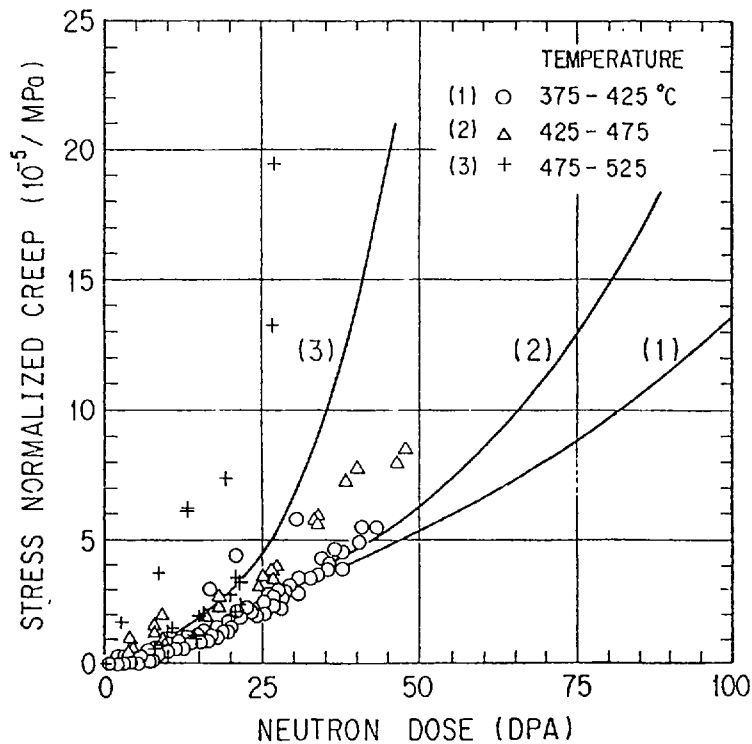


Fig. 3 Irradiation creep strain as a function of neutron dose with fitting curves at temperatures of 400 to 500°C for 20% cold-worked Type 316 stainless steel.

On the fatigue behavior, the relationship between total strain range $\Delta\epsilon_t$ and number of cycles to failure N_f was assumed to be fitted to the following form,

$$\Delta\epsilon_t = E \cdot N_f^{-0.12} + F \cdot N_f^{-0.5} \quad (6)$$

as reported by Grossbeck [13]. The coefficients E and F have been related to ultimate tensile strength and fracture ductility, respectively [14], while the ultimate tensile strength is not much

changed, the fracture ductility is decreased drastically with neutron irradiation. Then, the coefficients E and F are estimated to be 0.012 and $0.7 \cdot \exp(-0.12 \cdot D)$ respectively from the experimental data at 430 °C[13] with assumption that E is a constant whereas the F decreases exponentially with neutron dose. The equation

$$\Delta \epsilon_t = 0.012 \cdot N_f^{-0.12} + 0.7 \cdot \exp(-0.12 \cdot D) \cdot N_f^{-0.5} \quad (7)$$

can be used for failure lives to 10^6 cycles in the temperature range up to 430 °C; a fatigue-design curve for austenitic steels is used at temperatures up to 427 °C (800 °F)[15]. The fitting curves given by eq.(7) are presented in Fig. 4 along with experimental data reported by Grossbeck [15].

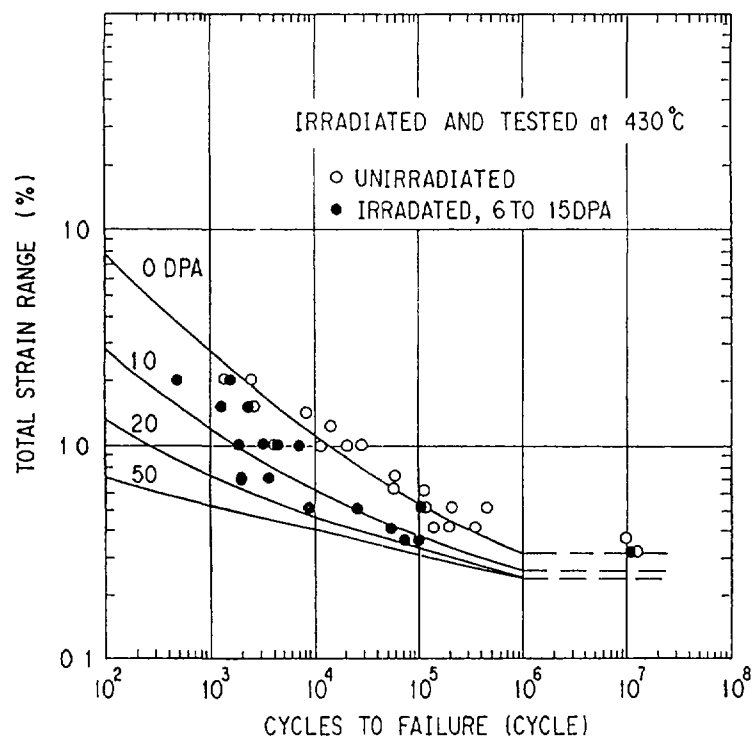


Fig. 4 Relation between total strain range and fatigue life with fitting curves at neutron dose of 0 to 50 dpa for 20% cold-worked Type 316 stainless steel.

It is expected that Type 316 stainless steel and PCA (Ti-modified 316 steel) are reasonably ductile after neutron irradiation at temperatures below 500 °C in fusion reactors, when the steel are used in cold-worked condition. As a blanket structure material, welding of the cold-worked steel should be closely examined from both the sides of blanket design and material properties. Radiation damage to the weldment and compatibility with coolants are major subjects to be investigated in the material development. It has been believed that the swelling behavior is well understood for austenitic stainless steels. However, swelling data at high fluences are required to be provided, especially the data at relatively low temperatures are urgent for the lifetime prediction of the blanket structure (Fig. 2).

Irradiation creep experiments are requested for Type 316 steel with optimized chemical composition and PCA; appreciable swelling is not expected to occur up to a dose of about 50 dpa in the steels [16]. As to fatigue properties, practically no data have been published for the lifetime prediction. Crack growth rate is required to be measured at least after irradiation to high fluences. With so-called fission-fusion correlation, the effects of nuclear transmuted helium on materials properties are considered to be carefully examined; high concentration helium in austenitic stainless steel irradiated in HFIR may alleviate degradation of materials properties as compared with fusion reactor irradiations [17].

2.3 Heat sink material

Oxygen-free high-conductivity (OFHC) copper is adopted as a heat sink material of divertor and its swelling, creep and fatigue properties are considered in the lifetime prediction.

Based on the experimental data [18-21] given in Fig. 5, the dose dependence of swelling is assumed to be independent of temperature. With the theoretical temperature dependence proposed by Gomolinski and Brebec [22], swelling $S(\%)$ is expressed by

$$S = 0.85 \cdot D \cdot \exp\left[-\left(\frac{T - 362}{126}\right)^2\right] \quad , \quad (8)$$

as function of neutron dose $D(\text{dpa})$ and temperature $T(^{\circ}\text{C})$.

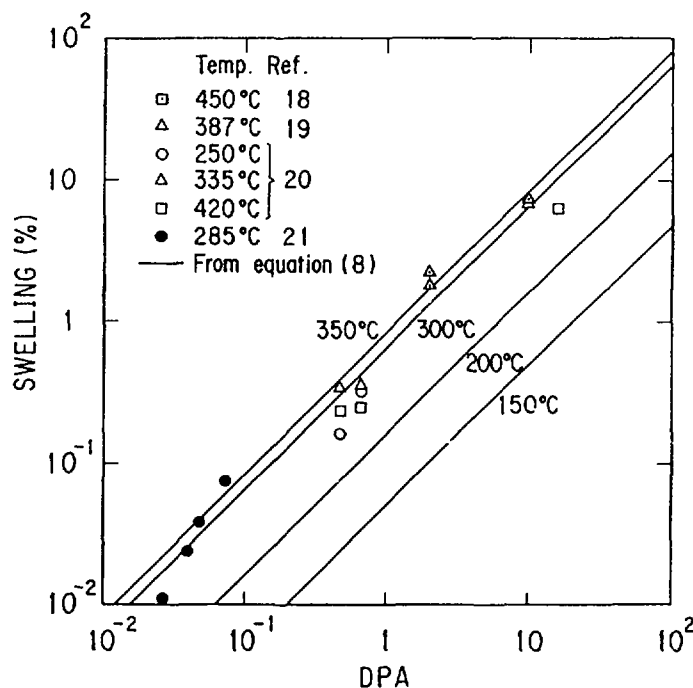


Fig. 5 Swelling as a function of neutron dose for copper.

Thermal creep is appreciable in copper above 100°C . Irradiation creep rate is expected to be smaller than the thermal creep rate. The relationship of steady state creep rate $\dot{\epsilon}$ to externally applied stress $\sigma(\text{MPa})$ is fitted to experimental data [23] by following equation,

$$\dot{\epsilon} = 10^{-6} \cdot [1.853 \times 10^{-3} \cdot \sigma \cdot \exp\left(\frac{T}{68.92}\right)]^{\frac{4.08 \cdot 2}{T}} \quad . \quad (9)$$

The fatigue properties are expected to be a little affected by neutron irradiation in the creep regime by analogy of type 316 stainless steel [24]. It is, on the other hand, experimentally showed that there is no significant change in fatigue life at temperatures up to 200°C [25]. Then, the fatigue property of irradiation copper at temperatures of 100°C to 200°C is presumed to be little different from the property of unirradiated copper at room temperature, though fatigue data is not available for irradiated copper. The total strain range $\Delta\epsilon_t$ is related to the number of cycles to failure N_f in annealed copper [26] by

$$\Delta\epsilon_t = 1.758 \cdot N_f^{-0.7} + 0.0075 \cdot N_f^{-0.1} \quad (10)$$

Irradiation data on swelling, creep and fatigue below 200°C are required to reduce uncertainty.

2.4 Divertor armor material

In the present work, tungsten is used as an armor material of divertor at temperatures below 300°C. Though the data of tungsten is not enough for prediction of swelling in tungsten at present [27-31], the swelling, at least up to the neutron dose of about 20 dpa, is presumed not to cause serious influence on the lifetime prediction.

Thermal creep is not considered to cause appreciable strain in tungsten at temperatures below 300°C. Furthermore, the dose rate is low in heavy element of tungsten. Thus, the creep would not inflict any damage on tungsten.

The equation of fatigue life in unirradiated tungsten at 300°C is expected to be not much different from that at room temperature. The equation is experimentally [32] given by

$$\Delta\epsilon_t = 0.05124 \cdot N_f^{-0.620} + 0.007425 \cdot N_f^{-0.053} \quad (11)$$

where $\Delta\epsilon_t$ is total strain range, and N_f is number of cycles to failure. The fatigue life may be reduced by neutron irradiation.

It is necessary to evaluate irradiation data on swelling, creep and fatigue below 300°C for the lifetime analysis in the future.

3. ONE-DIMENSIONAL LIFETIME ANALYSIS

3.1 Methods of analysis

For a wide variety of operating conditions and design parameters a one-dimensional computer code has been developed to obtain a comprehensive understanding about the influence of critical material properties and their change resulting from radiation damage and the synergistic effects on lifetime predictions of first wall and divertor components. An inelastic stress analysis has been performed based on the plate model [4] in which the plate is constrained from bending, but is free to expand. The code is capable of analyzing the stress in a plate composed of either a single or duplex material structure. The flow diagram of the code is shown in Fig. 6.

The lifetime analysis is focused on the first wall and the divertor plate for a pulsed-operation experimental reactor, and on the first wall for a steady state operation power reactor. The operation conditions and design parameters for a reference case are listed in Table 1. The high heat flux for an experimental reactor corresponds to localized power deposition to the wall due to rippled-induced losses of highly energetic ions. The nuclear heating and the damage

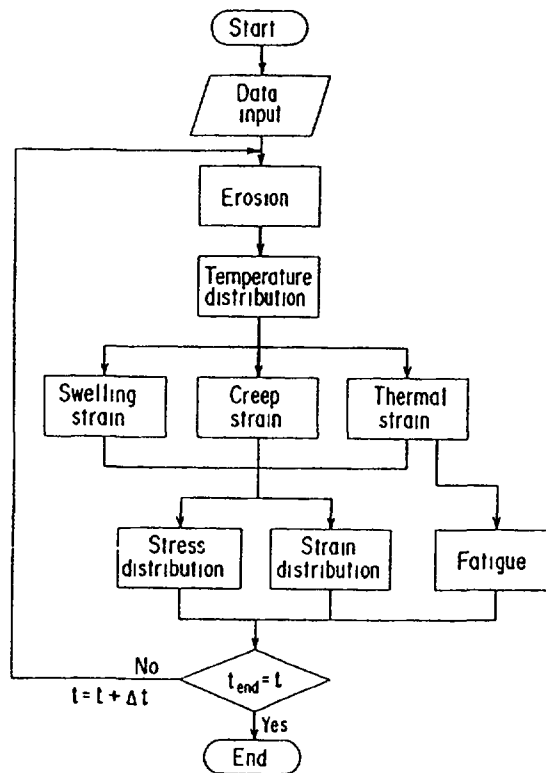


Fig. 6 Flow diagram of lifetime analysis code for a plate model.

Table 1 Operation conditions and design parameters for reference cases.

Parameter	F/W of ER *	F/W of PR *	Div of ER
Neutron wall loading (MW/m ²)	1	3	1
Surface heat flux (W/cm ²)	12.5~100	75	200
Burn time (s)	2000	Steady state	2000
Reactor cycles (y ⁻¹)	1.58 x 10 ⁴	20	1.58 x 10 ⁴
Coolant	Water	Water	Water
Coolant temperature (°C)	100	320	50
Coolant pressure (MPa)	1.5	15	1.5
Material	20% CW316SS	20% CW316SS	Armor Tungsten Heat sink Copper
Thickness (mm)	5	1.5	Armor 2 Heat sink 2.5
Coolant tube	5mm x 10mm	10mm #	15mm #
Coolant velocity (m/s)	3	5	6
Heat transfer coefficient (W/cm ² K)	198	3.49	2.41
Membrane stress (MPa)	x 3.0+50 y 0.25+50	x 58.5 y 21.7	x 5.36 y 1.93

* ER Experimental reactor, PR Power reactor

rates corresponding to 1 MW/m^2 are shown in Table 2. Material properties data other than those described in Sec. 2 were adopted from ASME Section III [33] and some handbooks [23, 34-35].

Table 2 Nuclear heating and damage rates corresponding to 1 MW/m^2 .

Material	Heating rate (W/cm^3)	Damage rate (dpa/y)
316 SS	10	9.47
Copper	9.9	10.3
Tungsten	20.6	2.77

3.2 Results and discussions

(1) First wall

The sensitivity of the predicted lifetime to first wall thickness, erosion rate and burn time for pulsed-operation conditions of the experimental reactor is shown in Fig. 7. The material temperature during plasma-off conditions is assumed to be the coolant temperature (100°C). The lifetime is governed by the erosion and fatigue damage. We define an erosion limit by the minimum wall

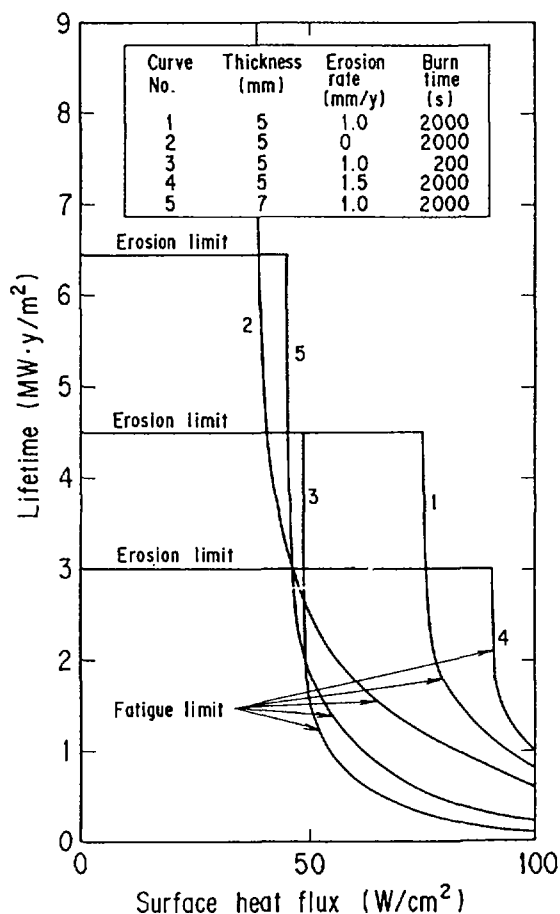


Fig. 7 Predicted lifetime of the first wall for the experimental reactor as a function of surface heat flux.

thickness in which the stress due to the internal coolant pressure meets the allowable stress. According to ASME Code, the allowable stress given by 1.5 S_m is 350 MPa for 20% cold worked 316 stainless steel, which requires a minimum thickness of 0.55 mm based on the beam theory. The impact of creep and swelling to be expected at high heat fluxes (i.e. high temperatures) does not appear, since the lifetime is determined by the fatigue damage at low irradiation fluences. At high heat fluxes where the fatigue damage is a life-limiting factor, higher erosion rates give longer lifetime.

No erosion is assumed in the lifetime analysis of the power reactor first wall. Major stress in the initial operation are the thermal stress and the membrane stress due to the internal pressure of coolant. The thermal stress is relaxed by irradiation creep within low fluences, and at high fluences the stress due to the swelling gradient through the wall causes creep strain.

Figure 8 shows the lifetime limited by either creep strain, swelling strain, or inelastic strain for specified criteria as a function of wall thickness. The inelastic strain here is a sum of creep and swelling strains. When the wall thickness is thinner than 1 mm, the membrane stress by the coolant pressure is a major cause of creep strain, and the maximum of creep strain appears at the coolant side. In case of the wall thicker than 1.5 mm, on the other hand, the stress due to the swelling gradient is a major cause of creep strain and the maximum creep strain generated at the plasma side is compressive. In Fig. 9 the lifetime as a function of neutron wall loading is shown for specified criteria of each strain. The surface heat flux is assumed to be 1/4 of neutron wall loading.

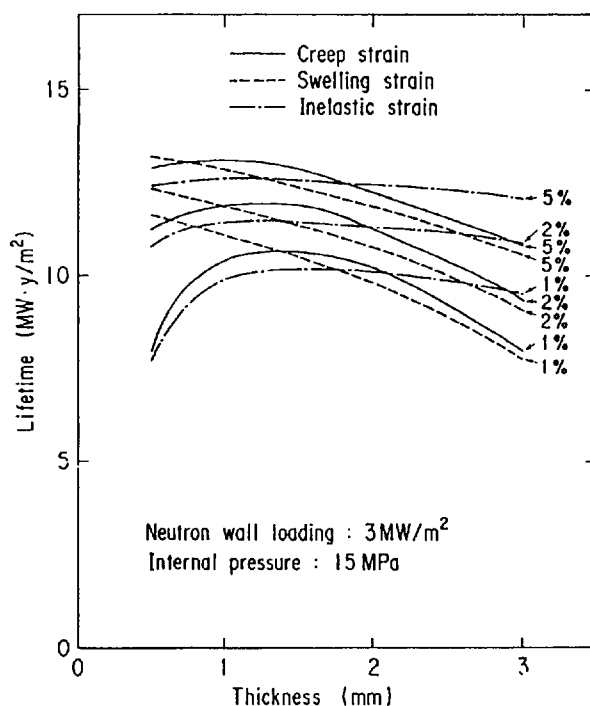


Fig. 8 Predicted lifetime of the first wall for the power reactor as a function of wall thickness.

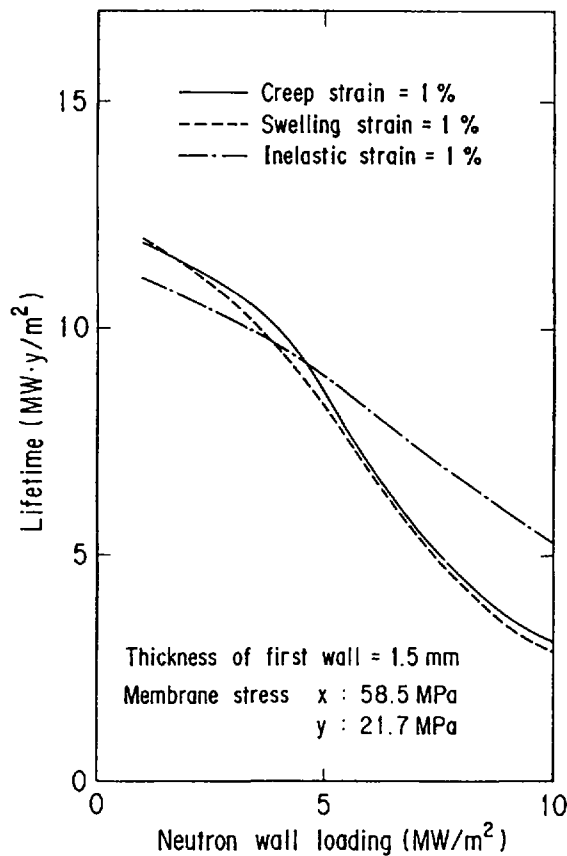


Fig. 9 Predicted lifetime of the first wall for the power reactor as a function of surface heat flux.

In the ASME Code Case N-47 [36], the strain limits (average through thickness: 1%, surface: 2%, local: 5%) are given for the accumulated inelastic (plastic and thermal creep) strain of the components served at elevated temperatures ($>427^{\circ}\text{C}$). In the present analysis, however, irradiation creep and swelling strains at the surface (coolant side) appear even at low temperatures ($<427^{\circ}\text{C}$). If those strains correspond to the inelastic strain in the ASME Code, another criteria taking account of the creep rupture time under neutron irradiation is required.

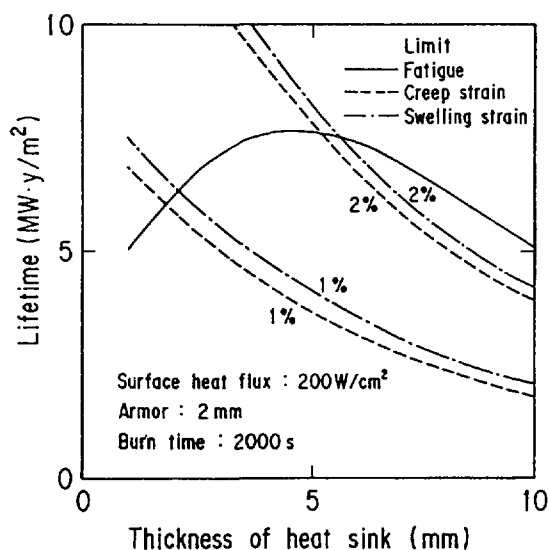


Fig.10 Predicted lifetime of the divertor plate for the experimental reactor as a function of heat sink thickness.

(2) Divertor plate

Lifetime predictions of the divertor plate with the duplex structure composed of tungsten armor and copper heat sink are performed. In Figs. 10 and 11, predicted lifetimes as a function of the thickness of heat sink and as a function of the thickness of armor are shown, respectively. The temperatures of two materials during plasma-off conditions and the initial stress-free temperature are assumed to be a coolant temperature of 50°C.

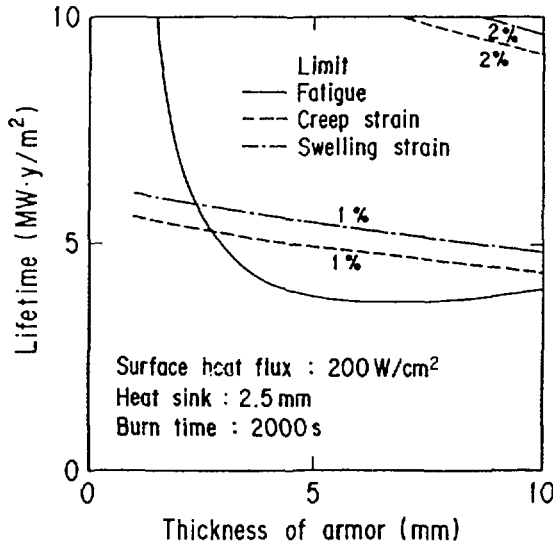


Fig.11 Predicted lifetime of the divertor plate for the experimental reactor as a function of armor thickness.

The lifetime analysis for the normal operation indicates that the fatigue damage of the tungsten armor due to the thermal stress is not accumulated and that the lifetime of this divertor is determined by the thermal fatigue of the copper heat sink. As shown in Fig. 10, for the surface heat flux of 200 W/cm², the maximum lifetime limited by the fatigue damage appears at the heat sink thickness of 4.5 mm when the thickness of armor is 2.0 mm. On the other hand, the minimum lifetime limited by the fatigue damage appears at the armor thickness of 6.5 mm when the thickness of heat sink is 2.5 mm as shown in Fig. 11. Lifetime limited by either the creep strain or the swelling strain decreases monotonously as either the thickness of heat sink or armor increases, since the distance from the coolant and nuclear heating raise the temperature at the interface. Inelastic strain in the copper heat sink, however, is small since the tungsten armor having very low creep rate and low swelling level constrains the deformation of the copper heat sink. In other words, creep strain rapidly occurs in the opposite direction to swelling strain in copper heat sink to relax the stress generated by swelling.

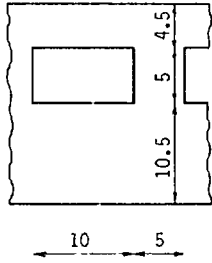
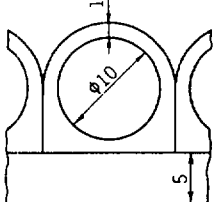
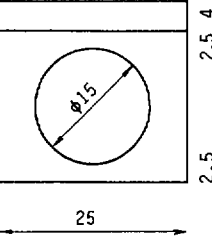
As shown in Figs. 10 and 11, the copper suffers damage from fatigue and creep simultaneously. Thus, the lifetime of the divertor must be discussed by the fatigue and creep damage in the copper heat sink, if the lifetime should be evaluated according to ASME Code Case N-47[36]. Since experiments in copper [25] and in Type 316 stainless steel [37] show that compression creep affects little on fatigue life, the contribution of creep to the fatigue and creep damage is considered to be small in the present design condition. However, it may be necessary to discuss the allowable creep strain from the viewpoint of rupture.

4. TWO-DIMENSIONAL ELASTIC-PLASTIC STRESS AND STRAIN ANALYSIS

4.1 Methods of analysis

In previous section, inelastic strains have been calculated by one-dimensional plate model considering the effects of thermal strain, internal pressure, irradiation creep, and swelling. When yielding occurs in the material, elastic-plastic analysis is required. In this section, elasto-plasticity and two-dimensional effects are analyzed by the finite element method to discuss in detail failure mechanisms in the first wall and divertor.

Table 3 Conditions for two-dimensional elastic-plastic analysis.

	first wall of experimental reactor	first wall of power reactor	divertor of experimental reactor
analysis model (unit. mm)			
Young's modulus	180 GPa	165 GPa	400 GPa (W) 120 (Cu)
Strain hardning modulus	2.3 GPa	2.1 GPa	1.2 GPa (Cu)
Yield stress	174 GPa (200°C)	161 GPa (400°C)	50 GPa (Cu) (200°C)
disruption condition	8.5 kW/cm ² 15 ms	—	54 kW/cm ² 5 ms

Configurations and conditions of the analysis are shown in Table 3. Conditions are the same as those in Sec.3 unless mentioned. Total strain ϵ^t is expressed as follows,

$$\epsilon^t = \epsilon^e + \epsilon^{in} + \epsilon^{th} \quad (12)$$

and

$$\epsilon^{in} = \epsilon^c + \epsilon^s + \epsilon^p \quad (13)$$

where ϵ^e , ϵ^{in} , ϵ^{th} , ϵ^c , ϵ^s , and ϵ^p are elastic strain, total inelastic strain, thermal strain, irradiation creep strain, swelling strain, and plastic strain, respectively. Elastic-plastic analysis is performed with ADINA code [38], where flow theory of plasticity, von Mises yield condition, kinematic hardning rule for stainless steel, isotropic hardening rule for copper, and BFGS equilibrium iteration method are used. It has been modified to consider irradiation creep and swelling strains, which are divided into both

normal and shear components from uniaxial strains by

$$\dot{\epsilon}_{ij}^c = \frac{3\dot{\epsilon}^c}{2\bar{\sigma}} \sigma'_{ij} \quad , \quad (14)$$

and

$$\dot{\epsilon}_{ii}^c = \dot{\epsilon}^s \quad \left(= \frac{S}{3} \right) \quad , \quad (15)$$

where $(\dot{})$, $\bar{\sigma}$, and σ' mean time derivative, equivalent stress, and deviatoric stress, respectively.

In the first wall analysis, yield strength data [39] for annealed stainless steel are adopted to examine the plastic behavior at high heat loads and high irradiation fluences.

4.2 Results and discussions

(1) First wall

Figure 12 shows the inelastic strain component change at the plasma side of the first wall of experimental reactor during the pulsed operation. Plastic strain occurs at the beginning of the operation, and it remains unchanged during the operation because the applied loads are constant. The stress relaxation appears by irradiation creep at an early stage ($\sim 2 \text{ MW}\cdot\text{y}/\text{m}^2$). Fluences higher than around $3 \text{ MW}\cdot\text{y}/\text{m}^2$ generate swelling strain which increases with fluence. This swelling strain causes irradiation creep strain in reverse direction (compression) to the swelling strain. The swelling and irradiation creep strains increase with heat flux because material temperature increases with heat flux, for example, 423°C for $100 \text{ W}/\text{cm}^2$, 277°C for $50 \text{ W}/\text{cm}^2$, and 154°C for $12.5 \text{ W}/\text{cm}^2$.

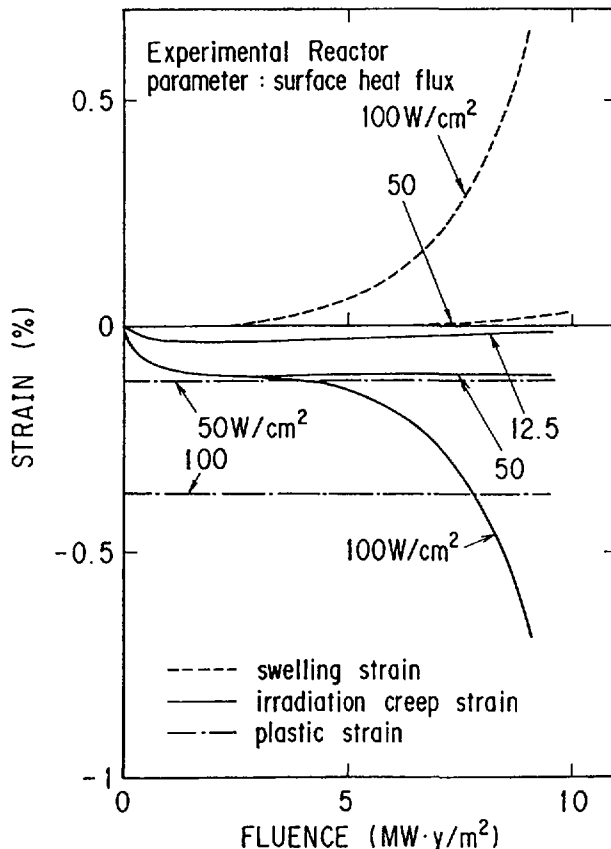


Fig.12

Inelastic strain component at the plasma side of the experimental reactor first wall as a function of fluence.

According to ASME Code Case N-47 [36], accumulated total inelastic strain has to be limited for structural integrity. But in the case of the experimental reactor first wall where the heat load is dominant, large tensile swelling strain and large compressive irradiation creep and plastic strain produce smaller total inelastic strain through their cancelation. Since irradiation creep strain and plastic strain will yield damage in the material, each inelastic strain component, namely creep and plastic strains as well as total strain, has to be limited. The swelling strain should be limited since it causes an extra stress in the material. Elastic-plastic analysis is preferable to elastic analysis to evaluate creep strain since elastic analysis predicts larger stress level and excessive creep strain. In this analysis, each strain component is small enough to meet strain limit of 1% up to 10 MW.y/m². The reason comes from the use of creep and swelling data for cold worked stainless steel first wall.

Strain and stress history at the plasma side of the first wall after plasma disruption is shown in Fig. 13. Compressive stress and compressive plastic strain occur initially by the plasma disruption heat load, and then the stress turns to tensile after the occurrence of the plasma disruption because of plastic deformation. The stress relaxation resulting from the appearance of tensile creep strain occurs during the subsequent normal operation. If a disruption occurs after the stress relaxation has finished, the same value of strain will be accumulated as ratchetting strain enhanced by irradiation creep. But only a part of inelastic strain will be accumulated for the experimental reactor conditions in which plasma disruptions are

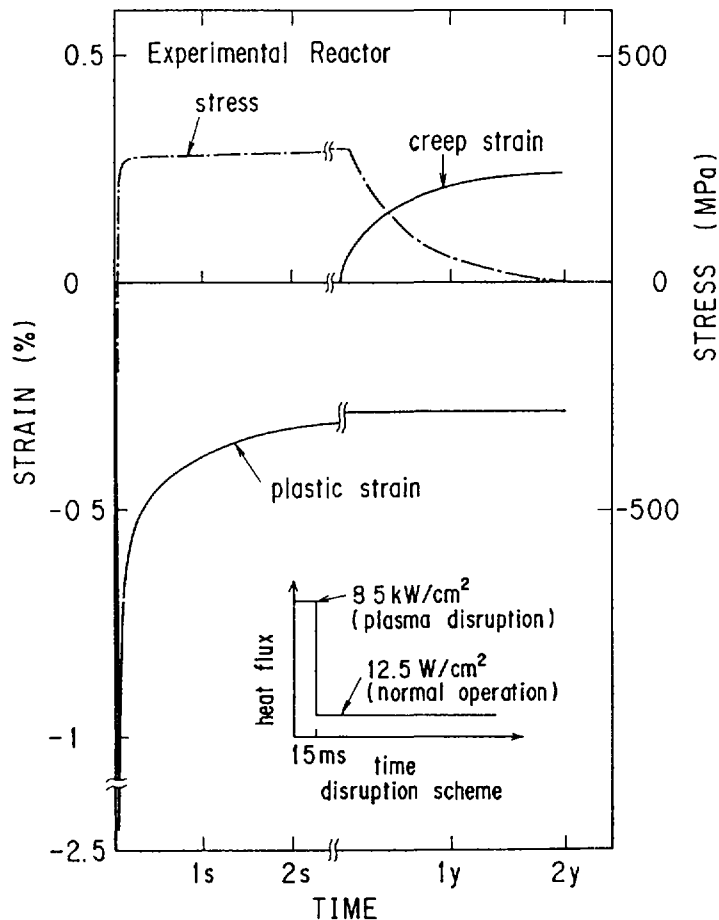


Fig.13

Strain and stress history at the plasma side of the first wall after plasma disruption.

supposed to occur relatively frequently before the stress relaxation completes. Since the plastic strain and creep strain appear in reverse direction each other, as discussed in normal operation case, each inelastic strain component has to be limited. In case of the elastic analysis, stress and strain caused by plasma disruption vanish after plasma disruption. To evaluate residual stress, plastic strain, and irradiation creep strain which are important for the lifetime prediction, elastic-plastic analysis is inevitable.

Figure 14 shows swelling and irradiation creep strains history at the plasma side of the power reactor first wall during the normal steady state operation. The swelling strain increases with neutron wall loading because of increasing temperature. The tensile irradiation creep strain in the figure is caused by the internal pressure, but at high fluences it turns to compression due to compressive stress produced by swelling difference through the wall. The plastic strain is not pronounced because relatively high yield stress [39] is used in the analysis. Results obtained for different wall thicknesses indicate that the effect of thickness is almost the same as those in one-dimensional analysis.

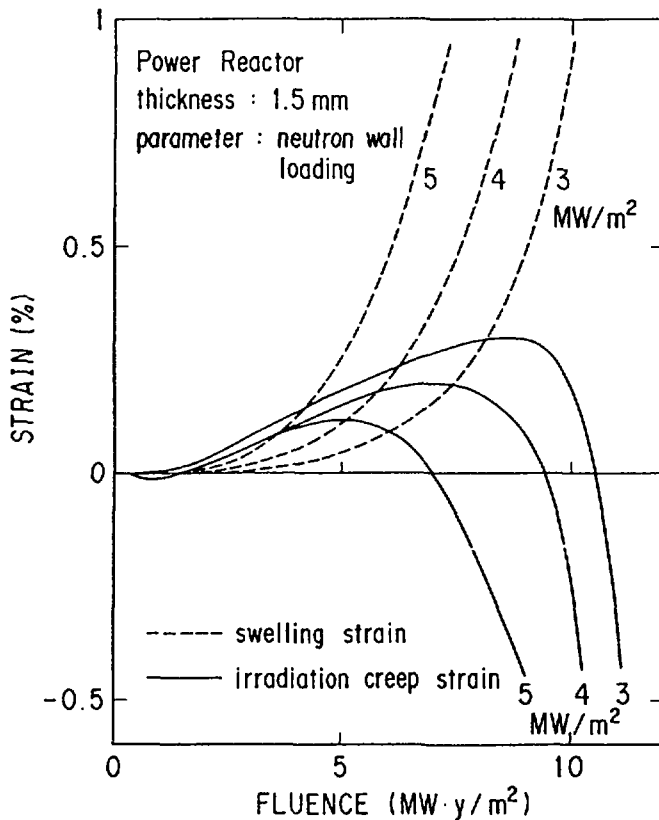


Fig.14

Swelling and irradiation creep strains at the plasma side of the power reactor first wall as a function of fluence.

Finally it should be noted that for the discussion of allowable minimum wall thickness by erosion it is necessary to evaluate membrane stress increase, buckling by disruption heat load, and break through of the crack. Consideration on these problems will be needed as a further work.

(2) Divertor plate

In the duplex structure (armor/heat sink), a large thermal stress due to the difference of the thermal expansions is caused at the interface and is one of the important factors for the lifetime prediction of the divertor plate. The lifetime of the divertor may be

limited by the stress if the failure of armor dose not restrict the lifetime. The amount of the stress is also dependent upon the difference between the stiffnesses of two materials (e.g. Young's modulus, bending stiffness).

Under the normal operating thermal load, the temperatuare at the interace is almost independent of the armor thickness, but the structure with thin armor gives a smaller thermal stress in copper near the interface than that with thick armor, due to the difference in the stiffness between two materials. At a plasma disruption, on the other hand, the increment of the surface temperature of the armor is not dependent on the armor thickness, and hence the thermal stress caused in the structure with thick armor does not become large since the heat capacity of the armor is large.

Here, the thermo-elastic-plastic stress analyses have been performed to examine the above characteristics and to predict the lifetime of the copper heat sink by taking account of two-dimensional deformation and the thermal loads at cyclic normal operation and plasma disruption. The surface heat flux at the normal operation is 200 W/cm^2 . The heat flux at plasma disruption is 54 kW/cm^2 [1] with the decay time of 5 msec, which is assumed to be constant during 5 msec. The coolant temperature is 50°C . The thicknesses of copper at plasma side and tungsten are 2.5 mm and 4.0 mm, respectively. In this case, the fatigue lifetime of copper is estimated to be around minimum from the one-dimensional analysis as shown in Fig. 11.

Figure 15 shows the shear stress-strain history under the thermal loads at normal operation and at plasma disruption, respectively. A large plastic strain appears during the first operation cycle because of the low yield strength of copper (50 MPa). Since the copper is assumed to be an isotropic work hardening material, however, copper deforms elastically in the range of shakedown after the first few

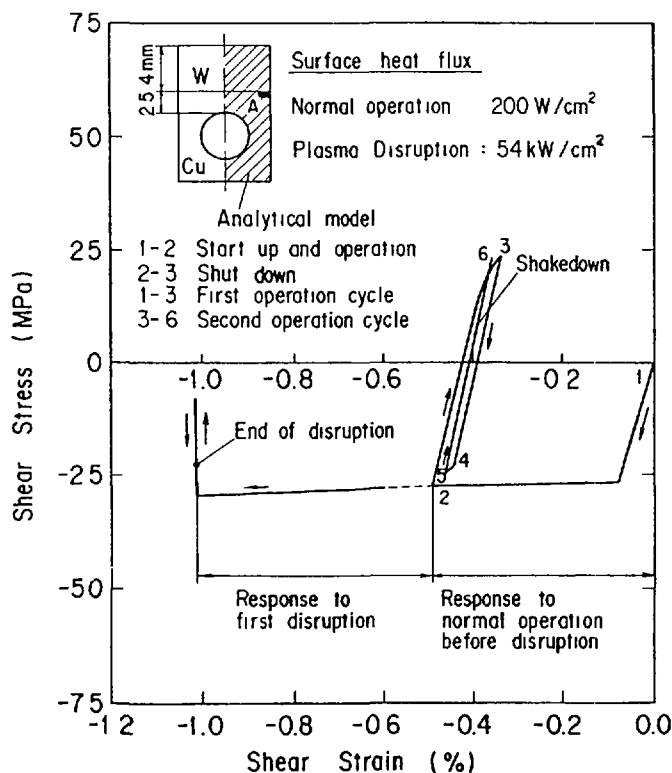


Fig.15

Shear stress strain history in copper at interface near edge (Point A) under two normal operation thermal load and first plasma disruption thermal load.

operation cycles. By the two-dimensional deformation obtained from the analysis, a large shear strain appears in copper at the interface near the edge. The equivalent strain range [36] at that point is used to evaluate the fatigue lifetime. From the fatigue curve of copper used in one-dimensional analysis, for the long burn time of 2000 sec the lifetime is larger by about one order than values estimated by one-dimensional analysis since the strain used for the lifetime is obtained by two-dimensional elastic-plastic analysis and the equivalent strain range is used. Therefore, one-dimensional analysis is not adequate for the lifetime evaluation of the divertor since the amount and direction of the strain components are affected by the two-dimensional deformation and/or the shakedown behavior of the copper.

After the plasma disruption, the temperature at the interface rises by about 50°C. The plastic strain increases as same as one of the first normal operation cycle. As mentioned previously, however, a large ratchetting strain will not increase after the first plasma disruption. It should be noted that the lifetime of copper will be limited by the time dependent inelastic strain (thermal creep, irradiation creep and swelling strains) for the long burn time operation.

From the results obtained by these analyses, the fatigue lifetime of copper dose not reduce significantly with the increase of the armor tungsten thickness. The optimum thickness of armor should be determined by taking account of the fatigue damage of copper for the short burn time operation (<200 sec) and by taking account of the inelastic strain (plastic strain, thermal and irradiation creep strains and swelling strain) in the copper heat sink for the long burn time operation. Among them, since the plastic strain depends upon the yield strength, the use of copper alloy with high yield strength is preferable for the divertor heat sink material.

5. FATIGUE EXPERIMENTS FOR TUNGSTEN-COPPER DUPLEX STRUCTURES

5.1 Mechanical fatigue tests

(1) Experimental procedure

The specimens used for tests consist of 99.9% purity tungsten and oxygen-free high-conductivity (OFHC) copper. Tungsten was prepared from powder metallurgy tungsten followed by a cross-rolled process at 1500°C. The bonding of tungsten and copper was carried out by brazing. The brazing filler metal is the nickel-based braze alloy (BNi-6). The silver-based braze alloy (BAG-13) was eliminated because of the poor wettability and the lower shear strength.

The static shear strength test was performed on the lap joint tensile specimens for various parameters (lap length, temperature). For example the average shear strength across the interface of the tungsten-copper lap joint is about 70 MPa for the overlap joint distance of 10 mm. The fatigue test was not conducted for the lap joint specimen, since the peak shear stresses appear at the edge of interface and make the fatigue life evaluation difficult.

The butt joint torsion specimens were prepared for the fatigue test. Figure 16 shows the specimen configuration. The solid specimen of copper was prepared to compare the fatigue life of the brazed butt joint specimen with that of copper. The torsion specimen may have a merit in regard to the simulation of shear stress distribution on the divertor plate. On the divertor plate, the shear stress at the interface fall off rapidly with distance from the edge of plate, and there is no shear stress at internal points away from the edge. The

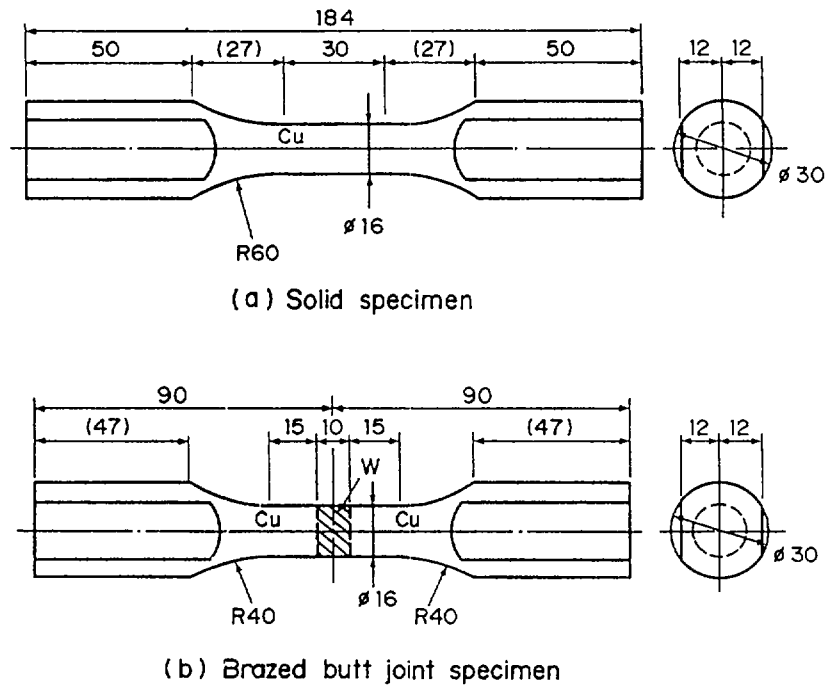


Fig.16 Torsion fatigue test specimen.

maximum stress for the torsion specimen also occurs at the boundary, and the stress decreases linearly to the value of zero at the center of the specimen.

Torsion fatigue tests have been performed in strain control utilizing a triangular wave form. Tests were performed on a servohydraulic fatigue system with the capacity of maximum torque of ± 1 kN.m and maximum torsional angle of $\pm 50^\circ$.

(2) Results and discussions

The stress response with cycles for the brazed joints is shown in Fig. 17. The brazed joints exhibit the cyclic hardening for various strain range. It is thought that both tungsten and Ni brazed metal of specimen are in an elastic stress-strain state, and the cyclic hardening of specimen occurs mainly in OFHC copper annealed by the brazing process.

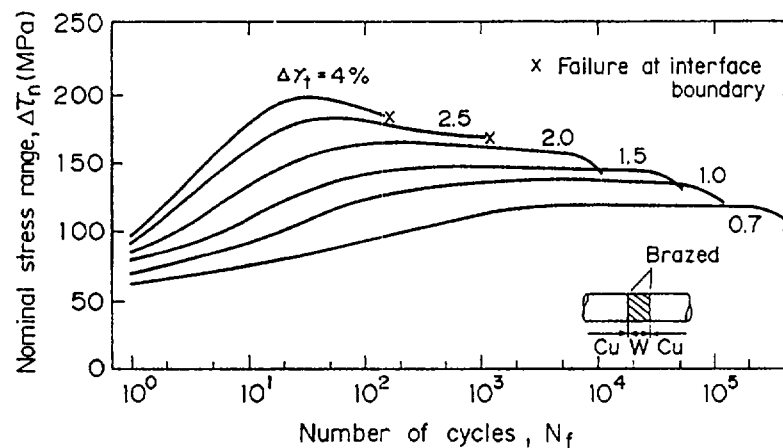


Fig.17 Stress response to cycles for brazed joint tested at various strains.

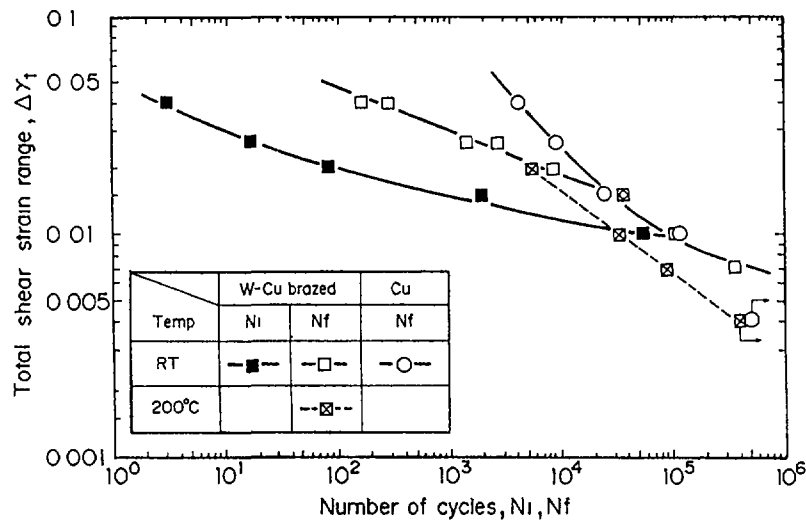


Fig.18 Total shear strain range as a function of cycles to lmm crack initiation and cycles to failure for W-Cu brazed joint and copper.

The results of fatigue tests are plotted for the tungsten-copper brazed specimen and the copper solid specimen in Fig. 18. The crack initiation is generally determined at the onset of rapid reduction in stress range. However, this definition could not be applied to the torsional test using the solid specimen since there is little change of torsional torque even with a large crack propagation. The crack initiation life of the solid specimen was defined by the crack propagation of 1 mm length on the surface of the specimen. The failure life was defined by the onset of a reduction of 5 % torque range compared with a period of stable stress-strain behavior.

The fatigue life to failure for the brazed specimen tested at room temperature agrees well to that of the copper specimen at 5×10^4 cycles and above (a low strain range), as shown in Fig. 18. This result shows that the fatigue life of the brazed specimen in the low strain range depends on the strength of copper base metal. At 5×10^4 cycles and below (a high strain range), the fatigue life of the brazed specimen is inferior as compared with that of the copper specimen. The fatigue life of the brazed specimen in the high strain range depends on the strength of interface and tungsten base metal. Examinations of the crack propagation indicate that the fatigue cracks have been propagated from the interface to copper in the low strain range, and from the interface to tungsten in the high strain range.

Figure 19 shows the nominal shear stress amplitude as a function of the cycles generating 1 mm crack initiation for the tungsten-copper brazed joint. This curve is obtained from Fig. 18 in consideration of the cyclic stress-strain response curve. The shear stress amplitude for the fatigue crack initiation life of 10^4 cycles has been estimated to be 70 MPa.

The fatigue life of the interface obtained may be used for the lifetime prediction of the divertor plate. Test results imply that under thermal cycles with large strains the fatigue crack appears to be generated in the tungsten layer of the plate. As shown in Fig. 18, a large number of cycles is required from the crack initiation to

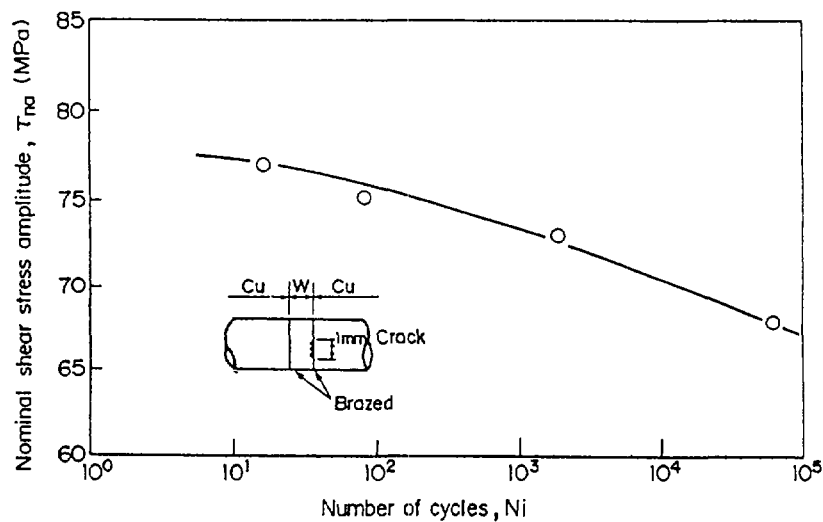


Fig.19 Nominal shear stress amplitude as a function of cycles generating 1mm crack growth for W-Cu brazed joint tested at RT.

failure for W-Cu brazed joint. The divertor plate will also have the long lifetime to failure after the crack initiation. So it will be important to evaluate crack propagation life.

5.2 Thermal fatigue tests

(1) Experimental procedure

Tungsten and copper have been successfully bonded by both means of brazing and direct casting. Direct casting is made by heating a copper rod placed on a copper-plated tungsten disk up to 1200-1300 °C. Thus, the directly casted bonds have no interlayer between tungsten and copper. Three test pieces made by silver brazing and one test piece made by direct casting were prepared for testing. A schematic drawing of the experimental apparatus used is shown in Fig. 20. The tungsten surface was heated by high temperature argon plasma flow.

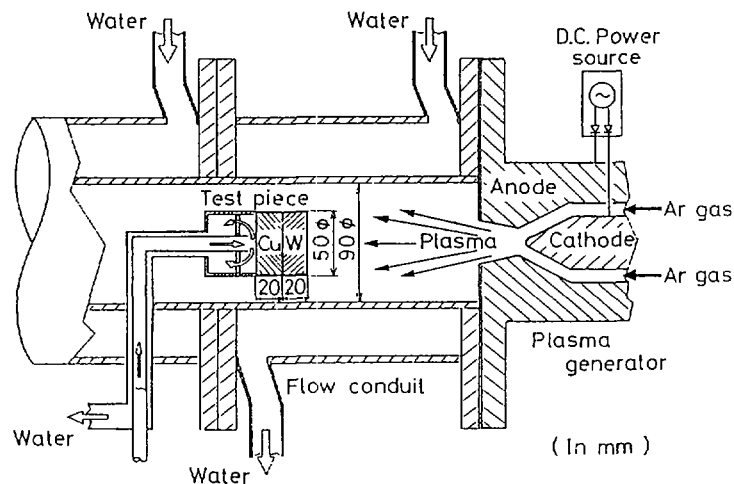


Fig.20 An experimental apparatus.

Figure 1: Schematic diagram of the test piece and its thermocouple locations. The top part shows a cross-section A-A' of a circular test piece with 12 thermocouples (TC-1 to TC-12) arranged in a grid. The bottom part shows a side view of the test piece with dimensions (67, 20, 20, 5, 10, 10, 50, 110, 150) and thermocouple locations (TC-1, TC-2, TC-3, TC-4, TC-5). The test piece is labeled 'Test piece' and 'A-A' cross section'. The side view also shows 'Water flow' direction and 'Cu' (copper) and 'W' (tungsten) components.

(2) Results and discussions

129

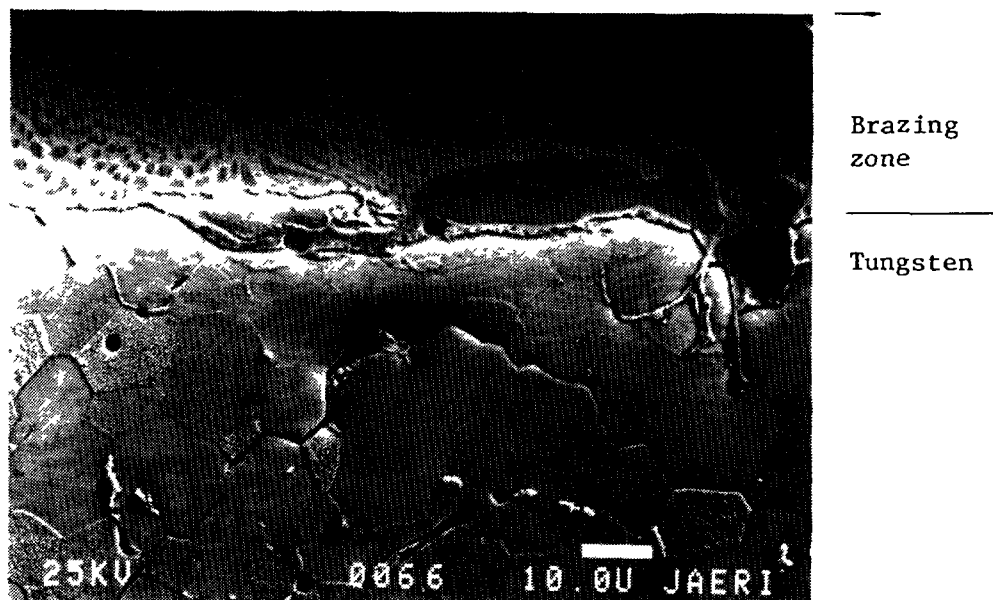


Photo 1 Microcracks found in the tungsten grain boundaries of the silver brazed test piece exposed to 1100 times of thermal cycles

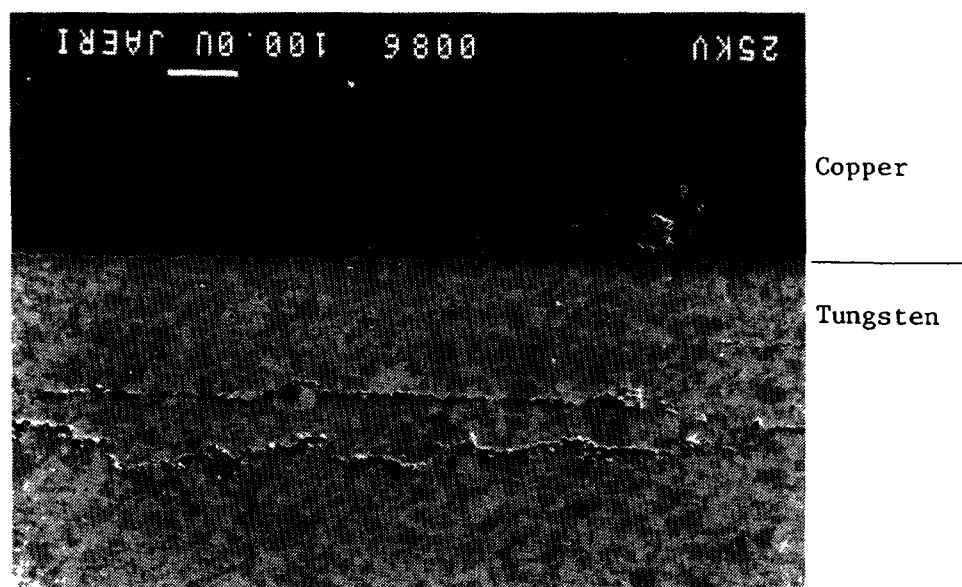


Photo 2 Large cracks found in the tungsten layer running parallel to the joint interface of the casted test piece exposed to 2200 times of thermal cycles

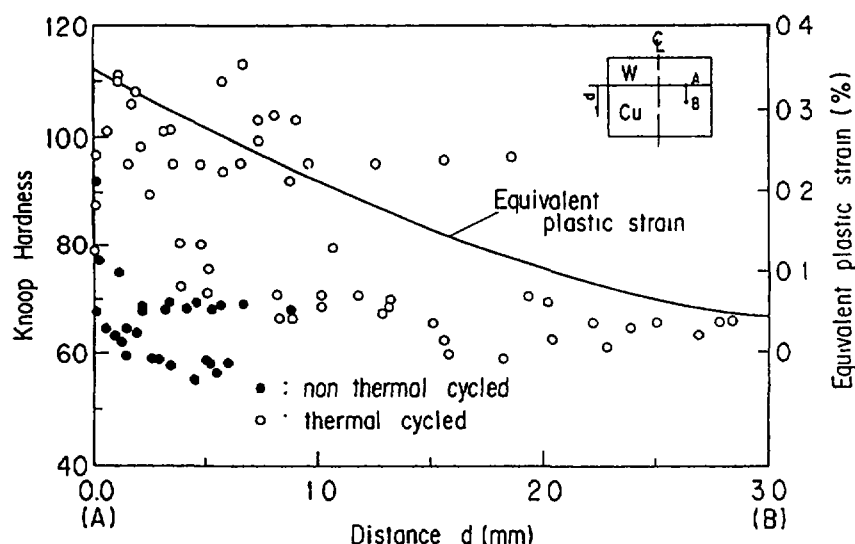


Fig.22 Knoop Hardness distribution in the copper layer of the casted test pieces and equivalent plastic strain distribution by elastic-plastic analysis.

Figure 22 shows Micro-Knoop Hardness in the copper layer adjacent to the joint interface of the casted test piece. Solid and open symbols indicate the data of non thermal cycled and thermal cycled test pieces, respectively. The solid line shows the distribution of the plastic strain which was calculated by the finite element method. The yield strength of copper is assumed to be 50 MPa in the analysis. Although the quantitative relation between the Hardness and the amount of the plastic strain of copper is not clarified at present, the qualitative agreement is observed in the distribution through the thickness of copper.

A large amount of the plastic strain is caused during the first thermal cycle. Since copper is an isotropic work hardening material, copper deforms in the range of shakedown after a few thermal cycles and a large increment of plastic strain dose not appear. The amount of the plastic strain is limited to prevent the failure due to the large deformation.

6. CONCLUDING REMARKS

- In case of the first wall of pulsed-operated experimental reactors, the lifetime is governed by erosion and fatigue damage rather than swelling or irradiation creep according to the results of the present analyses.
- From the two-dimensional elastic-plastic analysis, swelling and irradiation creep are negligible small at low irradiation fluence below 6 MW.y/m² (highest fluence adopted in experimental reactor designs [8]).
- As for the effect of plasma disruption on the first wall of the experimental reactor, compressive stress initially generated at the plasma side turns to tensile after plasma disruption because of plastic deformation. The stress relaxation by irradiation creep occurs during about 1~2 year normal operation, and disruptions

occurring during the relaxation period will enhance the ratchetting strain. To analyze these behavior the elastic-plastic model is needed.

- In case of the power reactor first wall which is subjected to high heat flux, the maximum thickness is limited by the swelling gradient through the wall rather than thermal stress, while the minimum thickness is limited by the mechanical stress caused by coolant pressure. These stresses cause irradiation creep strain.
- The two-dimensional elastic plastic stress analysis is inevitable for the lifetime evaluation of the divertor plate since the amount of the strain components for the evaluation of the fatigue damage is affected by the two dimensional deformation and the shakedown of the copper.
- The lifetime of the divertor will be limited by the fatigue damage for the short burn time (<200 sec).
- As for the tungsten-copper duplex-structure, the results obtained from mechanical tests indicate that in high strain range its lifetime is determined by tungsten failure, and in low strain range by copper failure. This fact is qualitatively understandable from the fatigue-life equations (10) and (11).
- Though microcracks are observed in tungsten side by thermal fatigue test carried out up to about 2000 cycles, there is much room for further consideration of the results obtained in low strain range (below 1%). Further tests with different strain range and with more cycles are needed.
- Among the configurations adopted in this study, the first wall and the divertor plate of the experimental reactor have two-dimensional effects, whereas one-dimensional analysis is a good approximation for the first wall of the power reactor. For normal operation, elastic analysis is a good approximation, but elastic-plastic analysis is required for the case of plasma disruption because of large plastic deformation. Especially, to evaluate the irradiation creep properly, elastic-plastic analysis is inevitable because the creep strain depends on the stress level.
- Large inelastic strain componetns can sometimes give small resultant inelastic strain through their cancelation. A problem remains to be discussed in terms of the influence of each component on failure and design criteria.

Acknowledgment

The authors would like to thanks Drs. K. Tomabechi, M. Yoshikawa and S. Tamura for their continued encouragement and advice.

References

- [1] T. Tone, et al., Fusion Technology, 8 (1985) 214.
- [2] T. Tone, et al., Proc. 3rd IAEA Technical Committee Meeting and Workshop on Fusion Reactor Design and Technology, Tokyo, Vol. I, 1981, IAEA, Vienna, (1983) 273; T. Tone et al., JAERI-M 83-031 (1983) (in Japanese).
- [3] C.K. Youngdahl, D.L. Smith, J. Nucl. Mater. 85 & 86 (1979) 153.
- [4] R.D. Watson, et al., J. Pressure Vessel Technol., 105 (1983) 144.
- [5] R.F. Mattas, Nucl. Technol./Fusion, 4 (1983) 1257.
- [6] R. Matera, et al., Nucl. Engrg. and Des./Fusion, 1(1984) 127.

- [7] A.O. Adegbulugbe, *ibid*, 301.
- [8] International Tokamak Reactor Phase One, IAEA, Vienna (1982).
- [9] S. Iwata, et al., *J. Nucl. Mater.*, 103 & 104 (1981) 173.
- [10] R. E. Gold, et al., *Nucl. Technol./Fusion* 1 (1981) 169.
- [11] P.J. Maziasz, *J. Nucl. Mater.*, 122 & 123 (1984) 472.
- [12] J.P. Foster, et al., *Proc. BNES Conf. on Irradiation Embrittlement and Creep in Fuel Cladding and Core Components*, BNES (1973) 273.
- [13] M.L. Grossbeck and K.C. Liu, *Nucl. Technol.* 58 (1982) 538.
- [14] C.R. Brinkman, et al., *ASTM STP-529* (1973) 473.
- [15] C.E. Jaske and W.J. O'Donnell, *J. Pressure Vessel Technol.*, 99, (1977) 584.
- [16] M. Koyama, et al., 1983 Fall Meeting of the Atomic Energy Society of Japan, H3.
- [17] R.E. Stoller and G.R. Odette, *J. Nucl. Mater.*, 103&104 (1981) 1361.
- [18] H.R. Brager, et al., *HEDL-SA-3174* (1984).
- [19] R.J. Livak, et al., *Trans. Amr. Nucl. Soc.*, 49 (1985) 106.
- [20] M. Labbe and J.P. Poirier, *J. Nucl. Mater.* 46 (1973) 86.
- [21] J.L. Brimhall and H.E. Kissinger, *Radiation Effects* 15 (1972) 259.
- [22] M. Gomolinski and G. Brebec, *J. Nucl. Mater.*, 43(1972) 59.
- [23] *Metals Handbook*, Ninth Edition "Volume 2, Properties and Selection: Nonferrous alloys and Pure Metals," American Society for Metals, Metals Park, Ohio (1979).
- [24] M.L. Grossbeck and K.C. Liu, *J. Nucl. Mater.*, 103&104 (1981) 853.
- [25] S. Sakurai, et al., *J. Japan Inst. Metals*, 48 (1984) 771.
- [26] H. Kojima, et al., *Fusion Tech.*, 6 (1984) 253.
- [27] F.W. Wiffen, *Proceedings of symposium on refractory alloy technology for space nuclear power applications*, CONF-8308130 (1984)252.
- [28] J. Matolich, et al., *Scripta Met.*, 8 (1974) 837.
- [29] V.N. Bykov, et al., *Atom. Energy*. 32, 4 (1972) 323.
- [30] R. C. Rau, et al., *J. Nucl. Mater.* 33(1969)324.
- [31] T. Adda, *Radiation Induced Voids in Metals*. CONF-710601 (1972)31.
- [32] R.E. Schmank and G.E. Korth, *J. Nucl. Mater.*, 103 & 104 (1981)943.
- [33] *ASME Boiler and Pressure Vessel Code*, Section III (1983).
- [34] Y.S. Touloukian and C. Y. Ho, Editor, *Thermophysical properties of matter*, The TPRC Data series, IFI/Plenum Data corporation, New York (1970).
- [35] D. Peckner and I.M. Bernstein, *Handbook of Stainless Steels*, McGraw-Hill Book Company, New York (1977).
- [36] *ASME Boiler and Pressure Vessel Code*, Code Case N-47, (1984).
- [37] M.L. Grossbeck and K.C. Liu, CONF-840404-9 (1984).
- [38] ADINA - A Finite Element Program for Automatic Dynamic Incremental Nonlinear Analysis, Report AE 81-1, ADINA Engineering Inc., Massachusetts (1981).
- [39] Report of Research Cooperation sub-committee 46, Japan Society of Mechanical Engineers, Tokyo (1977) (in Japanese).

Session 3

STRESS ANALYSIS AND LIFETIME EVALUATION (cont.)

LIFETIME ANALYSIS OF PLASMA SIDE COMPONENTS

R.F. MATTAS

Argonne National Laboratory,
Argonne, Illinois, United States of America

Abstract

A one dimensional computer code (FLIP, Fusion Lifetime Prediction) has been developed to examine the lifetime of first wall and impurity control components. The code incorporates the operating and design parameters, the material characteristics, and the appropriate failure criteria for the individual components. The major emphasis of the modelling effort has been to calculate the temperature-stress-strain-radiation effects history of a component so that the synergistic effects between sputtering erosion, swelling, creep, fatigue, and crack growth can be examined. The general forms of the property equations are the same for all materials in order to provide the greatest flexibility for materials selection in the code. The code is capable of determining the behavior of a plate, composed of either a single or dual material structure, that is either totally constrained or constrained from bending but not from expansion. The code has been utilized to analyze plasma side components for INTOR.

I. INTRODUCTION

Lifetime analyses for fusion reactor systems have been performed over the years as part of the design studies for the different reactor systems that have been proposed. Most of these analyses have emphasized particular aspects of the component lifetimes. For example, early studies emphasized radiation effects, particularly swelling and ductility loss.¹ The design limits on swelling range from ~ 2 -10%, and the limits on uniform elongation range from ~ 0.5 to 2%. The radiation limits were used since they depended only on the operating temperatures and neutron fluence, and they did not require detailed analysis of the material stresses or the operating scenario. Other studies have emphasized the mechanical property limitations, such as fatigue, thermal creep, and creep-fatigue interactions.^{2,3} In work by Mattas and Smith, both radiation effects and mechanical property effects were considered.⁴ A study by Cramer, et al., also examined both radiation effects and mechanical property changes.⁵ In addition, component design, and thermal and structural analysis were an integral part of the study.

More recent studies have examined the synergistic effects that occur during operation.^{6,7,8} In these studies the interaction of properties such as swelling, radiation creep, crack growth, and fatigue have been analyzed in considerable detail. The material most often studied is austenitic stainless steel because it is the most likely structural material in near term devices and it has the largest data base from which to draw.

The FLIP code was designed to study the behavior of first wall and limiter/divertor components. The approach used is to calculate the synergistic effects of various materials properties in a manner similar to previous studies. The major emphasis of this work is on studying the trends and trade-offs between materials properties, design, and operating environment. To provide the greatest flexibility, simple empirical equations are used to describe materials properties, so that only the coefficients need to be changed to study different materials. In addition, the code was designed to examine duplex structures, since many limiter/divertor designs employ a plasma side material bonded to a structural heat sink. Most recently, the FLIP code was used to study the first wall and divertor of INTOR.⁹

II. LIFETIME MODEL

The major emphasis of the modeling effort was to examine component response for a wide variety of operating conditions and materials. For this purpose, a one-dimensional model of a plate is believed adequate, although the model can, in principle, be adopted to 2 or 3 dimensional calculations. Only normal operating conditions (burn cycle and down periods) are included in the model.

The flow diagram for the FLIP code is shown in Fig. 1.¹⁰ The code first calculates the temperature, stress, and strain distribution through a plate based upon the selected operating and design parameters. Property changes are then determined for a specific time increment, and the effects of those changes on the initial distributions are evaluated. This process is repeated until failure occurs or the desired lifetime is reached.

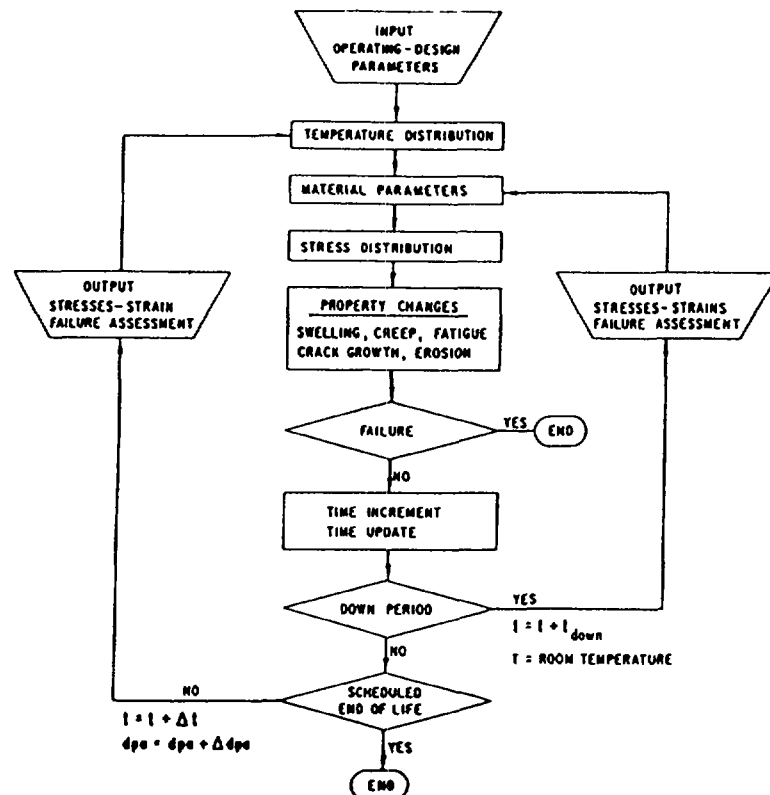


Fig. 1. FLIP code flow diagram.

The basic inputs to the code are the operating and design parameters. The design parameters include component material(s) selection, plate thickness, coolant characteristics, primary stress level, initial crack length, and plate constraint. The operating parameters include the burn cycle characteristics (ramp time, burn time, dwell time), down period duration and frequency, surface heat flux, neutron wall loading, and surface erosion rate. Finally, the failure criteria for swelling, deformation, and ductility are also provided.

Either a single or dual material plate can be analyzed by the code. The dual material plate is representative of impurity control components which are likely to have a low-Z material bonded to a structural material. The materials properties which are considered are the thermophysical, mechanical, swelling, and neutronic properties. Temperature is the primary parameter consi-

dered for the thermophysical properties. Radiation effects are also considered in the cases of the thermal conductivity and the elastic modulus. The mechanical properties considered are the tensile, crack growth, fatigue, and creep properties. A bi-linear elastic-plastic behavior is assumed for the tensile properties. Temperature, stress, fluence, flux, stress and strain ranges, and stress intensity are the parameters included in determining the mechanical behavior. Radiation swelling is dependent on the temperature and fluence, and the neutronic properties depend on the neutron flux and fluence.

The material properties are represented by empirical equations that incorporate the temperature, fluence, and stress dependencies. Whenever possible the predicted property values are based upon available experimental data. In many cases, the experimental data are sparse, and therefore data from similar materials or best estimates of property values are employed. The lack of data for many materials means that there is considerable uncertainty built into the model, and the predictions from the model should be viewed as showing qualitative trends rather than as an accurate representation of component behavior. Details of the material property equations and the property data base are given in Ref. 10.

A simple thermal-hydraulics subroutine calculates the temperature distribution through the plate at various times during the burn cycle. The temperature distribution is then used to calculate the thermal strain distribution, which is used as input to calculate the stress distribution. The stresses can be determined for a plate which is either totally constrained from expansion, allowed to expand but not bend, or is unconstrained. These three conditions span the possible range of component constraint in the reactor.

Once the temperature, stress, and strain distributions are determined, the long term response of the material to the reactor environment can be evaluated. The code determines the swelling change, creep change, fatigue damage, and crack growth for a time increment Δt . The swelling and creep which occurs during the period Δt results in a modified strain distribution that is used to calculate the changes in the stresses. The code also determines the amount of surface erosion during the time increment. The reduction in plate thickness results in a modified temperature distribution. The property change calculations are then repeated using the modified distributions until either the failure criteria are met or the component reaches the goal lifetime. For calculational purposes, the temperature and stresses are assumed to remain constant during the time increment. Therefore, Δt must be chosen such that the stress change is small compared with the total stresses in order for this approach to reasonably approximate in reactor behavior.

III. INTOR DIVERTOR COLLECTOR PLATES

The collector plates may be composed of either a single or duplex structure. The low edge temperature divertor utilizes a high-Z material, such as tungsten or tantalum, facing the plasma in order to reduce or eliminate sputtering erosion. A single material collector plate would be composed of a tantalum alloy like Ta-10W. The duplex structure plate consists of either Ta-10W or pure tungsten bonded to a heat sink composed of Cu-0.5Be-2Ni. The design and operating conditions are shown in Table 1, and the materials assumptions used for the calculations are presented in Table 2. The thickness of the material facing the plasma is low in order to accommodate the high heat loads. The combination of the low plasma edge temperatures in INTOR ($\lesssim 30$ eV) and the use of high-Z materials means that the erosion rate is essentially zero.⁹

Table 1. Material Assumptions - Collector Plates

General

1. No influence of stress on swelling.
2. Unirradiated behavior for fatigue and crack growth.
3. Radiation damage rates, helium generation, and nuclear heating calculated for fusion neutron spectrum.
4. No coolant stress corrosion effects.

Tantalum

1. Fast reactor swelling rates for pure Ta.
2. Radiation creep like HT-9.
3. Fatigue behavior like vanadium and niobium alloys.
4. Low temperature radiation embrittlement similar to vanadium and niobium alloys.
5. Crack growth rates like HT-9.

Tungsten

1. Fast reactor swelling behavior.
2. Radiation creep like HT-9.
3. Crack growth rates like HT-9.

Cu-.5Be-2Ni

1. Swelling rate 1/10 rate of pure Cu.
2. Fatigue and crack growth behavior of pure Cu.
3. Radiation creep like 316 stainless steel.
4. Ductility losses like 316 stainless steel.

Table 2. Design and Operating Conditions for Collector Plate Analysis

Parameter	Value
Material	
Surface	Ta-10W, W
Structure	Ta-10W, Cu-.5Be-2Ni
Thickness	
Single Material	4 mm
Duplex	
Surface	2 mm
Structure	4 mm
Neutron Wall Load	1.3 MW/m ²
Surface Heat Load	4.1 MW/m ²
Availability	50%
Lifetime Goal	2 y
Lifetime Cycles	1.3 x 10 ⁵
Burn Time	200 s
Dwell Time	40 s
Down Periods/Year	3
Stress Condition	Allowed to expand but not bend
Primary Stress Level	50 MPa
Erosion Rate	0
Stress Free Temperature	700, 400 K
Coolant Temperature	363 K
Heat Transfer Coefficient	40,000 W/mK

The temperature distributions through the collector plate are shown in Fig. 2. The all tantalum design exhibits the highest surface temperature due to tantalum's relatively low thermal conductivity. There is a $\sim 100^\circ\text{C}$ temperature drop between the structure and the coolant. These temperature distributions are assumed to remain unchanged during the life of the collector plates.

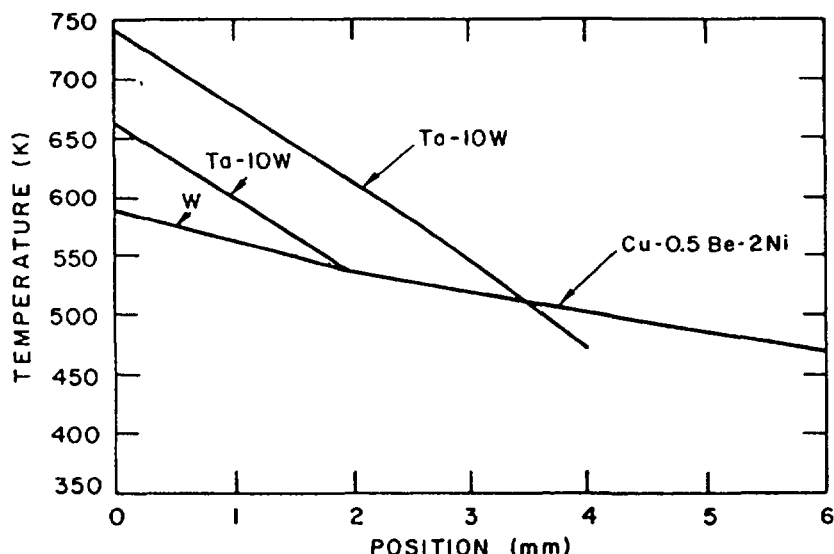


Fig. 2. INTOR divertor collector plate temperature distribution.

The thermal gradients are largely responsible for the generation of the operating stresses. Another important factor for duplex structures is the stress free temperature; i.e., the temperature where there are no stresses generated in the two materials as a result of the mismatch in the thermal expansion coefficients. This temperature generally corresponds to the temperature of bonding. For this analysis the stress free temperature has been taken to be either 700 or 400 K. The 400 K value might correspond to the stress free temperature for plasma spraying. The effect of the stress free temperature on the initial stress distribution during the burn period is shown in Fig. 3 for tungsten bonded to Cu-.5Be-2Ni. For a 700 K stress free temperature, the stress in the tungsten is highly compressive and, in fact, exceeds the yield strength of powder metallurgy recrystallized tungsten. For the 400 K stress free temperature, the stress in the tungsten is highly tensile. The 400 K stress free temperature is preferred, however, because of the reduced stresses through the plate.

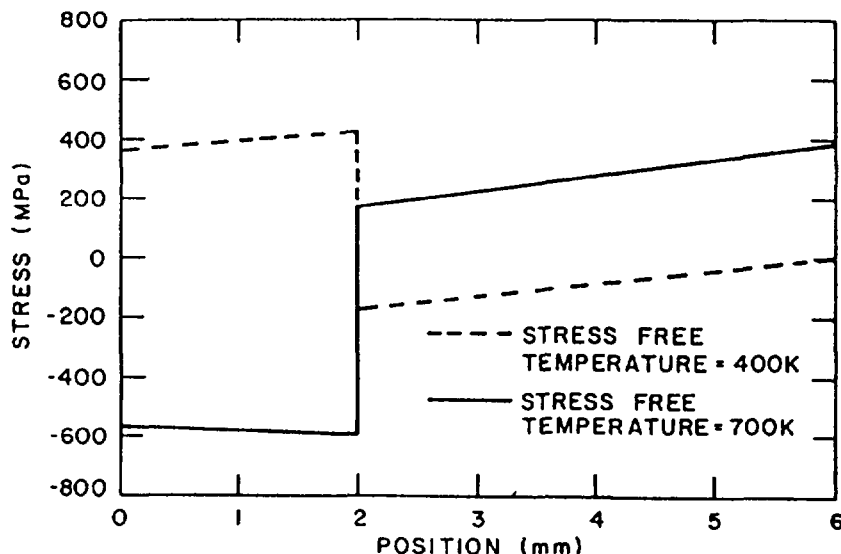


Fig. 3. Collector plate stress distribution - W-Cu.5Be-2Ni.

The stress distributions for collector plates composed of W bonded to Cu-.5Be-2Ni are shown in Fig. 4. When W is bonded to the copper alloy (Fig. 4), the magnitude of the stresses is increased due to the large mismatch in the thermal expansion coefficients. As radiation creep proceeds, the magnitude of the stresses during the burn cycle is reduced. In essence, radiation creep will tend to change the stress free temperature to the operating temperature of the collector plate. In this case, however, the stresses never reach zero during the burn due to swelling in the copper alloy and due to the 50 MPa primary stress. The swelling of the copper alloy results in a trend towards compressive stresses in the copper and tensile stresses in W. The swelling related stress levels reached in the structure will depend on the difference in the swelling rates of the two materials.

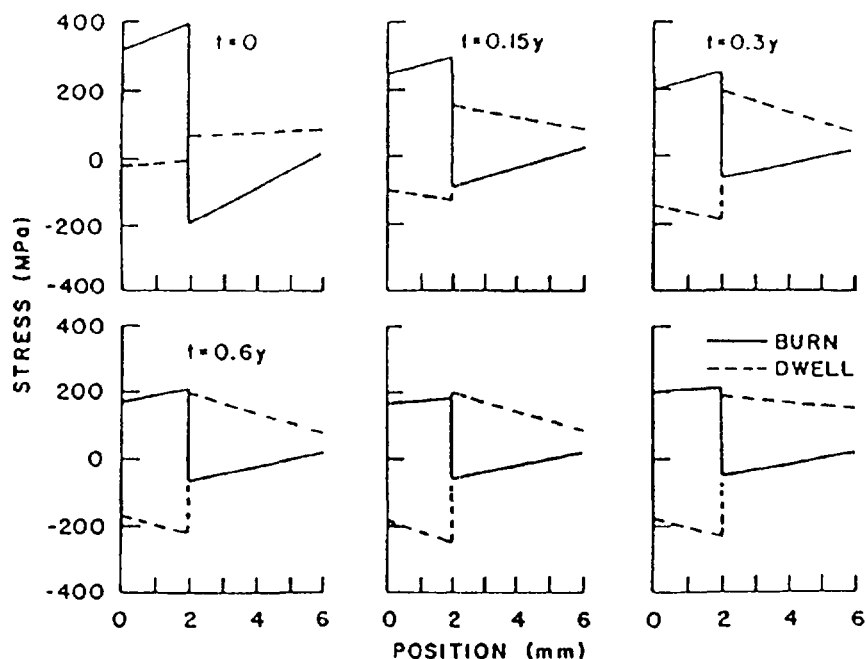


Fig. 4. W-Cu collector plate - stress relaxation.

IV. INTOR First Wall

The INTOR first wall is composed of 20% cold-worked Type 316 stainless steel. The plate facing the plasma is 14 mm thick and the coolant is water at 90°C. The reactor operating conditions are presented in Table 3 and the material assumptions are shown in Table 4.

The temperature distributions through the first wall at several times during the reactor lifetime are shown in Fig. 5. The surface of the plate exposed to the plasma for this and all other relevant figures in this section is the zero point of the abscissa. The temperature at the plasma side surface is 558 K, and it drops to 380 K adjacent to the coolant. The temperature gradient deviates from linearity because of the temperature dependence of the thermophysical properties and the significant contribution from nuclear heating. As the plate thickness is reduced by surface erosion, the surface temperature decreases such that after 10 y of operation the peak temperature is only 421 K.

The thermal gradients through the plate are largely responsible for the generation of the operating stresses. The stress distributions for a plate

Table 3. Design and Operating Conditions for INTOR First Walls

Parameter	Value
Material	20% CW Type 316 SS
Thickness	14 mm
Coolant Temperature	90°C
Heat Transfer Coefficient	20,000 W/mK
Surface Heat Flux	.14 MW/m ²
Neutron Wall Load	1.3 MW/m ²
Availability	50%
Lifetime Goal	10 y
Lifetime Cycles	7 x 10 ⁵
Lifetime Fluence	52 dpa
Burn Time (s)	200
Dwell Time (s)	200
Down Periods/Year	6
Stress Condition	Free to expand but not bend
Primary Stress Level (MPa)	50
Erosion Rate (m/s)	7 x 10 ⁻¹¹ m/s
Initial Flaw Size	0, 0.5, 1.0 mm
Minimum Structural Thickness	4 mm

Table 4. Materials Assumptions 20% Cold-Worked Type 316 Stainless Steel

1. Fast reactor swelling and creep rates.
2. No influence of stress on swelling.
3. Unirradiated behavior for fatigue and crack growth.
4. Radiation damage rates, helium generation rates, and nuclear heating calculated for a fusion neutron spectrum.
5. No coolant stress corrosion effects.

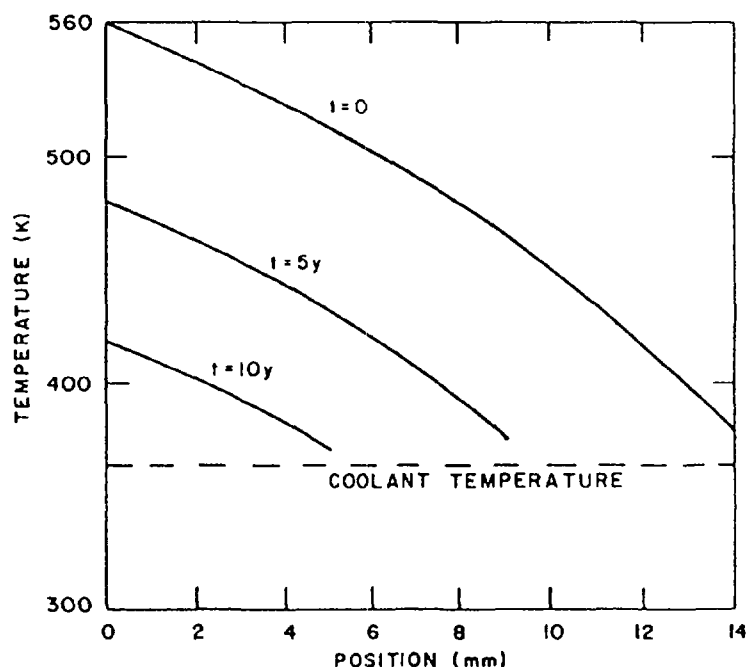


Fig. 5. Temperature distribution through first wall.

that is allowed to expand but not bend are shown in Fig. 6 for various times during the reactor life. Early in life ($t = 0$), the stress is compressive on the plasma side and tensile on the coolant side during the burn. The stress levels are near zero during the dwell period. The peak thermal stress ~ 600 MPa is well within the $3 S_{mt}$ design guideline. Radiation creep results in stress relaxation during the burn period such that the stress levels are near zero after ~ 1 y of operation. The stress levels during the dwell cycle move towards the opposite of the initial stress distribution during the burn. As the plate erodes, the peak stress levels are reduced ($t = 10$ y). Void swelling is predicted to reach only .02% after 10 y and hence it has no impact on the first wall stress distribution.

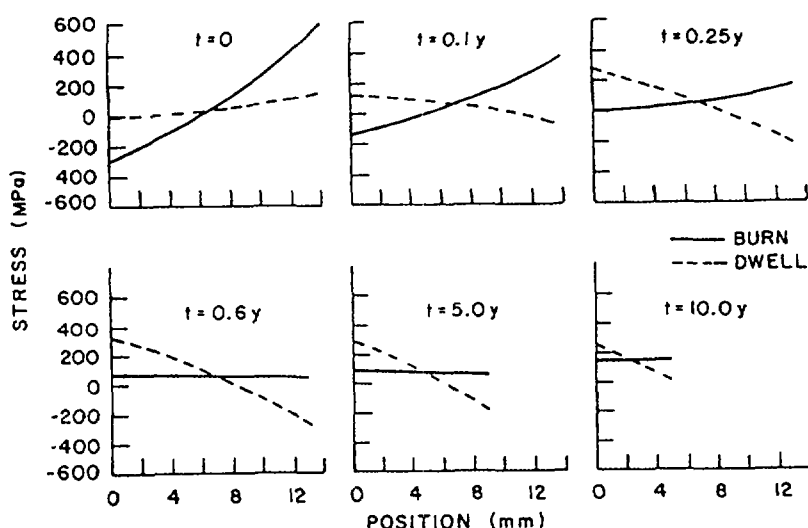


Fig. 6. INTOR first wall distribution.

Radiation creep at the coolant side of the plate is illustrated in Fig. 7. The creep rate is initially high as the thermal stresses relax during the burn. At ~ 0.5 y the thermal stresses are almost zero during the burn, and additional radiation creep is due to the primary stress in the structure. As the plate erodes during the 10 y lifetime, the primary stress is assumed to increase as the ratio of the original plate thickness to the eroded plate thickness. The increased primary stress results in an increased creep rate

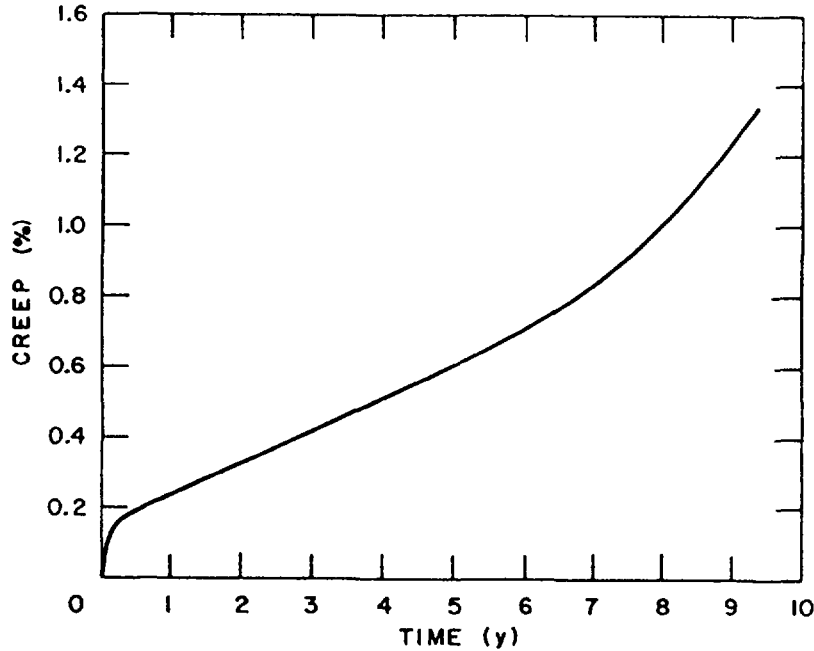


Fig. 7. INTOR first wall radiation creep.

towards the end of life. The total amount of radiation creep is calculated to be $\sim 1.25\%$ during the operating lifetime.

Failure of the first wall could also occur by crack growth from a flaw in the structure. Fig. 8 illustrates the crack growth rate from the coolant side of the plate for assumed flaw sizes of 1 mm and 0.5 mm. Failure occurs if the

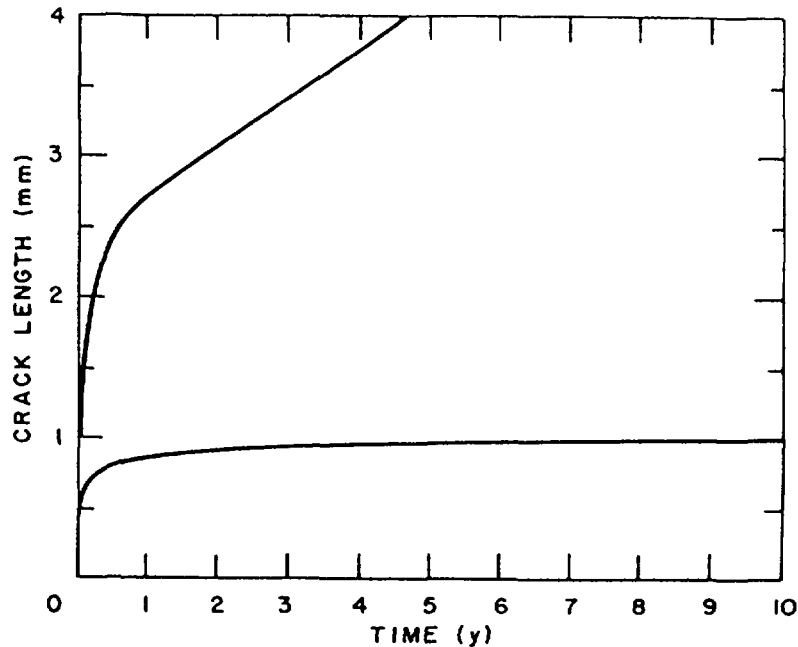


Fig. 8. INTOR first wall - crack growth.

flaw grows beyond 4 mm which is the minimum required structural thickness assumed for the first wall. The 1 mm flaw is predicted to grow to failure in ~ 4.7 y, whereas the 0.5 mm flaw remains below 1 mm in length after 10 y.

Loss of ductility is another major concern for the first wall structural material. The change in the uniform elongation in the INTOR first wall is shown in Fig. 9. The uniform elongation is predicted to reach a level of only 1% after ~ 10 y. The loss of ductility to these levels must be considered as being serious, but there are no established guidelines for acceptable ductility values. A major effort is required to develop such guidelines. The yield strength of the first wall is expected to rapidly increase up to a value of ~ 925 MPa. The increase in strength is predicted to saturate after ~ 1 y.

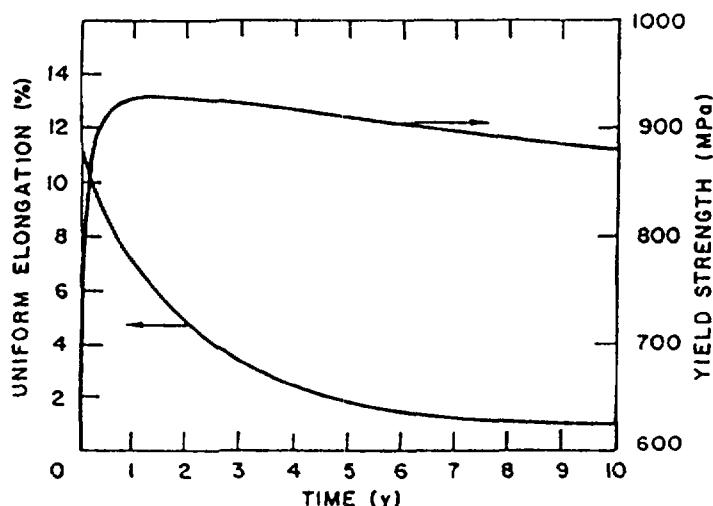


Fig. 9. INTOR first wall - uniform elongation - yield strength coolant side.

V. CONCLUSIONS

The analysis of the lifetime of plasma side components indicates that both the first wall and divertor in INTOR will have acceptable lifetimes. This conclusion should be considered as tentative, however, due to the considerable uncertainties in the analysis.

First, there are uncertainties concerning the operating environment. For plasma side components, the parameters of greatest importance are the surface heat load, the plasma edge parameters, and the disruption parameters. The surface heat load will in large part determine the operating temperatures and thermal stress distribution, and the plasma edge and disruption parameters will establish the erosion rate. The first wall in INTOR has little operating margin, and a small increase in surface heat load or erosion rate could reduce the lifetime to an unacceptable level.

Second, there are large uncertainties in the materials properties, particularly radiation effects. There is a sizable data base for stainless steels, but other materials are poorly characterized. A large effort is needed to establish the necessary materials data for plasma side components.

Third, the FLIP code is limited to 1-D calculations. There is a need to study component response in 2-D or 3-D calculations to more realistically calculate temperature and stress distributions. It is important that such calculations include dimensional changes due to plastic deformation or radiation

swelling and creep. They should also include the effects of radiation on the degradation of all materials properties.

Finally, off-normal events should be incorporated into the lifetime studies. A single off-normal event could alter the component stress distribution or be enough to cause catastrophic failure. The most common off-normal event is a disruption which will result in large electromagnetic forces in addition to surface erosion.

In order to verify code predictions, there is a need to compare the calculations with experimental results. This comparison is possible for the study of thermo-mechanical effects, but it is difficult or impossible when the effects of radiation and erosion are included. In the absence of direct verification by experiment, it is desirable to compare predictions of different codes with each other. The use of benchmark problems would allow such a comparison and would serve to establish the similarities and differences between code predictions. Finally, there is a need to analyze the uncertainties in the code predictions. The output of such an analysis would be a range of lifetime estimates that would depend on the ranges of uncertainty of the input parameters.

REFERENCES

1. G. L. KULCINSKI, R. G. BROWN, R. G. LOTT, and P. A. SENG, "Radiation Damage Limitations in the Design of the Wisconsin Tokamak Fusion Reactor," Nucl. Tech., 22, 20 (1974).
2. S. MAJUMDAR, "Computer Modeling of CTR First Wall Behavior," Argonne National Laboratory, MSD/CTR/TM-35 (1974).
3. C. K. YOUNGDAHL and D. L. SMITH, "Stress and Lifetime Limitations of First Wall Structural Materials," J. Nucl. Mater., 85 & 86, 153 (1979).
4. R. F. MATTAS and D. L. SMITH, "Model for Life-Limiting Properties of Fusion Reactor Structural Materials," Nucl. Tech., 39 (2) 186 (1978).
5. B. A. CRAMER, et al., "An Approach for Determining the Lifetime of First Wall Structure in a Tokamak Reactor," Proc. of the Second Topical Meeting on the Technology of Controlled Nuclear Fusion, CONF-760935-P4, 1513 (1976).
6. S. D. HARKNESS and B. CRAMER, "A Review of Lifetime Analyses for Tokamaks," J. Nucl. Mater., 85 & 86, 135 (1979).
7. R. D. WATSON, R. R. PETERSON and W. G. WOLFER, "The Effect of Irradiation Creep, Swelling, Wall Erosion and Embrittlement on the Fatigue Life of a Tokamak First Wall," J. Nucl. Mater., 103, 97 (1981).
8. J. P. BLANCHARD and N. M. GHONIEM, "Inelastic Structural Analysis of the MARS Tandem Mirror Reactor," Nucl. Eng. Design, 2 (1985), 19 (1985).
9. W. M. STACEY, et al., "U.S. Contribution to the Phase 2A, Part 2 INTOR Workshop, 1983-1985," USA INTOR/85-1 (1985).
10. R. F. MATTAS, "Lifetime Analysis of Fusion Components," Argonne National Laboratory, ANL/FPP/TM-160 (1983).

ESTIMATED THERMAL FATIGUE LIMITS FOR THE FIRST WALL OF NET*

G.O. VIEIDER, A. CARDELLA
The NET Team,
Max-Planck-Institut für Plasmaphysik,
Garching near Munich

Abstract

For an early tokamak reactor like NET with modest temperature- and fluence targets, the life of the first wall panels (F.W.) and divertor plates will be mainly limited by:

- thermal fatigue during about 10^5 burn cycles with peak heat loads of up to 0.3 MW/m^2 for the F.W. and 7 MW/m^2 for the divertor plates;
- sputtering erosion and disruptions which are (insufficiently understood) mechanisms for a potential local loss of material of up to 1 cm.

A 1-D thermo-mechanical model has been developed for the prediction of the cyclic thermal strain in plate-like F.W.-components. In this model:

- the bending deformation due to the heat flux was assumed to be restrained, which is close to the real boundary conditions;
- plate crosssections with different coolant channels and protection arrangements can be analysed;
- a calibration factor for 3-D effects has been derived from finite element analysis of several cases.

For given operating conditions and material data, this model permits to assess the thermal fatigue limits:

- A solid F.W. in austenitic stainless steel could endure 10^5 cycles if it has an initial thickness of about 8 mm. If significantly larger erosion margins than 5 mm were needed a grooved protection layer or a ceramic protection would be required.
- Divertor plates made of tungsten bonded to a copper heat sink and an all-molybdenum concept have been analysed. It appears that thermal fatigue is more life time limiting than erosion.

* At the time of publication only the abstract was available.

Major uncertainties in the life time evaluation of NET F.W.-components are associated with an insufficient data base on fatigue including irradiation effects as well as a lack of data concerning erosion and disruptions.

STRESS ANALYSIS OF THE NET OUTBOARD FIRST WALL BOX

A. CARDELLA, H. GORENFLO
The NET Team,
Max-Planck-Institut für Plasmaphysik,
Garching near Munich

Abstract

A very important topic related to the F.W. designs in form of a tight box that envelopes the breeding blanket is the overall behaviour under the severe operating conditions of NET fusion reactor.

In this paper the results of the 3-D stress analysis of the NET outboard F.W. box is presented. These results have been incorporated in the preliminary evaluation of the thermal fatigue limits for the F.W. of NET. (Paper presented in the same Technical Committee Meeting by G. Vieider).

1. Introduction

In most of the present design concepts, the F.W. in form of tight box envelopes each breeding blanket segment and consists of a front wall in view of the plasma, two side walls, top and bottom plates and a stiff back plate.

A very important topic related to this type of F.W. designs is the overall behaviour of the box under its severe operating conditions.

It has been then performed a 3-D stress analysis of the NET F.W. box subjected to the thermal, internal pressure and dead weight loads. Similar thermal stress analyses for different configurations can be found in Ref. 1,2.

Electromagnetic effects during normal operation and plasma disruption will be studied separately in a next analysis. Preliminary results for this type of loads but for a different configuration and scenario can be found in Ref. 3. The material considered is austenitic steel AISI 316. The NET configuration adopted is the 2.2.B.

The present analysis was restricted to the outboard part with reference to the designs which consider an independent separate inboard F.W. segment.

The inboard F.W. can be studied with similar analyses. For the designs which consider a continuous F.W. from the outboard to the inboard part (e.g. horse shoe geometry), the analysis should consider the entire F.W. .

The number of outboard F.W. segments can range from a minimum of 24 to a maximum of 48 segments. These two extreme cases have been included in the analysis and for each of them, two different F.W. thicknesses have been analyzed.

The analyses have been performed with the finite element code ADINA. The mesh generation and the pre- and post-processing have been made with the PATRAN code.

The detailed description of the analysis can be found in REF. 4.

The scope of these analyses is:

- to evaluate the stress level and distribution in the F.W. box due to the load induced
- to perform a comparative evaluation of different geometrical parameters.

2. F.E.M. MODEL

The shape of the F.W. box and the thermal load distribution is such that a 3D analysis is required to better evaluate the overall behaviour. A complete schematization of the F.W. geometry for each design solution would result in a very large number of elements and nodes. Infact the schematization of the F.W. cross section requires a very fine mesh to represent pipes and or cooling channels, collectors etc. and this mesh should be extended to the entire box which has much bigger global dimensions.

For this reason and because the scope of the analysis is the overall behaviour, the F.W. box has been modelled as a simple shell with a constant equivalent thickness. This shell has been rigidly attached to a stiff 10 cm thick back plate. In the top and bottom part, the F.W. box is closed with proper plates which have been considered to have the same thickness as the F.W. shell. The front wall edges of the shell in connection with the side wall and the top and bottom plates are rounded with a proper radius of curvature (70 mm) in order to have a smoother stress distribution. Of course the results of the analyses are more applicable to the F.W. designs that are better approximated by the model. In the cases in which the shape or the cross section deviates strongly from the model, the indications given by the analysis should be carefully considered.

Four F.E. models have been analysed;

- 1) F.W. Box width corresponding to 48 outboard segments and an equivalent thickness of 10 mm
- 2) F.W. Box width corresponding to 48 outboard segments and an equivalent thickness of 20 mm
- 3) F.W. Box width corresponding to 24 outboard segments and an equivalent thickness of 10 mm
- 4) F.S. Box width corresponding to 24 outboard segments and an equivalent thickness of 20 mm.

Due to the symmetry of the box, only a quarter of it has been modelled.

For all the models, 3-D solid elements have been used to better represent the temperature distribution.

The F.W. box is supposed to be free to expand in order to allow the thermal expansion of the structure. The restraints at the boundary have been applied accordingly. The same restraints have been applied for the pressure and dead weight load. For the dead weight the structure is then supposed to be hold in the equatorial plane. This choice has been taken to keep the same simplified model. If in the real F.W. box design the box is hanging from the top, the dead weight stresses should be reconsidered. Fig. 1 show the undeformed geometry of model 1. Fig. 2 shows a detail of the top or bottom plate. The other models have a similar shape.

3. DESIGN CONDITIONS

Thermal loads

The conditions affecting the F.W. can vary considerably depending on the assumptions made of the behaviour of the plasma edge.

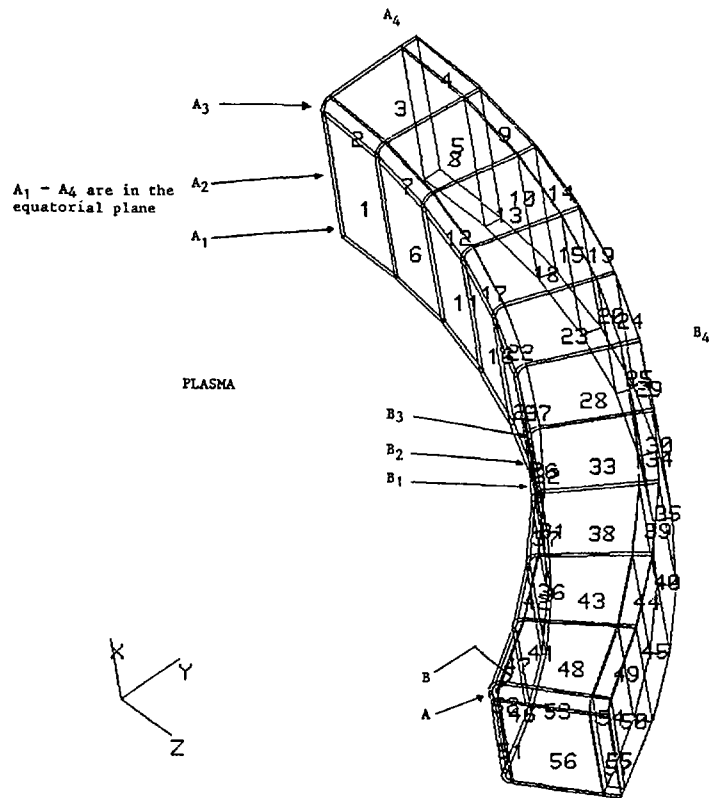


FIGURE 1 F.W. MODEL FOR F.E.M. STRESS ANALYSIS

IPP-CRAY HH6796

1

F1-11

14/10/85 13:19:56

TOP OR BOTTOM PLATE

BACK PLATE

PLASMA

MODEL S-0.001/TY-0,4.8,4.15/Z-130/Y-30/TX--10./S-1.0/0-0.1

FIG. 2 PARTICULAR OF THE TOP OR BOTTOM PLATE

The thermal loads, which the F.W. is subjected to, are derived from the expected operative conditions of NET. These loads are cyclic with a period that ranges from 200 to 1000 sec.

Due to the small thermal transient response time of the the F.W., the analyses have been performed in steady state conditions. The heat deposition inside the F.W. due to neutrons and gamma rays is assumed to be in order of 20 W/cm^3 in the front wall and almost linearly decreasing with the distance from the plasma to a value of 0.4 W/cm^3 in the zone attached to the backplate.

The surface heating on the F.W., due to radiation and particle interactions is assumed to be 10 W/cm^2 constant along the front wall surface.

The internal surface of the F.W. shell (front wall and side walls) has been considered as uniformly cooled by water with the following parameters:

Water average temperature	200°C
heat transfer coefficient	$2.8 \text{ W/cm}^2/^\circ\text{C}$

The back plate has been kept at a constant temperature of 200°C corresponding to the coolant temperature. The reasons for this choice are the following:

- It is useful to avoid large temperature differences in the box between the shell and the back plate
- In some designs the blanket and/or F.W. shell coolant passes also through the back plate.

Internal Pressure loads

The operating pressure of the F.W. box has not been assessed yet. Nevertheless, it is useful to know the stress levels due to this load. It has been decided to consider a reference pressure of 0.1 MPa (1 at). For different pressures, the stresses and displacements can be scaled since the analysis is supposed to be in the elastic range.

Dead weight

The stresses induced by the dead weight can be automatically computed by the code used so that it was considered useful to have a first evaluation with the results made available by the computer code. However, the analysis does not include all the other distributed (such as the coolant weight) or lumped weight in the structure.

4. MATERIAL PROPERTIES

In the present analysis the structural material considered is only the AISI 316 SS solution annealed. The results of the previous stress analyses have shown infact that solutions with AISI 316 are critical and necessitate further study.

For the loads considered in these analyses the martensitic steel is more appropriate because the thermal stresses are much lower and the allowable stress is much higher, living space for the other primary loads. Nevertheless the use of the martensitic steel have these main problems:

- The martensitic steels exhibit the ductile-brittle transition phenomenon

- The DBTT in the unirradiated conditions is determined by the composition and thermal-mechanical treatment of the steel and is increased by fast neutron irradiation
- The martensitic steel is ferromagnetic. Its use in a tokamak machine must be studied from the electromagnetic point of view
- Welding is more problematic.
- There is less information on martensitic steel than austenitic with respect to the effect of irradiation.

If these problems will be solved in the next future, the use of the martensitic steel for the NET F.W. box should be preferred.

Properties	AISI 316	
	21°C	537°C
Thermal conductivity (W/cm/°C)	0.145	0.215
Thermal expansion (°C ⁻¹)	15.46E-06	19.76E-06
Young's Modulus (Kg/cm ²)	2.1E06	1.72E06
Poisson's Ratio	0.29	0.34

5. RESULTS

Thermal analysis

The temperature distribution is similar in the four models. It is almost constant on the front wall bulk surface. The temperature slowly increases in the bended zone at the front wall edges where it reaches the maximum values. In these zones infact the external surface exposed to the plasma is larger than the internal cooled surface. The temperature decreases immediately after the bended zones to reach near the back plate the temperature of the coolant.

Along the front wall thickness the temperature decreases rapidly from the hot part in view of the plasma to the cold part in contact with the coolant. The temperature of the surface in contact with the coolant is almost uniform in the zone in front of the plasma and in the bended zones. It decreases to reach the temperature of the coolant in the back plate.

The maximum temperature is found for all the models in the curved zone of the bottom plate (point A in Fig. 1).

The structure expands in the X positive direction and in the Z direction and tends to diminish the curvature in the poloidal direction. The sidewalls if not fixed to the backplate would tend to enter in the blanket region. The backplate prevents this displacement, giving small additional stresses on the front wall edge.

The displacement values seem acceptable.

The stresses are high and mainly due to the strong temperature gradients along the front wall thickness. There, compressive stresses are present in the plasma side (hot part) and tensile stresses in the cooled side (cold part). The tensile stresses in the cold part are somewhat higher than the compressive in the hot part. This is due to the non linear temperature distribution along the thickness. Stress concentrations are present at the frontwall edges and at

the top and bottom plate edges as expected. The maximum Von Mises stress is found in point B (Fig. 1).

The maximum temperature, displacement and Von Mises Stress are reported in Tables 1-2 for the models 1 and 3 together with values at specific location shown in Fig. 1. The stress values for model 2 and 4 are far beyond yield strength.

TABLE 1

MODEL 1 1 cm thick 48 segments

TEMPERATURE

$T_{\max} = 342^{\circ}\text{C}$ Point A
 $D_{\max} = 30\text{mm}$
 $\sigma_{\max}^{\text{vm}} = 364 \text{ MPa}$ Point B

POINT	T	σ^{vm}	POINT	T	σ^{vm}
A ₁	hot 322°C	270 MPa	B ₁	hot 320°C	278 MPa
	cold 211°C	331 MPa		cold 210°C	335 MPa
A ₂	hot 323°C	286 MPa	B ₂	hot 322°C	302 MPa
	cold 211°C	296 MPa		cold 211°C	301 MPa
A ₃	hot 318°C	313 MPa	B ₃	hot 317°C	321 MPa
	cold 206°C	316 MPa		cold 206°C	321 MPa
A ₄	hot 221°C	55 MPa	B ₄	hot 221°C	53 MPa
	cold 200°C	67 MPa		cold 200°C	59 MPa

PRESSURE

$D_{\max} = 2.1 \text{ mm}$
 $\sigma_{\max}^{\text{vm}} = 85 \text{ MPa}$

WEIGHT

$\sigma_{\max}^{\text{vm}} = 11.4 \text{ MPa}$

TABLE 2

MODEL 3 1 cm thick 24 segments

TEMPERATURE

$$T_{\max} = 345^{\circ}\text{C} \quad \text{Point A}$$

$$D_{\max} = 28 \text{ mm}$$

$$\sigma_{\max}^{\text{vm}} = 362 \text{ MPa} \quad \text{Point B}$$

POINT	T	σ^{vm}
A ₁	hot 320°C	249 MPa
	cold 210°C	314 MPa
A ₂	hot 320°C	264 MPa
	cold 210°C	327 MPa
A ₃	hot 320°C	284 MPa
	cold 211°C	286 MPa

PRESSURE

$$D_{\max} = 9.7 \text{ mm}$$

$$\sigma_{\max}^{\text{vm}} = 161 \text{ MPa}$$

WEIGHT

$$\sigma_{\max}^{\text{vm}} = 23 \text{ MPa}$$

Internal pressure and dead weight

The location of the maximum stresses due to internal pressure is the front wall end where it is attached to the side wall.

The maximum V.M. stresses for models 1 & 3 are reported in Tables 1-2.

Considerations and conclusions

The applied thermal loads cause very high stresses to this type of F.W. box designs.

Although the necessary evaluation criteria has not been established yet, it can be said that for an AISI 316 F.W. box with an equivalent thickness of 1 cm the maximum stresses go beyond the allowable limits for primary plus secondary stresses. Considering only the thermal stresses, the gap between the allowable stress and the computed stress is not very high. Still ameliorating the box shape and, if possible, reducing the stiffness of the structure could bring

the stresses below the allowable limits but the space left for other primary loads will be very probably little. A better situation can be achieved decoupling the backplate from the F.W. sidewalls (Ref. 1) or more decoupling the F.W. front wall from the rest of the structure and still keep the box idea with other means if feasible (e.g. bellows). Another possibility could be to let some part of the F.W. work in full elastoplastic conditions. This requires longer and more difficult analyses and the F.W. lifetime will be affected very much. Furthermore a partial or total coverage of the F.W. with protection tiles could be required. This will affect the F.W. designs and other analysis will be required. An evaluation of the effect of the protection in the F.W. can be found in REF. 5.

The F.W. design solutions that are not in form of a box should be in a better situation for thermal stresses. Of course the stresses inherent to the thermal gradients are still present and the more a single F.W. panel is free to expand the bigger are the displacement to cope with.

In this case the advantages and drawbacks of a separate F.W. panel compared to the F.W. box must be analysed.

The main advantages of a F.W. box type are the following:

- reduced outgassing problems
- better containment of internal leakages
- possibility to use the F.W. panel as a partial passive loop for plasma vertical stability
- reduced structure for T breeding (with present situation)
- lower number of collectors/pipes
- easier maintenance of the F.W. blanket unit.

The main drawbacks are the following:

- higher thermal stresses
- higher electromagnetic loads
- easier maintenance of a single F.W. panel.

The stresses caused by an internal pressures of 0.1 MPa (1 bar), considered separately for the other stresses are low for model 2 that has a high stiffness (2 cm thick and 48 segments), and acceptable for model 1 and 4 in operating conditions.

They are surely beyond the allowable limits for model 3 where reinforcing devices are needed.

In faulted conditions the allowable limits for primary loads will probably be much higher (say twice), so that these pressures or even higher, depending from the box design, could be admitted if the F.W. box normally operate at lower pressure.

At present when the pressure stresses are combined with all the other primary and secondary stresses (including the stresses due to the electromagnetic loads), none of the models considered is very likely admissible mainly because of the too high thermal stresses.

When the analysis criteria for these type of reactor will be established a proper evaluation will be done.

Dead weight loads should not be a big problem unless very heavy components are attached to the F.W.

Considering only the above loads, the impact of the segmentation on the F.W. box can be summarized as follows:

- Thermal stresses are reduced by a small quantity when the segmentation is reduced (from 48 to 24 segments)

- Electromagnetic forces should be much higher when the segmentation is reduced. Since they go roughly with the surface they should be the double for the 24 segment solution. Because the stiffness of a larger F.W. is reduced the resulting stresses could be even higher than the double.
- Stresses caused by internal pressure in the box due to leakages or rupture are higher when the segmentation is reduced (roughly the double).
- Dead weight stresses are double when the segmentation is halved but the absolute value is low.

With the above considerations and again looking only at the above structural aspects, the 48 segment solution is better than the 24 segment solution.

These results should nevertheless be considered together with the other segmentation problems e.g.:

- neutronic performances are reduced with the higher segmentation
- vertical stability better with lower segmentation
- maintenance

A final consideration to be made is that the results of this and the previous stress analyses show that solutions with AISI 316 are problematic for the considered wall loadings. There is few or no room for other loads than thermal loads.

Therefore incentive should be given to the martensitic steel even for NET if the major uncertainties are solved.

REFERENCES.

1. A. Cardella, F. Farfaletti-Casali, M. Biggio, A. Inzaghi, "3-D Thermal Stress Analysis of the First Wall for the Outboard Breeding Blanket of NET" T.N. No. 1.05. B1.84.144 PER/918/84, JRC Ispra.
2. M.G. Turri, M. Biggio, F. Farfaletti-Casali, O. Jop, F. Munsch, "Thermo-mechanical analysis of outboard first wall", F.W./Blanket Workshop Culham, 19/20 June 1985.
3. E. Coccoresse, R. Martone, C. Rubinacci, M. Biggio, L. Deleanu, A. Inzaghi, 'Electromagnetic forces distribution and mechanical analysis in the first wall structure for INTOR/NET, 13th SOFT, Varese / Italy).
4. A. Cardella, H. Gorenflo, "Stress analysis of the NET outboard first wall box", NET/IN/86-03.
5. G. Vieider, "Estimated fatigue limites for the F.W. of NET", presented at this meeting.

POSSIBILITIES AND LIMITATIONS OF FIRST-WALL LIFETIME ANALYSES BY MEANS OF ANALYTICAL METHODS

W. DÄNNER
The NET Team,
Max-Planck-Institut für Plasmaphysik,
Garching near Munich

Abstract

This paper summarizes the scope of the problem of first-wall lifetime prediction as a comparison of the wall response to the typical loads in a fusion reactor environment and the material properties. Ways for solving the problem by computation are indicated and the procedure used in the FWLTB program is described. Some essential results obtained with this program are presented which show up the usefulness of analytical methods. The restrictions with respect to geometry and loading assumptions typical for analytical methods pose limitations which, together with the uncertainties in the materials data base, permit only rough lifetime estimates.

1. Introduction

Fairly early in the design of fusion reactors it has been recognized that the first wall will not withstand the loads to which it is exposed for the whole reactor life. This feature, of course, reflects into the economic and ecologic characteristics of a fusion power plant. If the first wall has to be exchanged several times in the plant life both the consumption of raw materials and the production of radioactive waste will be increased. In addition to the corresponding direct costs for fabrication and disposal of the spare parts further costs will have to be paid for the necessary remote handling equipment and another adverse economic impact arises from the reduced plant availability due to the time needed for the replacement. Hence, irrespective of the feasibility problem itself there is a strong economic incentive for finding a methodology to predict the lifetime of the first wall.

2. Scope of the Problem

In the absence of the possibility to perform lifetime tests in a real fusion reactor environment the problem of first wall lifetime prediction is clearly only accessible from the calculational side. In order to do a

calculation the following features have to be known:

- the detailed geometry of the first wall
- the loads on the first wall
- the properties of the wall material and
- the environment in which it is operating.

For the geometry it is not sufficient to know about the overall shape which is roughly dictated by the plasma shape. More essential are the details of the cross-section including, for instance, the size, shape, and location of cooling channels or those of protective components together with the means of their attachment. The loads which typically have to be considered are thermal loads in the form of both surface and volumetric heating, and mechanical loads originating from a coolant pressure and from forces and bending moments introduced by mechanical supports. The thermal loads are subjected to variation with time during an operation cycle; the time dependence may even be different for the surface and the volumetric part of the heat load.

As a consequence of the operation environment additional loads will arise in the first wall structure. During long term operation in the neutron environment inelastic strains due to swelling and irradiation creep, if operated at elevated temperatures even due to thermal creep, will be generated. At least the differential strains will in turn induce stresses which superimpose on those produced by the mechanical and thermal loads. Hence, the response of the wall to the loads is not only a function of time on the scale of an operation cycle but also on the long-term time scale.

The environment has also an impact on the geometry. Irrespective of the dimensional changes due to swelling and creep there is the special problem of erosion in a fusion reactor which - like corrosion - leads to a continuous decrease of the first-wall thickness.

The radiation environment is also responsible for a substantial change of the materials properties, especially of the mechanical ones. This means that the relation between the wall response and the respective property limitation (e.g. stress and strength) may be subjected to a continuous change. Just this relation, however, and its evolution with time is the essence of any life prediction methodology.

3. Ways for Solving the Problem

The scope of the problem which was roughly outlined in Section 2 is once more summarized in Fig. 1 in form of an information flow diagram which can be made the basis for a calculation procedure. In principle, it can be separated into two parts: the evaluation of the first wall responses and that of the material properties.

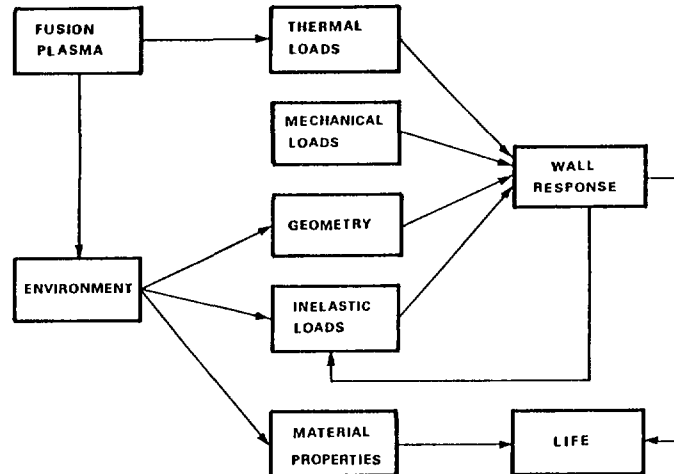


Fig.1 Information flow in procedure for lifetime prediction

In order to obtain the first wall responses a thermo-mechanical analysis is required. Depending on the complexity of the wall geometry either an analytical or a finite element procedure can be applied. Such a procedure has to include both nonstationary analysis on the time scale of an operation cycle and inelastic analysis on the long term time scale. This difference in time scales makes the solution of this problem complicated. Especially in the case that finite element methods have to be applied the size of the problem and the computer time needed for its solution may become excessive.

An additional problem arises from the fact that the finite element programs as they are available today cannot necessarily cope with the whole problem /1/. Nonstationary thermo-elastic analysis belongs to the standard capabilities of any program and most of them are even able to deal with plasticity problems. To a fair extent there are also algorithms implemented by means of which thermal creep problems can be treated. Equivalent procedures for irradiation creep and swelling, however, are only available in a few programs and are often restricted to a very specific material. Therefore, an appreciable R & D effort is

still needed in order to adapt these programs to the needs of the first wall lifetime prediction procedures. In the meantime simplified methods have to be used.

In the field of materials property evaluation the situation is also far from being satisfactory. What is actually required is a full description of the various life limiting properties as a function of the neutron irradiation dose with the data being measured in a typical fusion neutron spectrum. Today large programmes are underway to collect the information at least for a few materials envisaged for use in the next generation fusion devices. Within the procedure of lifetime prediction these data can be used in two different ways. One is to utilize the original data in evaluated form directly in the procedure and to compare them with the calculated response. This leads to a lifetime which may be qualified as "time to failure". A second way is to evaluate this information independently from the analysis and to derive design codes and guidelines in the form of admissible limits. Using these limitations in lifetime prediction leads to a result which is rather to be qualified as "service life".

With regard to the multinational efforts towards the next generation fusion machines like NET or INTOR the second way is surely the better one but it involves a lot of time to achieve the necessary agreement on the basis of the results of the experimental programmes. The first approach provides quicker answers even on a preliminary basis and can therefore provide guidance for the task of code development.

When comparing the needs and the current status in the field of first wall lifetime prediction the obvious conclusion is that an accurate treatment of the problem for realistic first wall designs is a matter of the farer future. Neither the computer programs nor the materials property data base are sufficiently well developed as to allow a precise answer to the question of lifetime now. Nevertheless, efforts have been made and are still being made to attack the problem with simplified methods. Examples are the SMILE code developed at JRC ISPRA /2/, the TSTRESS-WISECRACK program system developed at the University of Wisconsin /3/, and the FWLTB program developed at IPP Garching /4/. Recently KfK Karlsruhe joined this activity in the framework of the development of NET /5/. All these codes use analytical methods for

evaluating the first-wall response. They differ in the treatment of the inelastic effects and in the way of utilizing the materials data.

In the following the FWLTB program shall be described in order to demonstrate the possibilities and limitations of analytical methods.

4. The FWLTB program

4.1 Layout of the program

FWLTB is a computer program for simulating the First Wall Long Term Behaviour in a fusion reactor and for predicting its lifetime. Its development was started in 1975 with the goal to find a methodology for describing the long-term effects in simple wall geometries, specifically in cylindrical and spherical shells. Although this restriction to one-dimensionality implies the exclusion of perhaps more realistic wall geometries and of inhomogeneous loads, two advantages were attributed to this kind of approach: the geometrical simplicity facilitates interpretation of the results especially with regard to the interaction of the various phenomena occurring during long-term operation; the application of analytical tools for the thermo-elastic analysis provides the possibility of performing extensive parametric studies.

While concessions were made with respect to the geometry, much emphasis was put on a fairly correct representation and mathematical treatment of the loads and the responses of the wall to these loads. Internal heat sources in the wall resulting from neutron and gamma interactions with the wall material are based on the results of one-dimensional neutronics/photonics calculations from which the spatial profiles are derived. The time variation of the neutron wall loading and that of the surface heat load are based on the results of zero-dimensional plasma physics calculations. This input is analytically treated in a non-stationary thermo-elastic analysis which additionally takes into account the existence of a coolant pressure within the cylinder or sphere. Temperature, stress, and dose rate variations during an operation cycle are used to calculate the inelastic response in terms of average strain rates resulting from thermal creep, irradiation creep, and swelling. These are assumed to be valid during a prescribed interval on a so-called macro time scale. The strains developing within that period of

time build up additional stresses because temperature and stress are not uniform across the wall. These additional stresses superimpose on the initial stress level, which was only determined by the pressure stresses and the temperature profile. A new non-stationary thermo-elastic analysis including this alteration is performed at the end of the macro time interval, and the results form the basis for evaluating the inelastic response during the next interval. It should be mentioned that no iterative procedure is being used to enhance the accuracy with regard to the long-term variation of the stress fields; the accuracy is only controlled by an appropriate choice of the macro time interval lengths.

By using this procedure the stress and strain fields are obtained for discrete instants on the macro time scale. This information constitutes the one ingredient necessary for estimating the lifetime. The second one is the information about the mechanical properties. In parallel with the inelastic effects the evolution of the yield strength, ultimate tensile strength, uniform and total elongation, time rupture and fatigue life is followed on the macro time scale. This requires that a full description of these properties be included as a function of the irradiation exposure expressed in terms of neutron fluence, displacement dose, and helium concentration. A comparison of the two sets of information is performed after completion of every macro-time interval. The lifetime is terminated if the maximum stress occurring during an operation cycle exceeds certain fractions of the actual yield or ultimate tensile strength, if the maximum strain exceeds certain fractions of the actual uniform or total elongation, or if the sum of the life fractions consumed by time rupture and fatigue exceeds unity. In addition to these five criteria, the accumulated amounts of swelling and irradiation creep strains and of the total volume increase due to both effects are checked against prescribed limits which are determined by design features rather than by mechanical properties.

At a later stage the calculation of the stress intensity was added as was the evaluation of crack growth rates. By checking both the stress intensity against the fracture toughness and the crack length against the wall thickness two further life criteria could be evaluated.

4.2 Capabilities of the program

The mathematical procedure roughly described above forms the basis of the FWLTB computer program. It is of modular construction, readily allowing extensions, modifications and refinements. This feature pays off especially when new materials data emerge from the experimental programs.

Two separate subroutine packages are available which contain a fairly complete set of property relations for two different austenitic stainless steels: the German type DIN 1.4970 and AISI type 316 SS, both in the coldworked condition.

They represent the status of published knowledge up to 1981. The irradiation dependence of the properties was modelled from experimental results and evaluated design equations originating from fast breeder reactor development programmes. In the case of 316 SS results from HFIR irradiation tests have been additionally included which give a more representative picture of the material behaviour in a fusion reactor environment. Many of the data subroutines can be controlled via input in such a way that they provide property values deviating from the nominal ones. Sensitivity studies with respect to data accuracy can thus be performed.

Apart from management of the property data, the FWLTB program offers great flexibility with regard to operating modes. Besides the possibility of exactly treating arbitrarily shaped periodic time variations of neutron wall loading and surface heat load as obtained from plasma physics calculations, the program can also be run with the assumption of idealized pulse shapes. This is a valuable simplification for scoping studies. The program is also suitable for performing steady-state thermo-elastic analyses, which extends its applicability to analyses of the lifetime problem for reactor concepts allowing continuous operation. As a unique feature, provision is made in the program for varying on the macro time scale some load and design parameters, which in the usual operating mode are fixed by input specification. This allows not only the effects of wall erosion and corrosion to be included but also various types of load histories to be simulated.

In order to allow effective use of the program, it is equipped with a versatile system of output routines providing both print and plot output controlled by simple input specifications.

5. Some essential results

The results of the many investigations performed with the FWLTB program have been published in the proceedings of various conferences. A complete list of references may be found in /4/. Here only the most important results of general nature shall be summarized which document the usefulness of studies with analytical methods.

5.1 The inelastic response

The inelastic response of the wall resulting from swelling and creep processes modifies the stress and strain fields in the first wall to an extent which cannot be neglected. Thermal creep strains and, even at lower temperatures, irradiation creep strains partially equilibrate the operational thermal stresses such that stress relaxation occurs at the cold surface. This process may either be amplified or partially balanced once additional stresses are produced by differential swelling. Upon amplification or balancing decides the relative position of the operational temperature range of the wall with respect to the maximum swelling temperature of the material. For that reason it is conceivable that different materials behave differently and even the same material may behave differently in different environments, as is shown in Fig.2.

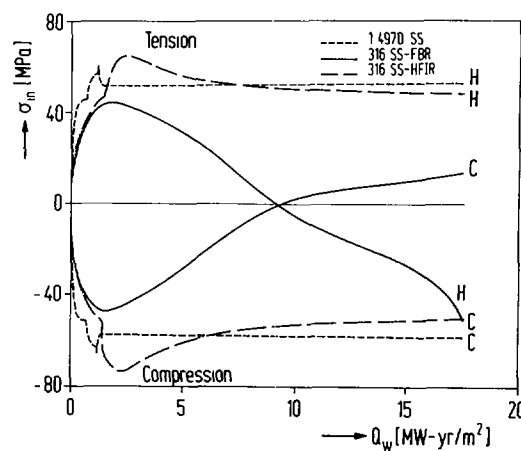


Fig.2 Stresses due to differential in-elastic strains for different materials in different environments.

The relation between swelling and creep is likewise of big importance as is shown in Fig. 3. Only if the ratio of the swelling and creep rates is linear in time or dose the additional stresses saturate. If it is nonlinear with an exponent $n > 1$ a continuous stress increase has to be expected leading to an early life termination.

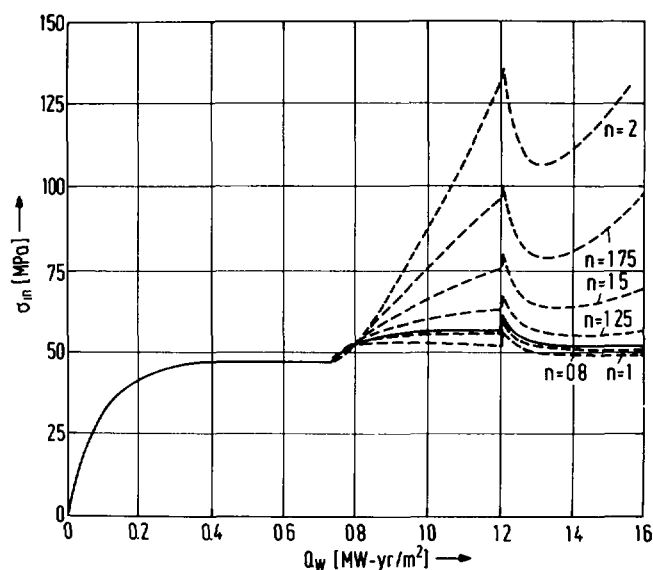


Fig.3 Influence of dose exponent n on the evolution of stresses due to inelastic effects

5.2 Important life limitations

Based on the experience from a number of studies it has turned out that the problem of first wall lifetime can best be discussed by means of a picture as shown in Fig. 4. This diagram generated for the case of a DEMO power reactor first wall made of 20% cold worked 316 SS shows that the most important lifetime limitations are the tolerable amounts of swelling and creep deformation, SW5 and IC5, both assumed to be 5%, and the limit due to creep-fatigue interaction, CF, which includes the effect of helium embrittlement. For given coolant pressure and thermal loads, creep deformation and creep-fatigue life are strongly dependent on the first wall thickness d . It is this dependence which makes erosion play a major role in assessing the life expectancy. A typical erosion rate $\dot{R}_e = 0.3$ cm/yr is represented by the dashed line in Fig. 4.

Within the frame defined by the solid lines optimization of the lifetime is possible. For the example shown in Fig. 4 the potential of 6 MW-yr/m^2 offered by swelling limitations can just be utilized under the condition of a 0.3 cm/yr erosion rate if the initial wall thickness d_0 is chosen about 1.05 cm. Under these conditions the creep-fatigue life consumption is large at the beginning of operation, but decreases with proceeding erosion. The creep deformation grows slowly at the beginning, but increases rapidly as the remaining wall thickness d approaches the IC5 limit.

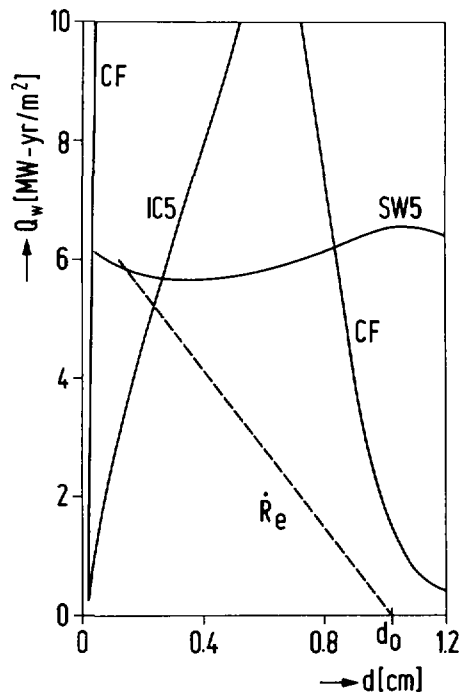


Fig.4 Lifetime limitations as dependent on the wall thickness d for a DEMO reactor

Longer lifetimes can only be achieved if this frame is enlarged. Of primary importance is the improvement of the swelling behaviour or, alternatively, admission of larger swelling deformations. The lifetime potential thus provided can, however, only be utilized if at the same time either the erosion rate is reduced or the creep-fatigue life is improved. The latter needs either effective means for suppressing the helium embrittlement which would shift the CF limit vertically upward, or a significant reduction of the external heat load on the wall shifting the limit to the right.

Just this relation between external heat load, erosion rate, and creep-fatigue life underlines the importance for reducing the uncertainties not only on the materials data, but also on the plasma physics side.

Out of the further materials properties only the short-term ductility seems to play a major role in machines operating at low temperatures as, for instance, INTOR. The problem of crack propagation emphasized over a long period of time appears in a more favourable light if both erosion and the inelastic response are taken into account in the analysis. Of course, the problem may come up again if the present predictions of lower erosion rates should survive.

6. Conclusions

As was demonstrated by the FWLTB program development and operation, analytical methods are well suited for combining non-stationary thermo-elastic and inelastic long-term analysis in an interdependent way. This allows to study the synergism and interaction of the various phenomena occurring during first-wall operation. The big benefit of analytical methods with respect to computer time requirements permits to perform extensive parametric studies and sensitivity analyses. With regard to the still existing big uncertainties in both the materials data and the physics loading conditions, investigations of this kind were more urgently needed in the past than precise predictions of the lifetime. The restriction to simple geometries was in fact very useful because it facilitated the interpretation of the results and it hence promoted the understanding of the first-wall long-term behaviour.

On the other hand, the restrictions to simple geometry as well as to uniform load distributions are the most serious limitations for analytical methods. From their application we have learned that the significant effects are attributable to the existence of any kind of profiles across the wall. Real first-wall structures look far more complicated than simple tubes and therefore the profiles will greatly differ from those of simple one-dimensional bodies. If, however, the geometry should be simple the loads will be non-uniformly distributed and the profiles will be affected accordingly. The best way to overcome this problem is to proceed in the development of existing finite element methods, i.e. especially to include suitable algorithms for swelling and irradiation creep. Nevertheless, it should be kept in mind that even with a refined calculational procedure the precision of lifetime prediction will still depend on the data accuracy.

Acknowledgements:

The author is deeply indebted to K. Ehrlich, J.D. Elen, D.R. Harries, J. Raeder, and P. Schiller for valuable comments and advice received during the development of the FWLTB program. He also gratefully acknowledges the programming work done by H. Gorenflo. He finally thanks A. Cardella and E. Zolti for many helpful discussions during the preparation of this paper.

References

- /1/ D.R. Harries, E. Zoltti: Structural mechanics and material aspects of the Next European Torus, Nucl. Eng. and Design (to be published).
- /2/ R. Matera et al.: SMILE - a computer program for evaluating the lifetime of fusion reactor structural components, Nucl. Eng. and Design, Vol. 1, No. 2 (April 1984).
- /3/ R.D. Watson et al.: The effect of irradiation creep, swelling, wall erosion and embrittlement on the fatigue life of a Tokamak first wall, J. of Nucl. Mat. 103 & 104 (1981).
- /4/ W. Dänner: FWLTB - a computer program for estimating the first wall lifetime in a fusion reactor: a status report, Res Mechanica 6 (1983).
- /5/ T. Fett, D. Munz: Stress and Lifetime Calculations for first wall and blanket structural components, Part I: Crack propagation in tubes, KfK 3875 (Jan. 1985).

TOOLS AND PROCEDURES FOR STRUCTURAL LIFETIME EVALUATION OF NET FIRST WALL DESIGN CONCEPTS

E. ZOLTI

The NET Team,
Max-Planck-Institut für Plasmaphysik,
Garching near Munich

Abstract

The problems, the available technology and the needed advances on the theoretical evaluation of the NET First Wall design concepts with respect to the structural lifetime are described. Major areas are:

- Computational methods to determine the First wall deformations, stresses and strains under conditions of cyclic elasto-plasticity, swelling, irradiation and thermal creep and computational fracture mechanics in situations of inelasticity and high thermal gradients.
- Criteria for the evaluation of the calculated thermostructural response with respect to the integrity and functional requirements.
- Approaches to handle very complex First Wall geometries through a combination of 2 and 3 dimensional models.

Uncertainties and open questions in these lifetime analyses tools and procedures are discussed and an example of first simple localized studies is given.

1. Introduction

Envisaged as the sole step between JET and a first fusion power reactor (DEMO) the Next European Torus (NET) aims at the demonstration, as far as possible, of reactor relevant technologies with reactor like plasma parameters /1/. The development of the First wall (FW) and other structural components facing or located close to the plasma poses a major technological challenge as compared to the magnet system structures, which benefit of a more advanced technology, and to the "conventional" components subjected to less onerous service conditions and structural requirements. During the current pre-design phase several FW design concepts (/2/,/3/) are evaluated comparatively also with respect to the structural lifetime. This is performed on the basis of the existing knowledge on the behaviour of the two candidate steels, namely the austenitic 316L (s.a. or cw) and ferritic-martensitic 1.4914.

The purpose of these lifetime evaluations is to assist in the final selection of the material and reference solution of the first wall for the detailed design.

This paper summarizes the main problems, the approaches available and the advances needed for the FW lifetime estimations, addressing particularly the areas of computational methods, structural design evaluation criteria and analysis modelling and procedures.

2. Structural failure modes

The potential failure modes determining the FW structural lifetime can be grouped in 2 categories, related respectively to:

- a) material damages impairing the FW integrity and
- b) excessive deformations impairing the FW functional adequacy.

The phenomena and factors associated with these failure modes have been extensively described in the literature, e.g. /4/.

The major areas are summarized in Fig. 1 and in the following:

- 1) Fatigue damage due to cyclic stresses and strains resulting from cyclic loadings.

These are not only the pulsed surface heat flux ($\sim 0.15 \text{ MW/m}^2$) and volumetric heat generation ($\sim 15 \text{ W/cm}^3$) (thermal fatigue) but also any repeated variation of mechanical (e.g. coolant pressure) and electromagnetic loads.

In some design solutions the yield limit is exceeded at every cycle (cyclic plasticity).

The fatigue damage can be divided in a crack initiation and a crack propagation phase.

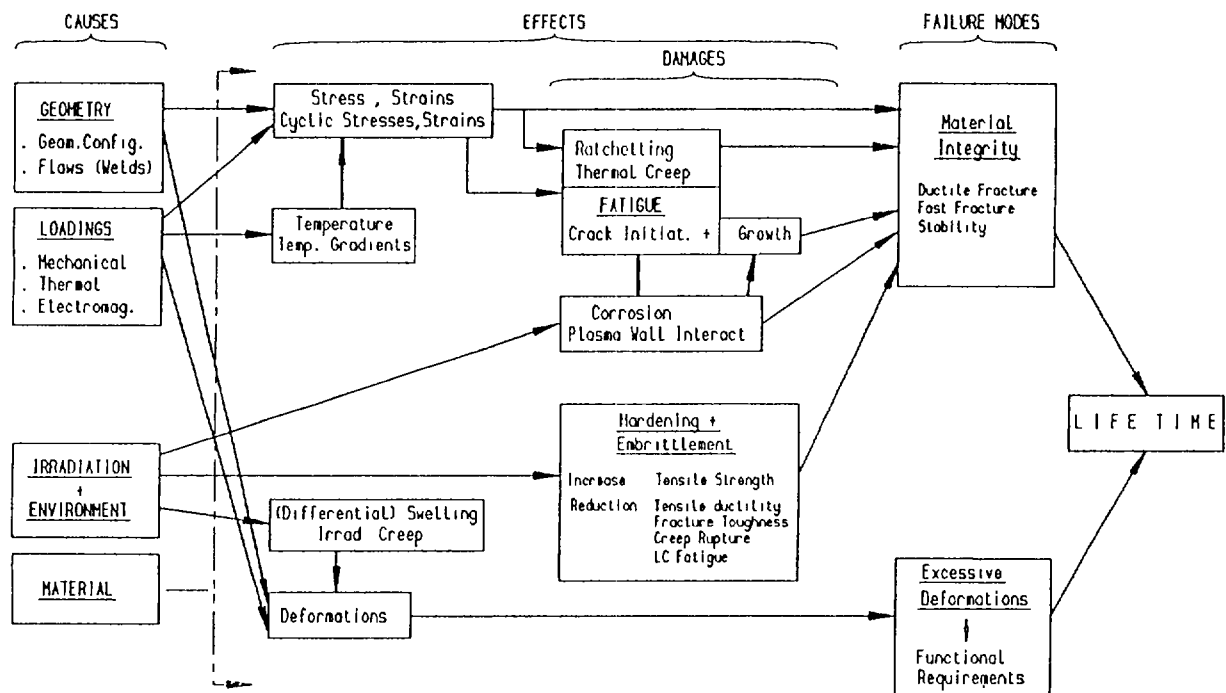


Fig. 1 Main potential failure modes and related factors affecting the FW structural lifetime

- 2) If a crack-like defect is already present, as always to be assumed in welds, the crack initiation phase is bridged and the deterioration considerably accelerated.
- 3) Neutron irradiation, gas (He and H) production and liquid metal effects determine a material embrittlement with a reduction of almost all the strength and ductility properties of the structural material.
- 4) Erosion on the plasma site, due to physical and chemical sputtering of the bare wall, and/or corrosion effects on the coolant site limit the lifetime because of the reduction of the thickness essential for the primary stresses and because of the possible generation of crack-like defects.

- 5) The temperature could be sufficiently high at large or localized zones for thermal creep and thus additional damage to be present. Fatigue, creep, irradiation and corrosion effects can interact, thus accelerating further the material damage.
- 6) An unfavourable combination of cyclic thermal stresses and a sustained primary stress could give rise to an incremental accumulation of inelastic strains from cycle to cycle (ratcheting). That can lead to a ductility exhaustion or to unallowable excessive deformations.
- 7) Neutron irradiation induced swelling and creep-strains are supposed to add directly no material damage. However, particularly the differential strains due to temperature and stress gradients, result in dilations and/or distortions of the FW. These could exceed the allowable deformation limits specified to avoid interferences or excessive frictional forces during maintenance, or plasma limiter effects.
- 8) During plasma disruption heat fluxes of 200 to 1000 J/cm² are deposited mainly on the inboard wall in a time of order 20 ms and large electromagnetic forces with a complex distribution and a clearly dynamic nature arise.

3. Lifetime evaluation steps and requirements.

In the FW lifetime investigations the material bulk and surface properties are undoubtedly in the foreground and especially the fracture toughness and the thermal fatigue of the irradiated material and the sputtering rate are presently among the major uncertainty sources.

However in addition to these "macroscopic" material properties, which are obtained on laboratory specimen geometries and loading, also the actual construction geometry and operational loading conditions of the FW are essential factors.

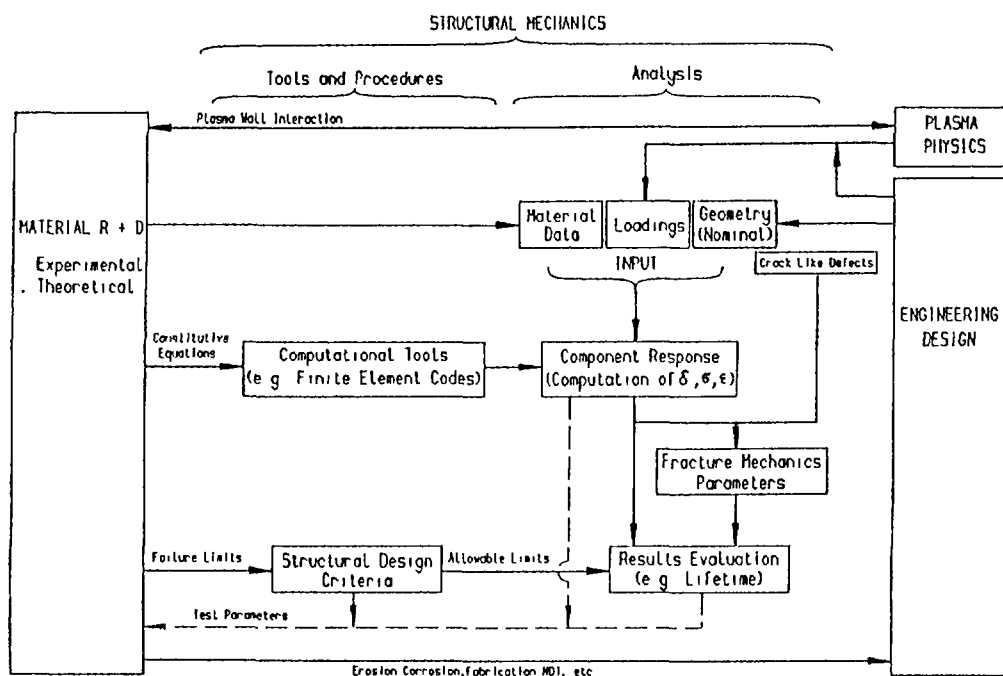


Fig. 2 Interactions between areas of structural mechanics, material, engineering design and plasma physics

The flow diagram of Fig 2 shows the steps of a lifetime analysis, the connection with the essential tools and the relationship with the engineering design, the material R and D and the plasma physics. At first the thermostructural response of the first wall has to be determined in terms of time and space distribution of the temperatures, deformations stresses and strains on the basis of a conservative schematization of the geometry and loadings. The results are then used directly or through the determination of "damage factors" and of fracture mechanics parameters to estimate the lifetime and thus to assess the structural design adequacy. This evaluation is carried out on the basis of the allowable limits included in the design criteria.

4. Computational methods

The basis for the prediction of the FW deformations stress and strains is:

- a) a mathematical representation of the material behaviour (constitutive equations) under multiaxial stress and strain states and under conditions not only of thermoelasticity (linear stress-strain relation), but in general also of cyclic plasticity, thermal and/or irradiation creep and swelling (non linear stress-strain relation) as mentioned in section 2;
 - b) a computational algorithm on the basis of a direct analytical or iterative numerical method.
- a) Methods for temperature and elastic calculations are well established. For plasticity and thermal creep there are many and varied models, addressing different materials and types of loadings. However no model describes completely the complex plastic and creep behaviour, which actually is not clearly understood. Of concern for FW plastic and thermal creep analysis is the material model developed by Oak Ridge National Laboratory, (ORNL), applicable to the stainless steels 304, 316 and 2 - 1/4 Cr - 1 Mo /5/. The model has been implemented in general purpose finite element computer codes, as e.g. ADINA, MARC, ANSYS, and used in the fission technology, particularly for high temperature design of fast breeder (LMFBR) components. In the ORNL model the total strain components (ϵ_{ij}) are considered to result from the sum of the elastic (ϵ_{ij}^{el}), plastic (ϵ_{ij}^{pl}), and thermal creep ($\epsilon_{ij}^{th.cr}$) strains. The loads histogram is divided in small but discrete time intervals (Δt) and the corresponding increments of the plastic strains ($\Delta \epsilon_{ij}^{pl}$) and thermal creep strains ($\Delta \epsilon_{ij}^{th.cr}$) are calculated separately and summed to get the total strain. Thus at every time $t + \Delta t$

$$(1) \quad \epsilon_{ij}^{tot.} (t + \Delta t) = \epsilon_{ij}^{el} (t + \Delta t) + \sum \Delta \epsilon_{ij}^{pl} + \sum \Delta \epsilon_{ij}^{th. cr.}$$

where the \sum refers to all the time steps from $t=0$ to $t + \Delta t$.

The model assumes no interaction of plasticity and creep, i.e. no effects of prior plastic strains or subsequent creep strains and viceversa; but prior creep strains are considered to contribute to the hardening similarly to plastic strains.

The relationship to calculate plastic strains are:

- the stress-strain relationship in the uniaxial case,
- the von Mises yield condition, specifying the onset of plasticity for the multiaxial stress state,
- a hardening criterium, specifying the changes of the yield condition during the plastic flow (e.g. isotropic or kinematic hardening).

Analogously, for the calculation of creep strain it is required:

- a creep law relating the creep strain to the time, stress and temperature in the uniaxial case, including primary and secondary creep;
- a hardening criterium specifying the creep strain accumulation in conditions of variable stresses and temperatures.

Furthermore a relationship is required to relate the multi-axial strain increments components to the multi-axial stress- and stress increments- components (Flow rule). For both plasticity and creep these flow equations are formulated assuming:

- isotropic material and constant volume with respect to plastic and creep strains, and
- plastic strain increments and creep strain rate not dependent on the hydrostatic stress states and proportional to the deviatoric part of the stress tensors.

The validity of these hypotheses for the conditions of the first wall materials is to be verified.

- b) The classical inelastic calculation approach is based on a linearization of the problem through the iterative time increment method and the initial strain- or initial stress- or variable stiffness matrix- procedure /6/. At every time step several iterations are carried out and in each one the deformations, total strains and stresses are calculated elastically accounting for the values of the inelastic strains of the previous iterations. The iterations are continued until the equilibrium conditions and the stress-strain relationships are satisfied within a convergence tolerance.

Procedures to calculate inelastic strain due to swelling and irradiation creep, although presenting no further difficulties, have been implemented in quite few inelastic finite element codes, probably because of the limited applications.

In the special purpose code IAFETIN /7/ developed for structural analyses of fast breeder core components, swelling strains depending on temperature and neutron fluence, are handled similarly to thermal strain; irradiation creep strains, depending on stresses and neutron fluence, similarly to thermal creep strains. Both are incorporated in the iterative time increment procedure, so that at every step either the time independent (plasticity) or the full time dependent (swelling, thermal and irradiation creep) behaviour can be considered.

However, for the cases where thermal creep and plasticity effects are irrelevant, the procedure can be simplified, taking advantage of the fact that the existing irradiation creep empirical correlations for stainless steel show a linear dependence of the creep strain on the stress. That permits to define an equivalent E modulus and an equivalent Poisson ratio accounting for the fluence dependent factor of the creep law, and thus to reduce the time increment calculations to only 1 elastic iteration.

Detailed elasto-plastic and creep calculations of the first wall structural response could be considerably more expensive and time consuming than the simple thermoelastic analysis, even for 2D models. The effort and also the results can strongly vary depending on the calculation strategy (subdivision of the load histogram in increments, convergence error, preliminary preparatory analyses etc).

The necessity of analysis procedures considering extensive simplifications in the geometry, loadings and material model is therefore evident.

5. Structural Design criteria

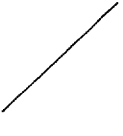
Besides adequate computational procedures to determine the FW structural response, as described in Sect.3 , the assessment of the structural design requires also a set of rules to evaluate the predicted deformations, stresses and strains with respect to the potential failure mode (structural design criteria).

A simple, even if very conservative set of rules is needed for common use within the NET project in the predesign phase to evaluate different design options. Furthermore, complete and qualified criteria are needed for the full validation of the selected reference solution in the successive detailed design phase.

Because of the peculiar operational conditions and of the complex material behaviour the needed criteria exceed the bounds of the present-day technology. The most complete reference basis can be the structural design codes in use for fission technology as e.g. ASME code sect III /8/, and in particular for the high temperature components of a fast breeder reactor (LMFBR), as e.g. the code case 47 /9/. Unfortunately, there is no standard code for the highly irradiated fast breeder core components, whose lifetime problematic, despite the different structural requirements, is in several points analogous to that of the FW.

Therefore, development work in this area has been initiated within the NET project. Table 1 shows a first draft of simplified criteria, proposed for use in the predesign phase. The symbols used in Table 1 are the usual ones of the ASME code.

Table 1 : Proposal for structural design criteria for the predesign of the NET plasma facing components

LOAD CONDITIONS	STRUCTURAL INTEGRITY			FUNCTIONAL REQUIREMENTS
	DUCTILE AND FAST FRACTURE	FATIGUE (+CREEP)	INSTABILITY	
CATEGORY 1 • Normal pulsed operation • Scheduled transients • Anticipated likely abnormal conditions. (disruptions ?)	$\sigma_{p,m} \leq S_m^{unirr} = \min(\frac{2}{3} \sigma_{ps}, \frac{1}{3} \sigma_{ps} \frac{1}{3} \sigma_{ps})$ $\sigma_{p,mib} \leq 1.5 S_m$ $E_{pl,cr} \leq \begin{cases} E_{all} \text{ (base mat. , T, } \phi t) \\ 1/2 E_{all} \end{cases} \rightarrow \text{welds}$ $\sigma_{p,ma} + \sigma_{sc} \leq S_m$ $E_{cr}(\sigma_o) \leq E_{all}$ $K_I^{EOL}(\sigma_o + \Delta \sigma_{fat,avg} + \Delta \sigma_{creep}) \leq \frac{1}{3} K_{IC}^{EOL}(T, \phi t)$	$\sum \frac{n}{N} (+ \sum \frac{t}{t_R}) \leq 1$	Load strain $L_{max} \leq E_{max}$ $\leq \frac{L_c}{3} \leq \frac{E_c}{15}$ (time indep) $\leq \frac{L_c}{15}$ (time dep)	$\delta_{max}(T, S_{wd}, cr)$ $\delta_{all} \text{ (plasma)}$ $\delta_{all} \text{ (mainten)}$ $\delta_{all} \text{ (divertor heat flux)}$ $\delta_{all} \text{ (RF anten.)}$
CATEGORY 2 • Anticipated unlikely abnormal conditions • Design faults	$\sigma_{p,m} \leq 2 S_m$ $\sigma_{p,mib} \leq 3 S_m$ $K_I(a^{EOL}) \leq 0.5 K_{IC}^{EOL}(T, \phi t)$		$L_{max} \leq E_{max}$ $\leq \frac{L_c}{15} \leq \frac{E_c}{4.1}$	δ_{max} $\leq \delta_{all \text{ safety}}$

Among the major differences between these interim FW predesign criteria and the ASME-code are the following:

- The operational loading conditions are grouped in only 2 categories. The 6 groups classification foreseen in the ASME Code Case 47 is at present considered premature, because of the nature and frequency of abnormal transients or fault situations, particularly those that arise from the plasma, cannot yet be clearly specified.

The classification of plasma disruptions associated thermal and electromagnetic loadings deserves special consideration because of the severity and the high number of the disruptions (~ 1000 in 2 years blanket lifetime). Pending progress in the plasma physics and a reduction in the probability of such events (say, down to ≤ 10), the disruption loadings will be included in the 1 category. Therefore, the design of the plasma facing components is required to accommodate the structural effects so that the components can withstand the conditions without operational impairment and thus without need of repair or replacement.

b) Emphasis is placed on the material irradiation damage and failure modes by consideration of:

- the fluence dependence of fracture toughness, thermal fatigue limits and strain limits to guard against ductility exhaustion.
- swelling and irradiation creep in the deformation rules for functional requirements.

The irradiation induced increases of the yield and ultimate stresses are not normally considered for the allowable limit S_m on the primary stresses. Sufficiently reliable values of the irradiated material strengths can be taken into account only if the time at which the max. stresses arise can be clearly identified. This is the case of primary stresses computation based on thickness reduction due to sputtering erosion and/or corrosion.

Due to the potential presence of flaws or any crack-like defects (welds, craters with cracks following disruptions, arcing etc) fracture mechanics considerations are essential part of the evaluation criteria. For the elastic case the methods of fracture mechanics are within certain limitations quite well established. Further development and/or qualification work is needed for the cases of extensive inelastic zones and of large stress gradients at the crack tip. Fracture mechanics aspects are handled in another presentation of this IAEA meeting /10/.

Since the determining failure mechanisms are not yet known and because of the close dependence of the allowable limits on the material properties which are in continuous state of development, the preliminary structural design criteria are also to be continuously updated on the basis of the latest knowledge resulting from the corresponding R & D programmes.

6. Lifetime analysis modeling and computations

In addition to the uncertainties in the material behaviour and in its mathematical representation, as described in section 4(a), further difficulties of the FW lifetime analysis arise in the modelling of the complex geometry and of the complex space and time distribution of thermal, mechanical, electromagnetic and neutron irradiation loading.

In the first wall design concepts currently studied by the NET Team (Fig.3), the FW of each toroidal sector consists of an inboard and an outboard panel with poloidal coolant channels, possibly containing additional coolant tubes, or alternatively with toroidal coolant tubes. This global geometrical configuration and the presence of a protection layer in the form of additional thickness steel with or without grooves, or mechanically attached or bonded ceramic tiles result in a highly 3-dimensional geometry.

Thus the total schematization of the inboard or outboard geometry with a mesh of finite elements, although in principle possible by means of the

general purpose finite element computer codes, would require an exorbitant effort even for the simplest case of thermoelasticity and constant loads. A first problem of approaching the structural lifetime evaluation is therefore to find a proper combination of global analyses, with 2 or 3 dimensional simplified models, and of 2 dimensional localized analyses.

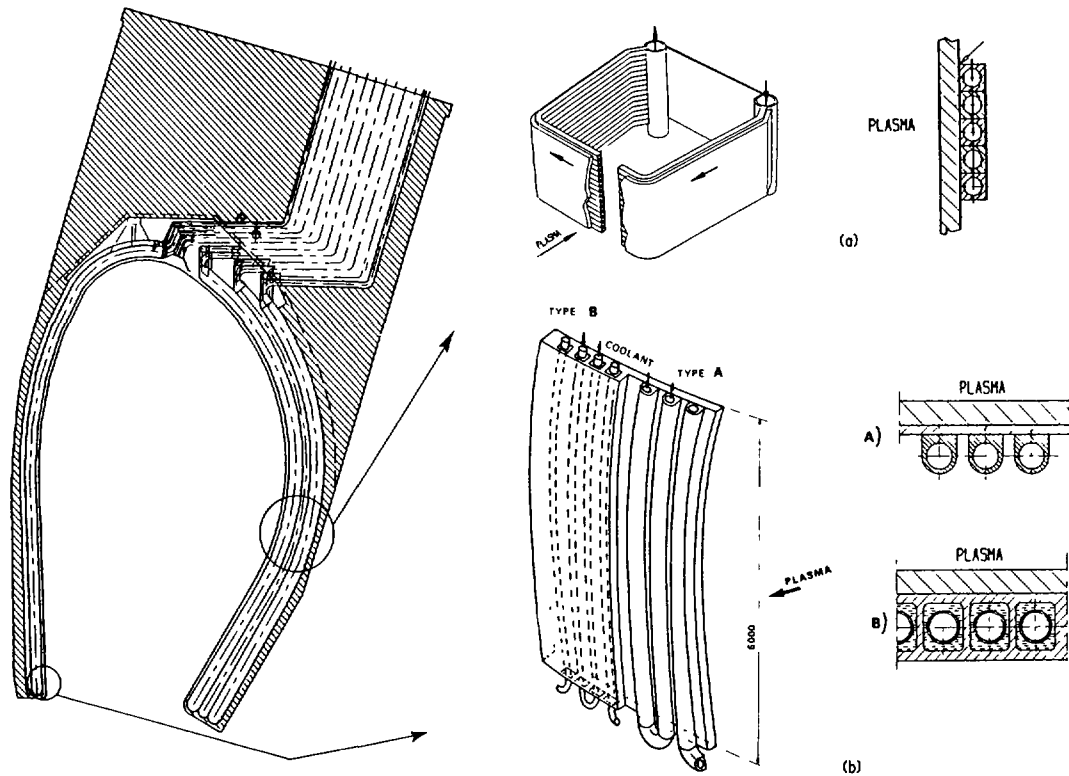


Fig. 3 Examples of design concepts of NET FW integrated in the blanket segment box, with (a) toroidal coolant flow /3/ and (b) poloidal coolant channels and/or U-tubes /2/

The purpose of the global analysis is to investigate the bending behaviour of the box configuration. Thereby the real FW geometry can be simulated through continuous shells equivalent to the original panels with respect to the deflections and membrane plus bending stresses. For the cases of mechanical and electromagnetic loads the equivalence can be achieved through adequate choice of the shell thickness and of the 2 different E-Moduli of a fictitious orthotropic material, thus restoring conservatively the bending stiffness in both the poloidal and toroidal directions.

The main objectives of the 2 dimensional localized analyses are:

- to compare different protection solutions in terms of temperatures, steady state stresses, cyclic stresses,
- to identify essential design improvements, e.g. grooves, coolant channels, location of welds, geometry of the mechanical attachment,
- to investigate the effects of the pulse times, especially dwell times on temperature gradients and thus on fatigue lifetime through instationary analysis,
- to obtain the temperature distribution through the cross section for other considerations, e.g. surface chemistry, tritium permeation,
- to quantify the approximation of simple handcalculations.

Relatively to these objectives the simplest approach to the localized analyses is a two dimensional thermoelastic model considering:

- the smallest symmetrical (with respect to geometry, loadings and material properties) zone of the FW horizontal and vertical cross section,
- plane strain or generalized plane strain finite elements, corresponding to the assumption of total or partial strain prevention in direction perpendicular to the considered plane, respectively.
- a translation without rotation of the cut-sites, corresponding to the assumption of a free lateral expansion without bending, or, more realistically, displacement boundary conditions derived from the results of the global bending analyses.

Fig. 4 shows an example of the geometrical schematization for localized analyses which was used for a parametric study of the NET-FW through the computer code IAFETIN. To minimize the computational effort an adequate finite element mesh was selected, so that the geometry of the single case could be easily obtained with minor changes or making inactive the elements of the zones not involved.

Fig. 5 shows some results of the case of an instationary, thermal and elastic mechanical analyses and the assumed loads histogram and material data.

The evaluation of the elastically calculated stress range in the cycle in terms of allowable number of cycles was made on the basis of the code case 47 fatigue curves (/9/).

From Fig. 5 one can see the conservatism of fatigue considerations based on the stationary stresses, the large negative effects of increasing the sacrificial layer up to 10 mm, and the beneficial effect of every dwell time reduction. The latter is due to a larger temperature gradient at the end of the dwell time and thus to a lower stress range.

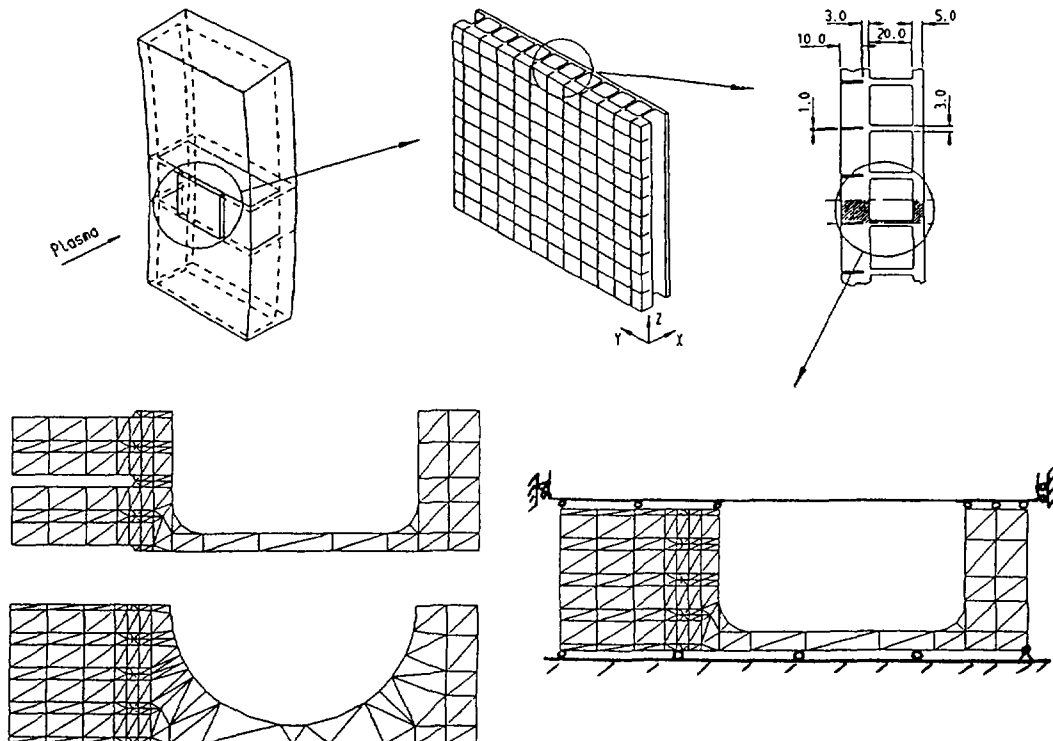


Fig. 4 Geometry schematization and boundary conditions for a parametric local analysis of NET FW

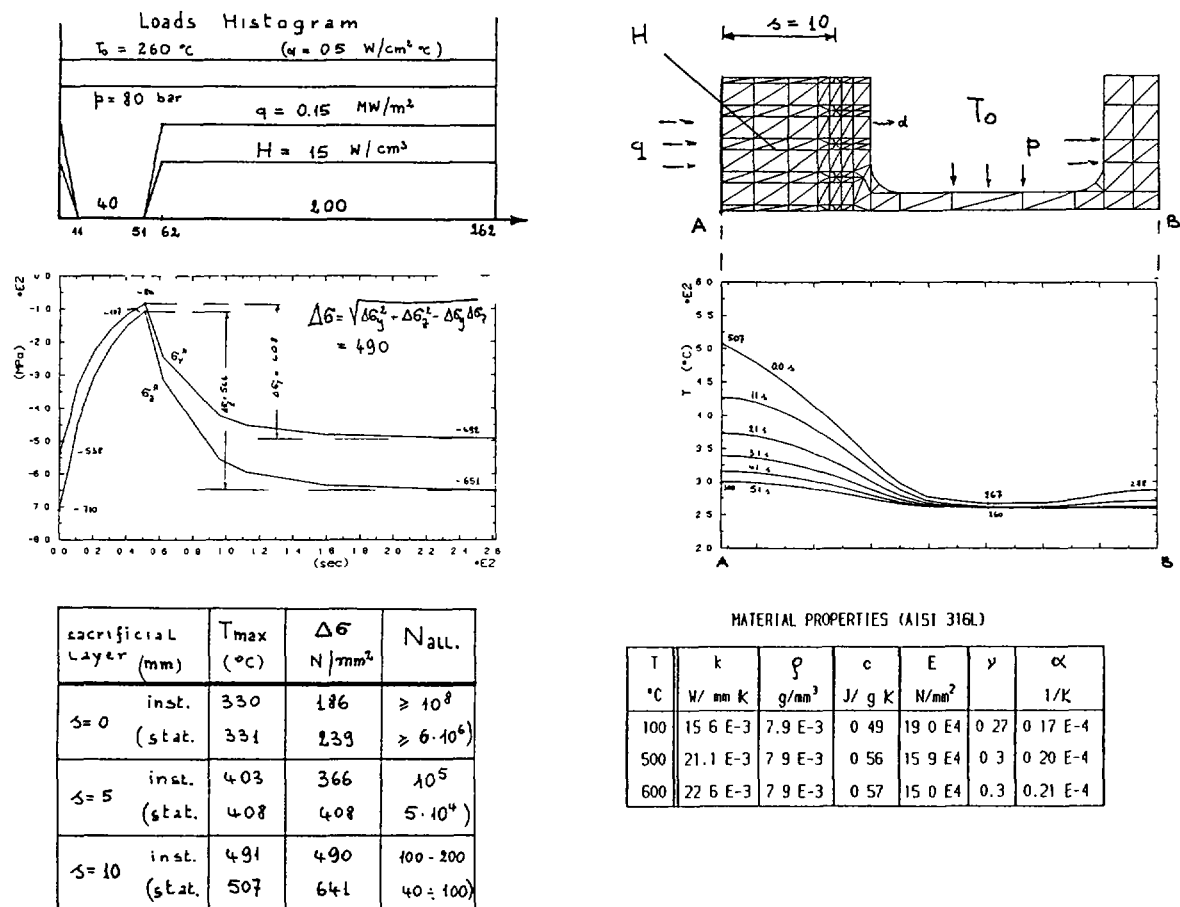


Fig. 5 First Wall parametric local analysis. Case of instationary thermal and mechanical elastic calculation for the ungrooved FW.

7. Summary and conclusions

In this brief review of the tools and procedures needed for the theoretical evaluation of the NET first wall design concepts with respect to the structural lifetime it was attempted to highlight the limitations and the uncertainties of the correspondent available technology.

The main points can be summarized as follows:

- 1) Computational methods to determine the structural response in terms of displacements, stresses and strains are available or easy to be developed. However the validity of the basic assumptions in the available mathematical models describing the material behaviour under conditions of cyclic plasticity, thermal and irradiations creep has to be verified for the NET materials, loading and environmental conditions.
- 2) FW-appropriate swelling and irradiation creep laws are to be still developed.
- 3) Structural design criteria for the evaluation of the calculated structural response can be derived from existing design codes in use for fission reactor components. However, the material allowable limits, relative especially to fatigue, ductilites, fracture toughness will remain the major uncertainty area in FW lifetime assessments until the

real effects of gas production and neutron irradiation damage on the material properties are known.

- 4) The sputtering rate, the disruption loadings magnitude and frequency are also a considerable source of uncertainty. However, the lifetime assessment problem is alleviated if an adequate protection design solution is found.
- 5) The modelling of the complex 3D-FW geometry with a combination of simple 2 and 3D models requires expertise to avoid excessive or insufficient conservatism and is correspondently, a source of uncertainty.
- 6) Inelastic analysis are presently impractical because, in addition to the above points 1 to 5, they are normally very expensive and time consuming.

Main conclusion is:

- Simplified methods for lifetime assessment including extensive simplifications in the modelling of the geometry, of the material behaviour and loading conditions or a combination in all these areas are essential especially in this predesign phase to keep the structural analysis effort commensurate to the overall predesign effort;
- the simplifications should be generously conservative to attempt to cover at least partially the present uncertainties;
- as long as the material behaviour in fusion environment (especially the embrittlement and swelling) is not sufficiently quantified, lifetime studies are valuable for comparative evaluation of different design options rather than for absolute service time assessment.

References

- /1/ R Toschi, Trans 8th SMIRT, Brussels, August 1985, Paper N2/1
- /2/ G. Vieider et al., Proc. 13th SOFT, Varese, September 1984, PergamonPress, 1984, I, 297.
- /3/ G. Casini et al., Trans. 8th SMIRT, Brussels, August 1985, Paper N4/1
- /4/ INTOR Report, Phase One, IAEA, Vienna 1982
- /5/ K.M. Corum et al., Interim guidelines for detailed inelastic analysis of high temperature reactor system components, ORNL 5014, Dec. 1974.
- /6/ O.C. Zienkiewicz, The Finite Element Method in Engineering Science, Mc Graw-Hill, London 1971.
- /7/ E. Zolti, Localized Thermostructural Analysis of LMFBR-Core Components through the FEM-code IAFETIN, Trans. 6th SMIRT, Paris, August 1981, Paper D4/6.
- /8/ ASME Boiler and Pressure Vessel Code, Sect. III, Division 1, Subsection NB. ASME.
- /9/ ASME Sect. III, Division 1, Code Case N-47, Class 1 Components in Elevated Temperature Service.
- /10/ D. Munz, Lifetime Limitation of First Wall Structures by Fatigue Crack Propagation. Presentation at this IAEA Meeting.

Session 4

EROSION AND DEPOSITION EFFECTS

MATERIAL DAMAGE IN THE FIRST WALL OF TOKAMAKs BY PLASMA WALL INTERACTION

K. KOIZLIK, H. NICKEL

Institut für Reaktorwerkstoffe,
Kernforschungsanlage Jülich GmbH*,
Jülich, Federal Republic of Germany

Abstract

Materials of the first wall in near fusion plasma machines are subjected to a complex load system resulting from the plasma wall interaction. These processes cause life-limiting damage or structural changes in the material. Investigations of samples of real first wall components from different TOKAMAKs allow a systematic classification of the induced damage and other effects. Material tests in an operating TOKAMAK and in suitable laboratory devices give access to the limiting or critical load above which a first wall material suffers severe damage or fails due to thermal fatigue.

1. Introduction

During operation, the hot plasma in near-fusion plasma machines and in fusion reactors interacts with the first wall materials. The plasma wall interaction, on the one hand, give rise to contaminations of the plasma with wall material atoms and ions and, on the other hand, causes material damages. These induced structural changes can be life-limiting for first wall components. In special cases, plasma induced material damage can cause spontaneous failure of a wall component. This is primarily true for high heat flux components such as limiters and armor tiles.

There exist three typical procedures to come to a valuation of the different types of material damages and their significance with respect to first wall life time:

- Plasma wall interaction and the resulting material defects can be investigated directly by real first wall components or samples of them.

* Association EURATOM-KFA.

- Material tests can be carried out in operating TOKAMAKs either by applying special sample manipulators or by preparing real first wall components from test materials.
- Special types of plasma wall interaction can be studied with a broad variability of process parameters in simulating laboratory experiments.

Some typical investigations and experiments and their results shall be discussed subsequently.

A highly important type of plasma wall interaction remains unconsidered here and is only mentioned under the aspect of necessary further work on material damage: the influence of the 14-MeV fusion neutrons on material lifetime.

2. Plasma Wall Interaction

The complex processes of plasma wall interaction can be examined in two groups: plasma wall interaction during "normal" or stable operation and those processes during unstable operation of the plasma, fig. 1.

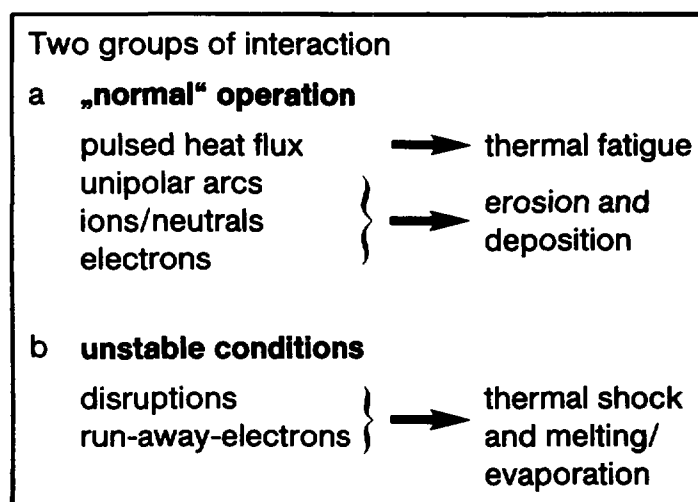


Fig. 1:

Classification of plasma states and effects on materials due to plasma wall interaction.

The type and intensity of the plasma-wall interaction depends on the one hand on the component itself - vacuum vessel, liner, limiter -, but on the other hand also on the mentioned operating state of plasma. Interactive

mechanisms affecting the vacuum vessel or, for example in the case of the TEXTOR TOKAMAK, the liner, under all operating conditions are

- continuous erosion (sputtering) by high-energy neutral particles, ions and electrons,
- chemical interaction between the plasma and the first wall, or its alloying constituents; a typical process is the reaction of hydrogen and carbon to methane (chemical sputtering) at the surface of the graphite internals (limiter, armor tiles),
- erosion and evaporation of first wall materials by unipolar arcing and
- thermal fatigue by the pulsed transport of thermal energy in the case of TOKAMAKs.

Thermally highly stressed components of the first wall such as limiters are subjected to the same interaction processes as the vacuum vessel and liner during normal operation of a fusion reactor.

However, the effects on the materials of the limiters are considerably more intensive even in normal operation since the main limiters extend into the boundary layer of the plasma. During plasma instabilities or during plasma states with low particle densities the following can occur additionally:

- thermal shock load through plasma disruptions and
- thermal shock loads, material melting and evaporation by "run-away" electrons.

Furthermore, selective erosion or evaporation at the surface of the first wall components can cause metallurgical changes which influence, for example, heat transfer or erosion behaviour. The same is true of the redeposition of evaporated material from a plasma, whereby surface layers of different chemical composition and/or different morphology can arise on the first wall and its components.

As an example for selective erosion/evaporation, the evaporation of Ti from TiC-layers on coated first wall graphite components shall be mentioned. After TEXTOR operation, for example, the TiC-layers are more or less depleted from Ti, whereas the Ti appears in the plasma as contamination.

Some mechanisms of plasma wall interaction are not taken into consideration in this discussion. They will be mentioned here but not further discussed.

These include:

- the short-term ability of the surface of the first wall to store hydrogen which is favourable to a certain extent for stable plasma shots, especially for concluding the pulse without disruption (soft landing),
- influencing the material properties by implanting helium, the "ash" of fusion reactors, and finally
- changing the material properties by irradiation with high-energy fusion neutrons (14-MeV neutrons).

3. Material damage in first wall components of existing TOKAMAKS

The term "plasma wall interaction" summarizes some typical processes which affect the surface and - to some extent - also deeper zones of the bulk material of first wall components, fig. 2.

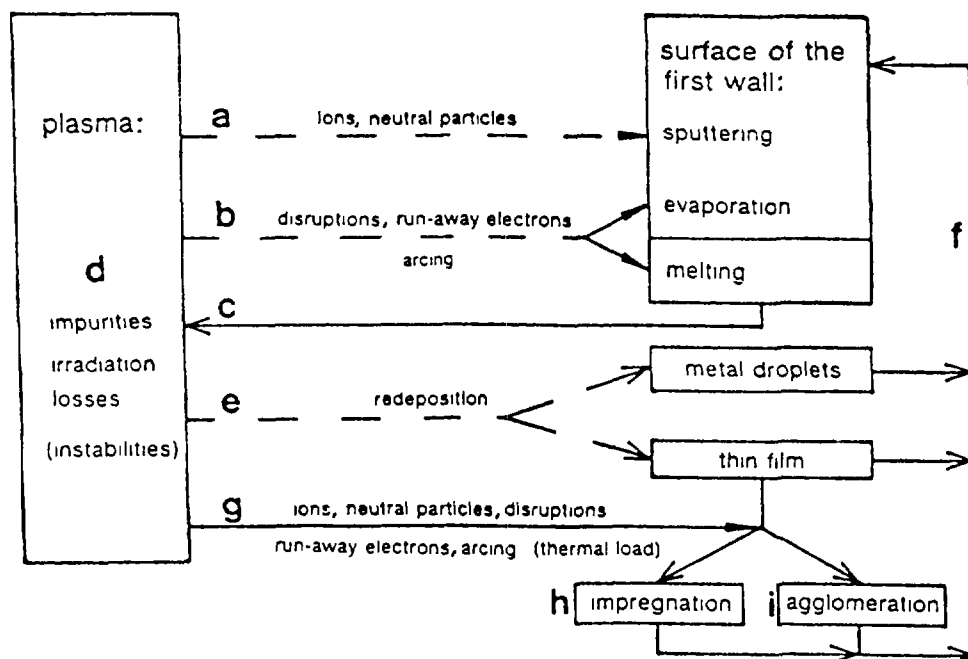


Fig. 2:

Plasma wall interaction processes and the resulting effects on the first wall materials.

The effects on the material (or wall) side range from pure surface effects like erosion by electrons and ions, fig. 3, droplet deposition - when the droplets themselves are generated by high energetic processes like arcing or disruptions/run away electrons -, fig. 4 a, 5 and redeposition of "plasma born" material which afterwards is submitted to secondary processes by high heat loading of the redeposition layer, fig. 4 b and 6: the layer can remain

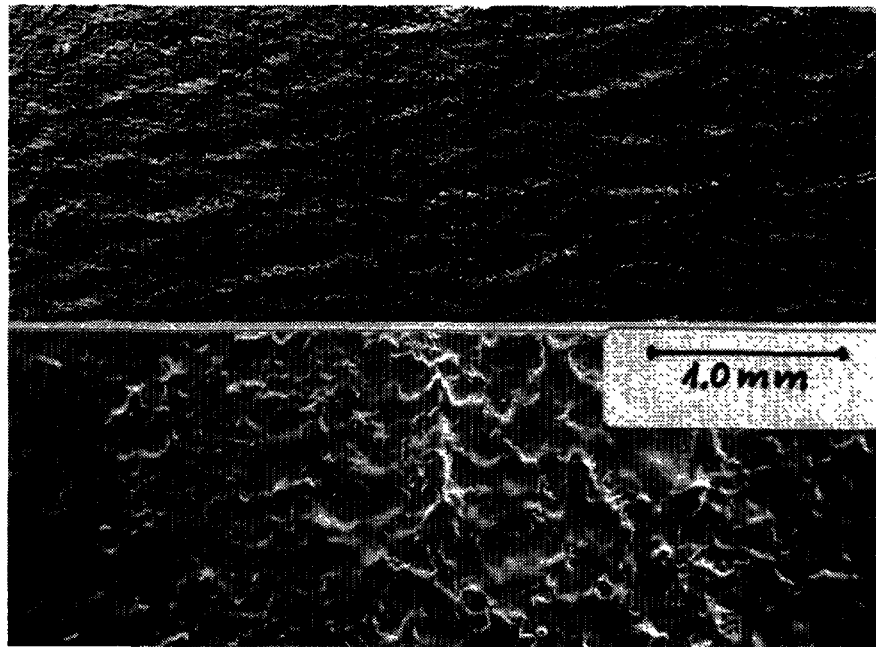


Fig. 3:

Surface areas of INCONEL 600 limiters in TEXTOR after erosion by ions (ion drift side) - above - and by electrons (electron drift side) - below -.

a) deposition of liquid metal droplets

b) atomic deposition by condensation

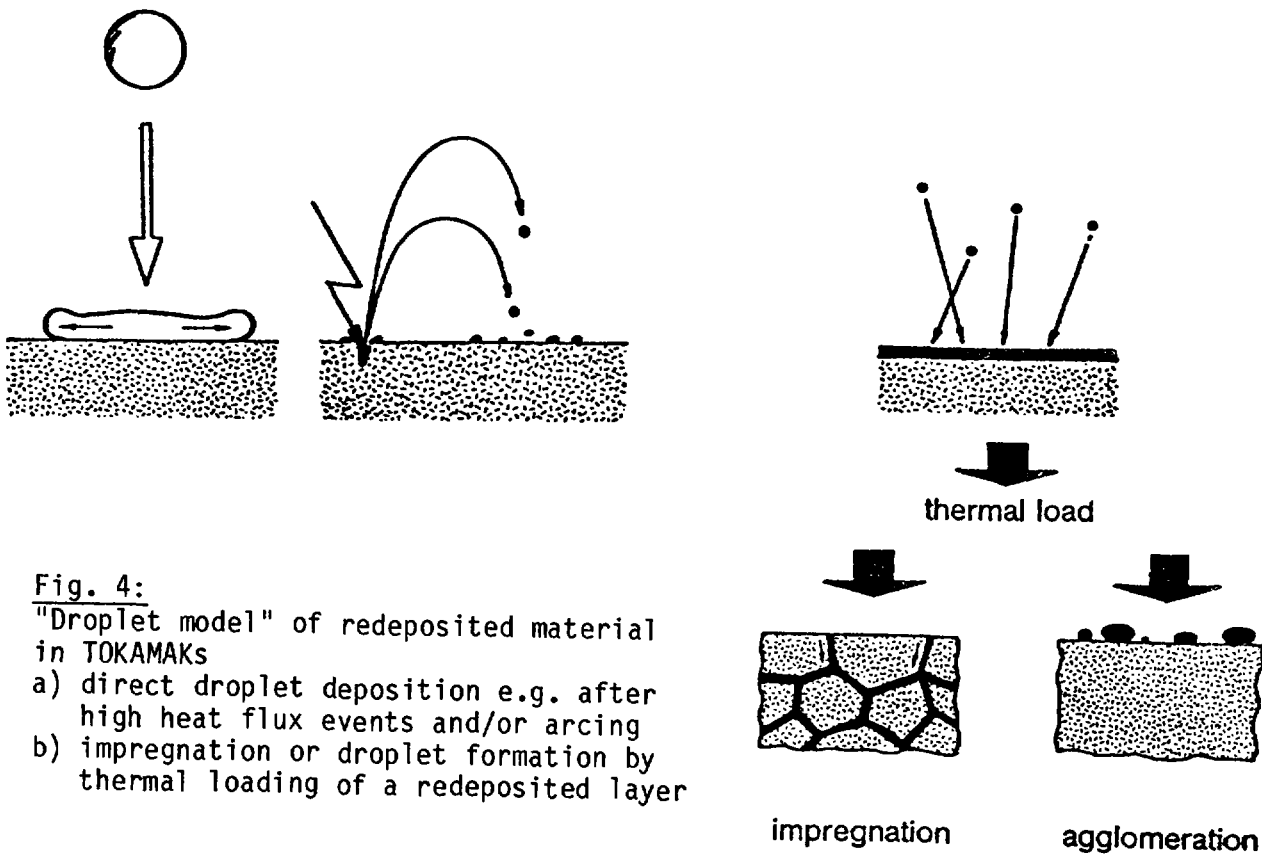


Fig. 4:

"Droplet model" of redeposited material in TOKAMAKs

- a) direct droplet deposition e.g. after high heat flux events and/or arcing
- b) impregnation or droplet formation by thermal loading of a redeposited layer

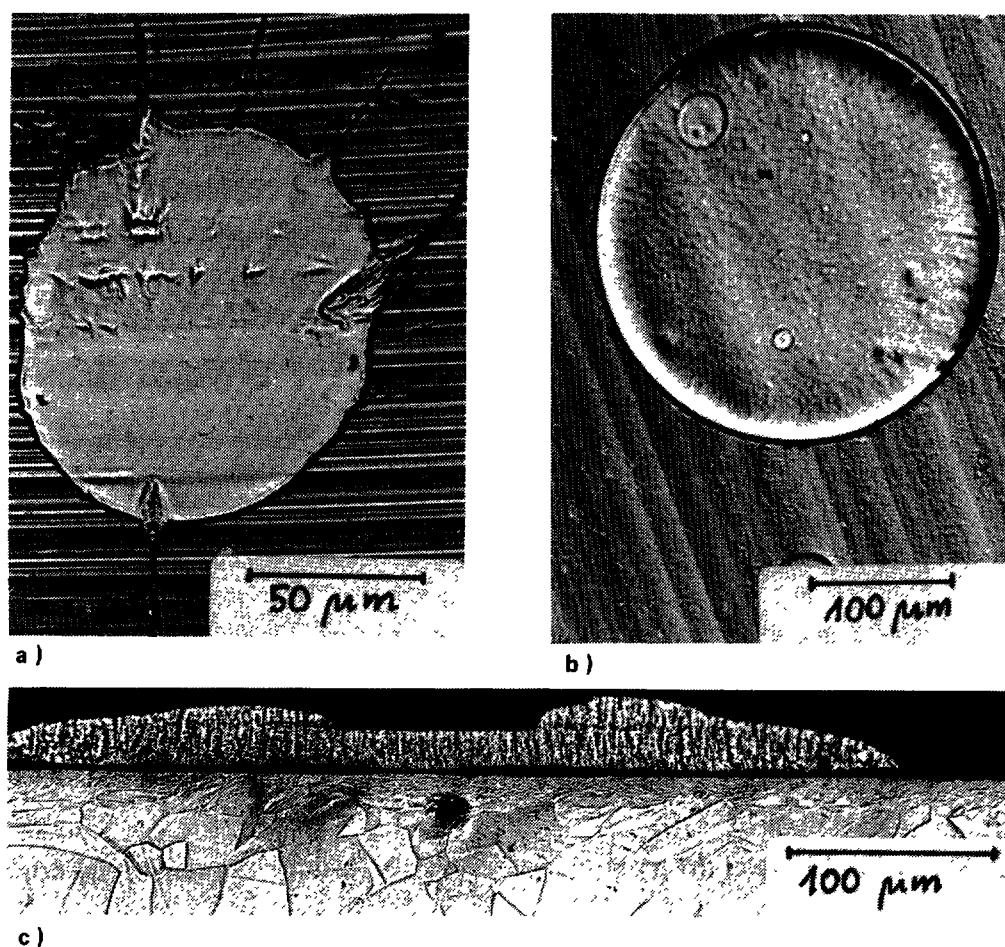


Fig. 5:
Metal droplets on long term samples in the first wall of JET (a, b), and metallographic section through such a very large droplet (c).

more or less unchanged, it can agglomerate to small droplets, fig. 6 a, or it can impregnate the near-surface bulk of the resp. component material, fig. 6 b. The type of these secondary processes is determined by the duration and amount of subsequent heating of the redeposited layer, on the one hand, and by the surface energy in the concerned surfaces of layer and substrate.

All surface-affecting processes cause severe changes of the material properties and thus give rise to lifetime decrease. This is especially true for lifetime reduction of thin coatings by erosion and droplet-enhanced arcing and for serious changes of material properties by impregnation processes.

Very severe, long-range material damage is caused by plasma disruptions and/or run-away-electrons, fig. 7. The interaction process is a type of thermal shock loading with pulse durations up to some 10 ms and power densities -

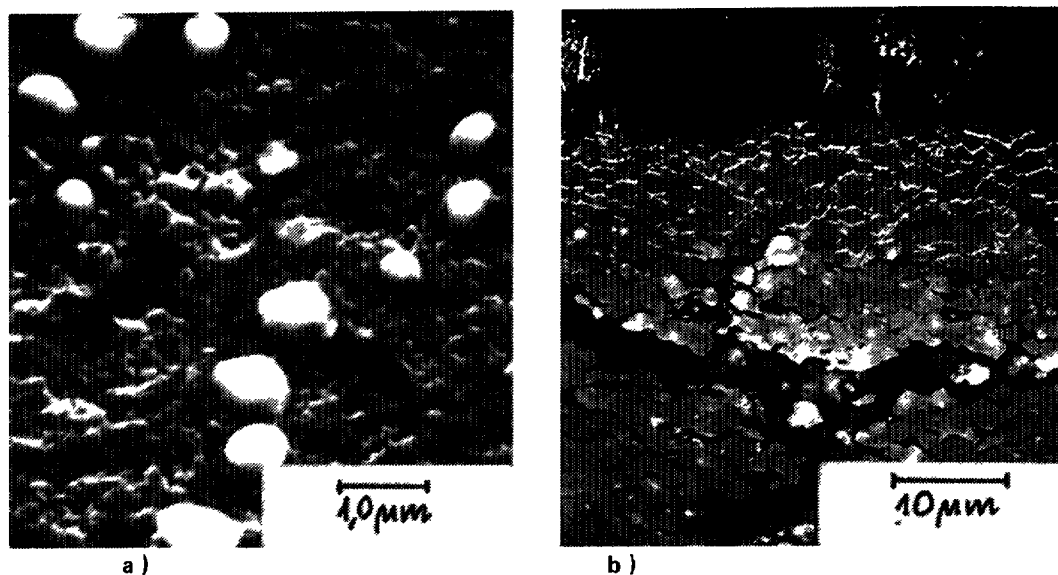


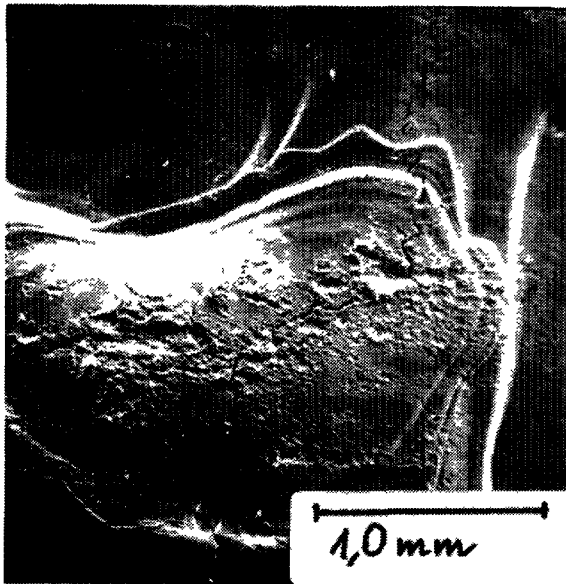
Fig. 6:
Transformation of a redeposited metal layer on a first wall component by high heat flux loading
a) droplet formation by agglomeration after heating of the redeposited layer in an arcing trace (Doublet III armor tile)
b) impregnation of a near-surface zone by redeposited materials and cracking in a SiC + 2 % AlN limiter sandwich in TEXTOR (in pile - TEXTOR material test).

of course, depending on the special event and on the type of plasma machine - few 100 MWm^{-2} . This thermal shock loading results in large area melting, dendritic recrystallisation, and cracking. Subsequent disruptions and run-away-electron events to the same area of a first wall component produce deep multi-layer remelt zones, fig. 8.

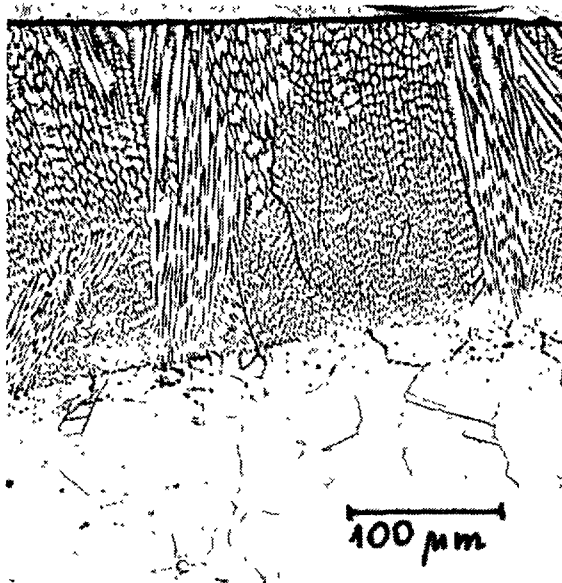
4. Material tests in the TOKAMAK TEXTOR

An important possibility for studying lifelimiting effects of plasma wall interaction on selected materials are in pile tests in existing TOKAMAKs, such as TEXTOR. For some first test series a sandwich limiter is used for screening tests of different coated and uncoated metallic alloys and ceramics.

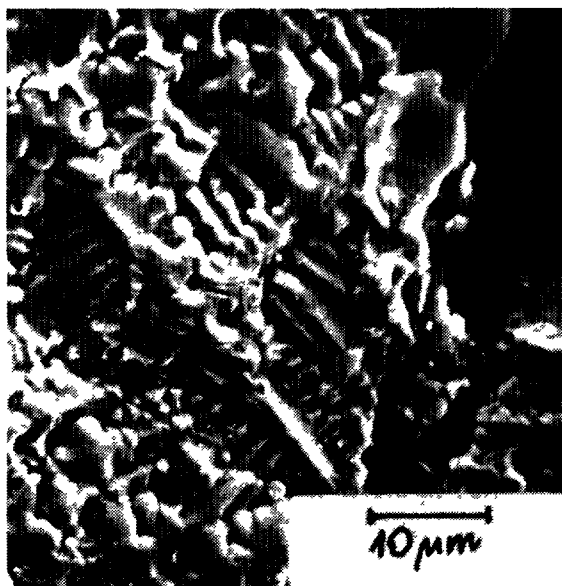
After a series of plasma discharges the test limiter shows the typical plasma attacks: arcing, erosion and redeposition, droplet formation and material impregnation, fig. 9 and 10. It is interesting that the unipolar arcs running over the surface of the sandwich limiter seem to "jump" over the non-conducting ceramic sandwiches after having burned deep craters at the boundaries between metal and ceramic causing severe chipping of the ceramic, fig. 11.



a)



b)



c)

Fig. 7:
Melted area in the surface of an INCONEL 600 limiter from TEXTOR after thermal shock by run-away-electrons:
a) surface area with arcing traces and thermal shock induced cracks
b) metallographic section through the melted and recrystallized zone; no temperature effects on crystalline structure of the material are visible below the melted area due to the short pulse duration of the event
c) dendritic surface recrystallization and thermal stress cracking.

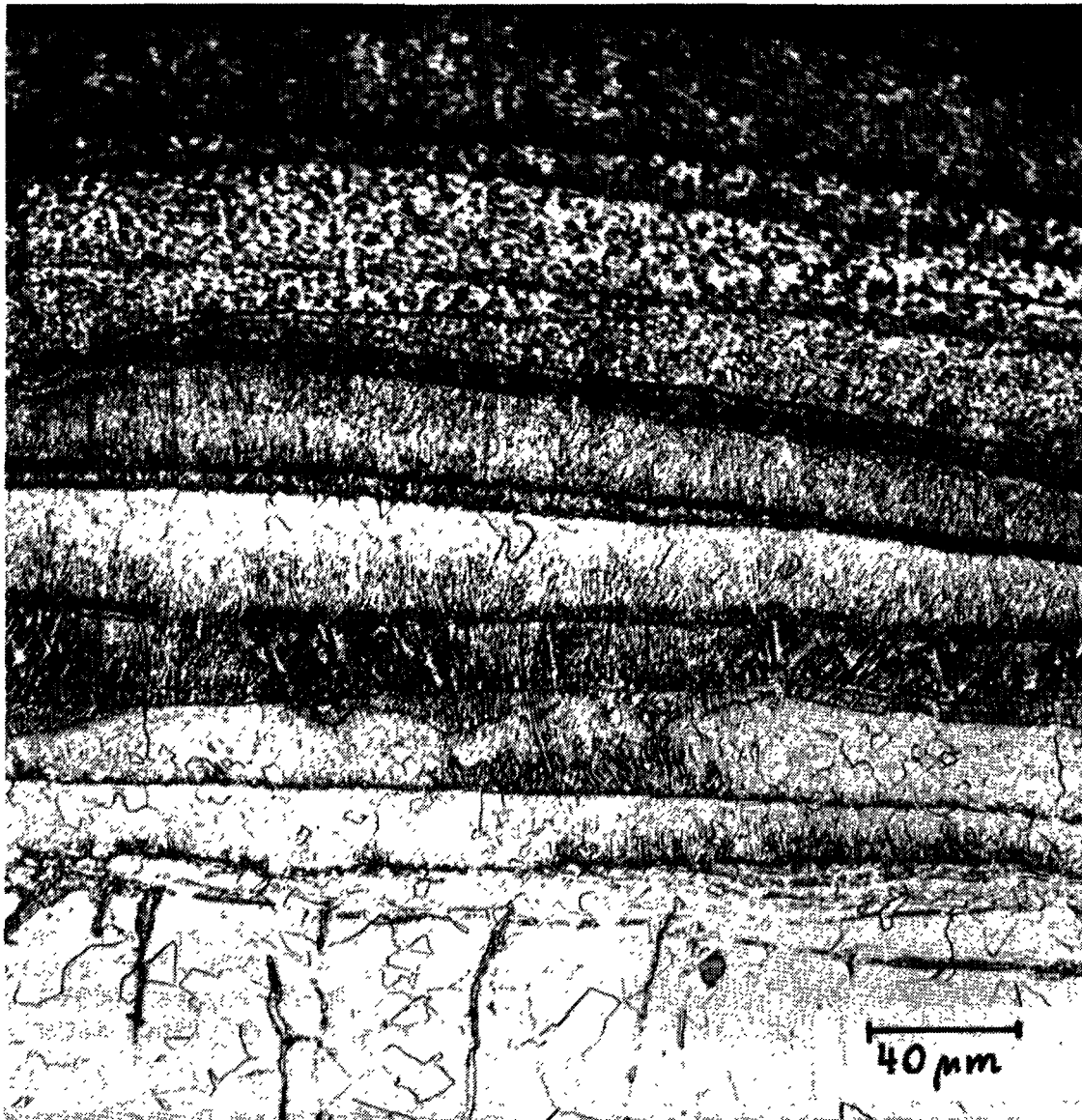
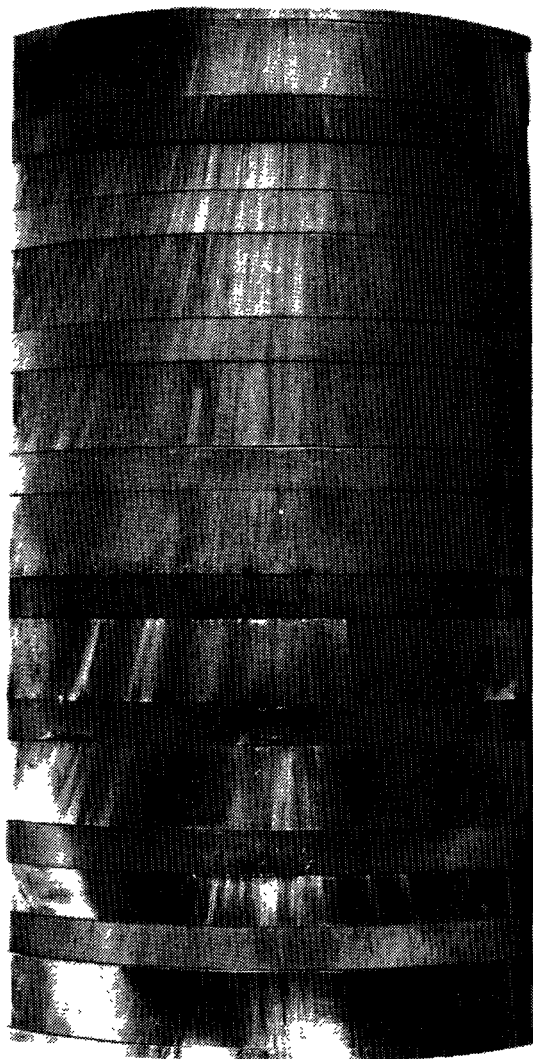


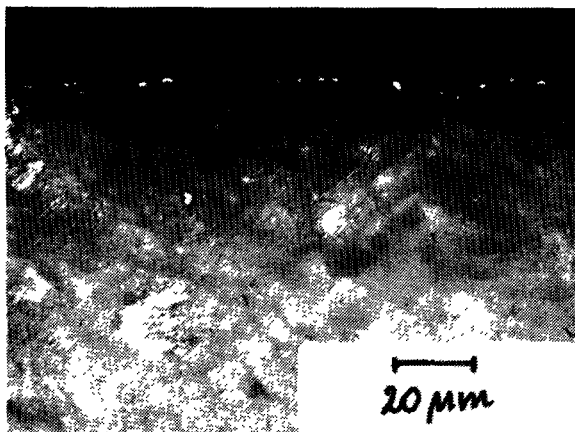
Fig. 8:
Multi-layer remelt zone by several successive high heat load events (disruption/run away electrons) to the same area of a 1.4311-alloy limiter in TEXTOR.

This experimental procedure is especially interesting for material tests under normal plasma conditions. Under the elevated loading of the material sandwiches in a limiter position, bulk ceramics showed very bad, thin coatings such as TiC or Cr_2C_3 acceptable behaviour even under the moderate plasma wall interaction of normal plasma discharges, fig. 12.

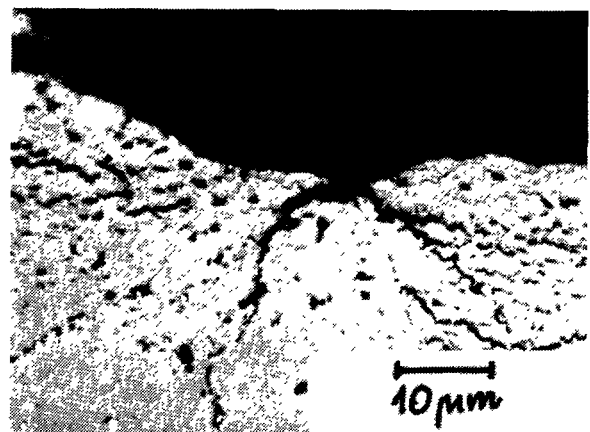


1.4311
 IN600
 POCO
 IN600
 EK98 + Cr₂C₃
 IN600
 EK98 + TiC
 IN600
 IN625 + TiN
 IN600
 ROSINIT
 IN600
 ALN
 IN600
 AS-BN
 IN600
 SiSiC
 IN600
 1.4311

Fig. 9:
 Sandwich limiter after in pile
 test in TEXTOR after about 80
 plasma discharges INCONEL 600
 acts as a reference material.



a)



b)

Fig. 10:

Cross sections through sandwich-samples after TEXTOR test:

a) droplets on the surface of a BN-sample

b) impregnation and cracks in a SiC + 2 % AlN-sample

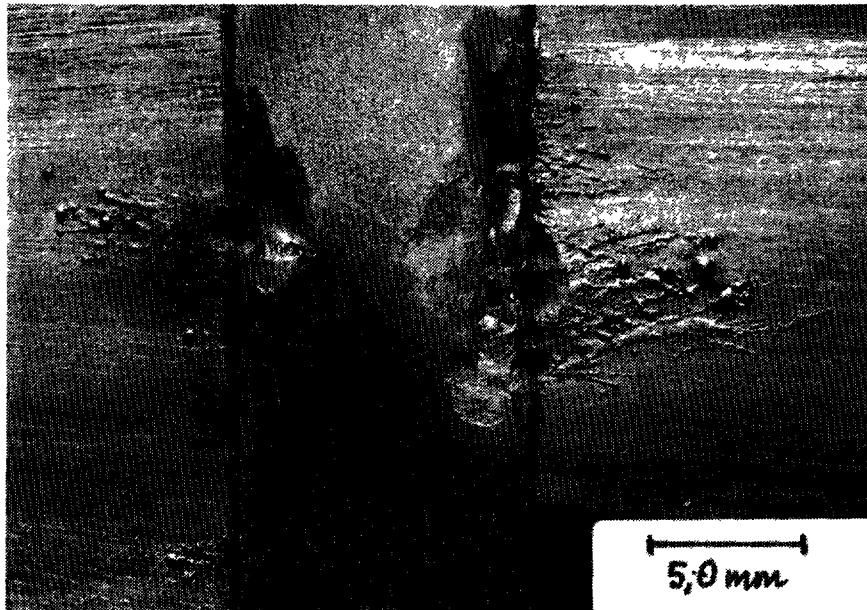


Fig. 11:
Detail of sandwich limiter after TEXTOR test, deep crater at the end of arcing trace at the boundary metal-ceramic on the metal side and severe chipping on the ceramic side.

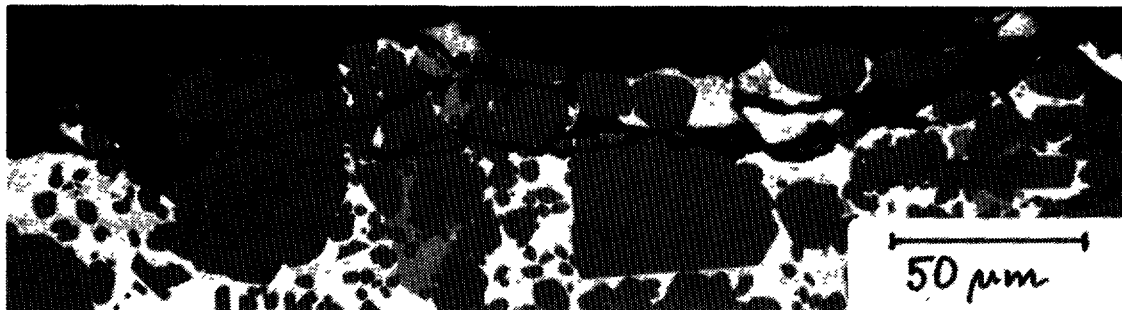


Fig. 12:
Material sandwiches after in pile test in TEXTOR: severe surface cracking by normal plasma operation in a SiSiC-sample (above), few cracks more or less vertical to the surface in a Cr_2C_3 -layer on a graphite sample (below).

5. Laboratory tests of material behaviour

Isolated loading processes out of the complex real system of plasma wall interaction can be applied to first wall materials in special laboratory tests. Besides this advantage of studying isolated damaging mechanisms, the most important aspect is the possibility of varying the process parameters over a very wide range to find the critical or threshold values of interaction processes above which life-limiting material attacks occur.

As far as the maximum thermal power density for thermal shock tests is concerned two realistic laboratory test procedures are available, namely the electron beam test and the material test in a neutral particle/ion hydrogen beam, for example in a neutral beam injector test facility. Both can fulfil the conditions of maximum thermal power density up to few hundred MW/m², pulse durations few ten ms and maximum energy deposition to the sample surface up to 100 MJ/m². Both meet also the requirement of sufficiently large sample sizes and test areas, resp., of up to few cm² in the case of electron beam test and some 100 cm² in the case of neutral particle/ion beam test.

With more moderate parameter combinations, power density up to 1 MW/m², pulse duration up to few seconds, that is the normal plasma discharge time in a TOKAMAK, and total energy depositions to the sample surface up to 10 MJ/m², the thermal fatigue behaviour of materials can be tested, also by the two already mentioned test procedures. For this purpose, a sequence of pulses is applied to the material, interrupted by realistic cooling down times. For these tests, a third procedure is available, too, namely the material loading by infrared electromagnetic radiation by suitable types of lamps.

Thermal fatigue tests under independent variation of applied number of pulses and thermal power density, with fixed parameters of pulse duration and pulse spacing time, give for each investigated material the connection between power density loading and maximum tolerable number of plasma discharges - pulses - before life-limiting effects or other material damage occurs.

Electron beam tests are also useful for studying the erosion behaviour and possible segregations and preferred evaporation of single alloying constituents in candidate first wall materials.

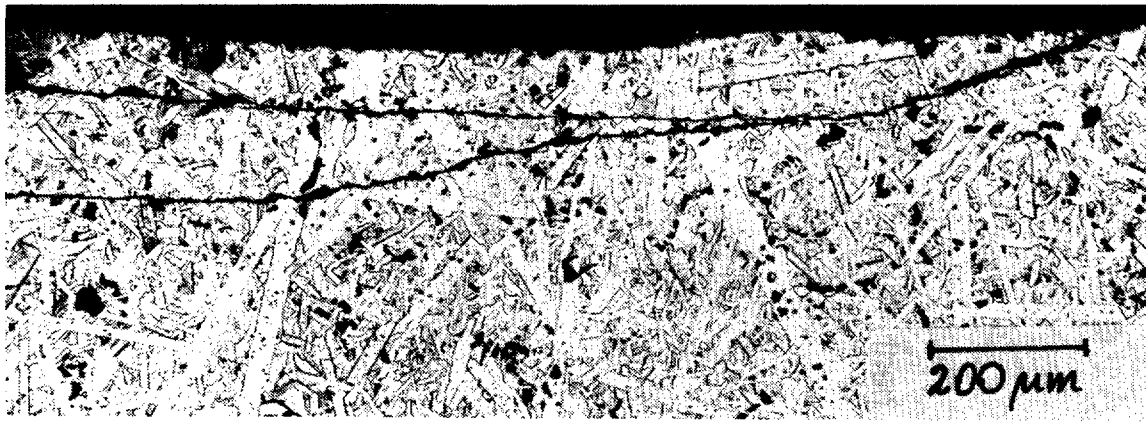
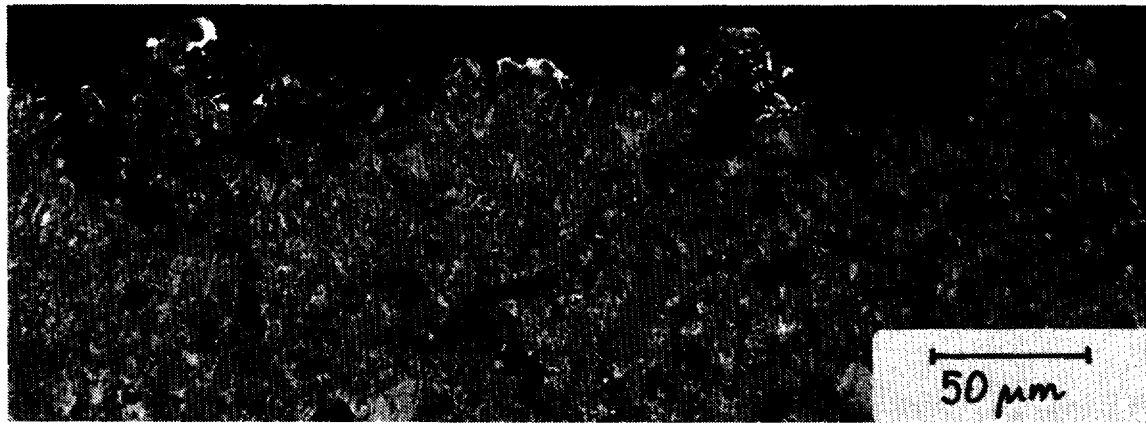


Fig. 13:
A graphite sample (above) and a SiC-sample (below) after one shot electron beam test (100 WM/m^{-2} , 0.1 s).



Fig. 14:
TiN-coating after a one shot electron beam test (100 MW/m^{-2} , 0.1 s).

Some typical results of thermal shock behaviour of materials in an electron beam test are given in fig. 13 and 14, showing the erosion of graphite, the severe cracking and chipping of SiC, and the total destruction of thin coatings by a single thermal shock event - the parameters of these experiments were 100 MW/m^2 and 0.1 s pulse duration.

A possible way of quantifying these results is given in fig. 15.

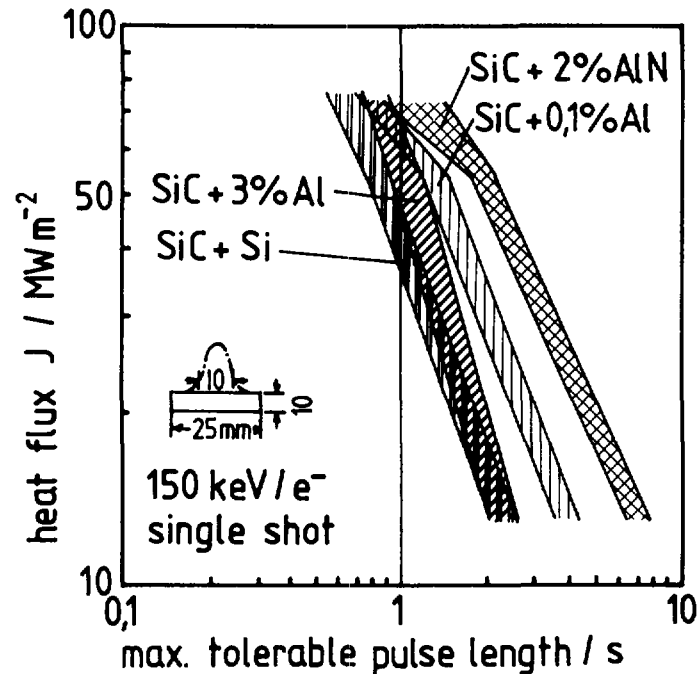


Fig. 15:

Critical heat loads which cause sample surface fracture for different qualities of SiC; electron beam thermal shock tests (one shot experiments).

The quantification of thermal fatigue behaviour can be realized in a similar way by plotting the critical heat load density in a diagram "heat flux (MW/m^2) versus number of pulses" for each candidate material and for pulse lengths equal to the discharge durations of a resp. plasma machine (e.g. TEXTOR 2 s, JET 20 s...). For these experiments the power density varies, as has been mentioned above, in the range for normal plasma discharges, i.e. between 5 MW/m^2 as an upper limit and $\dots 0,1 \dots \text{MW/m}^2$ as a lower limit.

It is, of course, necessary to quantify the term "critical heat load", that means to quantify the material damage caused by plasma wall interaction:

- erosion depth, eroded area and amount of eroded material per unit area,
- chemical composition of eroded material (preferential erosion),

- depth and size of melted area,
- total crack length and depth of cracks,
- type of cracks (vertical/parallel to surface).

This work is under preparation in the Institute für Reactor Materials in the Nuclear Research Center in Jülich.

6. Conclusions

By plasma wall interaction, the first wall materials can change their structure and their chemical composition and thus also their material properties. These effects can influence only a very thin surface zone - few μm thick - or, and that is obviously the case that is mostly found, affect after few plasma discharges already a relatively extensive part of the first wall material. So it seems necessary to consider plasma wall interaction e.g. in mathematical/theoretical models quantitatively by adjusted variations of the material property values.

MECHANISMS OF WALL EROSION IN FUSION DEVICES

R. BEHRISCH

The NET Team,

Max-Planck-Institut für Plasmaphysik,

Garching near Munich

Abstract

Owing to the limited particle confinement in magnetic fields, the walls of high-temperature plasma experiments and future fusion reactors are subjected to bombardment with high currents (10^{14} to 10^{19} cm⁻² s⁻¹) of plasma ions, electrons and atoms with energies in the 10 eV to 3.5 MeV range. As the plasma electrons have a higher velocity than the ions a sheath potential of about $3 kT_e$ builds up which accelerates the plasma ions toward the walls and reflects low energy electrons. In unstable discharges runaway electrons produce heat pulses at the wall and electric arcs can be ignited and burn between the plasma and the wall surfaces.

These different loads lead to erosion of the solid walls facing the plasma. The major processes are: physical sputtering, chemical sputtering, sublimation (which may be enhanced under the particle irradiation) melting and evaporation as well as erosion by electric arcs. Furthermore the thermophysical properties of the wall material may be degraded owing to deposition and implantation of ions from the plasma and the thermal pulses and microscopic debris, or even larger pieces may break off at the walls. They can partly evaporate after entering the plasma or fall onto the bottom of the discharge vessel.

Only a fraction of the material released at the walls can enter the central plasma, where it adds to the impurities. The other part is redeposited mostly close to the area of erosion. The wall atoms which have penetrated into the plasma finally also return onto the vessel walls.

The major erosion processes and the redeposition observed are reviewed and their importance in today's tokamaks is assessed.

I. INTRODUCTION

The lifetime of the first wall in a fusion reactor will be limited owing to the damage caused by the energetic neutron bombardment and the temperature fluctuations owing to surface layer modifications caused by interaction with the hot fusion plasma. Thus, the first wall will very likely be degraded much faster than the structural materials of the reactor. In order to obtain information about the limitation of the 1st wall lifetime due to the surface layer modifications various ways are followed:

- Investigation of 1st wall modification and of the boundary plasma causing them in today's tokamaks, stellarators and the other high-temperature plasma experiments.
- Investigations of the atomic processes that contribute to these 1st wall modifications in separate experiments and collection of a reliable data base.

- Extrapolations from this knowledge to the boundary plasma parameters and the conditions at the first wall in a future fusion reactor.

In today's plasma experiments the first wall is already deliberately modified before the main plasma discharges are started. In order to remove surface layers due to machining, assembling and washing of the vessel or adsorbed during opening of the vessel, low-density glow discharges or low-power plasma discharges are performed /1/. Besides removing loosely bound adsorbates, this discharge conditioning can damage the walls by ion implantation, arcing and sputtering and may cause a redistribution of the wall materials on all surface areas of the vessel.

The wall modifications occurring during normal plasma discharges in today's experiments are determined by plasma temperatures, densities and confinement times, which are still a factor 1.5 to 3 below those needed for a fusion reactor. Furthermore, the discharge times are only of the order of seconds and the times between discharges are relatively long. All wall modifications observed today are therefore caused by a plasma with reduced parameters, and they can be largely dominated by the start-up and shut down phases of the plasma discharge.

Finally, the plasma experiments are performed partly with the aim to extend the operation regime. The plasma parameters are pushed to higher plasma densities and temperatures by different schemes of fuelling and additional heating. Many discharges are thus unstable or are terminated by a plasma disruption. This generally causes for a very short time a large local power deposition, and several wall modifications occur during such badly controlled discharges.

For understanding the different processes contributing to the 1st wall modifications detailed time-resolved measurements of the plasma conditions near the walls, the particle and energy fluxes to the walls, and particle implantation, erosion and deposition have to be performed. The atomic processes contributing to these wall modifications have to be known in the relevant parameter range.

The following contribution will concentrate on those atomic processes which are a necessary basis for understanding the 1st wall modifications in today's experiments and for extrapolation to the next generation of experiments.

II. MECHANISMS OF WALL MODIFICATIONS

The modifications of the first wall in high-temperature plasma experiments are caused by particle bombardment and energy deposition as well as by electric fields which build up between a plasma and solid surface. The major processes to be considered are:

- 1) Surface erosion by physical and chemical sputtering due to wall bombardment with energetic ions and neutrals.
- 2) Sublimation, local melting, evaporation and droplet emission at overheated areas due to very local energy deposition.
- 3) Cathode spots from electric arcs on the 1st wall due to electric fields which develop at the plasma-solid transition.
- 4) Microparticle emission due to 1st wall modifications by ion implantation, thermal stresses and shocks.

In the following, the physical basis of these processes is briefly outlined and their contribution to wall modification in fusion devices is discussed.

1) Sputtering

Sputtering is the erosion of a surface due to energetic particle bombardment. Different processes can contribute to erosion, such as physical sputtering, chemical sputtering and radiation-enhanced sublimation /2-5/.

a) Physical sputtering

Physical sputtering is caused by collision cascades in the solid that are initiated by the incoming ion. If an energy larger than the surface binding energy is transferred to a surface atom in the direction normal to the surface it will be emitted, i.e. sputtered (fig. 1) /5,6/. There is a threshold energy for sputtering below which the energy transfer to a surface atom is smaller than the surface binding energy.

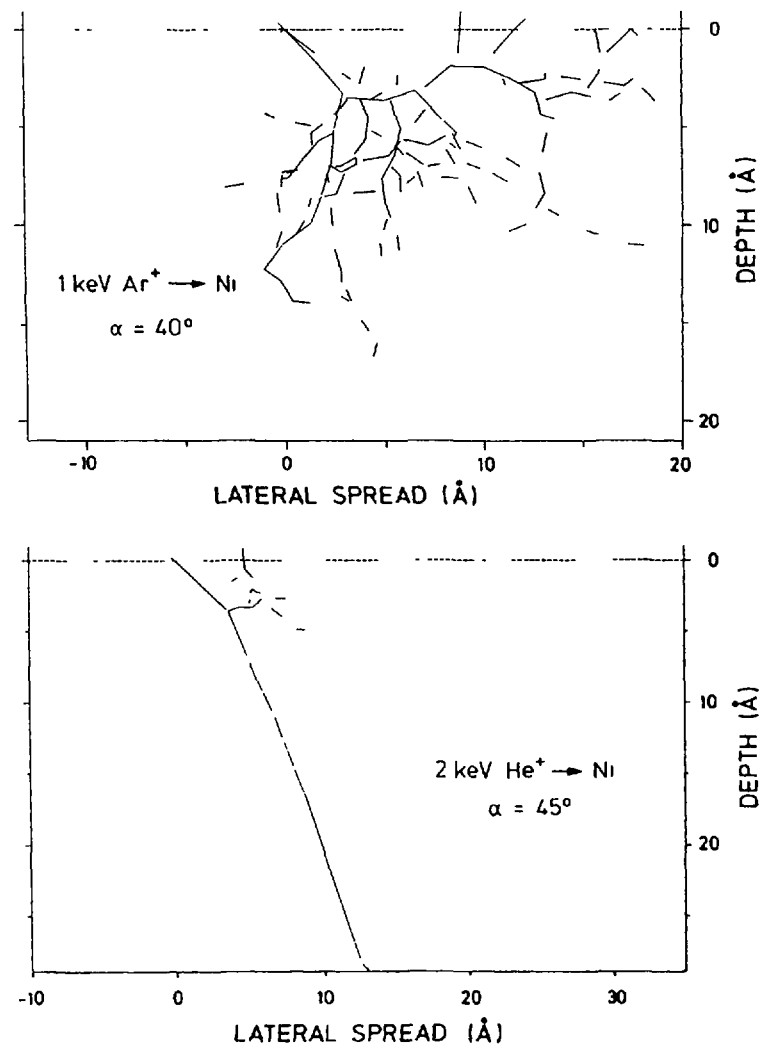


Fig. 1 Collision cascades in Nickel for the incidence of 1 keV Ar⁺ ions (top) and 2 keV He⁺-ions (bottom). The trajectories calculated with the computer simulation program TRIM are shown in the projection on the plane of ion incidence. At bombardment with Ar⁺ two atoms are sputtered while for He bombardment one atom is sputtered /5, 6/.

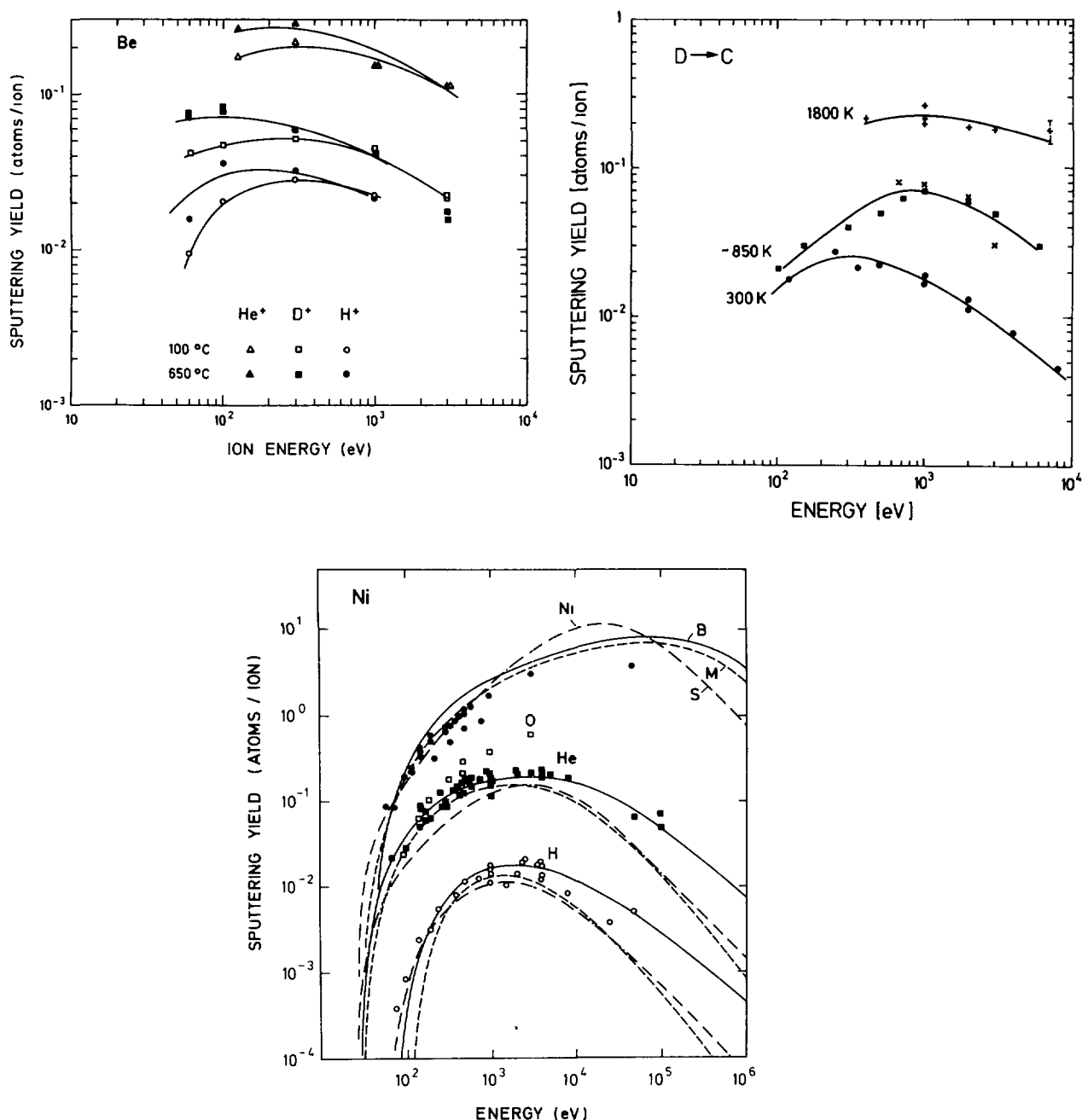


Fig. 2 Measured sputtering yields for Be, C and Ni for normal ion incidence at different energies [3-7]. For Ni the results of different analytical fitting formulae are shown. The solid line corresponds to equation (1).

Sputtering is a very general phenomenon which is observed during any energetic particle bombardment [2]. It can only be avoided by reducing the bombardment energies below the threshold energy for sputtering (between 20 to 40 eV for hydrogen and half of these values for deuterium). It can be reduced by increasing the surface binding energy.

Sputtering yields, their dependence on the bombardment energy and angle of incidence, as well as the energy and angular distributions of the sputtered material have been investigated for many elements [2-9]. The yields for

light ion sputtering of Be, C and Ni and their energy dependence are shown in fig. 2a-c. However, there is still a lack of many important data such as the distribution of the sputtered atoms and the yields for other solids in the parameter range of interest for fusion research.

An analytical formula for the dependence of the sputtering yield Y of single-element solids, on the incident energy E_0 covering light and heavy ion bombardment at normal incidence has been proposed /5,9/:

$$Y(E_0) = \frac{1}{U_0} \frac{M_1 M_2^{2/3}}{(M_1 + M_2) M_1^{2/3}} \cdot \frac{Z_1 Z_2}{(Z_1^{2/3} + Z_2^{2/3})^{1/2}} \cdot \frac{R_p}{R_1} s_n(\epsilon) f\left(\frac{E_0}{E_{th}}\right) \left[\frac{\text{atoms}}{\text{ion}}\right] \quad (1)$$

where M_1, M_2, Z_1, Z_2 are the masses and atomic numbers of the incident ions and the target atoms, U_0 is the surface binding energy, $R_p/R_1 = kM_2/(M_1 + 1)$ is a measure of the number of surface crossings if the cascade is initiated in an infinite medium with k between 0.1 and 0.4, $s_n(\epsilon)$ is a fit to the universal nuclear stopping power function given by

$$s_n(\epsilon) = \frac{3.44 \sqrt{\epsilon} \log(\epsilon + 2.718)}{1 + 6.35 \sqrt{\epsilon} + \epsilon(6.882 \sqrt{\epsilon} - 1.708)} \quad (2)$$

with ϵ being the reduced energy

$$\epsilon = 32.55 \frac{M_1}{(M_1 + M_2) Z_1 Z_2 (Z_1^{2/3} + Z_2^{2/3})^{1/2}} E_0 (\text{keV}) \quad (3)$$

and

$$f\left(\frac{E_0}{E_{th}}\right) = \left[1 - \left(\frac{E_{th}}{E_0}\right)^{2/3}\right] \left[1 - \frac{E_{th}}{E_0}\right]^2 \quad (4)$$

where E_{th} is the threshold energy for sputtering given by

$$E_{th} = \begin{cases} \frac{U_0}{\gamma(1-\gamma)} & \text{for } \frac{M_1}{M_2} < 0.2 \\ 8U_0 \left(\frac{M_1}{M_2}\right)^{2/5} & \text{for } \frac{M_1}{M_2} > 0.2 \end{cases} \quad (5)$$

and $\gamma = 4M_1 M_2 / (M_1 + M_2)^2$ is the energy transfer factor. The yields calculated with formula (1) are also introduced as black lines in fig. 2a-c and there is good agreement within the uncertainties of the experimental values /8/.

Generally, the first wall is made out of an alloy. Here preferential sputtering is observed, especially for light ion bombardment, i.e. one component is sputtered faster than the others. At temperatures where bulk diffusion occurs a relatively thick surface layer can be depleted and the thermophysical properties are modified /2/.

b) Chemical sputtering

For bombardment with ions, which form a volatile compound with the atoms of the solid, the erosion yield can be enhanced in a certain temperature range owing to the formation and release of molecules. Such a chemical sputtering effect has been observed especially for hydrogen ion bombardment of carbon in the temperature range between 400° and 900° C (fig. 3) /2,3,5/. An enhanced erosion yield and a peak in the CH₄ formation were measured. The enhanced erosion is less pronounced for carbon containing a few per cent of metal, boron, or silicon (SiC) in the surface layers. There is an indication that the relative contribution of chemical sputtering of carbon is also reduced on bombardment with high hydrogen ion current densities. For oxygen bombardment of carbon chemical sputtering effects are not so pronounced /2,3,5/.

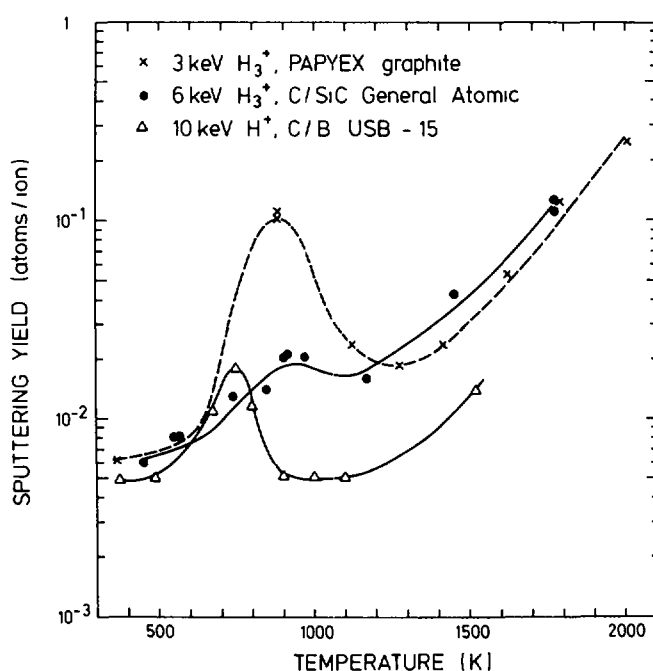


Fig. 3 Temperature dependence of the sputtering yield of Carbon, C+SiC and C+B /3,5/.

c) Radiation-enhanced sublimation

During particle bombardment of carbon at temperatures above 1000° C the erosion yield was found to increase with temperature, independently of the chemical nature of the incident ions (fig. 3). This effect has been observed up to now only for carbon and was explained by the damage created in the solid by the ion bombardment. Interstitial atoms produced in the solid which diffuse to the surface may immediately evaporate /5,8/.

This model predicts that radiation-enhanced sublimation is reduced at low bombardment energies, i.e. at energies below about 100 eV (fig. 4)/8/. Experimentally, no influence was found for Si or metal admixtures in carbon, as was observed in chemical sputtering. This may be either due to evaporation of the admixtures at the surface or due to diffusion into the bulk at temperatures above 1000° C so that only a clean carbon surface is exposed to the bombarding ions /5/.

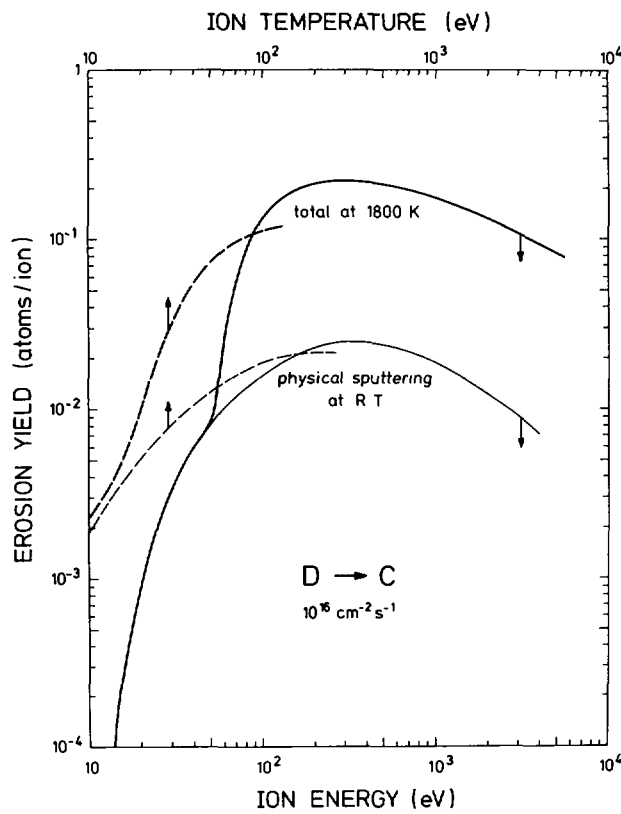


Fig. 4 Calculated yields for radiation enhanced erosion and physical sputtering of Carbon at RT and 1800 K /8/.

Generally physical sputtering by hydrogen ions is a low-yield process ($\sim 10^{-2}$ atoms/ion), whereas the yields for chemical sputtering and radiation enhanced sublimation as well as those for heavy-ion bombardment can be considerably larger, i.e. of the order of 0.1 to 1 atoms per ion.

2) Sublimation evaporation, melting and droplet emission

If a surface is heated to temperatures close to the melting point, sublimation may become important. The sublimation yield \dot{n} is given by /10/

$$\dot{n}(T) = \alpha \frac{3.5 \cdot 10^{22}}{\sqrt{M \cdot T}} p(T) \left[\frac{\text{atoms}}{\text{cm}^2 \text{ s}} \right] \quad (6)$$

Here α is the sticking probability of metal atoms on the surface, $p(T)$ is the equilibrium vapour pressure in mbar at temperature, T and M the atomic mass of the solid. Evaporation yields for Be and C are shown in Fig. 5 assuming $\alpha = 1$. /10/.

If the surface of a thick solid is heated by a pulse of energy for just a short time τ , the temperature increase, $\Delta T = T_2 - T_1$ is given by

$$\Delta T = \frac{2}{\sqrt{\pi} \rho c k} F \sqrt{\tau} \quad (7)$$

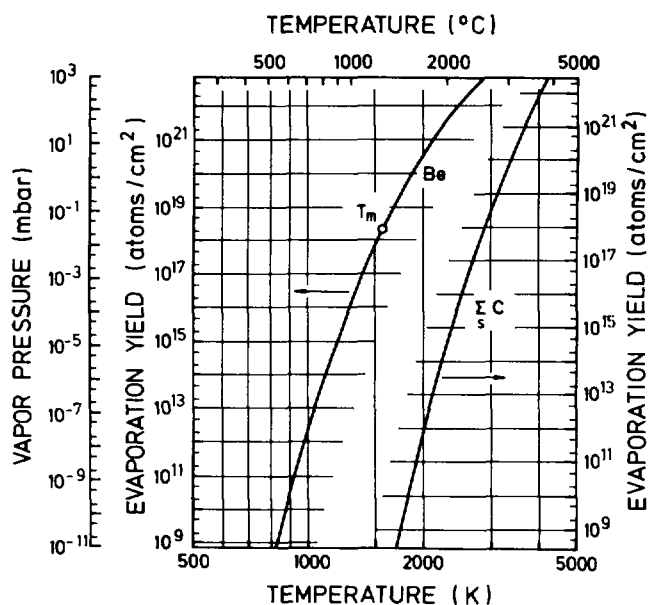


Fig. 5 Vapour pressure and evaporation yields calculated with formula (6) /10/.

where ρ is the density, c the specific heat, k the heat conduction and F the power flux. This gives an evaporation per pulse /11/ of

$$n = \dot{n}(T_2) \frac{2T_2}{\Delta T} \frac{k_B T_2}{\Delta H} \tau \quad \left[\frac{\text{atoms}}{\text{cm}^2} \right] \quad (8)$$

where, k_B is the Boltzmann constant and ΔH the heat of sublimation per atom.

Evaporation yields during heat pulses were recently determined experimentally, giving reasonable agreement with the simple formula (8) /12/. For very large heat pulses the vapour cloud formed during the pulse can absorb part of the incoming energy at the end of the pulse. It will shield the surface from excessive heating and thus reduce the evaporation.

If the heat pulse $F \sqrt{\tau}$ leads to melting at the surface, liquid material can be released owing to the pressure on the melt layer or to gravity. Carbon melts only at pressures above 100 bar and temperatures above 4000° C /13/, thus just a large sublimation is observed at high heat loads /11, 12/. Thermal pulses can further degrade the material by inducing cracks. The depth and the width of the cracks depend on the thermophysical properties of the material and on the deposited energy as well as the deposition time /11, 14-16/.

3) Cathode spots from electric arcs /3, 17-20/

An electric arc is a very short and concentrated plasma discharge with currents of 10 to 100 A between two electrodes. The electron-emitting cathode spot with a radius of a few μm is heated by ion impact from the arc plasma and by the concentric current in the cathode. Metal erosion from the cathode spot provides the ions for the plasma, so that the arc also burns also in high vacuum. Such cathode spots are initiated by field emission from dielectric layers or, at clean surfaces, from protrusions.

Electric arcs always ignite if the electrical field at a surface is larger than a critical value which depends on the surface conditions. The arcs generally burn for about 100 μ s at one cathode spot. When the cathode crater gets too large, the arc spot moves to a new area. In a magnetic field the movement occurs in the retrograde direction, i.e. opposite to the $\mathbf{J} \times \mathbf{B}$ force.

The material eroded from the arc spot consists primarily of the ions from the arc plasma, which amounts to about 10 % of the electron current. For metals liquid droplets about 10 μ m in diameter are emitted toward the sides.

Droplets become important especially at high cathode temperatures. Erosion yields thus increase with temperature (fig. 6) [21]. For carbon droplet emission has not been observed because carbon does not melt under normal conditions.

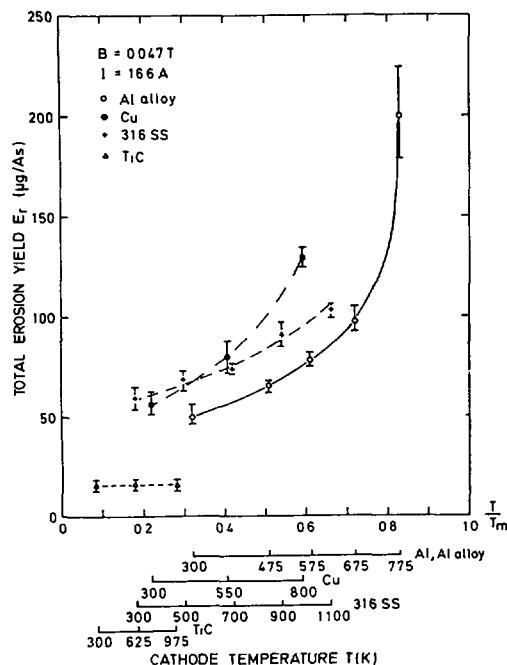


Fig. 6 Erosion yields due to electrical arcs for TiC, stainless steel, Cu and Al as a function of the surface temperature normalized to the melting temperature [16,17].

4) Microparticle emission

The implantation of high fluences of hydrogen ions into the surface layers of a solid leads to a build-up of large stresses and can severely embrittle the materials. Furthermore the deposition of material from the solid or of a getter material or a coating will produce a surface layer which is generally less tightly bound to the substrate and may be very brittle. Thermal shocks, ion implantation or mechanical shocks can lead to the release of microparticles by flaking.

III. WALL MODIFICATIONS IN FUSION DEVICES

All erosion processes described in the previous section have been observed at the vessel walls in today's high-temperature plasma experiments. The eroded material enters the boundary plasma and partly penetrates into the central plasma. Finally, it is redeposited on some areas of the first wall.

Table 1: 1. Wall Processes in Fusion Devices

Event	discharge conditioning	down time between discharges	Start B_{tor}	Start discharge current and density increase	flat top OH discharge	additional heating to max. temperature	burning plasma $T_i \approx T_e \approx 12 \text{ keV}$ $n_e \tau_E \sim 10^{14} \text{ sec cm}^{-3}$	current drive	burning plasma	shut down current and density decrease
plasma	low density plasma	-	-	poor plasma confinement	stable discharge	plasma may become unstable	stable plasma, high wall load: plasma particles, α -particles 14 MeV neutr.	low density plasma		reduced plasma confinement
wall effects	desorption of surface layers, ion implantation, sputtering arcing	degassing of walls, surface reactions, wall cooling	mechanical stress, micro-particles	sputtering by ions & CX-neutrals, desorption (adsorbates), arcing, droplets	sputtering by ions & CX-neutrals desorpt. (contam. walls)	sputtering by ions & CX-neutrals (high energy) run away electrons, heat pulses, droplets, arcing	sputtering by ions & CX neutrals (high energy) wall temp. increase, evaporation, desorption arcing?	sputtering, arcing, droplets, micro-particles		sputtering, arcing, run-away electrons, wall cooling
today	$10^5\text{-}10^6$	500	1	0.3-3	1-10	0.5-5				3
times (s)	fusion reactor	$10^5\text{-}10^6$	10-100	3-300	1-10	5-50	$2\text{-}4 \cdot 10^4$ (5-10 min)	5-50		3-30
							$10^5\text{-}10^7$ (1-100 days)			

The amount of eroded and redeposited material largely depends on the geometry of the first wall, on the parameters of the plasma discharge, such as the plasma density, plasma position and their fluctuations, and on the fuelling and particle exhaust schemes. In addition, major plasma disruptions can give rise to more intense wall damage than many days of normal discharges. Generally, on all wall areas both erosion and redeposition of wall material has been observed /22,23/. However, on areas close to the plasma, such as limiters, erosion dominates, while on more remote areas deposition dominates. /23/.

The possible importance of different wall processes during the phases of a plasma discharge are schematically summarised in Table 1. During conditioning and start-up, desorption and degassing seem to be important, while sputtering probably dominates during plasma discharges. Up to now the wall processes are still not extensively investigated in plasma experiments. Detailed measurements are being performed only at few selected wall positions, and extrapolations to the other wall areas have to be regarded with caution. Changes of larger areas of the walls and limiters have been investigated only by integration over many discharges. A discussion of these wall modifications observed in JET is presented in the following contribution /31/.

Sputtering

The vessel walls are bombarded with ions and neutral particles from the plasma. As the ions flow mostly along the magnetic field lines, they impact predominantly on areas where magnetic field lines intersect the vessel walls. The fluxes are largest near the central plasma and amount for hydrogen to 10^{15} to $10^{19}/\text{cm}^2 \text{ s}$. The impurity fluxes are a factor of 10 to 1000 lower, depending on their concentrations in the boundary plasma. The energy of the ions is about $2kT_i + 3.5q_i kT_e$, where T_i and T_e are the ion and electron temperatures and q_i is the charge of the ions.^e The second term originates from the acceleration in the sheath potential.

Owing to recycling and charge exchange processes, especially for hydrogen, an additional flux of neutral hydrogen atoms hits the wall. The total neutral flux has about the same intensity as the ion flux but is more uniformly distributed. Only on areas of strong recycling and around the gas inlet are the neutral fluxes enhanced. The neutrals have a much broader energy distribution, with average energies close to those of the ions /24,25/.

Physical Sputtering

Physical sputtering is caused by the hydrogen ions (in a fusion plasma also by helium ions), by energetic neutrals as well as by impurity ions such as oxygen and by ions from the wall material. It is still an open question which particles make the major contribution. For a clean plasma sputtering by hydrogen (deuterium and tritium) should dominate /26/. On limiters and wall areas perpendicular to the magnetic field, ion sputtering is likely to dominate, while on areas parallel to the magnetic field sputtering by CX neutrals is important.

In ASDEX direct erosion measurements averaged over several discharges have shown that of the order of $3 \cdot 10^{13}$ Ni atoms/ $\text{cm}^2 \text{ s}$ have been eroded on first-wall areas parallel to the magnetic field, while it is more than an order of magnitude more on areas perpendicular to the magnetic field. The erosion probes were positioned in the shadow of a protection limiter outside the boundary plasma flowing into the divertor /24/.

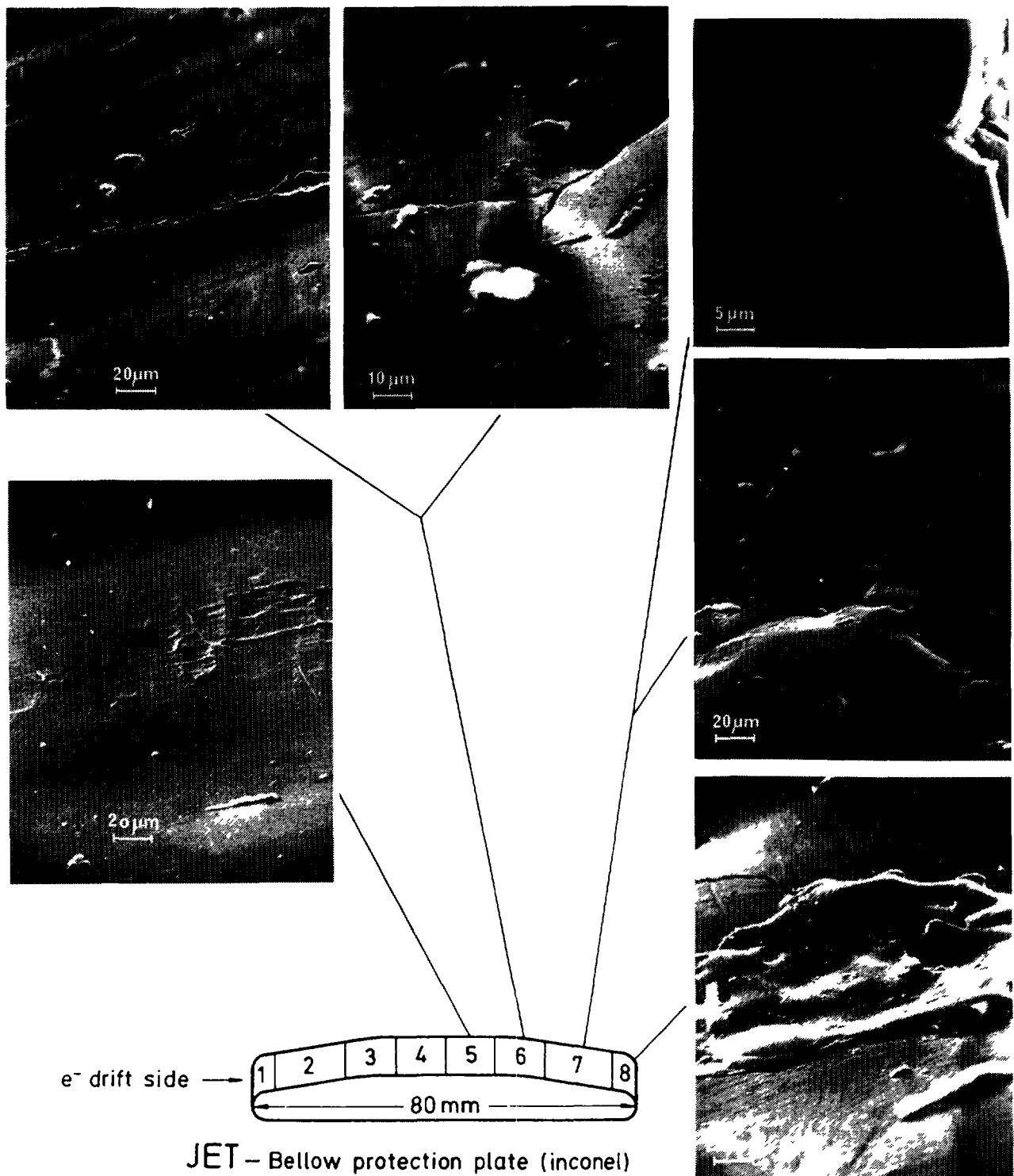


Fig. 7 Surface features on the inconel bellow protection plates used in JET during the 1984 operation period.
 Top left : traces from electric arc.
 Top middle: Cracks due to thermal shocks, surface melting, surface debris and metal splashes.
 Top right : a cut perpendicular through the surface showing that the surface crack penetrates about 30 μm.

If we take for a fusion reactor a wall flux of 10^{16} to 10^{17} deuterium and tritium ions and neutrals per $\text{cm}^2 \text{ s}$, an value of 10^{14} wall atoms are eroded per $\text{cm}^2 \text{ s}$. Just hydrogen sputtering would give a total erosion at the walls of 10^2 to 10^3 kg per year. The sputtered material are mostly neutral atoms with energies in the eV range. They are finally deposited or implanted mostly non-uniformly on the different wall areas.

Chemical Sputtering

In today's tokamaks mostly carbon is used for limiters and protection plates. However, the contribution of chemical sputtering to erosion is still contradictory. A possible reason for this is the very high hydrogen flux density and/or the metal deposition found on all carbon samples after being in a tokamak for a few discharges /5/. Further atoms and molecules released by chemical sputtering generally have low energies, i.e. corresponding to the wall temperature. These low-energy particles are probably ionised very effectively in the boundary plasma and will be redeposited at near-wall areas and will not enter the central plasma.

Radiation-enhanced sublimation

At a carbon probe in PLT a very high erosion was found on an area where energetic particles from loss cones hit the walls. This effect has been explained by radiation-enhanced sublimation /27/.

Sublimation, melting, droplets

In today's high-temperature plasma experiments typically 5 to 10 % of all discharges are unstable and are partly terminated by a disruption. The densities of the locally deposited power may reach up to several kW/cm^2 for times of the order of ms.

During such plasma disruptions major wall damage, i.e. large molten areas, the release of metal droplets from the first wall and surface cracks, have been found (fig. 7). A fusion reactor may have to be designed to survive a few of these disruptions, and they will probably limit the lifetime of the first wall. It will be necessary to find schemes for carefully controlling the plasma in order to avoid hard disruptions.

Electric arcs

Electric arcs can be ignited at the vessel walls if the electric field is above the critical value depending on the surface state. The electric field of the Langmuir sheath potential is generally not sufficient to ignite arcs at a clean surface in today's plasma experiments. Arcs are ignited at contaminated surfaces and/or during unstable plasma phases by runaway electrons or by magnetic islands touching the limiter, the divertor plates or the vessel surface. Detailed measurements have shown that arcs burn during current ramp-up of a tokamak, during additional heating, during the current ramp-down as well as during unstable plasma phases. Generally, traces of cathode arcs are found on all areas of the vessel which are not too remote from the plasma. (fig.7) .

The material released consists primarily of ions from the arc plasma. Most of them will be redeposited on the vessel walls before entering the central plasma. The molten droplets emitted by arcs from metal surfaces, especially at elevated temperatures, are found in large numbers as small metal splashes on the first wall (fig. 8) /22,23/.

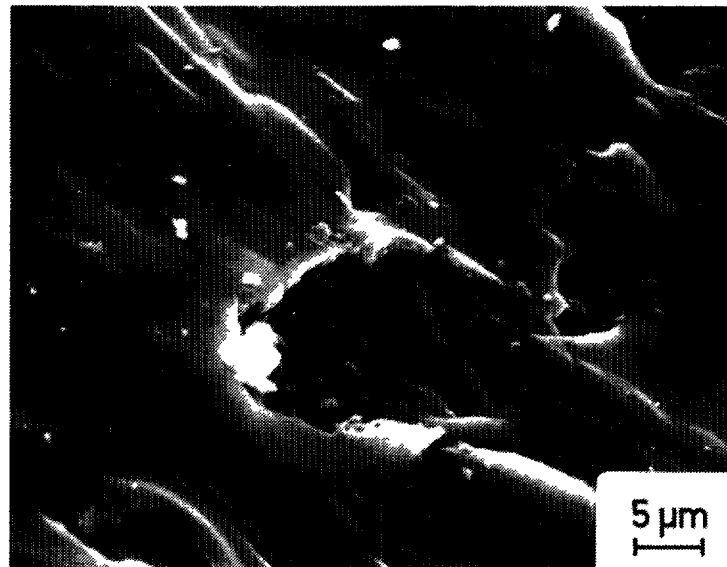
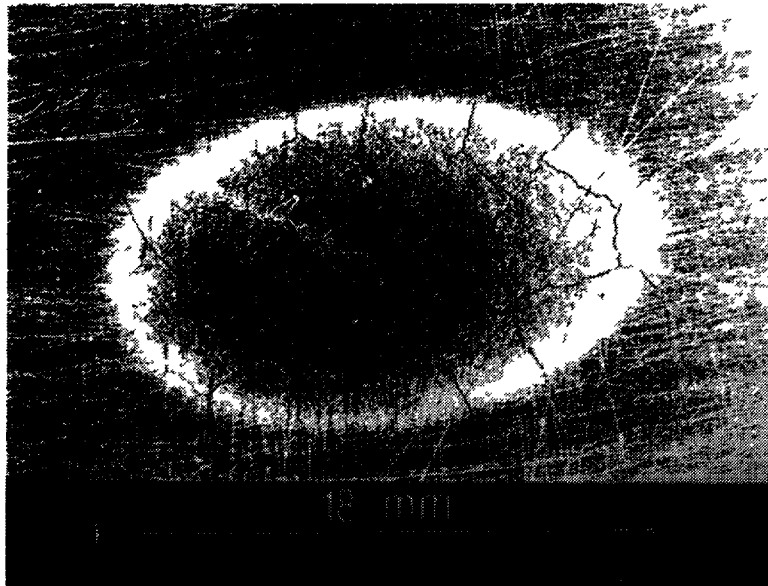


Fig. 8 top: Cracks on the surface of a carbon mushroom limiter from ASDEX,
bottom: Flaking of a Carbon layer deposited on the sides of the Carbon limiter of JET (1985 operation period).

In a future fusion reactor the erosion by arcing at first-wall components such as limiters may become a crucial problem when the densities and temperatures of the boundary plasma are increased compared with those in current plasma experiments.

Microparticle emission

In plasma experiments where the vessel walls had been covered with evaporated Ti for gettering of impurities, the plasma discharges occasionally showed abnormally high impurity concentrations. In filming the

plasma of such discharges sometimes bright objects, UFO's, have been found /28/. The number of these bright objects is drastically increased when referred to as at the vessel was hit with a hammer during a discharge. This indicates that the objects are small metal flakes which very likely originate from the getter layer evaporated on the vessel wall. Such bright objects were considerably reduced in number when the vessel walls were cleaned from all loosely bound material.

However, after an extended discharge period, the surface layers of the first wall are transformed. A new surface layer is formed owing to condensation and implantation of material from other wall areas and to simultaneous erosion. Furthermore, droplets and splashes are deposited /29, 30/. The surface layer is modified by the implanted hydrogen and helium and by thermal pulses and we may assume a rough surface topography. Some examples are given in figs. 8 and 9 showing carbon limiters from ASDEX and JET /31/ and a TiC-coated Poco graphite limiter from ISX /32/. Such modified surfaces may be again a source of microparticles released at mechanical or thermal pulses.



Fig. 9 Cracking and melting of a TiC coating on the carbon mushroom limiter used in ISX /32/.

IV. SUMMARY

From the different processes contributing to first-wall modification and the examples given from today's fusion machines it is not yet possible to make definite predictions of the lifetime of the vessel components in future fusion reactors.

Even if hydrogen sputtering is the only wall erosion mechanism a total amount of about 10^2 to 10^3 kg of wall material can be removed per year and will probably be redeposited on other wall areas. Especially at limiters, divertor plates and other comparable areas exposed close to the central plasma, erosion and net material loss will most likely dominate as found in today's experiments. There will be few areas where wall material erosion and redeposition just balance. The erosion processes which occur predominantly during plasma instabilities, i.e. sublimation and evaporation, melting and droplet emission, arcing and microparticle emission, may represent mechanisms even more severe than sputtering in limiting the lifetime of the first wall in a fusion reactor.

Acknowledgements

It is a pleasure to thank my colleagues from the Plasma Wall Interaction group at Garching, especially J. Roth, B.M.U. Scherzer, G. Staudenmaier and H. Verbeek for many helpful comments and suggestions.

References

- /1/ H.F. Dylla, J. Nucl. Mat. 93/94 (1980) 61
- /2/ R. Behrisch (ed) "Sputtering by particle bombardment Vol. I, Topics in Applied Physics, Vol. 47 (1981) and Vol. II Topics in Applied Physics, Vol. 53 (1983), Springer Verlag, Berlin, Heidelberg, New York.
- /3/ R.A. Langley, J. Bohdanský, W. Eckstein, P. Mioduszewski, J. Roth, E. Taglaier, E.W. Thomas, H. Verbeek, K.L. Wilson: "Data compendium for plasma-surface interactions" Nuclear Fusion, special issue (1984).
- /4/ N. Matsunami, Y. Yamamura, Y. Itikawa, N. Itoh, Y. Kazumata, S. Miyagawa, K. Morita, R. Shimizu and H. Tawara, Report IPPJ-AM-32, Institute of Plasma Physics, Nagoya University, Chikusa-ku, Nagoya 464, Japan (1983)
- /5/ J. Roth in "Physics of Plasma Surface Interactions in Controlled Fusion", D. Post, R. Behrisch (eds) Plenum Press, New York, London, (1985).
- /6/ J.P. Biersack, W. Eckstein, Appl. Phys. A34 (1984) 73
- /7/ J. Bohdanský, Max-Planck-Institut für Plasmaphysik, D-8046 Garching bei München, FRG, IPP-JET-Report (1985)
- /8/ J. Roth, W. Möller, Nucl. Instr. Meth. in Physics, Res. B 718 (1985) 788
- /9/ J. Bohdanský, Nucl. Instr. Meth. B2 (1984) 587
- /10/ R.E. Honig, D.A. Cramer, RCA Review 30 (1969) 285
- /11/ R. Behrisch, Nucl. Fusion 12 (1972) 695 and J. Nucl. Mat. 93/94 (1980) 498
- /12/ C.D. Groessmann, G.L. Kulciski, J.B. Whitley, J. Nucl. Mat. 128/129 (1984) 816
- /13/ Gmelin's Handbuch der anorganischen Chemie. "Kohlenstoff", 8. Auflage, p. 188 (IB) (1968)
- /14/ H. Vernickel, J. Nucl. Mat. 111/112 (1982) 531
- /15/ A.M. Hassanein, G.L. Kulcinski, W.G. Wolfer, J. Nucl. Mat. 111/112 (1982) 554
- /16/ M.F. Smith, J.B. Whitley, in "Physics of Plasma Surface Interactions in Controlled Fusion", D. Post, R. Behrisch (eds) Plenum Press, New York, London (1985)

- /17/ G.M. McCracken, P. Stott, Nucl. Fusion 19 (1979) 889
- /18/ B. Jüttner, Plasma physics and Controlled Fusion 26 (1984) 249
- /19/ G. Ecker, Proc. Int. Symp. Plasma Wall Interactions, Jülich (1976), Pergamon Press 245 (1977) and Proc. ICPIG, Düsseldorf (1983)
- /20/ R. Behrisch in: "Physics of Plasma Surface Interactions in Controlled Fusion", D. Post, R. Behrisch (eds.), Plenum Press, New York, London (1985)
- /21/ A.W. Nürnberg, D.Y. Fang, H.U. Bauder, R. Behrisch, F. Brossa, J. Nucl. Mat. 103/104 (1981) 305
- /22/ G. Staudenmaier, J.Vac.Sci.Techn. A3 (1985) 1091
- /23/ EQUIPE TFR with collaboration of P. Staib, G. Staudenmaier, Int.Symp. on Plasma Wall Interaction, KFA Jülich 1976, p. 59, Pergamon Press EUR 5782 e
- /24/ D.E. Voss, S.A. Cohen, J.Nucl.Mat. 93/94 (1980) 405
- /25/ H. Verbeek and the ASDEX-Team. Proc. 12th Europ. Conf. Controlled Fusion and Plasma Physics, Budapest, Sept. 1985
- /26/ H. Vernickel, B.M.U. Scherzer, J. Bohdanský, R. Behrisch, Int. Symp. on Plasma Wall Interaction, KFA Jülich 1976, p. 209, Pergamon Press EUR 5782 e
- /27/ D. Manos, P.C. Stangeby, R.V. Budny, S.A. Cohen, S. Kilpatrick, T. Satake, J.Nucl.Mat. 129 (1984) 319
- /28/ D.H.G. Goodall, J.Nucl.Mat. 111/112 (1982) 11
- /29/ Ph. Staib, G. Staudenmaier, J.Nucl.Mat. 76/77 (1978) 78
- /30/ R. Behrisch, R.S. Blewer, H. Kukral, B.M.U. Scherzer, H. Schmidl, P. Staib, G. Staudenmaier, J.Nucl.Mat. 76/77 (1978) 437
- /31/ J. Ehrenberg, R. Behrisch, P.E. Stott, J.P. Coad, L. de Kock, G.M. McCracken, these proceedings
- /32/ R.A. Langley, L.C. Emerson, J.B. Whitley, A.W. Mullendore, J.Nucl.Mat. 93/94 (1980) 479

REDISTRIBUTION OF LIMITER AND WALL MATERIALS IN JET

J. EHRENBERG, R. BEHRISCH
The NET Team,
Max-Planck-Institut für Plasmaphysik,
Garching near Munich

P.E. STOTT, J.P. COAD, L. de KOCK
JET Joint Undertaking,
Abingdon, Oxfordshire

G.M. McCracken
Culham Laboratories,
Abingdon, Oxfordshire

United Kingdom

Abstract

The study of plasma wall interactions serves two interrelated fields in fusion research: Impurity release and transport from the walls of the vacuum chamber into the plasma and wall erosion and damage done by the plasma.

The first is a serious problem for plasma discharges in today's fusion devices (see for example /1/) whereas the second becomes more important with the increase of input power into large machines, such as TFTR, JT60 or JET.

In JET specific diagnostics have been used from the start of the operation to monitor the variation of the wall state after long term tokamak operation (typically half a year). One of the main purposes is to quantify the amounts of eroded and redeposited wall and limiter material and to investigate its redistribution in the vacuum vessel. On limiters this has been performed after each operational period whereas the wall investigations started after the 1984 period, giving for the first time an overview of wall and limiter changes dependent on different operational periods of a large tokamak. Some of the important and relevant results are reported here.

1) EXPERIMENTAL METHODS AND CONDITIONS

Two experimental methods are employed: 1) Post mortem analyses of the JET carbon limiters by surface analysis techniques (described below). 2) Exposure of wall long term samples (LTS) to the plasma. The LTS have been evenly distributed across the vessel wall during shutdown periods and were later on taken out in subsequent shutdowns to undergo surface analyses.

Four different sample materials were used: Carbon - to detect deposited metals; Inconel 600 - to detect deposited carbon and to see how the wall material (inconel 600) changes; Silicon, Nickel - to have a well known material for further fundamental studies (not reported here).

Fig.1 shows one of the four JET carbon limiter consisting of 8 tiles. Analyses have been performed at the bottom of tile 4 which is the location of the plasma midplane.

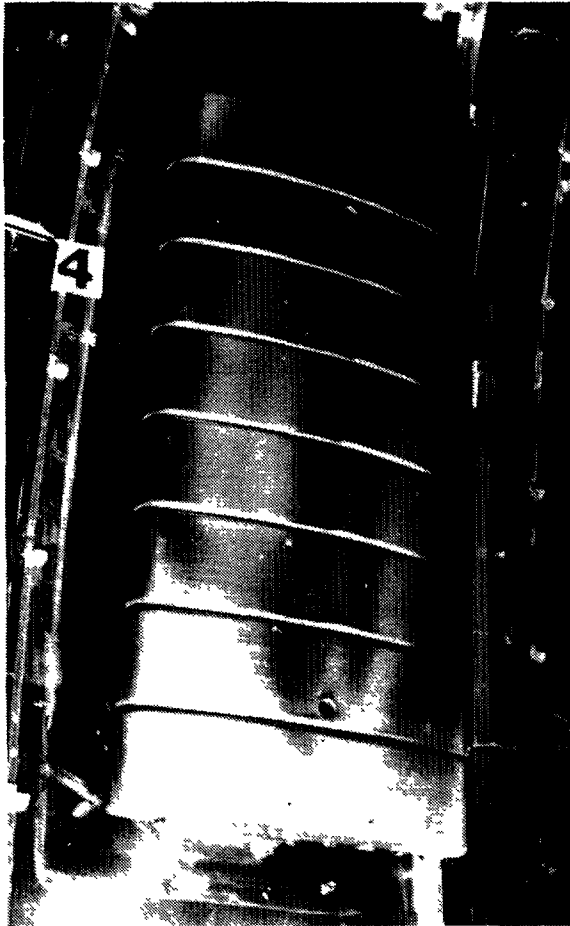


FIG.1: A JET Carbon Limiter

Fig.2 gives an impression of the relative arrangement of limiters and LTS. The latter were all placed well in the shadow of the bellows protection plates.

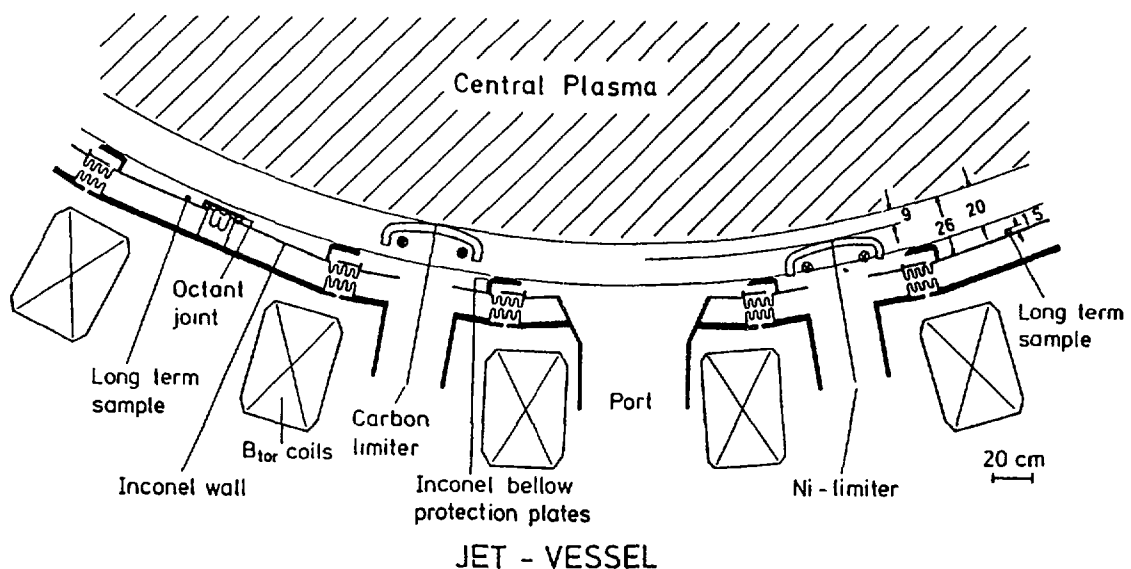


FIG.2 Local arrangement of limiters and wall long term samples (LTS)

The analysis techniques were: Proton induced X-Ray Emission (PIXE) to detect mainly deposited metals up to a depth of about 10 μ m on a carbon sample; Backscattering Spectroscopy to measure deposited carbon on metal samples; Scanning Electron Microscopy (SEM) to get a qualitative impression of the deposit topography; Sputter Auger Electron Microscopy to look at the very surface composition of a sample and to perform depth profiling. Besides these techniques visual inspections of the torus wall were performed in shutdown periods in order to reveal macroscopic damages.

The experimental periods after which investigations were carried out can be characterised as follows:

- i) 1983, about 200 flat top plasma discharges, a maximum plasma current of 3MA and a discharge time of up to 10s.
- ii) 1984, about 400 flat top plasma discharges, a maximum current of about 4MA and up to 15s discharge time.
- iii) 1985, roughly 900 flat top discharges, currents of up to 5MA and up to 20s discharge time.

In 1984 and 1985 wall carbonisation was performed to study the effect of an all carbon wall. Carbonisation is carried out by adding a few percent of CH₄ to a glow discharge in hydrogen. This deposits carbon on the walls of the vessel /12/. In 1985 the inside wall was covered with carbon tiles (see Fig.5) and first tests of RF heating were performed with a maximum RF-power of 4MW for two seconds. Typical ohmic heating powers were 3 to 4MW.

II) RESULTS

1. Erosion and Redeposition of Wall Material

1.1 Metals Visual inspection of the torus wall after the 1984 experimental period revealed three regions with different surface features /2,3/:

- (i) The inside wall was heavily damaged by massive melting processes.
- (ii) Top and bottom of the vessel showed mostly arc tracks.
- (iii) The outside wall was not significantly changed indicating the protective action of the limiters which have been placed there.

Most of the damage was observed on bellows protection plates, covering the rigid sector junctions. The wall itself, about 6cm behind, was much less affected. The distribution of deposited wall material as found on carbon LTS (see Fig.3), shows a correlation to the damage distribution: maximum deposition on inside wall LTS. Toroidally differences are smaller than poloidally.

Results from the 1985 period, also shown in Fig.3, indicate different toroidal and poloidal distributions. In particular the metal ratio of Fe/Ni+Fe+Cr, Fig.4, differs significantly from its inconel value except at the bottom of the torus. The excess deposition of iron was due to the melting and evaporation of a stainless steel containing Langmuir probe hit by runaway electrons /3/. Comparing absolute amounts of Ni (which may serve as an indicator for wall erosion) no major

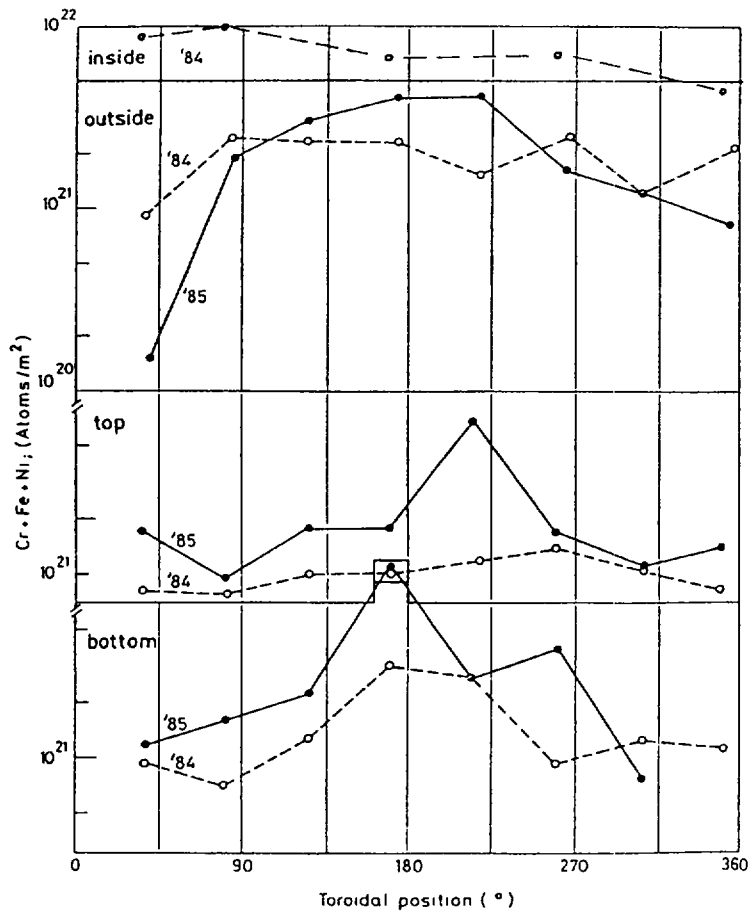


FIG.3:

Toroidal distribution of deposited metals on wall LTS as found after the experimental period of 1984 and 1985.

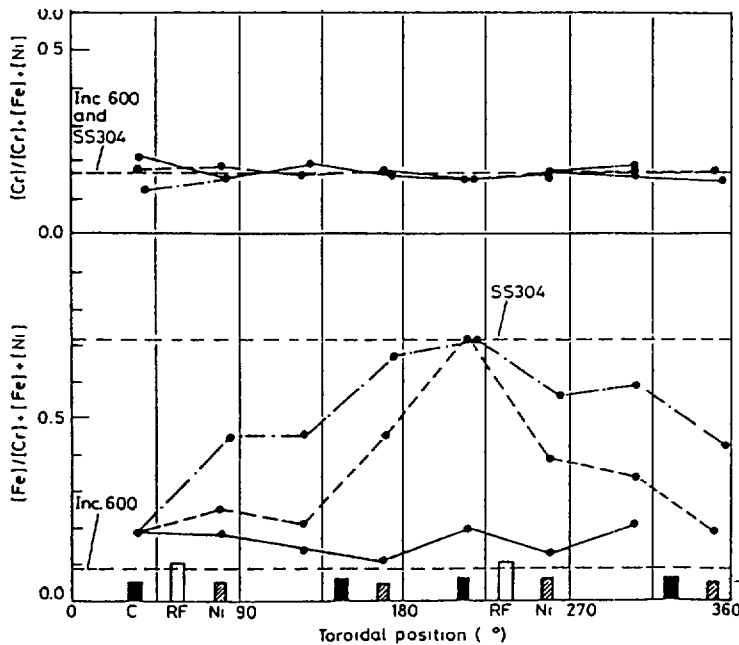


FIG.4:

Relative distribution of Cr and Fe as found on the 1985 LTS.

differences between 1984 and 1985 could be detected especially not at the top side of the wall /3/: Mo, surprisingly found on limiters and walls after the 1983 and 1984 period, has been accidentally introduced into JET by contaminated limiters. Before the 1985 period they were thoroughly cleaned, thus no Mo appeared on the 1985 LTS. Mo was found predominantly on

the outboard wall LTS of 1984, which is the same poloidal position as that of the limiters.

1.2 Non metals The most abundant impurity in the JET plasma (2-3%) is carbon. Comparing the inconel LTS analyses of 1984 and 1985 Fig.5 shows an enhanced deposition during 1985 owing possibly to the enhanced carbonisation carried out during 1985. In contrast to metals carbon is sensitive to chemical reactions with hydrogen which complicates erosion and redeposition phenomena. Recent results /4/ indicate a stronger deposition of carbon at the outside wall than elsewhere, similar to the Mo distribution in 1984.

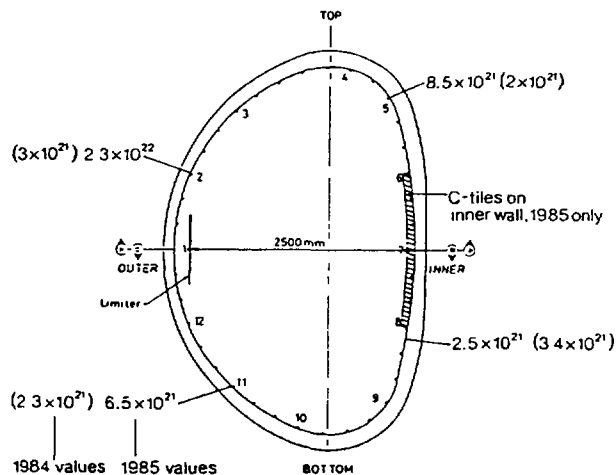


FIG.5:
Distribution of carbon
as found on Inconel LTS
(amounts in atoms/m²)

Chlorine was also found at wall samples of the 1985 period. Typical amounts were below 10²⁰ atoms/m². The origin of Chlorine is unclear.

Oxygen is also an abundant element on the samples (10²⁰-10²¹ atoms/m²). However, we cannot make conclusive interpretations until the influence of post oxidation in air has been clarified.

2. Redeposition on the Carbon Limiters

Visual inspection of the limiter surface did not usually reveal surface features which could characterise important erosion mechanisms. Only a few arc tracks have been observed at the side edges.

In general, the distribution of metals on limiters from all three periods show large deposited amounts at the side edges (>10²¹ atoms/m²) and lower ones at more central parts (<10²¹ atoms/m²), Fig.6. There is a tendency for increased deposited amounts at the side edges starting from the 1983 period. The different shapes of the distributions can be correlated to different experimental conditions as discussed below. The Molybdenum as found on the 83 and 84 limiters exhibits the same distribution as Ni although it is not present in the wall material.

Ti is a trace element in inconel, and K, Ca are trace elements in the carbon bulk (only shown for the 83 limiter). Cl was

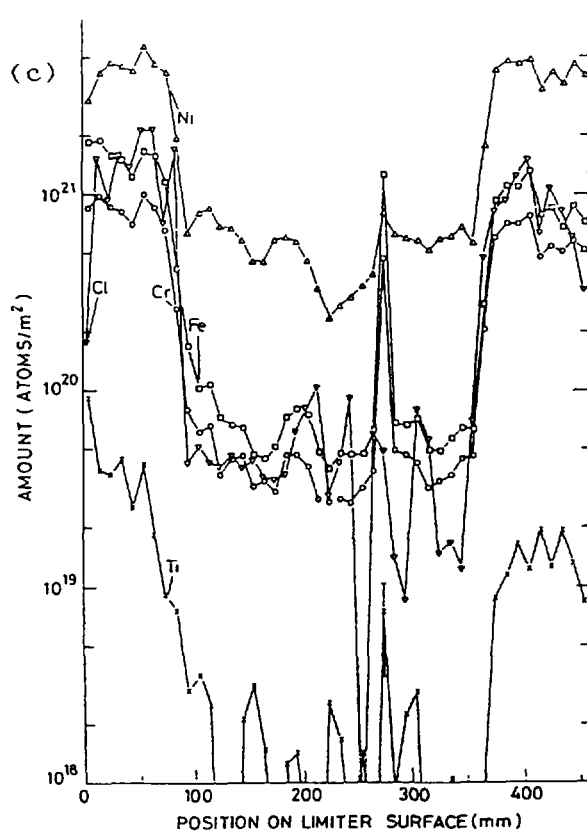
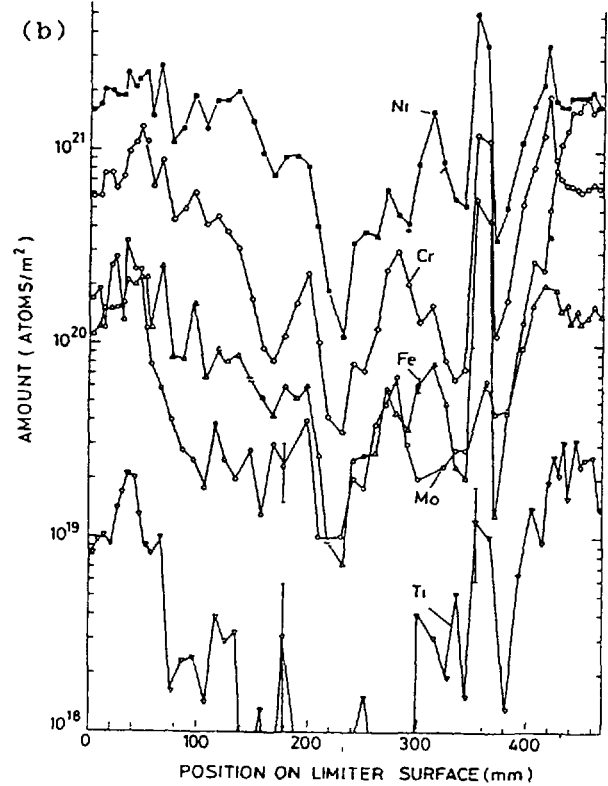
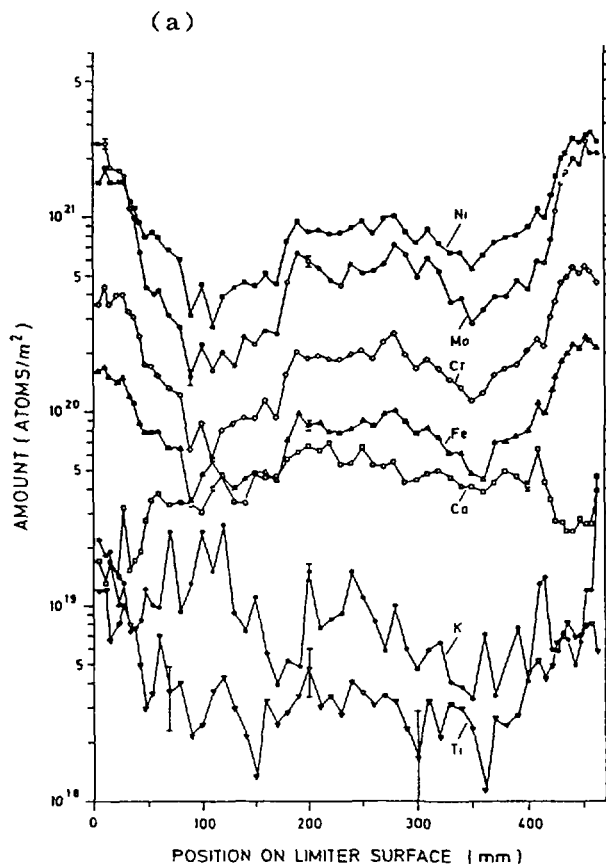
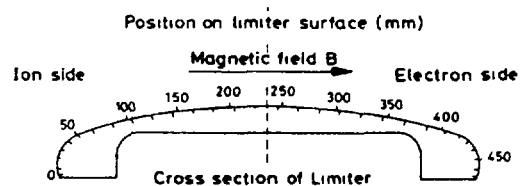


FIG.6:

Toroidal distribution of metals
as found on JET carbon limiters
after three different
operational periods:

- a) 1983
- b) 1984
- c) 1985



also detected on the 85 limiter showing a similar distribution to other contaminants.

3. Surface Topography of Deposits

There are three different features of topography on wall LTS:

- (i) Uniform metal layers.
- (ii) Metal splashes from melting process, $\varnothing < 100 \mu\text{m}$.
- (iii) Droplets, possibly formed on the surfaces $\varnothing < 10 \mu\text{m}$.

They appear on all wall sites with an enhancement of (ii) on the bottom of the machine, part of it found in form of debris (=30g in 1984 /6/).

The metal on the limiters was distributed in the carbon bulk /7/ and droplets appear to be embedded in carbon grooves at the surface /2/. Because of this depth distribution the very surface of the limiter is still about 90% carbon, as measured by Auger analysis.

III) DISCUSSION

1. Identification of Erosion and Redeposition Zones at the Wall

All surfaces which have been exposed to tokamak operations are subject to erosion and deposition processes. The relative importance depends on the actual location of a specific surface relative to the plasma. The inside wall of JET was more affected by disruptions and run away electrons than other locations. The main heat load went to the protection plates while the inside wall itself acted much more as a deposition zone for the eroded material. A similar correlation between erosion and redeposition can be inferred from the Fe distribution of the 1985 period, Fig.4. The location of the peak maximum coincides with that of the Langmuir probe which was destroyed by runaway electrons. A more detailed analysis /3/ shows the Fe distribution depending primarily on the solid angle between a specific LTS and the probe suggesting vapour distribution. Although this probe accident happened at the beginning of the 1985 period all the subsequent discharges did not change the original distribution showing that erosion at the wall was relatively weak. Most of the erosion and deposition appears to occur in unstable or disruptive discharges. The Mo distribution on the 1984 LTS, /2/, may serve as an example for erosion and redeposition during all discharges. The poloidal distribution of redeposited Mo also suggests the presence of a source-sink correlation as most of the Mo is found at the same poloidal position as that of the limiters.

From these observations we may draw the following conclusions: The closer a surface is to the plasma the more likely it is to be subject to erosion in normal discharges. Melting and evaporation events caused by disruptions or run away electrons may occur everywhere and are locally confined. All these erosion processes are well recorded by the deposits found at the wall indicating low re-erosion from there.

2. Relative Importance of Different Wall Erosion-Processes

In this section we will make some order of magnitude estimates of some erosion processes. We shall first consider the possible contribution of charge exchange neutral sputtering (CXNS). From the energy distribution of the measured /8/ CX-neutrals and from known sputtering yields /9/ we may estimate possible erosion yields. In order to take into account the most important low energy (<1keV) part of the CXN-distribution we have to extrapolate the measured curves. At the maximum of the product of sputtering coefficient and flux density we have, for the 1984 period, assuming a 2π source distribution and uniformity:

$$Y_{CXN} = 3.10^{18} \text{atoms/m}^2\text{s} \times 3 \times 10^{-2} \times 1000 \text{ discharges} \times 15\text{s} \\ \approx 1.4 \times 10^{21} \text{atoms/m}^2$$

For the ions we take the temperature (+10eV) from recent Langmuir-probe measurements /12/ and assume a uniform distribution and similar fluxes as for CXN. We then get for 1985

$$Y_{ion} \approx 3.10^{18} \text{atoms/m}^2$$

The influence of a disruption or run away electrons is difficult to assess. Analysis of the Langmuir probe melting process indicated the presence of at least 20MeV electrons which deposit at least 25kJ into the metal parts /11/, leading to evaporation and melting of 85g SS304. This amount may be converted to an equivalent of

$$Y_{disruption} \approx 5 \times 10^{21} \text{atoms/m}^2$$

if eroded evenly from the entire vessel wall. No damage was observed on the inside wall carbon tiles during 1985 which showed that there were no powerloads significantly over 5MW/m² for 10s since this is the maximum heat load the tiles could withstand.

Besides tokamak discharges glow discharge cleaning processes also contribute to wall erosion /12/. Assuming sputtering and taking the GDC data for 1985 we end up with an amount of

$$Y_{GDC} \approx 2 \times 10^{21} \text{atoms/m}^2$$

assuming again uniformity over the vessel wall.

These estimates indicate that rather than normal discharges alone erosion by disruptions/runaway electrons and GDC, are also important. The contribution of CXNS is very uncertain and might be higher if non isotropic flux distributions are taken into consideration. However, the data, especially the experimental results from wall LTS indicate that stable plasma discharges do not contribute significantly to wall erosion. Although we do not know the influence of arcing on the overall erosion in JET there are indications /2/ that it also occurs predominantly in unstable discharges.

3. Modeling of Erosion and Redeposition Processes at the Carbon Limiters

Besides the effect of wall damage, wall erosion leads also to the contamination of carbon limiters with metals /2,5/ thus reducing the advantage of making them out of a low Z material. In JET, the limiters are the dominant source for metal influxes into the plasma /13/. Taking the spectroscopically measured fluxes of Ni for instance and calculating the time which would be needed to clean the surface of the limiter gives 10s to 100s or 1 to 10 discharges. This is obviously in contrast with the surface analysis results where up to 10^{21} Ni/atoms/m² have been still detected after several hundred discharges. The most likely explanation for this is that significant impurity recycling occurs on the limiter itself. This is supported by the observation that Mo exhibits the same distribution on the limiter as Ni does but without having a source on the wall. We may therefore model the erosion and deposition processes at the limiters, integrated over all discharges in the following way:

We assume a net, constant and uniform deposition concentration C_0 on the limiter surface. This may be caused by vapour deposition occurring during disruptions for example or by glow discharge cleaning.

In plasma discharges we assume an erosion flux due to a power flux decaying exponentially radially outwards beginning from the leading edge of the limiter:

$$E = E_0 e^{-(r-a)/\lambda_E}$$

with r = radial position

a = radial position of the limiter leading edge

λ_E = decay length

Power fluxes have been measured thermographically /14/ giving λ - values from 10 to about 20mm.

We now assume that the plasma impurities are partially redeposited on the limiter by a radially outward decaying deposition flux:

$$D = D_0 e^{-(r-a)/\lambda_D}$$

λ_D is not known but may be different from λ_E .

For simplicity we assume $\lambda_D = \lambda_E$ and, taking into account the angular (α) dependence of the fluxes on the limiter surface owing to its cylindrical geometry in toroidal direction, we get the following normalized deposition distribution:

$$\frac{C(\tau)}{C_0} = C^X(\tau) = 1 + P_0 e^{-(r-a)/\lambda} \cos \alpha$$

$$\text{with } P_0 = \frac{D_0 - E_0}{C_0}$$

P_0 may be considered as the net deposition or erosion constant depending on whether it is larger or smaller than zero.

Fig.7 shows a comparison between this model and the experimental data from 1983 and 1984, taking values for P and λ as indicated.

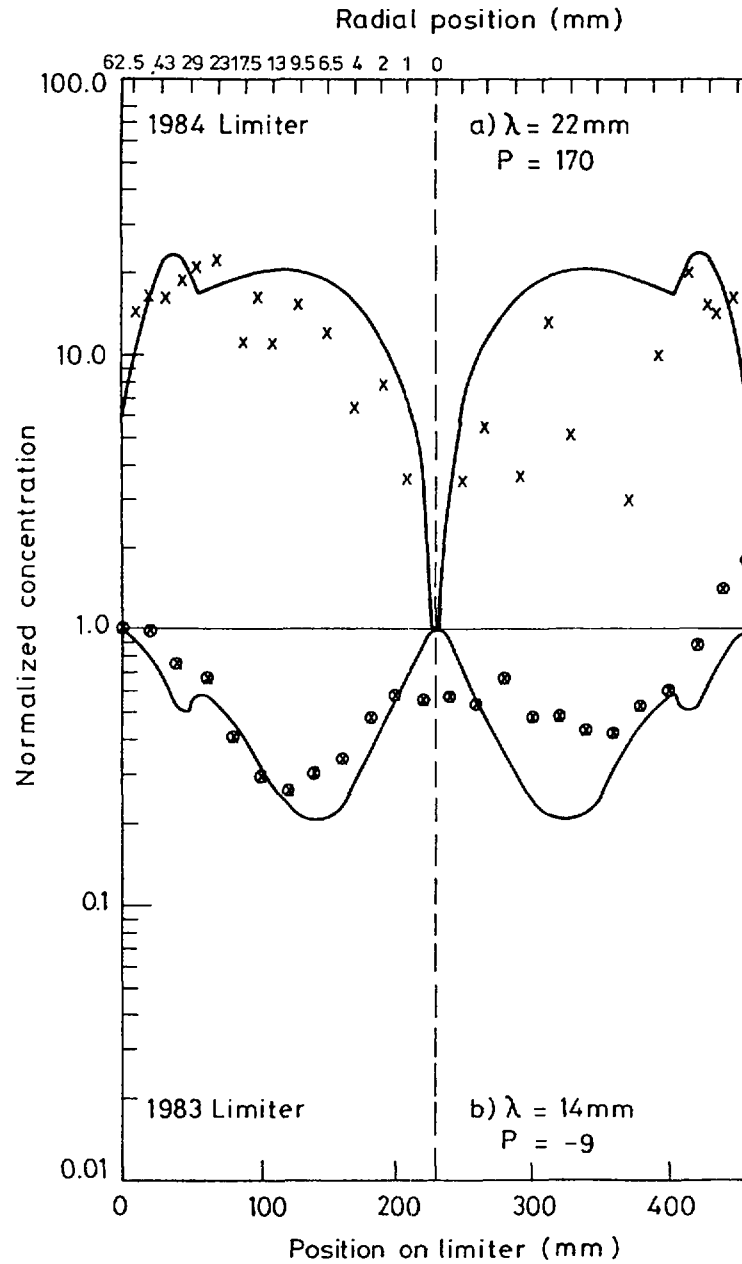


FIG.7: Modelling of erosion and deposition processes on the limiter surface. Crosses are experimental data.

Obviously the 1984 distribution can be approximated to some extent by a deposition determined process ($P>0$) while the 83 distribution is better described by an erosion determined plasma limiter interaction ($P<0$). The reason for this is yet not fully understood. The 1984 distribution was in addition affected by much higher limiter temperatures ($\approx 1500^\circ\text{C}$ compared to less than 650°C in 1983) which have distributed metal by diffusion into the limiter bulk /7/ thus protecting it from re-erosion.

The 1985 limiter metal distribution cannot be explained with this model because of the interfering action of the RF antennae.

The antennae shadowed the limiter such that regions below 80mm and beyond 370mm on the limiter surface received lower fluxes. Thus the steep increase in surface concentration there is not caused by mechanisms as mentioned above.

In general we may conclude that not only metal but other impurities including the limiter material carbon are redistributed in the same way. From unexpectedly high deuterium amounts found on the side edges of the 1984 and 1985 limiters, suggesting the presence of carbon-deuterium codeposition /2,3/, we may evaluate the amount of deposited carbon. The amounts could be in the range of 10^{22} to 10^{23} atoms/m², about an order of magnitude more than for Ni. This is in agreement with spectroscopical observations showing a factor of 10 larger C-fluxes than Ni fluxes.

A calculation of impurity erosion on the limiter surface employing spectroscopically measured particle fluxes for hydrogen, metals, carbon and oxygen /12/ indicates that a large part of the carbon erosion may be due to oxygen and self sputtering. There is, so far, no experimental indication for chemical erosion of carbon by hydrogen. Chemical erosion would not be expected to be significant for such high incident fluxes as measured on the limiters (10^{21} - 10^{22} ions/m².s) /15/.

IV) CONCLUSIONS

Erosion and deposition investigations in JET indicate that in stable discharges wall erosion is negligible while most of the wall damage is due to singular events such as disruptions and runaway electrons, hitting the wall. Glow discharge cleaning runs integrated over a total experimental period may also contribute significantly to wall erosion.

All erosion processes may contribute to the contamination of the carbon limiter surface with metals. In plasma discharges contaminants are re-eroded from there and probably redeposited undergoing a recycling process on the limiter. During a discharge only a minor part of the limiter material seems to be transmitted to the walls.

LITERATURE

- /1/ G.M. McCracken and P.E. Stott, Nuclear Fusion, Vol.19, No.7 (1979) pp.889-980
- /2/ J. Ehrenberg, R. Behrisch, A.P. Martinelli, H. Kukral, IPP-JET-Report No.29, May 1985
- /3/ J. Ehrenberg to be published
- /4/ M. Braun and B. Emmoth, Private communication
- /5/ J. Ehrenberg and R. Behrisch, IPP-JET-REPORT No.23 May 1984
- /6/ D.H.J. Goodall, Private communication
- /7/ J. Ehrenbertg and P. Børgesen to be published
- /8/ S. Corti, G. Bracco, M. Brusati, A. Gondhalekar, G. Grono, F. Hendriks, S. Segré and V. Zanza, Proceed. 12th Europ. Conf. Contr. Fus. Plasma Phys., Budapest 2-6 September 1985, Vol..I, pp.219-222
- /9/ J. Roth, J. Bohdansky, W. Ottenberger, IPP-Report 9/26 May 1979
- /10/ P.C. Stangeby, S.K. Erents, J.A. Tagle, G.M. McCracken, L. de Kock, Proceed. 12th Europ. Conf. Contr. Fus. Plasma Phys., Budapest 2-6 September 1985, Vol.II, pp.579-582
- /11/ G.M. McCracken, P. Stangeby, B. Denne, S.K. Erents, D. Goodall, H. Krause, G. Sadler, M. Stamp, D. Summers, T. Tagle, Internal JET-Report, JDN/E(85)8
- /12/ J.P. Coad, G.M. McCracken, S.K. Erents, J. Ehrenberg, L. de Kock, P.C. Stangeby, T. Tagle, Proceed. 12th Europ. Conf. Contr. Fus. Plasma Phys., Budapest 2-6 September 1986,, Vol.II, pp.571-574
- /13/ M.F. Stamp, K.H. Behringer, M.J. Forrest, P.D. Morgan, H.P. Summers, Proceed. 12th Europ. Conf. Contr. Fus. Plasma Phys., Budapest 2-6 September 1986, Vol.II, pp.539-542
- /14/ D. Summers, Private communication
- /15/ P.D. Morgan, S. Corti, J. Ehrenberg, M. Forrest, A. Gondhalekar, C.W. Gowers, G. Magyar, J.J. O'Rourke, M.F. Stamp, D.D.R. Summers, A. Tanga, M.L. Watkins, Proceed. 12th Europ. Conf. Contr. Fus. Plasma Phys., Budapest 2-6 September 1986, Vol.II, pp.535-538

THE DEPOSITIONS OF HYDROGEN ISOTOPES ON CARBONISED FUSION REACTOR WALLS

B.Y. EMMOTH, H. BERGSÅKER
Research Institute of Physics (AFI),
Energy Research Commission,
Stockholm, Sweden

Abstract

Results from recent tokamak experiments, with a carbonised surface covering the first wall, could give information on the surface content of hydrogen isotopes in the surface layer of a fusion reactor, and the risk for surface embrittlement. An important tool for such studies is the use of long term samples exposed in larger tokamaks of today for extended periods. Varying plasma conditions and disruption events is the cause of an ununiform deposition distribution. The total surface inventory of hydrogen isotopes can be estimated from these results.

1. INTRODUCTION

The idea to generate electricity by thermonuclear fusion has led to large scale experiments with tokamak reactor chambers, having the purpose to study plasma physics and plasma-wall interactions. Long term changes of the wall surfaces may change its stability and influence the wall lifetime. Equally important is that such changes may influence the control of the plasma performance, since gradual changes of the surfaces affect the recycling of the fuel gases. Hydrogen recycling is an interchange of hydrogen fuel between plasma and wall /1/. Recycling is a complex phenomenon, strongly influenced by plasma-wall interactions and is determined by the bulk diffusion of thermally activated hydrogen, and the surface conditions /2/, which are influenced by erosion and deposition of materials during the discharge /3/, as well as of wall treatments such as wall conditioning and carbonisations /4/.

Surface conditions and roughness, hydrogen content and the surface layer composition is thus of major concern for both the wall lifetime and plasma performance. Long term changes of the fusion first wall surface can already be studied by exposing samples during longer periods to discharges in larger tokamaks. Recently, carbonisation procedures have been developed /5/, which seem to improve plasma performance, but it is still not known whether such layers have the necessary stability as fusion reactor first walls. It is known, however, that such layers contain high amounts of the fuel gas or the hydrogen

isotope used in the wall treatment operations. In this paper we will, on the basis of recent results from JET and TEXTOR, describe the expected distribution and the concentration limits found from experiments and estimate the expected fuel inventory within this surface layer and the possibility of a degradation of the layer stability due to the high gas content, the radiation impact and problems related to erosion/deposition of impurities.

2. HYDROGEN DEPOSITIONS ON WALLS AND LIMITERS

Samples mounted on inner walls of the torus at different tokamaks, have been exposed for shorter or longer periods in order to study the end results from long term exposure of surfaces facing the plasma. Samples from large tokamaks were exposed up to several months and in some cases for hundreds of discharges. Such samples may give a relatively correct picture of the final surface modification that will result, although the history of the surface is complicated with respect to exposure conditions, plasma parameters and wall treatments. In this work our interest has been focused on carbonised walls and where deuterium has been used as filling gas.

Measurements of the net deposition of deuterium shows a larger scatter in the amount of detected surface concentrations for the wall samples. Investigating carbon limiters yield, however, more repetitive results, but the distribution is clearly related to the heat flux distribution. Fig. 1 shows within which concentration range deuterium varies. The area marked with lines between two dashed curves, covers an areal density of deuterium between approximately 1×10^{20} to 1×10^{22} atoms/m², where the upper curve is an indication of a typical toroidal variation, whilst the distance between the upper and lower curves indicates a typical poloidal variation. Fig. 2 shows a distribution which can be found on the limiters. In the middle of the limiter, which is facing the plasma more perpendicular and which is in closest contact with the plasma, the deuterium surface concentration is least due to the influence of the heavy power flux /5,6/. The region in the middle of the limiter tiles that receive a higher power flux, as also indicated in the figure. Towards the sides of the limiter tile the deuterium concentration increases to unexpected values, as will be explained below, whilst the concentration fall down, when we reach the points on the limiter that are not facing the plasma core directly.

The highest concentrations in the surface regions found are around 1×10^{22} atoms/m² both for wall samples and limiters. It should be noted that these numbers refer to studies when wall carbonisations have been performed routinely.

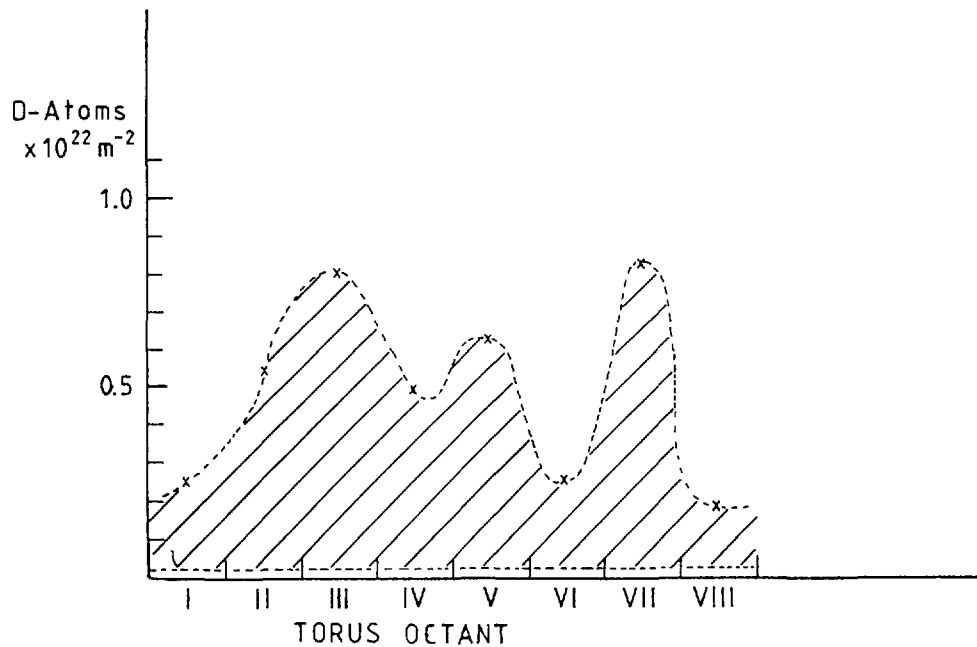


Fig. 1. Showing the variation of the deuterium areal density on samples exposed for a large number of discharges and at many positions within the torus. The results fall between the upper and lower dashed curves. The upper curve shows the maximum densities and the toroidal variation for all eight segments.

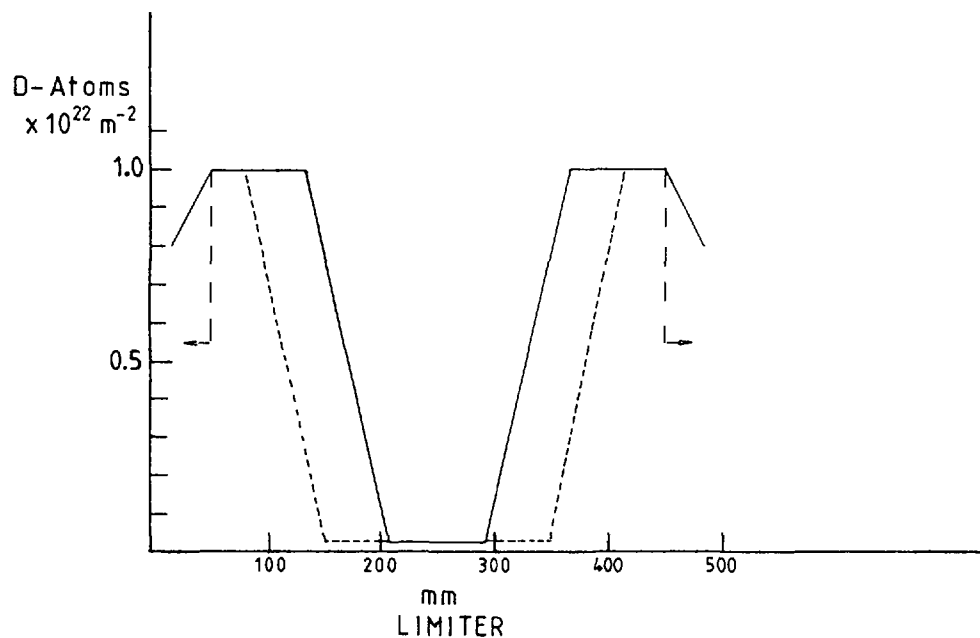


Fig. 2. Showing areal densities of deuterium on limiter tiles and the variation when the analysis is done from the side of the tile which faced the ion direction to the other side facing the electron drift. In a middle region of the limiter tile, which is nearly perpendicular to the plasma core, the deuterium density is lowered due to the heat flux. This region becomes broader for higher power fluxes, as indicated by the dashed lines.

3. TOTAL HYDROGEN INVENTORY IN THE WALL SURFACE LAYER

From the presentation in the preceding section we can make an estimation of the hydrogen inventory within the surface layer. We calculate the lower and upper limits from the figures. If the inner surface area of the torus is 200 m^2 , as for JET, we find a surface inventory of hydrogen

$$2 \times 10^{22} \text{ atoms} < \text{the H-isotope} < 1 \times 10^{24} \text{ atoms}$$

i.e. within a near-surface region of a few μm .

If we compare with a bare Ni surface, we find that for Ni the surface regions contains much less hydrogen, probably a factor 100 lower concentration. From our estimation we find that the amount of hydrogen in the carbon layer should be about 100 times that in the discharge. The trapped hydrogen will remain in the layer also after removal from the vessel and exposure to air.

4. DISCUSSION: CARBON LAYER LIFE-TIME

We have showed that the carbon layer on top of a metallic wall or a graphite limiter contain very high areal concentrations of deuterium. For metallic surfaces it has been reported earlier that a high load of hydrogen in the surface region can cause embrittlement /7/. The areal concentrations we report here have not been possible to reach in ion implantation experiments, a fact that explains why our knowledge about these coatings still is limited. It has been reported recently, that the stability of the carbon layer is good during normal discharges /8/ but it is destroyed by heavy disruptions. The carbonisation is done in a mixture of H_2 and methane, and a glow discharge. When successful the layer have diamond like bonds. Earlier, it has been showed that a diamond like layer has better sputtering properties than if the layer is amorphous /9/.

Although the carbon layer has been produced in a discharge with H_2 , long term exposure to deuterium tokamak discharges will result in mixture of the two gases within the layer /10/. We also conclude that we reach a deuterium level that probably is constant. Erosion and deposition together with recycling, take place simultaneously, but for a large number of normal discharges the layer seem to keep its composition and structure. Due to disruptions and accidents together with redistribution of material during glow discharge cleaning, the investigated samples always contain metallic impurities. The formed layers can therefore also be different types of carbides.

An important aspect on carbonisation is that the process in which the carbon layer is formed appears to be reversible /8/. Therefore the gases in the layer can be pumped off if necessary before parts of the surface is removed.

Our knowledge about carbon layers formed in carbonisation processes in tokamaks is still very limited. We need to investigate sputtering, embrittlement and even the composition and structure. Laboratory experiments may be difficult to perform, since we can not simulate conditions in a large plasma device. Long term sample and limiter analysis is probably the only way for a better understanding of these processes.

REFERENCES

- /1/ K. J. Wilson, J. Nucl. Mater. 103&104, 453 (1981)
- /2/ J. Winter, F. G. Waelbroeck, P. Wienhold, E. Rota and T. Banno,
J. Vac. Sci. Technol. A 2, 679 (1984)
- /3/ G. Staudenmaier, J. Vac. Sci. Technol. A 3, 1091 (1985)
- /4/ J. Winter, F. Waelbroeck, P. Wienhold, H.G. Esser, L. Konen, M. Braun,
B. Emmoth and H. E. S  therblom, J. Nucl. Mat. 128&129, 841 (1984)
- /5/ M. Braun and B. Emmoth, J. Nucl. Mat. 128&129, 657 (1984)
- /6/ S. Nagata, S. Yamaguchi, Y. Fujino, M. Hirabayashi and K. Kamada,
J. Nucl. Mat. 128&129, 760 (1984)
- /7/ I. Ali-Kahn, K. J. Dietz, F. G. Waelbroeck, and P. Wienhold,
J. Nucl. Mat. 85&86, 1151 (1979)
- /8/ J. Winter, TEXTOR, private communication
- /9/ N. Matuda, H. Sakamoto, K. Hashimoto, S. Baba and A. Kinbara,
J. Nucl. Mat. 128&129, 916 (1984)
- /10/ B. L. Doyle, W. R. Wampler and D. K. Brice, J. Nucl. Mat. 103&104,
513 (1981)

LIST OF PARTICIPANTS AND OBSERVERS

Chairman:

Mr. J. Vetter
Kernforschungszentrum Karlsruhe
Postfach 3640
D-7500 Karlsruhe 1
Federal Republic of Germany

Scientific Secretaries:

Mr. D. Röhrig
Kernforschungszentrum Karlsruhe
Postfach 3640
D-7500 Karlsruhe 1
Federal Republic of Germany

Mr. J. Kupitz
International Atomic Energy Agency
Wagramerstrasse 5
P.O. Box 100
A-1400 Vienna
Austria

Austria

Mr. H. Kny
Metallwerke Plansee
Reutte

Belgium

Mr. W. Vandermeulen
C.E.N./S.C.K. Mol
Boeretang 200
B-2400 Mol

France

Mr. D. Acker
DEDR/DEMT/SMTS
CEN/Saclay
F-91191 Gif-Sur-Yvette

Mr. G. Chevereau
DEDR/DEMT/SERMA
CEN/Saclay
F-91191 Gif-Sur-Yvette

Germany, Federal Republic of

Mr. M. Bocek
Kernforschungszentrum Karlsruhe
Institut für Material- und
Festkörperforschung
Postfach 3640
D-7500 Karlsruhe 1

Germany, Federal Republic of (cont.)

Mr. A. Ludwig	Kernforschungszentrum Karlsruhe Institut für Reaktorentwicklung Weberstrasse 5 Postfach 3640 D-7500 Karlsruhe 1
Mr. D. Munz	Universität Karlsruhe Institut für Zuverlässigkeit und Schadenskunde im Maschinenbau Postfach 3640 D-7500 Karlsruhe 1
Mr. T. Fett	Kernforschungszentrum Karlsruhe Postfach 3640 D-7500 Karlsruhe 1
Mr. E. Diegele	Kernforschungszentrum Karlsruhe Postfach 3640 D-7500 Karlsruhe 1
Mr. K. Anderko	Kernforschungszentrum Karlsruhe Postfach 3640 D-7500 Karlsruhe 1
Mr. M. Dalle Donne	Kernforschungszentrum Karlsruhe Postfach 3640 D-7500 Karlsruhe 1
Mr. K. Koizlik	Kernforschungsanlage Jülich GmbH Institut für Reaktorwerkstoffe Postfach 1913 D-5170 Jülich 1
Mr. R. Behrisch	Max-Planck-Institut für Plasmaphysik (IPP) D-8046 Garching
Mr. H. Schroeder	Kernforschungsanlage Jülich GmbH Postfach 1913 D-5170 Jülich
Mr. R. Krieg	Kernforschungszentrum Karlsruhe Institut für Reaktorentwicklung Weberstrasse 5 Postfach 3640 D-7500 Karlsruhe 1

Italy

Mr. Alberto Borello	ENEA, TIB-Chimica, C.R.E.-Casaccia S.P. Anguillarese301 I-00100-Roma (1)
---------------------	---

Italy (cont.)

Mr. Emilio Franconi

ENEA, Department of Fusion
C.R.E.-Frascati
C.P. 65
I-00044 - Frascati
Roma - I

Japan

Mr. T. Tone

Japan Atomic Energy Research Institute
Naka Fusion Research Establishment
Naka-machi
Naka-gun
Ibaraki-ken

Netherlands

Mr. B. Van der Schaaf

Netherlands Energy Research Foundation
Westerduinweg 3
P.O. Box 1
1755 ZG Petten

Sweden

Mr. B.Y. Emmoth

Research Institute of Physics (AFI)
Frescativ.gen 24
S-104 05 Stockholm

Switzerland

Mr. W. Green

Eidgenössisches Institut
für Reaktorforschung
CH-5303 Würenlingen

United Kingdom

Mr. J. R. Matthews

Theoretical Physics Division
Building 424.4
AERE Harwell
Oxon, OX11 0RA

United States of America

Mr. R. Mattas


Fusion Power Programme
Argonne National Laboratory
9700 South Cass Avenue
Argonne, ILL. 60439

International Organization


Commission of European Communities

Mr. R. Bünde	The NET Team Max-Planck-Institut für Plasmaphysik Boltzmannstrasse 2 D-8046 Garching
Mr. G.O. Vieider	The NET Team Max-Planck-Institut für Plasmaphysik Boltzmannstrasse 2 D-8046 Garching
Mr. F. Moons	The NET Team Max-Planck-Institut für Plasmaphysik Boltzmannstrasse 2 D-8046 Garching
Mr. A. Cardella	The NET Team Max-Planck-Institut für Plasmaphysik Boltzmannstrasse 2 D-8046 Garching
Mr. W. Dänner	The NET Team Max-Planck-Institut für Plasmaphysik Boltzmannstrasse 2 D-8046 Garching
Mr. E. Zolti	The NET Team Max-Planck-Institut für Plasmaphysik Boltzmannstrasse 2 D-8046 Garching
Mr. D.R. Harries	The NET Team Max-Planck-Institut für Plasmaphysik Boltzmannstrasse 2 D-8046 Garching
Mr. Ehrenberg	The JET Team Max-Planck-Institut für Plasmaphysik Boltzmannstrasse 2 D-8046 Garching

HOW TO ORDER IAEA PUBLICATIONS

 An exclusive sales agent for IAEA publications, to whom all orders and inquiries should be addressed, has been appointed in the following country:

UNITED STATES OF AMERICA UNIPUB — Bernan Associates, 10033-F King Highway, Lanham, MD 20706-4391

 In the following countries IAEA publications may be purchased from the sales agents or booksellers listed or through your major local booksellers. Payment can be made in local currency or with UNESCO coupons.

ARGENTINA	Comisión Nacional de Energía Atómica, Avenida del Libertador 8250, RA-1429 Buenos Aires
AUSTRALIA	Hunter Publications, 58 A Gipps Street, Collingwood, Victoria 3066
BELGIUM	Service Courrier UNESCO, 202, Avenue du Roi, B-1060 Brussels
CHILE	Comisión Chilena de Energía Nuclear, Venta de Publicaciones, Amunategui 95, Casilla 188-D, Santiago
CHINA	IAEA Publications in Chinese: China Nuclear Energy Industry Corporation, Translation Section, P.O. Box 2103, Beijing IAEA Publications other than in Chinese: China National Publications Import & Export Corporation, Deutsche Abteilung, P.O. Box 88, Beijing
CZECHOSLOVAKIA	S.N.T.L., Mikulandska 4, CS-116 86 Prague 1 Alfa, Publishers, Hurbanovo námestie 3, CS-815 89 Bratislava
FRANCE	Office International de Documentation et Librairie, 48, rue Gay-Lussac, F-75240 Paris Cedex 05
HUNGARY	Kultura, Hungarian Foreign Trading Company, P.O. Box 149, H-1389 Budapest 62
INDIA	Oxford Book and Stationery Co., 17, Park Street, Calcutta-700 016 Oxford Book and Stationery Co., Scindia House, New Delhi-110 001
ISRAEL	Heiliger and Co., Ltd, Scientific and Medical Books, 3, Nathan Strauss Street, Jerusalem 94227
ITALY	Libreria Scientifica, Dott. Lucio de Biasio "aeiou", Via Meravigli 16, I-20123 Milan
JAPAN	Maruzen Company, Ltd, P.O. Box 5050, 100-31 Tokyo International
NETHERLANDS	Martinus Nijhoff B.V., Booksellers, Lange Voorhout 9-11, P.O. Box 269, NL-2501 The Hague
PAKISTAN	Mirza Book Agency, 65, Shahrah Quaid-e-Azam, P.O. Box 729, Lahore 3
POLAND	Ars Polona-Ruch, Centrala Handlu Zagranicznego, Krakowskie Przedmiescie 7, PL-00-068 Warsaw
ROMANIA	Ilexim, P.O. Box 136-137, Bucharest
SOUTH AFRICA	Van Schaik Bookstore (Pty) Ltd, P.O. Box 724, Pretoria 0001
SPAIN	Díaz de Santos, Lagasca 95, E-28006 Madrid Díaz de Santos, Balmes 417, E-08022 Barcelona
SWEDEN	AB Fritzes Kungl. Hovbokhandel, Fredsgatan 2, P.O. Box 16356, S-103 27 Stockholm
UNITED KINGDOM	Her Majesty's Stationery Office, Publications Centre, Agency Section, 51 Nine Elms Lane, London SW8 5DR
USSR	Mezhdunarodnaya Kniga, Smolenskaya-Sennaya 32-34, Moscow G-200
YUGOSLAVIA	Jugoslovenska Knjiga, Terazije 27, P.O. Box 36, YU-11001 Belgrade

 Orders from countries where sales agents have not yet been appointed and requests for information should be addressed directly to:



Division of Publications
International Atomic Energy Agency
Wagramerstrasse 5, P.O. Box 100, A-1400 Vienna, Austria